THÈSE DE DOCTORAT

présentée et soutenue publiquement à

L'UNIVERSITE DE LILLE

Ecole doctorale des Sciences Pour l'Ingénieur (EDSPI)
pour obtenir le grade de

DOCTEUR

Spécialité: Mécanique des solides, des matériaux, des structures et des surfaces

par

Daniele MASSELLA

Preparation of biofunctional textiles by surface functionalization based on the nanoencapsulation technique.

Préparation de textiles biofonctionnels par fonctionnalisation de surface basée sur la nanoencapsulation.

Thèse en cotutelle avec le Politecnico di Torino et l'Université de Soochow (Chine)

Soutenue le 1 octobre 2020 devant la commission d'Examen composée de:

Yves CHEVALIER	Professor, Universitè de Lyon 1, France	Rapporteur
Raffaele SALADINO	Professor, Università degli studi della Tuscia, Italy	Rapporteur
Bernard MARTEL	Professor, Université de Lille, France	Président
Zhao HUIJING	Associate Professor, Soochow University, China	Examinateur
Meritxell MARTI-GELABERT	Researcher, IQAC, Spain	Examinateur
Francesco TROTTA	Professor, Università di Torino, Italy	Examinateur
Fabien SALAUN	Professor, ENSAIT-GEMTEX, France	Directeur de thèse
Ada FERRI	Professor, Politecnico di Torino, Italy	Co-directrice de thèse
Jinping GUAN	Professor, Soochow University, China	Invité
Yan Chen	Professor, Soochow University	Invité

Preparation of biofunctional textiles by surface functionalization based on the nanoencapsulation technique

Ph.D. Thesis by

Massella Daniele

In the fulfillment of the Erasmus Mundus joint doctorate program

SMD-TEX - *Sustainable management and design of textiles.*

In collaboration with

Politecnico di Torino – Department of Applied Science and Technology, Italy

ENSAIT, GEMTEX - Laboratory textiles materials and engineering, France

Soochow University – College of textile and clothing engineering, China.

Abstract

This study was performed in the frame of the SMD-Tex Joint Doctorate project. The doctoral research activities were carried out in three mobility periods at POLITO (Italy), Ensait (France), and University of Soochow (China). This work aims to propose novel approaches for the production of biofunctional textiles. These products consist of textile fabrics which underwent special finishing treatments to confer properties that display beneficial effects to the user's health.

In the last decades, pharmaceutical research has been investigating novel and more effective tools to administer a drug to the patient. The scope of these studies is to provide effective therapeutic dosages over a long time, minimizing the number of required administrations and the possible side effects. In this context, the skin has been regarded as a potential route for the release of local and systemic drugs. Such an approach is simpler and less invasive compared to other routes. Therefore, several strategies have been developed to effectively deliver drugs across the skin barrier. Among them encapsulation technology allows the incorporation of the active substances inside nanoparticles (NPs) to i) protect the drug, ii) effectively deliver it through the skin iii) control the release over time.

In the present work, drug-loaded NPs were produced by employing polycaprolactone (PCL) as shell material. The produced nanoparticles were then used to finish cotton fabrics producing biofunctional textiles to be employed as wearable drug delivery devices. The flash nanoprecipitation technique (FNP) was exploited for the nanocarrier production being identified as a simple, sustainable and efficient production process. The suitability of the FNP process to produce NPs to be used in the preparation of biofunctional textiles was investigated. The PCL nanoparticles were produced by loading three different drugs in the system i.e. caffeine, melatonin, and curcumin. Such drugs are indeed considered model drugs in terms of hydrophilicity level. The latter is a key property in determining the outcome of the encapsulation process and the dermal permeation.

The FNP process was run by dissolving the polymer in an organic solvent and making the solution stream collide against an antisolvent stream in a micromixer, resulting in the polymer precipitation in the form of nanoparticles. The drugs were precipitated together with the polymer upon being added either to the solvent or the antisolvent stream. For each active substance, the experimental protocols and analytical methods were adjusted to better investigated the drug-loaded NPs system. The effect of the formulation as well as the process parameters on the properties of the nanoparticles was investigated. The process was optimized to produce particles with a diameter lower than the one of skin pores. The amount of drug loaded in particles was investigated by loading capacity (LC) and

encapsulation efficiency (EE). Furtherly, the NP formulations were characterized to obtain insights on their physical, chemical, and morphological properties by various analytical techniques.

The particles were applied to the cotton fabric either by imbibition or impregnation methods. The effectiveness of the functionalization treatment was evaluated combining different analyses. The biofunctional properties were studied in terms of antioxidant activity, UV protection factors, and drug release. For the latter test, the Franz cell method was employed using either artificial and excised porcine skin membranes.

The study showed that the FNP allows producing drug loaded PCL NPs for all the three investigated substances. The proposed finishing treatment allowed to effectively functionalize the fabric surface. The treated textiles allowed to effectively deliver the active principles to the skin with permeation profiles dependent on the drug properties. The nanoparticle finishing also imparted cotton antioxidant and UV protection properties.

Keywords: Biofunctional textiles; Drug delivery; Nanoparticles; Encapsulation; Textile Finishing; Flash nanoprecipitation; Dermatological applications.

Résumé

La présente thèse a été réalisée dans le cadre du projet de doctorat joint SMD-Tex, en partenariat entre le POLITO (Italie), l'ENSAIT (France) et à l'Université de Soochow (Chine). Le but de ce travail est de proposer de nouvelles approches pour la production de textiles biofonctionnels. Ces produits sont constitués de textiles qui ont subi des traitements de finition spéciaux pour conférer des propriétés qui présentent des effets bénéfiques pour la santé de l'utilisateur.

Longtemp la recherche pharmaceutique a étudié des outils nouveaux et plus efficaces pour administrer un médicament au patient. Le but de ces études est d'admiistrer des dosages thérapeutiques efficaces sur une longue période, en minimisant le nombre d'administrations requises et les effets secondaires possibles. Dans ce contexte, la peau a été considérée comme une voie de libération de médicaments locaux et systémiques. Une telle approche est plus simple et moins invasive que d'autres voies. Donc, plusieurs stratégies ont été développées pour délivrer efficacement des médicaments à travers la barrière cutanée. Parmi celles-ci, la technologie d'encapsulation permet l'incorporation des substances actives à l'intérieur des nanoparticules (NP) pour i) protéger le médicament, ii) le délivrer efficacement à travers la peau iii) contrôler la libération au fil du temps.

Dans le présent travail, des NP chargés de médicament ont été produits en utilisant de la polycaprolactone (PCL) comme membrane. Les nanoparticules produites ont ensuite été utilisées pour finisser des tissus en coton produisant des textiles biofonctionnels destinés à être utilisés comme dispositifs portables de distribution de médicaments. La technique de nanoprécipitation flash (FNP) a été exploitée pour la production des NPs en raison de sa productivitè, et semplicité. La pertinence du procédé FNP pour produire des NP destinés à être utilisés dans la préparation de textiles biofonctionnels a été étudiée. Les nanoparticules PCL ont été produites en chargeant trois médicaments différents dans le système, à savoir la caféine, la mélatonine et la curcumine. Ces médicaments sont en effet considérés comme des médicaments modèles en termes de niveau d'hydrophilie. Ce dernier est une propriété clé dans la détermination du résultat du processus d'encapsulation et de la perméation cutanée.

Le procédé FNP a été exécuté en dissolvant le polymère dans un solvant organique et en faisant entrer le courant de solution en collision avec un courant d'antisolvant dans un micromélangeur, entraînant la précipitation du polymère sous forme de nanoparticules. Pour chaque substance active, les protocoles expérimentaux et les méthodes analytiques ont été ajustés pour mieux étudier le système de NP chargé de médicament. L'effet de la formulation ainsi que les paramètres du procede sur les

taille et la capacitè d’enrobement des nanoparticules ont été étudiés. De plus, les formulations de NP ont été caractérisées pour obtenir des informations sur leurs propriétés physiques et chimiques par diverses techniques.

Les particules ont été appliquées au textile de coton soit par des méthodes d'imbibition ou d'imprégnation. L'efficacité du traitement de fonctionnalisation a été évaluée en combinant différentes analyses. Les propriétés biofonctionnelles ont été étudiées en termes d'activité antioxydante, de facteurs de protection UV et de libération de médicaments. Pour ce dernier test, la méthode des cellules de Franz a été employée.

L'étude a montré que le FNP permet de produire des NPs de PCL chargées de médicament pour les trois substances étudiées. Le traitement de finition proposé a permis de fonctionnaliser efficacement la surface du tissu. Les textiles traités ont permis de délivrer efficacement les principes actifs à la peau avec des profils de perméation dépendant des propriétés du médicament. La finition des nanoparticules confère également au coton des propriétés antioxydantes et de protection contre les UV.

Mots-clés: Textiles biofonctionnels; Administration de médicaments; Nanoparticules; Encapsulation; Finition textile; Nanoprécipitation; Applications dermatologiques.

Riassunto

Il presente studio è stato condotto nell'ambito del progetto di dottorato internazionale SMD-Tex. Le attività di ricerca sono state svolte in tre periodi di mobilità presso il Politecnico di Torino (Italia), l'ENSAIT (Francia) e l'Università di Soochow (Cina). La presente tesi propone nuove metodologie per la produzione di tessuti biofunzionali. Questi materiali sono costituiti da tessuti sottoposti a speciali trattamenti di finissaggio al fine di impartire proprietà benefiche per la salute dell'utilizzatore.

Negli ultimi decenni, la ricerca farmaceutica ha studiato nuove tecnologie al fine di ottimizzare la somministrazione di molecole attive al paziente. Lo scopo di questi studi sul rilascio controllato è quello di somministrare dosaggi terapeutici efficaci riducendo il rischio di effetti collaterali. In questo contesto, la pelle è stata considerata una potenziale via per il rilascio di farmaci sia a livello topico che sistemico. Tale approccio è considerato più semplice e meno invasivo rispetto alla via enterale o a quella parenterale. Pertanto, sono state sviluppate diverse strategie per permettere alla posologia di attraversare efficacemente barriera cutanea. Tra queste la tecnica dell'incapsulamento consente l'incorporazione delle sostanze attive all'interno di nanoparticelle polimeriche (NP) al fine di i) proteggere il farmaco, ii) somministrarlo efficacemente attraverso la pelle iii) controllare la cinetica di rilascio.

Nel presente studio, diverse sostanze attive sono state incorporate in NP polimeriche usando il policaprolattone (PCL) come matrice di incapsulamento. Le nanoparticelle prodotte sono state quindi utilizzate per funzionalizare tessuti di cotone, ottenendo così tessuti biofunzionali impiegabili come dispositivi per il rilascio controllato. La tecnica di nanoprecipitazione flash (FNP) è stata scelta per la produzione dei nanocarriers essendo riconosciuta come una metodologia semplice, sostenibile ed efficiente. L'idoneità del processo FNP per la produzione di NP da impiegare nel finissaggio tessile è stata valutata testando il processo su diverse sostanze attive quali la caffeina, la melatonina e la curcumina. Tali sostanze sono state scelte come molecole modello in termini idrofilia. Quest'ultima proprietà risulta avere un ruolo chiave sia nel processo di incapsulamento sia nella permeazione cutanea.

Il processo FNP è stato condotto dissolvendo il polimero in un solvente organico e, mescolando tale soluzione con un antisolvente all'interno di un apposito micro miscelatore; andando così a provocare la precipitazione del polimero sotto forma di nanoparticelle. Per ogni sostanza attiva, i protocolli sperimentali e i metodi analitici sono stati adeguati per studiare al meglio il sistema particellare. Sono stati studiati gli effetti della formulazione e dei parametri di processo sulle proprietà delle

nanoparticelle. Il processo è stato ottimizzato per produrre particelle con un diametro sufficientemente piccolo al fine di permeare efficacemente la barriera cutanea. La quantità di farmaco caricato all'interno particelle è stata quantificata misurando i parametri Loading Capacity (LC) ed Encapsulation Efficiency (EE). Inoltre, le formulazioni NP sono state sottoposte a diverse caratterizzazioni al fine di per ottenere maggiori informazioni sulle loro proprietà fisiche e chimiche.

Le particelle sono state applicate al tessuto di cotone mediante metodi di imbibizione o impregnazione. L'efficacia del trattamento di funzionalizzazione è stata valutata combinando diverse analisi. Le proprietà biofunzionali sono state studiate in termini di attività antiossidante, fattori di protezione UV e rilascio del farmaco. Per quest'ultimo test, è stato impiegato il metodo delle celle di Franz.

Il presente studio ha dimostrato che la FNP consente di produrre nanoparticelle di PCL caricate con diverse sostanze attive. Il trattamento di finissaggio proposto ha permesso di funzionalizzare efficacemente il substrato tessile. I tessuti biofunzionali prodotti si sono rivelati efficaci nel somministrare le sostanze attive a livello cutaneo. Il processo di finissaggio ha inoltre conferito ai tessuti proprietà antiossidanti e di protezione dai raggi ultravioletti UV.

Parole chiave: Tessuti biofunzionali; Rilascio di farmaci; Nanoparticelle; Incapsulamento; Finissaggio tessile; Nanoprecipitazione flash; Applicazioni dermatologiche.

摘要

本研究在SMD-Tex欧盟联合培养博士学位项目的体系下进行。博士研究工作主要在意大利都灵理工大学、法国国立高等纺织工程师学院和中国苏州大学三个学校流动进行。本研究的主要目的是提出制备生物功能纺织品的新型方法，通过特种整理所制备的功能性纺织品对人体健康有益。

在过去的几十年中，药物研究者一直致力于开发新型、高效的给药方法。这些研究的主要目的是为了长期输送一定剂量的药物给患者，从而减少给药次数及其带来的副作用。在此背景下，皮肤被当作是局部释放和全身性药物释放的有效途径。与其它途径相比，这种方法更为简单且对人体侵入性更小。因此，研究者开发了一些方法可有效地使药物穿过皮肤这道屏障。其中，微胶囊技术可将活性物质混入纳米颗粒中，从而起到以下作用：(1) 保护药物；(2) 有效地将药物输送到皮肤内；(3) 控制释放时间。

本研究采用聚己内酯（PCL）作为外壳材料制备载药纳米粒子。然后将制备的纳米粒子采用整理的方法应用于棉织物，并将其用于可穿戴的药物输送装置。作为一种简便、可持续和有效的生产方法，快速纳米沉积法（FNP）被用于制备纳米装置。研究了采用FNP工艺制备纳米粒子和生物功能性纺织品的可行性。通过将三种不同的药物如咖啡因、褪黑素和姜黄素加载到体系中来制备PCL纳米颗粒。通过亲水性测试推断这些药物可作为模型药物。微胶囊的制备过程和皮肤渗透效果也是后期较为关键的性能。

首先通过FNP工艺将聚合物溶解在有机溶剂中，并使溶液在微型混合器中与溶剂流发生碰撞进行反应，从而使聚合物沉淀，制备纳米颗粒沉淀。将聚合物加入到溶剂或反溶剂中都可以使聚合物产生沉淀，得到药物颗粒。通过调整实验方案和分析方法来更好的研究每种活性物质载药NPC体系。研究了配方以及工艺参数对纳米粒子性能的影响。经过工艺优化可制备出直径小于皮肤毛孔的颗粒。通过负载量(LC)和包埋效率(EE)研究颗粒中的药物载量。此外，通过各种分析技术表征NP配方，从而对其物理性能、化学性能和表面形态等有更深的了解。

通过浸渍吸附的方法将纳米颗粒应用于棉织物。结合不同的分析评价功能整理的效果。研究了整理棉织物的生物功能性如抗氧化性能、抗紫外性能和药物释放性能。通过Franz细胞法采用人工皮肤和猪皮肤评价药物释放性能。

研究结果表明，FNP法可用于制备负载三种药物的PCL纳米颗粒。本研究所采用的整理方法可有效地对织物表面进行功能化改性。经过处理的纺织品可有效地将活性成分输送到皮肤，而其渗透性能与药物自身的特性有关。此外，纳米颗粒整理还赋予棉织物较好的抗氧化性能和抗紫外性能。

关键词：生物功能纺织品； 药物输送； 纳米粒子； 胶囊化； 纺织品整理； 瞬时纳米析出法； 皮肤病应用

Acknowledgments

Firstly, I would like to express my sincere gratitude to my supervisors Professors Ada Ferri, Fabien Salaün and Guan Jinping both under the professional and the personal point of view. They provided me guidance in the research development and gave me the tools to start taught me the necessary to develop my scientific work. Moreover, they helped me throughout my journey around the world providing continuous support, without this support the development of the present manuscript would have not been possible.

I want to thank the other professor that contributed to the present work starting with prof. Antonello Barresi who provided a great support and gave me a significant contribution that allowed me start my project in the best possible way. I wish to thank professor Stephane Giraud for being an awesome co-supervisor and for giving me a significant contribution especially during the French mobility and during the last month of redaction of the thesis. A special thanks goes to professor Yan Chen that continuously assisted me during my stay in China.

I wish to thank the European Union for funding the SMD-Tex thus giving me the possibility of continuing my education and taking this once in a life journey. Furtherly I wish to thank you prof. Zeng for his coordination of the SMD-Tex program.

I sincerely thank the rapporteurs/reviewers and the members of my defense jury for taking the duty of evaluating my work.

Special thanks go to the Ermenegildo Zegna company for the support of my mobility abroad through the “EZ founder scholarship” action.

I wish to thank the research groups with which I collaborated during the past four years which allowed me to tackle my research with a multidisciplinary mindset. I sincerely thank the group of Prof. Roberta Cavalli from the drug science and technology department of UNITO, particularly I acknowledge Doctors Monica Argenziano and Federica Bessone for the precious collaboration.

I sincerely thank the members of TNH lab group in POLITO, Prof Valentina Cauda, Dr Andrea Ancona and Dr Nadia Garino for the fruitful scientific collaborations and for their sincere supports during all my PhD journey.

A sincere thanks goes to the technical staff of the laboratories in which I worked, particularly to Dr Edvige Celasco for the XPS analysis, Mauro Raimondo for the FESEM observations, Sabine Chlebicki, Christian Catel and François Dassonville for the technical support and training in the GEMTEX labs.

A sincere and significant thank goes to the master thesis students whose work constituted a preliminary basis of the present work and those MS thesis students which I co-supervised and that gave me a substantial help in the collection of the data here present. Without their contribution the redaction of the present manuscript would not have been possible. I therefore thank, Giulia Delpiano, Ivan Bevilacqua, Marco Izzo and Matteo Baudino.

Lastly I want to thank my SMD-Tex fellows who shared with me the joys and the struggles of the PhD life. Indeed, I am going to write the personal acknowledgements later but since I will write it in Italian, maybe its better to take here the opportunity to thank Nett (aka Miss Petchprakai) for being my foody fellow and running partner in Roubaix, Prisca for making me understand I could never go on a diet and for saving me (and Nett as well) when could not exit the yard… Mulat (aka Quintaletto) for the beer after work and the great time spent in China, Molla (aka Patrick) for making me discover that Italy and Ethiopia are the same thing, Sheenam for being the smartest computer girl in China that can make everything work properly, Sweeta for having the coolest haircut in Suzhou and Marzi for being the biggest fan of my homemade liquors (with Sweeta as well).

Ed ora per un momento mi concedo di scrivere poche righe nella mia lingua madre per poter ringraziare le persone che più mi sono state vicine in questi anni.

Prima di tutto ringrazio mia mamma Stefania, per il suo amore incondizionato, per i suoi continui sacrifici, soprattutto quello di aver accettato e sopportato la mia lontananza in questi anni essendoci sempre per me. Al mio babbo Alessandro che si prendeva cura di me senza mai essere di troppo, nascondendo le sue preoccupazioni affinché io non dovessi portarne altro peso e cercando di togliere i possibili ostacoli sul mio cammino senza che io potessi accorgermene.

Ringrazio la mia zia Daniela perché è un portento, mi ha fatto appassionare alla scienza da quando ero bambino, il seme di questo dottorato forse è stata lei a piantarlo… e poi perché insieme stiamo sempre un gran bene.

Alla zia Petit Madeleine Roberta, perché noi abbiamo un legame speciale e forse, una delle cose più belle di questo percorso è stato per me quello di vivere in Francia, cosicché tra noi si è creata

un’ancora più forte rete di sottili connivenze, che racchiudano al loro interno la paradossale gioia di vivere.

Alla mia cugina Giulia per i nostri riti scaramantici prima degli esami, spero che potremmo farne presto uno per la difesa della tesi.

A miei zii Enrico e Maurizio per il loro importante e motivante supporto in questi ultimi mesi di lavoro di stesura. A miei cuginetti Filippo, Gabriele e Federico perché il tempo che sono riuscito a passare con loro nonostante sia stato fuori negli ultimi anni è stato stupendo.

Al nonno Cesare che mi guarda e veglia su di me dal cielo, la sua immensa stima e fiducia nei miei confronti mi hanno sempre dato la motivazione per superare ogni difficoltà.

Un Grazie speciale va agli amici ed ai fantastici colleghi incontrati in questi anni, che sono tantissimi e spero di non dimenticarne nessuno (soprattutto perché anche questa volta mi riduco all’ultimo per scrivere i ringraziamenti).

Un grazie speciale va a Sole che è sempre stato un amico impareggiabile su cui sai sempre di poter contare, una persona con la quale è stupendo condividere qualsiasi momento della propria vita.

Un grazie speciale va tutti gli amici, anzi fratelli incontrati sul cammino dello scoutismo che vissuto con grande passione in questi anni e qui parte una grande lista: Tony, Filo, Foro, Don Luca, Maria, Beatrice, Cesare, Cristina, Pasquale, Alessandra, Enrico, Laura, Massimo, Elena, Danilo, Roberto, Luca, Matteo King, Annalisa, Fausto, Giammarco, Emanuele Arcanda, Gianluca, Sara, Serena e tanti altri… a tutti voi la mia gratitudine ed il mio augurio di Buona Strada.

Un grazie ai miei colleghi, ma soprattutto amici incontrati al DISAT, Luigi, Fiora, Marco S, e Marco B e Luchino.

A Matteo Segantini, viterbese anema e core in perenne traferta.

Un grazie speciale ed enorme va ai miei stupendi coinquilini di Lille, Gianluca e Patrizia per la loro amicizia speciale, il loro supporto costante e il loro affetto incondizionato.

A tutti voi va la mia gratitudine per aver dato a questi anni un valore speciale e ve ne sono grato, senza di voi non sarei riuscito in tutto questo… vi voglio molto bene.

Daniele.

Table of contents

List of abbreviations

ACS	American Chemical Society
ATR	Attenuated Total Reflectance
CA	Cellulose Acetate
CD	Cyclodextrins
CE	Chemical enhancer
CIJM	Confined Impinging Jet Mixer
DLS	Dynamic Light Scattering
DME	Direct Membrane Emulsification.
DMPO	5,5-Dimethyl-1-Pyrroline N-Oxide
DSC	Differential Scaning Calorimetry
EE	Encapsulation Efficciency
EMA	European Medicines Agency
EPR	Electron Paramagnetic Resonance spectroscopy
FDA	Food and Drug Administration regulation agency
FTIR	Fourier Transform Infrared Spectroscopy
HaCat	Skin keratinocytes cell line
H-NMR	Hydrogen Nuclear Magnetic Resonance spectroscopy.
LC	Loading capacity
LDH	Lactate Dehydrogenase
LogP	Water Octanol partition coefficient
MCE	Mixed Cellulose Esters
ME	Membrane Emulsification
MIVM	Multi Inlet Vortex Mixer

MMLR	Maximum mass loss rate
MN	Microneedles
MTT	(3-(4,5-dimethylthiazol-2-yl)-2,5-diphenyltetrazolium bromide) cell viability test
MW	Molecular Weight.
NB	Nanobubbles
NC	Nanocapsules
NF	Nanofibers
NP	Nanoparticles
NS	Nanospheres
NSP	Nanosponges
O/W	Oil in water emulsion
O/W/O	Oil in water in oil emulsion
PA	Polyamide
PAA	Polyacrylic acid
PAC	Polyacrylic
PC	PolyCarbonate
PCL	Poly-ε-caprolactone
PEG	Polyethylene glycol
PEGDA	Polyethylene glycol diacrylate
PFC	Perfluorocarbons
PLA	Poly Lactic Acid
PLGA	Poly (lactic-co-glycolic acid)
PME	Premix Membrane Emulsification.
PI	Poly Imide.
pI	Isoelectric point.

PES	Poly Esters.
PSD	Particle Size Distribution
PTFE	Poly Tetra Fluoro Ethylene
PU	Polyurethane
PVA	Poly Vinyl Alcohol
PVP	Poly Vinyl Pyrrolidone
QR	Quenching Ratio
ROS	Radical Oxygen Species.
SC	Stratum Corneum
SEM	Scanning Electron Microscope
TEOS	Tetra Ethyl Ortosilicate
TGA	Termogravimetric analysis
THF	Tetrahydrofuran
TLC	Thin layer Chromatografy
TPP	Tripolyphosphate
W/O	Water in oil
W/OW	Water in oil in water
UPF	UV Protection Factor
UV	Ultraviolet
USA	United States of America
US	Ultrasounds
XPS	X-ray Photoelectron Spectroscopy

List of symbols

ΔH_{fus}: Enthalphy variation of the fusion process.

ΔP: Pressure drops.

ϵ: Molar extinction coefficient.

ϵ_0: The electrical permittivity of the vacuum.

ϵ_m: The electrical permittivity of the medium.

θ: Contact angle.

π: Greek letter pi.

ρ: Density.

A: Absorbance.

C: Concentration.

C_{PCL}: Concentration of PCL.

C_{Mel}: Concentration of Melatonin.

C_{Caf}: Concentration of Caffeine.

C_{Cur}: Concentration of Curcumin.

Dp: Average particle diameter.

E_λ: Relative erythemal spectral effectiveness.

K_{El}: Electrical conductivity.

K_0: Zero order constant.

K_f: First order constant.

K_H: Higuchi model constant.

K_{BL}: Baker and Lonsdale constant.

K_{hc}: Hixon Crowell constant.

$\frac{K}{S}$: Color strength.

l: Optical path.

MW: Polymer molecular weight.

$m_{drug,en}$: Mass of drug encapsulated.

$m_{drug,in}$: Initial mass of drug in the formulation

$m_{pol,in}$: Initial mass of polymer in the formulation

m_{tot}: Total mass of the NP system.

Q: Cumulative drug released at time t.

Q_∞ : Cumulative drug released at the end of the test.

Q_0: Drug released at the beginning of the test.

QR: Quenching ratio.

R: Spectral reflectance.

S: Supersaturation degree.

S_λ: Solar spectral irradiance.

T*:* Temperature in Kelvins.

$T_{5\%}$: Temperature at which 5% by weight of the sample was degraged during TGA analysis.

T_λ: Spectral transmittance of the fabric sample.

$T_{fus,\ onset}$: Onset temperature for the fusion process.

$T_{fus,\ peak}$: Peak temperature for the fusion process.

T_{max}: Temperature of maximum degradation rate.

U_{str}: Streaming potential.

V_Q: Volume of quenching water.

V_s: Volume of solution fed to the reactor.

X_c: Degree of crystallinity.

List of Figures

List of Tables

General introduction

In the last decades, research in the field of pharmaceutical technology has invested significant efforts to develop innovative ways to administer active principles to patients in more effective ways. This research field, commonly defined as drug delivery technology, aims to administer effective therapeutic dosages to the target tissues in a controlled way while minimizing possible side effects.

The common approaches to deliver drugs to the patient imply the enteral and parenteral drug administration routes. The enteral pathway mainly consists of the oral ingestion of the formulation by the patient. Such an approach is simple and not invasive, however, the effective delivery of the drug to the systemic circulation may be hindered by scarce uptake in the gastric environment or by the first pass metabolism in the liver. The parenteral administration includes the formulations which are injected in the circulation. Such an approach limits the metabolic degradation of the active principles, however, it is quite invasive and sometimes may not be operated independently by the patient. Furtherly, both for enteral and parenteral route multiple administrations of the posology are required; thus, strict patient compliance is necessary for the therapy to be effective.

In recent years the novel approach of exploiting skin for pharmaceutical administration has aroused significant interest. Being the skin the largest organ of the human body it offers a significant surface area for drug administration. Furthermore, the skin is the organ devoted to internal body protection and can act as a barrier for harmful substances thus reducing possible side effects. Therefore, the skin has been considered as a possible administration route both for systemic and local drugs.

This administration method displays several advantages compared to other classic drug delivery routes such as the enteral and parenteral ones. Firstly, it is noninvasive since it does not require injections. Secondly, it delivers the actives in the blood circulation avoiding the first pass metabolism in the liver. Lastly, given that transdermal delivery devices can stick on the patient for several days, the number of required applications is significantly reduced; thus easing the patient compliance to the therapy. Notwithstanding the numerous advantages of the transdermal route, its employment is still limited because the skin barrier is characterized by a great chemical complexity that limits the transport of the active substances across its numerous layers. Therefore, the transdermal delivery is commonly limited to a few classes of active molecules that can effectively cross the skin to reach the systemic circulation.

The encapsulation technique is a widely exploited approach in the context of drug delivery technologies. It mainly consists of incorporating the active substance inside a shell material. Such an

approach displays several advantages that can lead to higher therapeutic efficacy respect to the raw drug formulation. Firstly, encapsulation protects the active molecule and eases its storage, thus preventing its degradation until the target tissue is reached. Secondly, it allows structuring the drug promoting the penetration of the biological barrier and favoring cellular uptakes. Finally, the encapsulation makes possible to control the drug release over a long time, this feature prevents the burst release phenomenon and reduces the number of administrations required. Given the numerous advantages of the encapsulation technology, it had become of significant interest to produce drug carriers with improved therapeutic performances. In particular, nanosized drug carriers have proved to be more effective in overcoming the biological barriers and improving cellular uptakes while effectively controlling the drug release kinetics.

Such a nanotechnology based approach was considered particularly advantageous in overcoming the skin barrier. The nanocarriers can vector the active principle through the skin layers without the need of employing chemical penetration enhancers which can irritate the skin in the long run. Therefore, the encapsulation of the active principle was identified as an effective strategy to release drugs across the skin layers.

The nanocarrier formulations are generally available in the form of liquid suspensions and therefore their usage in the dermatological application requires multiples administrations unless the formulation is supported on a wearable platform. Such supports generally consist of adhesive patches that stick for several days on the patient skin. However, these adhesive patches are generally not breathable and therefore may cause skin irritation in the long run. Therefore, the usage of breathable support for the drug loaded nanocarriers was foreseen as a strategy to improve the state-of-the-art technology.

Textiles are a class of materials owning peculiar properties such as flexibility, mechanical strength and lightness. Besides the common use in the apparel industry, in recent years they have been employed in a wide range of industrial sectors such as automotive, construction, electronics, environmental and biomedical ones. These materials are defined as technical textiles, namely fibrous materials that are not used for their apparel and aesthetic properties but their technical performances. A particular category of technical textiles is the Medtech one, this includes those textiles materials whose main purpose is to benefit the user's health. The Medtech category includes products such as pressure garments to enhance muscular recovery, textiles with antibacterial properties used to produce bandages or garments for surgeons, textiles for protection against insects and ultimately for the release of active substances. These last mentioned products are obtained by applying peculiar finishes on commodity fabrics such as cotton, silk, wool or polyester that represent optimal support for the

nanocarriers. Such fabrics have been used as garments over years and they are well known to not cause any allergic reaction or inflammation upon long contact with the human skin. Furthermore, the porous and interlaced fibers networks typical of the fabric's structure acts as a reservoir for the drug loaded nanocarriers. Notwithstanding the high potential benefits of employing such textile substrates as support for dermatological delivery of drug loaded nanocarriers, such technology is still not widely developed.

The biofunctional textile technology has not reached technological maturity yet. Thus the production of these materials is still not sustainable under the technical and economic point of view. The first issue encountered is the fact that the production of pharmaceutical nanocarriers is still a niche technology. Thus, these nanocapsules are often produced in small batches with high production costs. On the contrary, the textile industry requires the finishing agent to available in high quantity at a cheap price. Concerning the finishing process, it must be designed to make the functionalized fabric act as an effective pharmaceutical formulation to be easily operated by the user. These considerations show that significant improvements should be done in the biofunctional textiles technology to make it available to the users.

This issue is not peculiar to the biofunctional textiles but regards several innovative technologies and processes being developed nowadays in the textile fields. To propose a novel design of textiles technologies that comply with the up-to-date sustainability issues, the SMD-Tex project was launched in 2013. The acronym stands for Sustainable Management and Design of Textiles and refers to international joint doctorate financed by the European Union under the Erasmus Mundus action. The involved parts in the SMD-Tex project are five academic institutions from different countries: Ecole Nationale Supérieure des Arts et Industries Textiles (ENSAIT) in France, Politecnico di Torino in Italy, the University of Boras in Sweden, Gheorghe Asachi Technical University in Romania and the Soochow University in China.

These universities cooperate to allow selected students to carry out a Ph.D. degree in the universities of the consortium. The structure and peculiarity of the Ph.D. program consist of the fact that the candidate carries out his/her studies in three of the previously mentioned academic institution over four years. In particular, the candidate spends the first two mobilities of 18 months each in two of the European partners while the fourth and final year is spent at Soochow University. The involvement of several partner universities allows the SMD-Tex project to tackle different areas of textile research including quality management, garment design, sustainability and environmental impact assessment,

supply chain management, innovative materials and process design. The latter theme tackles the issues of developing new textiles materials and process which own superior performances and added value while complying with the current issues of resource protection and environmental compliance. In this context, several projects have been financed in the frame of SMD-Tex to develop innovative materials for wastewater treatment, smart textile, protective garments or processes to reduce the environmental impact of the textile chain by LCA, upcycling and resource replacement approach.

In the context of the SMD-Tex program, the present thesis aims to propose a novel approach for the production of biofunctional textiles. The project was carried out by a collaboration of the Italian, French and Chinese partners as sketched in Figure I.1.

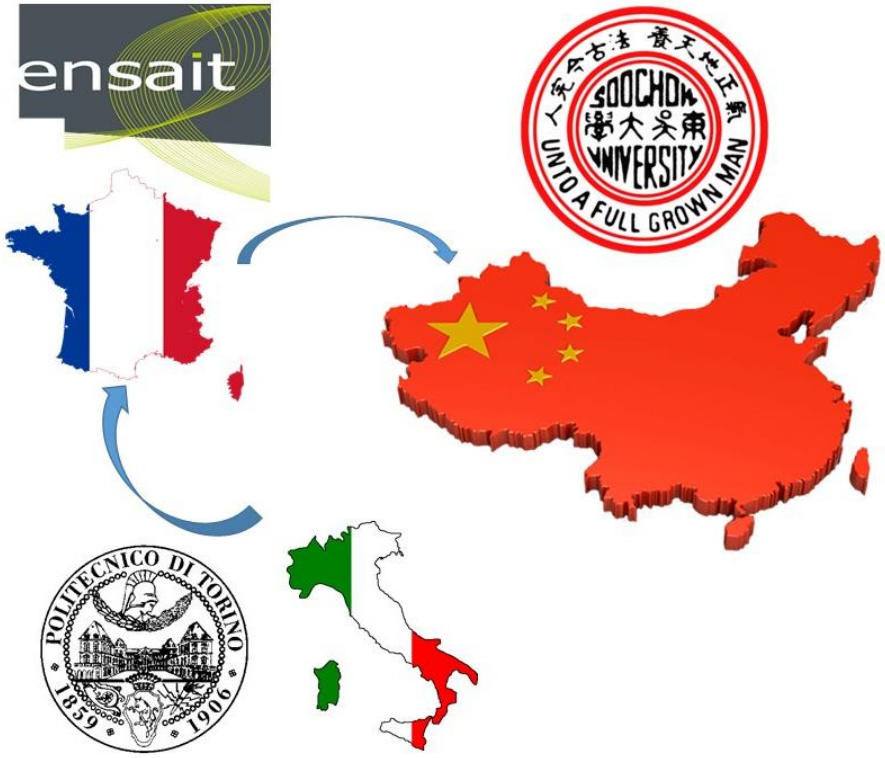

Figure I.1. Scheme of the mobilities and logos of the partner universities.

The first mobility was carried out in Italy at the applied science and technology department of Politecnico di Torino. The second mobility was carried out in France at the Gemtex laboratories of the Ecole National Supérieur des Artes et Industries Textiles. Lastly, the final mobility was carried out in China at the National Silk laboratories of Soochow University.

The approach used to tackle the issue of biofunctional textile production is sketched in Figure I.2. The first step consisted of the development of a suitable nanocarrier production method. The nanocarriers were then applied to the fabrics by finishing treatment to obtain the biofunctional textiles. The obtained fabrics were finally tested for their properties with a major focus on the capability of delivering the active principle.

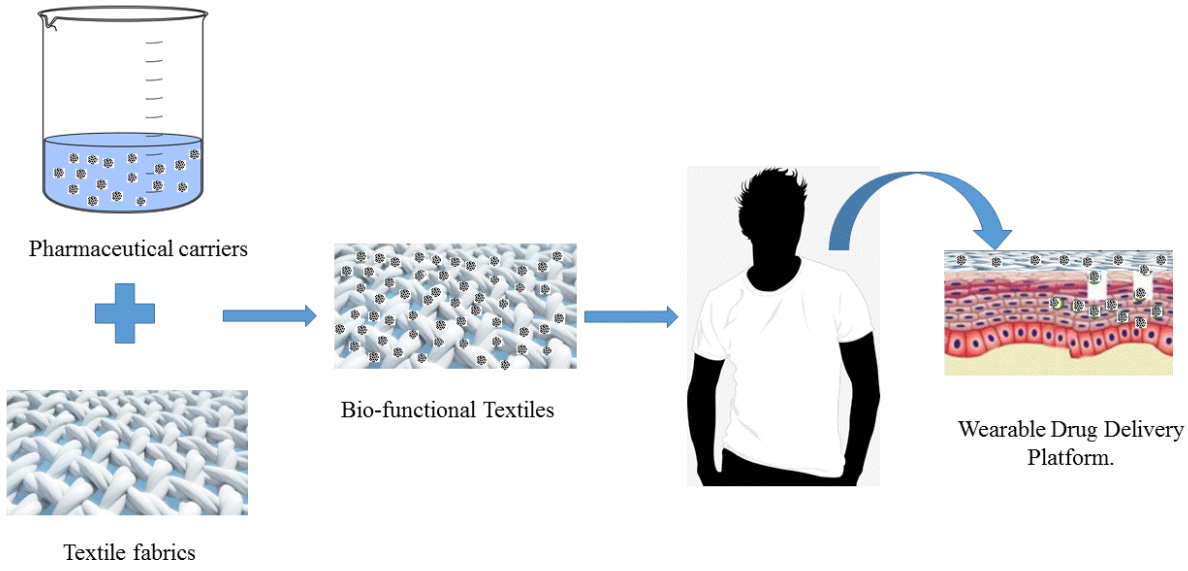

Figure I.2. Production approach for biofunctional textiles.

Specifically, the Flash Nanoprecipitation (FNP) technique was proposed for the production of the drug loaded carriers. In fact, FNP is known for its simplicity and scalability which allows an easy and productive synthesis of the nanocarriers. However, its employment in the textile finishing was still not investigated. In the present work, the FNP method was used to produce polymeric nanoparticles made of polycaprolactone (PCL). The latter was selected as polymeric shell due to its biodegradability and biocompatibility. Moreover, PCL is a hydrophobic polymer that can promote drug delivery in the epidermal layer. Lastly, it is known to be a suitable material for long lasting release applications.

The PCL nanoparticles were applied onto cotton fabrics. This textile was chosen for its breathability and compatibility with the skin tissue. The particles were applied onto the textiles by using a simple impregnation treatment with the scope of making biofunctional textiles eventually rechargeable by the user.

To investigate the suitability of the proposed processes, they were tested with three different model drugs i.e. caffeine, melatonin and curcumin. These drugs own different levels of hydrophobicity which is the main property affecting both the transdermal permeation and the extent of encapsulation in the FNP process. Moreover, these active substances were selected based on their antioxidant and therapeutic properties, with the scope of proposing a system with potential medical applications.

The first part of the present work was dedicated to the description of the state of the art. The literature analysis introduced and discussed the background knowledge and the issues that come into play in the production of biofunctional textiles. Above all, the basic concepts of skin physiology and pathology together with the ones of skin drug delivery were presented. Thereafter the different kinds of pharmaceutical carriers of interest for dermatological application were critically reviewed together with the different encapsulation methods. Thanks to such a literature review, the current weakness of the biofunctional textile technology and the points to be addressed in the experimental work were outlined.

In the second part of the thesis, the materials and methodology were presented. Firstly, the production methods for nanoparticles and textile finishing was described. Thereafter the testing methods and characterization techniques employed to investigate the quality of the produced materials were presented. Particular focus was paid on describing the peculiar properties of the selected raw materials.

Thereafter the results of the experimental activities were presented. Firstly the preliminary results on the PCL particle formation process were reported. By this study, it was possible to choose a proper solvent for the particle synthesis and to define the operating parameters to be employed in the drug loaded nanoparticles synthesis. Thereafter a preliminary study on drug loaded nanoparticle production and biofunctional textile finishing was conducted using melatonin as a model drug. Having performed such a proof of concept study on the intermediate hydrophilic drug allowed to tune the synthesis methods and analytical techniques for the other model substances.

A deep study was conducted on the production of caffeine and curcumin loaded nanoparticles. In the particular case of caffeine, significant attention was paid on developing and studying the effects of the process configurations onto the structure of the particles and on proving the possibility of effectively loading a hydrophilic active principle by the FNP method. In the study of curcumin loaded nanoparticles, the efficacy of the synthesis method for hydrophobic substances was evaluated. Moreover, the peculiar properties of the drug and the encapsulation process were exploited to obtain

an optimized nanoparticle formulation that displayed the best properties for biofunctional applications and textile finishing.

Finally, the optimized formulation of caffeine and curcumin loaded nanoparticles were applied to the textile substrate. Several analyses were run to gain insight into how the formulation characteristics and the drug hydrophilicity influence the textile properties. This was achieved by firstly assessing the effectiveness of the finishing treatment and thereafter by inquiring the features of the material which are beneficial to the user's health.

Part I The state of the Art

Chapter 1: Drug delivery in dermatological applications

1.1 Structure and physiology of the skin

Skin is the organ of the human body that presents the highest surface area and it complies with essential body functions. Above all, it is a physical and chemical barrier that protects the internal organs and tissues from the external harms such as pathogenic microorganisms, radiations and toxic substances. Moreover, skin contributes to thermal regulation, sensorial detection, water retention and self-healing (Wysocki, 1999; Zhang and Michniak-Kohn, 2012). Structurally speaking, skin consists of a series of stratified layers that are represented and described in Figure 1.1. The epidermis and the dermis are the two principal skin layers (Suñer-Carbó et al., 2019).

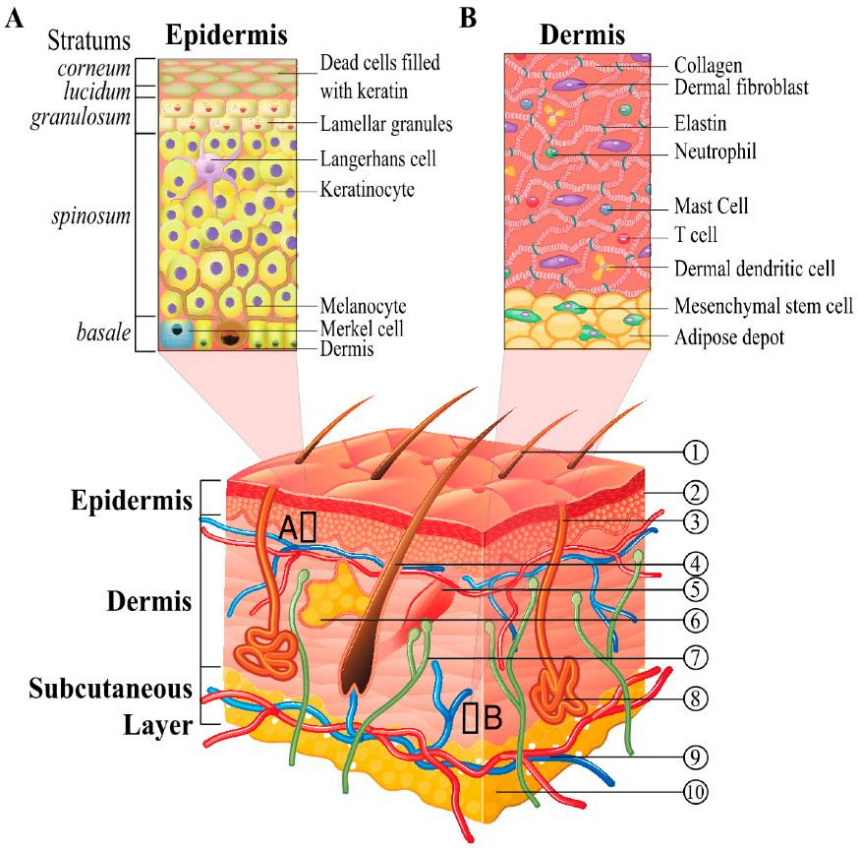

Figure 1.1. Scheme of the skin layers (Gaur et al., 2017). The references in the image point out: 1) hair shaft; 2) stratum corneum; 3) sweat-pore; 4) hair follicle; 5) arrector pili muscle; 6) sebaceous gland; 7) nerve; 8) eccrine sweat gland; 9) cutaneous vascular plexes; 10) adipose depot. Section A and B highlight a detailed structure of the epidermis and derma respectively.

The epidermis is the skin layer in contact with the external environment; it is formed by several sublayers. It is mostly constituted by keratinocytes which are the most diffuse skin cells. Keratinocytes are formed in the lowermost epidermal layer, the Stratum Basale and, throughout the cell life cycle, they raise to the outermost Stratum Corneum (SC) undergoing keratinization and cellular differentiation (Rincón et al., 2018). The keratinocytes present in the SC are normally referred to as dead cells, named corneocytes. Corneocytes are denuclearized flat cells bound together by lipids and cholesterol. The SC owns a "brick and mortar" structure where hair shaft and sweat pore are present (Eckhart et al., 2013; van Smeden et al., 2014). Right below the SC the Stratum Lucidum is found; in this skin layer, partially denuclearized keratinocytes are bound together by the eleidin, a lipoprotein with translucent appearance (Briggaman and Wheeler, 1975). By secreting the interlamellar lipids found in SC the cells of the Stratum Lucidum are responsible for skin barrier properties. The Stratum Granulosum is located under the Stratum Lucidum, in this layer, the keratinocytes are nuclearized and characterized by a granular shape (Freeman and Sonthalia, 2019). In the under-located Stratum Spinosum, the keratinocytes have spine shape and are arranged in rows. Here are present other epidermal cells i.e. the Langherans cells, responsible for immune response, and the Melanocytes where melanin synthesis occurs (Yousef and Sharma, 2019). Melanin is the molecule responsible for UV protection and skin pigmentation (Tolleson, 2005). On the bottom of the epidermis, the Stratum Basale is composed of a single layer of stem keratinocytes, these cells have large nuclei and high reproduction rate, once produced the stem cell raise to the upper layer gradually differentiating (Jackson et al., 2017). In the Stratum Basale, the Merkel cells which comply with the role of touch sensors are found (Abraham and Mathew, 2019).

The Dermis is connected to the epidermis by mean of the Dermal-Epidermal Junction (DEJ), a basement membrane made of collagen and other proteins (Goletz et al., 2017). The dermis is a vascularized tissue characterized by a layered structure that can be divided into the papillary and reticular dermis. The papillary dermis is mainly constituted by connective tissue and contains the Mast cells which mediate and counteract allergic reactions (da Silva et al., 2014). The reticular dermis is composed of proteins that are responsible for the skin mechanical properties. In this layer are found the sweat glands, which contribute to thermal regulation, and the hair follicles, which act as keratinocytes source during the re-epithelialization process (Arda et al., 2014).

The reticular dermis is attached to subcutaneous tissues without sharp distinctions. The hypodermis is mainly constituted of connective and adipose tissue and attaches the properly called skin to the muscular tissues. It is composed of three layers, the top one is rich in fatty substances while the bottom two are vascularized (Yu et al., 2019).

The overall skin architecture consists of a complex structure from the biochemical point of view. The alternation of fatty hydrophobic layers and vascularized hydrophilic exerts an effective shield, making it difficult for most of the chemicals to effectively cross it. Notwithstanding its barrier properties, skin can be the target of pathogens and illnesses (Nastiti et al., 2017). For these reasons, the skin has been considered as a possible administration route both for systemic and local drugs. According to Food and Drug Administration (FDA), the first case is defined as transdermal administration and involves the delivery of the drug through the skin layers to reach systemic circulation, while the latter is defined as topical administration and consists of the application of the active molecule on a particular area of the body surface (Prow et al., 2011; Sgorbini et al., 2017).

1.2 Topical administration and skin diseases

Topical delivery is among the most commonly used administration routes, in general consists of applying the medicament directly to the target tissue. It commonly applies to ocular or dermatological formulations, in the latter case, it is also referred to as dermal delivery (Marto et al., 2019; Tatke et al., 2018). Such a local administration approach is extensively used in dermatological therapies to treat the illnesses of the dermis and epidermis such as wounds, infection, and cancers (Nagula and Wairkar, 2019; Simitzis, 2018). Indeed, skin diseases have a significant impact on the quality of life of the patients both from the physical and the psychological point of view (Wu and Cohen, 2019).

Skin is a living organ and therefore goes through significant changes over the human lifetime. The accumulation of such biochemical and physical changes is commonly referred to as aging and is a phenomenon that occurs differently in every individual (Bessada et al., 2018). It is due to the progressive loss of elastin and collagen as age advances, which causes loss of structure and functions of the skin tissue. Besides causing unpleasant visual modifications, such as wrinkles and spots, aging makes skin more vulnerable to several diseases. This phenomenon is commonly attributed to endogenous and exogenous factors, the first ones are identified to the chemical and genic changes the tissues undergo over time. The exogenous factors are instead related to the environment and exposure to harmful substances and radiations (Tobin, 2017).

Radical oxygen species (ROS) are among the exogenous factors that can cause critical skin damages and are associated with several skin diseases. ROS are indeed very reactive oxidants species that can interact sharply with biomolecules causing damages to deoxyribonucleic acid (DNA), proteins and lipids; therefore, they are connected with the rise of eczema, dermatitis, and cancers. To counteract the oxidant activity of ROS, the body developed an antioxidant system based on enzymes (Lephart, 2016). However, excessive exposure to ROS generators may overcome the capability of such

endogenous antioxidants and lead to oxidative stress; in such conditions, the skin aging is accelerated and all the pathologies related have higher chances to arise (Poljšak and Dahmane, 2012). For this reason, the topical administration of antioxidants is a common strategy to reduce radical-induced damages. Indeed, antioxidants tend to rapidly react with ROS before they could damage biological macromolecules reducing their pathogenicity (Pisoschi and Pop, 2015).

UV solar radiation is the main cause of excessive ROS production and related oxidative stress. UVB rays are connected to the formation of free radicals. Such species are connected to lipid peroxidation and rupture of elastin and collagen chains. Furtherly, the UV induced radical species tend to attack the DNA chains promoting genetic mutation and cancer arises (Bessada et al., 2018). In particular, melanoma is the most aggressive form of skin cancer that arises from malignant melanocytes. In fact, during its progression, it tends to develop resistance to cytotoxic drugs making chemotherapies to progressively lose efficacy (Keller et al., 2017). Furtherly, it is one of the most common forms of cancer with an averagely 87000 diagnosis and 10000 casualties occurring per year in the US (Abdul-Karim and Cowey, 2017).

Bacterial infections are a common issue that can affect the skin. The action of pathogens onto the skin can lead to undesired effects such as inflammation or skin destruction (Bazbouz and Tronci, 2019). Moreover, the presence of infective species inhibits the skin regeneration mechanism and makes it impossible for the body to recover from wounds naturally (Mostafalu et al., 2017). These kinds of infections are normally tackled by antibiotics and anti-inflammatory drugs; however, such therapies present several drawbacks due to their scarce therapeutic windows and progressive loss of efficacy due to bacterial resistance (Bassetti et al., 2019).

Other common skin diseases include psoriasis, an autoimmune disease connected with keratinocytes overexpression, and *Acne Vulgaris*, due to the occlusion of hair follicles. They lead to the formation of red scales and itchy patches of skin. The common treatment of such diseases includes the topical administration antibiotic and anti-inflammatory drugs (Beylot et al., 2014; Lowes et al., 2014; Williams et al., 2012). Cellulite is a skin disorder connected to the accumulation of subcutaneous fat and scarce microcirculation. Although it usually does not implies pathological consequences, cellulite affects a large portion of the population and is regarded as an anti-aesthetic feature. Therefore, it is commonly treated with cosmetic creams and ointments which improve microcirculation and promote lipolysis in subcutaneous tissues (Rawlings, 2006).

All the above-mentioned skin pathologies are serious challenges in clinical research. Indeed, they compromise the patient's life quality and, for this reason, continuous efforts are being done to propose innovative treatments to heal or at least reduce symptoms.

1.3 Transdermal administration

Being the largest organ of the human body skin has been regarded not only as a potential administration route for systemic drugs. Transdermal administration displays several advantages compared to other classic drug delivery routes such as the enteral and parenteral ones (Roberts et al., 2017). Firstly, it is noninvasive since it does not require injections. Secondly, it delivers the active principle in the blood circulation avoiding the first pass metabolism in the liver (Al-Hashimi et al., 2018). Lastly, given that transdermal delivery devices can stick on the patient for several days, the number of required applications is significantly reduced; this improves patient compliance to the therapy (Rigon et al., 2016). Notwithstanding the numerous advantages of the transdermal route, its large employment in clinical practices is still limited. This is due to the great chemical complexity and barrier properties of the skin layers that make it difficult for many active substances to cross it (Chuang et al., 2017; Palmer and DeLouise, 2016).

The phenomena acting in the transdermal release are sketched in Figure 1.2. For a substance to reach the dermis, three penetration pathways are commonly identified (Carreras et al., 2015; Yang et al., 2011).

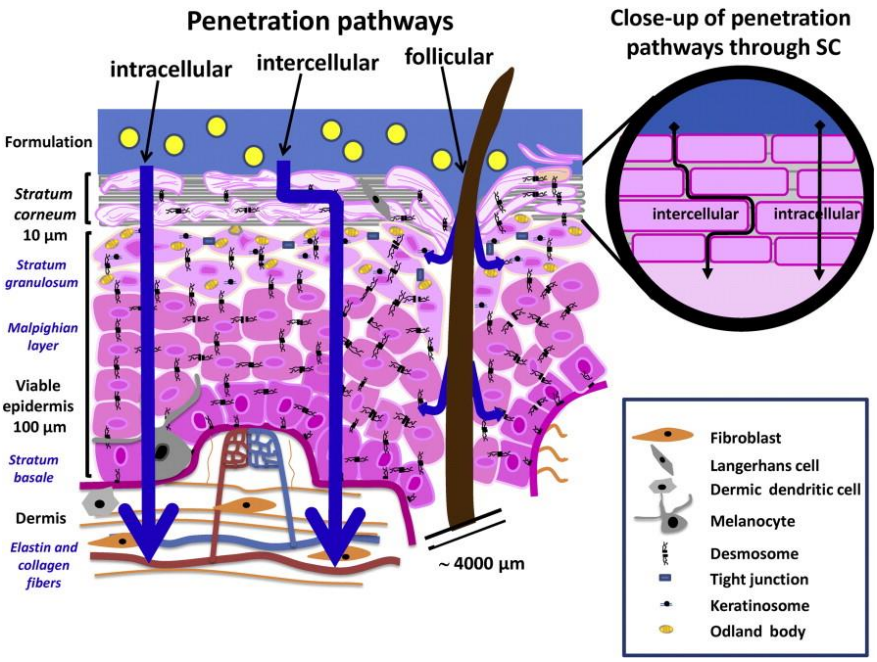

Figure 1.2. Transdermal transport and penetration pathway (Bolzinger et al., 2012))

The intercellular route involves the passage around the corneocytes, and the molecules diffuse in the lipid substances that hold the terminally differentiated keratinocytes together, thus such route is generally preferred by lipophilic substances (Hadgraft and Lane, 2016). Oppositely, the intracellular pathway is preferred by hydrophilic substances that cannot diffuse easily in the lipid extracellular network of the SC. This route involves the penetration of the drug through the corneocytes cells and therefore requires the substance to smoothly cross the cellular membranes (Alonso et al., 2018). A third path, defined as the annexial (or follicular) route, consists of the drug passaging through the skin annexes such as hair follicles or sweat glands (Lademann et al., 2008).

The percutaneous absorption of a drug can be regarded as a mass transfer phenomenon that involves several steps whose kinetics is mainly dominated by diffusion (Simovic et al., 2010, 2012). Firstly, it consists of the entry and penetration of the drug into the SC. Secondly, the drug must partition from the SC into the hydrophilic region of the epidermis reaching the Stratum Basale. The drug must then diffuse through the Stratum Basale to reach and permeate the Dermal-epidermal junction. Once reached the dermis, the drug must be absorbed by the blood vessels to finally enter the systemic circulation (Amjadi et al., 2017; Hao et al., 2016). The complexity of transdermal penetration lies in the fact that it requires alternate diffusion through different layers and permeation across the boundaries that separate them. Each layer and boundary have a different chemical composition and therefore different resistance to mass transfer. Since a limited diffusion in one single skin layer may hinder the overall penetration process, the amount of active substances easily deliverable transdermally is quite reduced (Schwöbel and Klamt, 2019).

Common rules found in the literature state that to cross the SC easily a molecule should have lipophilic character and small size, i.e., lower than 500 Da; the latter condition is widely known as the 500 Daltons rule (Cintra et al., 2016). However, also markedly lipophilic molecules have been recently considered not to have optimal penetration capability, indeed according to some authors they can easily cross the SC but thereafter cannot diffuse in the vascularized layers, and therefore they tend to accumulate in the SC (Şenyiğit et al., 2016).

The degree hydrophilicity of the active substance is the main factor affecting its skin permeation profile. A commonly used approach to classify the hydrophilicity of the active substances exploits the parameter logP; where P indicates the drug partition coefficient between octanol and water (Eugene Kellogg and Abraham, 2000). Negative values of the logP indicate that a substance is hydrophilic, while high positive values logP are associated with hydrophobic substances (Mannhold and Dross, 1996).

A further level of complexity in the transdermal release is represented by the variability of the skin in terms of thickness, chemical composition, and biological activity. Such parameters tend to change in different individuals, the factors that influence the skin physiology include but are not limited to age, sex, phototype and health practices of the patient (Vitellaro-Zuccarello et al., 1994). Moreover, the relative properties of the individual skin layers can also change in a different part of a single body. For these reasons, the transdermal penetration of a drug is an overall complex phenomenon (Darlenski and Fluhr, 2012).

1.4 Technologies for transdermal drug delivery

Despite the complexity of the transdermal administration route, its potential advantages have driven the scientific community to develop innovative technologies to improve skin penetration by active substances (McConville et al., 2018). Transdermal technologies are mainly divided into permeation enhancement methods and drug delivery devices (DDDs) (Yang et al., 2011). The permeation enhancement consists of the application of an external stimulus to make the drug to cross the skin barrier. These stimuli can be either of physical nature, such as electrical current or ultrasounds (US), or chemicals added in the formulation (Kapoor et al., 2017; Nguyen and Banga, 2018). DDDs include instead a wide class of technologies in which the drug is incorporated inside a material that improves its delivery to the target tissue. In the context of transdermal release, the most common DDDs are the microneedles (MNs), the transdermal patches (TPs) and the drug carriers (Czajkowska-Kośnik et al., 2019; Haj-Ahmad et al., 2015). The different transdermal delivery methods are reported in Table 1.1 together with their advantages and limitations.

Iontophoresis is a permeation enhancement technique that employs low electrical currents to promote the active molecules crossing of the epidermis (Takeuchi et al., 2017). Upon application of electric current, the drug transport across the skin is promoted through electrophoretic and electroosmotic phenomena. The first phenomenon exploits the repulsion of the drug from the electrode while the second is based on the charge gradient across the skin membrane (Ita, 2016). The extent to which the drug mass transfer is affected by iontophoresis strongly depends on the drug polarity and surface charge and the skin pH. Iontophoresis mainly enhances the drug permeation occurring by the annexial route (Karpiński, 2018).

The enhancement of skin penetration obtained by the application of ultrasounds is named sonophoresis (Polat et al., 2011). In this technique, the permeation of the drug is due to both the cavitation of gas microbubbles that disrupts the SC, and to the generation of a local temperature gradient that promotes diffusion (Park et al., 2014). Sonophoresis was proved to be efficient in

enhancing the penetration of high MW molecules or small hydrophilic ones (Katikaneni et al., 2010; Seah and Teo, 2018).

Table 1.1 Comparison of different transdermal delivery technologies.

Transdermal enhancement strategy	Drug applicability	Penetration mechanism	Patient usability	Administrations required	Possible side effects
Iontophoresis	Charged and polar drugs	Electro osmosis and electrophoresis	Electrical current to be applied	Several	Surface damages
Sonophoresis	Small substances (below 500 Da)	Transdermal penetration and cavitation	Ultrasound device needed	Several	SC disrupted
Chemical enhancement	Small drugs (below 500 Da)	CE-Drug and CE-Skin interactions	Topical formulation	Several	Skin irritation by CE
Transdermal patches	Small drugs (below 500 Da)	Passive diffusion	Simple patch application	Few	Skin irritation and contact dermatitis
Microneedles	Most drugs	Simple: direct release in the epidermis	Simple patch application	Few	Skin piercing and irritation
Drug carriers	Most drugs	Intracellular, extracellular and annexial route	Topical formulation	Several	Cytotoxicity to be tested for each carrier

The chemical enhancement method involves the addition of particular substances to the formulation to increase the permeation rate and extent. Various compounds such as organic solvents, oils or surfactants can be employed as chemical enhancers (Haque and Talukder, 2018). These chemical

enhancers (CEs) promote the drug permeation by different mechanisms depending on their interaction with both the skin and the drug. Usually, the CEs should both be a good solvent for the drug and have good diffusivity in the SC, in this way they can vehicular the drug. However, in the case of high solubility of the drug in the CE the release may be hindered by the tendency to remain in solution rather than partitioning in the skin (Benson et al., 2005). Also, CEs can act on skin properties, by disrupting or swelling the SC (Barry, 1987).

Among the DDDs, the transdermal patches were the first ones to be proposed. They are made of several layers with specific functions and characteristics (Pastore et al., 2015). TPs generally contain an adhesive layer that keeps contact with the skin, a drug reservoir where the active substance is stored and an outermost layer to protect the patch from the external environment. In more advanced products, the drug can be stored over multiple reservoir layers to control the released dosages. The release mechanism is mostly described by passive diffusion of the drug from the patch to the skin (Al Hanbali et al., 2019).

Microneedles technology consists of the production of patches equipped with several arrays of needles of small size. MNs aim to directly inject the drug inside vascularized skin layers, thus bypassing the issue of drug diffusion in the epidermis. Regarding MNs technology, the drug can be loaded in the patch, in the tip of the needle or just on its surface (Dharadhar et al., 2019). For the production of MNs metallic, ceramic and polymeric materials were used (Hartmann et al., 2015). However, in recent years, polymeric MNs have aroused the greatest interest. Indeed, they have been proven to be cost effective and simple to produce. Furtherly, the use of bioabsorbable polymers allows the needle to degrade inside the skin without causing side effects (Wang et al., 2017). The advantage of delivering the drug in the vascularized layers avoiding retention in SC makes MNs a very effective transdermal technology. On the other hand, some concerns are usually aroused by the invasiveness of such a technique which requires to pierce and hole the skin, risking to cause irritation. For these reasons, MNs are mostly studied for the administration of life-saving drugs such as insulin and chemotherapeutics. These drugs are generally quite expensive, so their effective administration must be maximized. Considering that the common administration route of these drugs is the parenteral one, MNs are a novel and less invasive administration route (Jin et al., 2018; Lan et al., 2018).

Drug carriers are among one of the most studied delivery devices in pharmaceutical technology. They consist of micro/nanometric structures that can incorporate different kinds of drugs and release them to the target tissue in a more controlled and effective way (Czajkowska-Kośnik et al., 2019). These nanocarriers have been studied for several kinds of medical applications that involve different

administration routes. In the context of transdermal release, it has been reviewed that they can enhance the delivery of a wide range of active substances. Indeed, it is possible to tailor the size and surface of the nanocarriers to enhance their capability to undergo the different penetration routes (Bornare and Saudagar, 2017).

In comparing these different transdermal delivery technologies several aspects were considered. Concerning the kind of drugs that can be delivered by each system, it is clear that CE, patches, ionto- and sonophoresis present stricter limitations compared to other technologies since they have to comply with 500 Da rule. In the case of iontophoresis, the drug must be electrically charged to be effectively delivered. In the case of drug carriers and MNs, less strict limitations on the kind of drug are present. In fact, once the active substance is incorporated in the carriers and the MNs, the release kinetic is less affected by the chemical structure of the therapeutic molecule.

The release phenomena occurring are also of different kinds. In MNs the permeation in the epidermis is bypassed making the release simpler. Ionto- and sonophoresis require instead the drug to permeate all the layers of the skin undergoing the already discussed phenomena. A similar permeation mechanism is observed in patches, CE and drug carriers in which classical penetration routes come in play; for the latter technology release mechanism is mainly dependent on the properties of the carrier.

Concerning the invasiveness of the systems, MNs require the outer layers of the skin to be perforated. Furtherly, if the polymer swells inside the epidermis, the needles enlarge, causing the holes to increase in size. Ionto- and sonophoresis require external stimuli that can damage the skin integrity. Moreover, proper devices should be used to apply electricity and ultrasounds. Therefore, ionto- and sonophoresis are probably more difficult to be operated by the patient. Oppositely, formulations based on CE or nanocarriers are easily applied topically.

Considering the number of administration required TPs and MNs devices present the advantage of sticking to the patient for longer times respect to other technologies. However, this advantage is counterbalanced by the fact that long contact with the skin may lead to irritation or damages (Musel and Warshaw, 2006). Particularly in the case of TPs, the scarce breathability of the adhesive layer was reported to cause contact dermatitis (Romita et al., 2018).

1.5 Drug carriers for dermatological application

Drug loaded carriers are among the most studied technologies in the context of pharmaceutical research. Such innovative formulation had been developed to administer active substances more effectively. The encapsulation process is the technique used to incorporate active molecules inside nanostructured materials with monolithic or core-shell structure (Lengyel et al., 2019). This process can indeed improve the performances of the active material under many points of view. Firstly, the nanomaterial can protect the drug from environmental factors that alter its biological activity (Salaün, 2016). Secondly, the encapsulation process allows to structure the core material to regulate its interactions with the environment, as an example, such technique is commonly used to enhance biostability and bioavailability of poorly water soluble drugs in the bloodstream (Parisi et al., 2017). Lastly, encapsulation allows releasing the drug in a prolonged and controlled manner providing an effective therapeutic dosage while minimizing side effects (Ancona et al., 2018). The encapsulation process allows producing different kinds of nanocarriers, which are classified according to their chemical nature, structure, morphology, and assemblies. Such different carriers have been employed for the treatment of a wide range of diseases and administered by different routes. In the context of dermal and transdermal delivery, the most studied carriers are particle based carriers, cyclodextrins, hydrogels and liposomes whose structure is sketched in Figure 1.3 (Chen et al., 2017; Jain and Thareja, 2019).

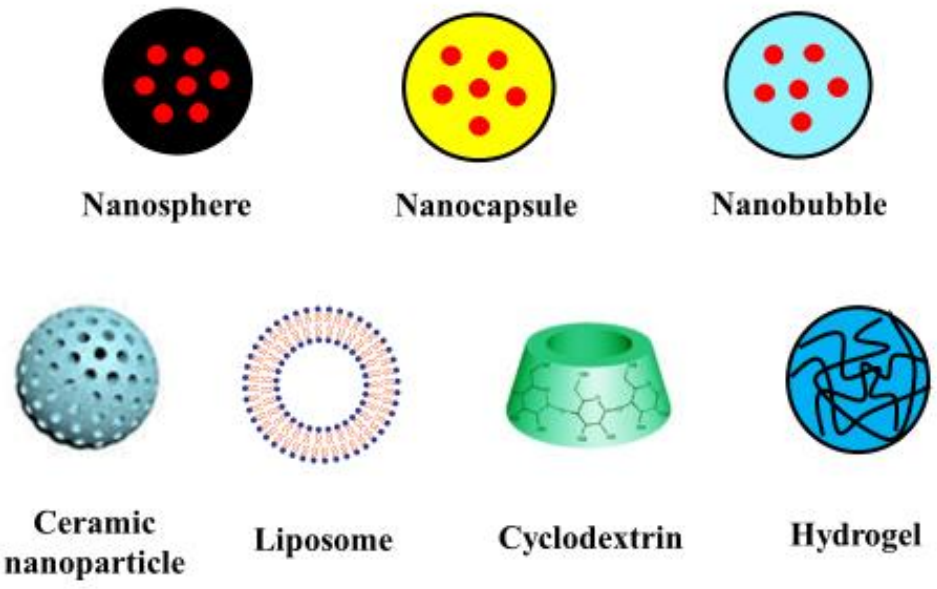

Figure 1.3. Schematic structure of the nanocarrier employed for dermatological applications.

The properties and application of such carriers in the context of dermatological application are summarized in Table 1.2.

Table 1.2. Characteristics and applications of nanocarriers in dermatological therapies.

Drug	Hydrophilicity	Carrier	Therapeutic target	Release test	Ref.
Vitamin D	Hydrophobic	Nanospheres	Transdermal supplement administration	Healthy and damaged porcine skin	(Lalloz et al., 2018)
Menthol	Hydrophilic	Nanospheres	Antioxidant and anti cellulite	Artificial Membrane	(Ferri et al., 2017)
Adapalene and adapsone	Hydrophobic and hydrophilic	Nanocapsules	Dermatitis treatment	Porcine skin	(Pereira et al., 2016)
HNE inhibitor	Hydrophobic	Nanocapsules	Psoriasis	In vitro and in vivo (rats)	(Marto et al., 2018)
Clobetasol propionate	Hydrophobic	Nanospheres and nanocapsules	Hair follicles	Ex vivo pig and human skin	(Mathes et al., 2016)
Vancomycin	Hydrophilic	Nanobubbles	Skin infection	Porcine skin	(Argenziano et al., 2017)
Rifampicin	Hydrophobic	Nanobubbles	Acne treatment	In vitro studies	(Hsiao et al., 2018)
Imiquimod	Hydrophobic	Nanosponges	Aberrant wounds	Porcine skin	(Argenziano et al., 2019)
Resveratrol	Hydrophobic	Nanosponges	Antioxidant	Porcine skin	(Ansari et al., 2011)
Econazole nitrate	Hydrophobic	Nanosponges	Fungal infection	In vitro studies	(Sharma and Pathak, 2011)
Sodium Fluorescein	Hydrophilic	Liposomes	Model system	Porcine skin	(Mahrhauser et al., 2015)
Quercitin	Slightly hydrophilic	Liposomes	Antioxidant	Human excised skin	(Hong et al., 2018)
Nobiletin	Hydrophobic	Hydrogel	Acne treatment	Porcine skin	(Jeong et al., 2019)

Heparin and Paclitaxel	Hydrophilic and hydrophobic	Hydrogel	Transdermal cancer therapy	In vitro and in vivo	(Taktak et al., 2019)
5-fluroracil	Hydrophilic	Silica nanoparticles	Cancer therapy	Rat skin	(Anirudhan and Nair, 2018)
Insulin	Hydrophobic	Silica nanoparticles and ZnO quantum dots	Transdermal diabetes therapy	In vivo in rats	(Xu et al., 2018)

1.5.1 Particle based carriers

Particulate systems are among the most studied carriers, they are classified according to their average size (microparticles, nanoparticles), shell material (organic, inorganic, hybrid) and their morphology and structure (spheres, capsules and bubbles/droplets) (Cavalli et al., 2016). In dermatology, the nanosized particles present a wider application range, indeed their small size enhances their capability of penetrating the skin barrier both by Intra/extracellular route and by annexial one. On the other hand, microparticles (MPs) have a size that hinders their penetration and is mostly applied in topical skin therapy (Bansal and Jamil, 2018; Nastiti et al., 2017). Concerning shell nature, mostly polymeric materials are used. This trend is due to the large availability of biocompatible and biodegradable polymers that allows sustained release of the drug by diffusion/erosion of the polymer matrix (Lam et al., 2012). Furthermore, ceramic materials, such as zinc oxide, can be also used for drug delivery, combining the therapeutic action of the drug with the functional properties of the shell such as antimicrobial or UV light protection (AbdElhady, 2012; Garino et al., 2019). According to the structure, nanoparticles are commonly classified into nanospheres (NSs), characterized by a solid structure in which the drug is dispersed in the polymer matrix, nanocapsules (NCs), which have a liquid core and a defined shell structure, and nanobubbles/nanodroplets, spherical core/shell structures filled by a gas or vaporizable compounds (Kumari et al., 2010).

1.5.1.1 Nanospheres and Nanocapsules

Nanospheres are polymeric nanoparticles in which the drug is dispersed in the polymer matrix without a distinct core-shell structure. Several authors proposed the application of nanospheres to enhance drug penetration, among them Lalloz et al. (2018) deeply studied the effect of the particle surface

charge on skin penetration. In their work, vitamin D was incorporated in block copolymers by employing flash nanoprecipitation. Permeation studies conducted both on healthy and damaged pig skin, showed a limited effect of the nanoparticle surface charge on the healthy skin while particle polarity affected the release kinetics in the case of damaged skin tissue. By employing a similar particle production methodology, Ferri et al (2017). designed PCL nanoparticles for the delivery of menthol for thermal body management and topical refreshment purposes. The results proved the production of high payload nanoparticles with the possibility of tuning the particle size by proper solvent choice and adjustment of process parameters.

Nanocapsules usually present a well-defined core and shell structure. Such devices can either penetrate SC as whole or disrupt and allow the oily core to diffuse in the epidermis. In the work of Pereira et al (2016) adapalene loaded PCL nanocapsules were produced and topically applied: the high hydrophobicity of both carrier and drug facilitated diffusion in the SC but no further penetration was observed, making the system suitable for topical administration. Marto et al. (2019) incorporated an anti-inflammatory drug in starch-shelled nanoparticles. The potential effectiveness of such topical formulation was evaluated both in vitro and in vivo on rats showing an improved efficacy compared to commercial cream formulations. In the study of Mathes et al. (2016), the relative performances of both nanospheres and capsules were compared to target hair follicles with glucocorticoids. The particles were produced, marked with fluorescent dyes and tested both on pig and human skin. This study evidenced how different particle structure and formulations played different roles on release kinetics and different penetration/accumulation in different skin layers.

1.5.1.2 Nanobubbles and nanodroplets

Polymer shelled nanobubbles (NBs) and nanodroplets (NDs) represent another nanotechnology exploited for cutaneous administration of active molecules. They are versatile multifunctional gaseous core nanocarriers that can simultaneously deliver gases, drugs, and genes (Banche et al., 2015; Cavalli et al., 2016). They have been proposed for the local delivery of antimicrobial drugs for the treatment of cutaneous infectious diseases. The combination of vancomycin-loaded NBs with ultrasound was studied to enhance drug penetration through the skin by sonophoresis and trigger drug release at the site of infection. In vitro permeation studies with porcine skin showed that the amount of vancomycin accumulated in the skin after US application combined with NBs was greater than the minimal inhibitory concentration value, whereas the passive transport through the skin of the free drug was negligible (Argenziano et al., 2017). The feasibility of the use of the NB system combined

with the US was also exploited to design a therapeutic tool to topically treat hypoxia-associated dermal pathologies and promote the wound healing process (Basilico et al., 2015; Sayadi et al., 2018). They showed effective oxygen storing capability and the ability to release oxygen to cutaneous tissues both in vitro and in vivo (Gulino et al., 2015; Khadjavi et al., 2015). Skin oxygenation of mice topically treated with oxygen-loaded NDs was monitored by visualizing the subcutaneous levels of oxy-hemoglobin and deoxy-hemoglobin through photoacoustic imaging and an increase in the tissue oxygenation with a prolonged oxygen release over time was observed (Prato et al., 2015).

1.5.1.3 Ceramic nanoparticles

Ceramic materials are also exploited for encapsulation and delivery of active principles. Indeed, these materials combine the therapeutic effect of the drug with the intrinsic biological activity of the glass (Baino et al., 2018). Ceramic materials such as silica, zinca and titania particles are commonly used in the dermatological application since their cations exert antimicrobial activity, and their morphology and surface properties may be tuned to enhance their bio-affinity (Leone et al., 2019, 2018; Limongi et al., 2019). Anirudhan and Nair (2018) succeeded in the production of drug loaded mesoporous silica particles with a size range of 200-300 nm. The surface of these particles was grafted with oligomeric chains that acted as thermally and ultrasound-activated gates for drug controlled release. Biocompatibility was assessed by keratinocytes cell culture assay while skin penetration was observed on excised rat skin. Xu et al. (2018) proposed a similar responsive system fully based on inorganic materials. The mesoporous silica nanoparticles were loaded with insulin and capped with ZnO quantum dots. Enzymes were integrated into the system to promote a local decrease of pH upon the increase of glucose concentration. The pH decrease triggered the ZnO dissolution allowing for insulin release. The system was proved to be effective in modulating the glucose level of rats.

1.5.2 Hydrogels

Hydrogels are constituted by polymeric chains dispersed in water whose content can constitute up 99% of the system weight. They have a significant efficiency in the encapsulation and the delivery of hydrophilic substances; moreover, their high content of water also makes them a suitable material for wound and burn recovery (Chatterjee et al., 2018). Jeong and co-workers (2019) proposed a nobiletin loaded hydrogel produced by crosslinking carboxymethyl chitosan with hydroxyethyl acrylate via a free radical polymerization mechanism. The hydrogel was proved to be not toxic to keratinocytes cells culture. The skin penetration test on micro pig dorsal skin showed that most of the incorporated drug was released. Taktak et al. (2019) used a tri-block co-polymer to produce hydrogels loaded with

paclitaxel and heparin for cancer therapy. The formulation showed that can be effective in cancer treatment in vitro and in vivo.

1.5.3 Cyclodextrin based carriers

Cyclodextrins (CDs) are oligosaccharides chemically constituted by glucose rings arranged in a toroidal structure (Carneiro et al., 2019). Common CDs are formed by 6-8 glucose units; while recent studies report the synthesis of cyclodextrins composed of 3 or 4 glucose units (Ikuta et al., 2019). CDs have been widely exploited in pharmaceutical sciences to include active substances in their cavity, thus improving drug dispersibility and bioactivity (Han et al., 2018; Jug and Mura, 2018). To improve their drug loading content several CDs based supramolecular assemblies have been proposed. Nanosponges (NSP) are cross-linked cyclodextrins nanostructured within a three-dimensional network (Trotta et al., 2012). Thanks to their porous nanostructure, they are capable of encapsulating hydrophilic as well as hydrophobic molecules, providing sustained and controlled release, improving solubility, stability, permeation and bioavailability (Chilajwar et al., 2014). Nanosponges have been proposed as promising multifunctional co-ingredient in topical monophasic and biphasic formulations. Skin permeation studies showed that NSP in gels and cream-gels containing diclofenac significantly modulate drug transport through the skin, increasing its amount in stratum corneum and viable epidermis (Conte et al., 2014). The same type of NSP was also exploited for the delivery of imiquimod (IMQ) to treat aberrant wounds. Loaded NSP acted as a drug reservoir, able to slowly deliver IMQ through the skin, favoring dermal accumulation (Argenziano et al., 2019; Bastiancich et al., 2014). Ansari et al. (2011) incorporated resveratrol in NSP evidencing how the incorporation enhances the drug permeation rate in porcine skin and rabbit mucosa. Nanosponge-based hydrogels have been also proposed for the treatment of skin infections. They were designed as alternative carriers for targeting econazole nitrate (EN) to the skin to contrast fungal infection with minimal side-effects (Sharma and Pathak, 2011).

1.5.4 Liposomes

Liposomes are vesicle based carriers, they are typically constituted by a phospholipidic bilayer with entrapping a core, which is usually an aqueous solution. Having an amphiphilic structure, liposomes can entrap either hydrophilic or hydrophobic molecules in the aqueous core and the lipid membrane, respectively. Marhauser et al. (2015) have shown that liposomes as efficient carriers enhancing transdermal drug release. Their approach consisted of preparing fluorescent labeled liposomes and testing their penetration through porcine skin. Deformable liposomes or transferosomes have been designed to enhance the penetration behavior of traditional liposomes. The high elasticity of these

liposomes allows them to squeeze and penetrate the skin by different pathways (Hussain et al., 2016). Hong *et al*. correlated the effectiveness of the skin transport of liposomal formulations to their mechanical properties. Several formulations with various surfactants were prepared and then their elasticity was measured and the transdermal release was studied on a porcine skin model. More recently, other vesicular nanosystems such as niosomes, ethosomes, transethosomes have been studied to enhance the transdermal drug delivery (Zorec et al., 2018). These novel liposomal carriers contain a high amount of ethanol together with surfactants and penetration enhancers, then they furtherly improve the SC penetration (Jondhalekar et al., 2017; Singh et al., 2015).

It can be observed that pharmaceutical nanocarriers have been employed for the release of both hydrophilic and hydrophobic substances. The therapeutic target for which the systems were designed are various and include both topical and transdermal formulations. Most of the reviewed work tested the produced formulations onto porcine skin. Such choice can be interpreted considering the easiness in obtaining pig skin and the proximity of the results obtained on this tissue with the human. In some cases, the formulations were tested in vivo.

1.6 Textile materials for healthcare

In the last decades, textile research and industry underwent significant innovative changes. Indeed, textile materials were no more produced only for apparel purposes but also to satisfy various needs. Therefore, the novel concept of technical textile was introduced; such innovative textile product does not only comply to body coverage but mostly to exert specific functionalities (Mather and Wilson, 2017; McCarthy, 2016). The application of these technical textiles is broad and includes fibrous materials employed in several fields such as electronics (Fernández-Caramés and Fraga-Lamas, 2018; Roudjane et al., 2018), automotive and aerospace (Islam et al., 2016; Lavagna et al., 2018a), construction and buildings (Cui et al., 2018; Lavagna et al., 2018b), flame retardants (Malucelli, 2016), bullet protections (Abtew et al., 2018) and healthcare (Sami Rtimi et al., 2017; Wenyi Wang et al., 2017). The latter category is wide broad and includes all technical textiles whose purpose is to deliver benefits to human health. Healthcare textiles have different properties and final applications.

Antimicrobial textiles are among the first examples of medical textiles that have been designed and proposed. Their main property consists in inhibiting the growth of microorganisms onto their surface. Indeed, regular textiles tend to be a good substrate for bacterial growth (Morais et al., 2016). This can lead to several undesired effects such as stains, material ruining and unpleasant odors. Moreover, textiles wore in particular environments such as hospitals or biological laboratories, as well as the

ones used for bandages, must comply with antibacterial properties to safeguard the user (Yuan Gao and Cranston, 2008). Antimicrobial textiles are produced by combining the fibrous material with an intrinsic antimicrobial agent. These can be either antibiotic drugs, inorganic materials such as zinc titanium and silver oxides, or polymers like chitosan (Bashari et al., 2018; Parisi et al., 2017). The antimicrobial activity of these materials is due to the fact that they own a positive surface charge that disrupts the microbial cell wall causing the bacterium death (Hoseinzadeh et al., 2017).

Cosmeto textiles are textile materials whose aim is to provide beneficial effects to the user in terms of skin care. They entrap and release substances with different effects such as perfumes, moisturizing agents, anti-cellulite agents, antioxidants, essential oils and ointments. Generally, they do not have a specific therapeutic target and their posology does not aim to have a systemic effect. They can be produced by embedding the substance in the fiber or by fabric finishing. In the latter case, encapsulation techniques are generally used to better apply the substance to the fabric and to control its release (Mathis and Mehling, 2011; Salaün, 2016).

Insect repellant textiles are designed to protect the user from insects, they have aroused significant interest in the context of preventing the spread of diseases like malaria that are vehiculated by mosquitoes. Their functioning is similar to cosmeto textiles: an active volatile substance is incorporated by different techniques into the textile material and thereafter released to the environment to repel the insects (Souza et al., 2014; Xin and Fei, 2007). Similarly, a category of technical textiles is employed for protection against radiations. The latter is generally associated with several health risks since they can cause DNA damaging and carcinogenesis; therefore, specific textiles are designed to shield the body from those radiations. Such effect can be obtained by combining textiles with specific materials either by fiber incorporation or by surface finishes (Agnhage et al., 2017; Javadi Toghchi et al., 2019).

Lastly, drug releasing textiles are a category of textile materials which are devoted to the release of active substances. They are distinguished from cosmeto textiles since they are designed for specific therapeutic applications. They are employed both for the release of topical drugs to treat skin diseases and for the transdermal administration of systemic active principles. The production of such textiles is carried either by bulk or surface treatments. The first approach consists of integrating the active principle inside the fiber core during the spinning process. The second approach consists of the finishing of a regular textile using a pharmaceutical nanocarrier. The products obtained by such an approach, hereby defined as biofunctional textiles, are the principal focus of the present work.

1.6.1 Drug releasing textiles by bulk treatment.

Drug releasing textiles can be produced by bulk treatment by integrating the active molecules inside the fiber core. These materials are produced by a special spinning process. In this context two main technologies have been reported. The first one employs the conventional spinning process to produce micron size fibers for healthcare applications (Zhuang et al., 2019), this method is of particular interest for the production such as bioactive suture yarns (Silva et al., 2020). The second bulk method, which has aroused significant interest over the last decades, employs the electrospinning technology to produce nanofibrous products.

Nanofibers (NFs) are class of nanomaterials characterized by a fibrous morphology whose diameter is below 1µm. They are usually arranged in a reticular mat structure which displays a high surface area; this property makes NFs very interesting for biomedical applications (Vineis and Varesano, 2018). Nanofibers are mostly produced by the electrospinning process (ES). It consists of the pumping of a viscous and electrically conductive polymer solution through a spinneret under the application of a strong electrical field. Then a fine jet is formed and collected on a metal plate. The solid fibers deposit on the collector with a random orientation giving the final non-woven structure (Doshi and Reneker, 1995; Greiner and Wendorff, 2007). This structure owns morphological properties similar to one of the extracellular matrices (Figueira et al., 2016). The electrospinning process allows us to spin a different kind of polymer and to easily embed active substances in the polymer solution (Miguel et al., 2018). For these reasons, the drug loaded nanofibers were found to display significant advantage respect to micro-sized ones; therefore, NFs have been widely studied as medical textiles for dermatological applications as reported in Table 1.3 By observing the Table, a wide range of polymers can be successfully electrospun. These include hyaluronic acid (HA), polylactic acid (PLA), poly-vinyl-pyrrolidone (PVP), poly-vinyl-alcohol (PVA), poly-acrylic-acid (PAA), poly-acryl-nitrile (PAN), poly(lactic-*co*-glycolic acid) (PLGA) and others. The kinds of active substances includable in the nanofibers are various. Indeed, such a mechanical incorporation method allows processing different drugs regardless of their chemical properties. Moreover, the mild temperature condition at which electrospinning is carried out to avoid the risk of damaging the active molecule. The therapeutic application of electrospun nanofiber includes wound recovery, transdermal and topical delivery. Moreover, such materials have been employed also for cosmetic application and treatment of specific diseases such as atopic dermatitis (AD) and keloids. It is interesting to notice that the electrospinning method has been adapted on the basis of the specific application of the material. As an example, for wound recovery application different materials are combined in order to obtain dual layer patches. Such dual patches are constituted by an inner hydrophilic layer absorbs

wound exudate and promotes cell regrowth and an outer hydrophobic layer which protects the damaged tissue from the external environment. Also in the case of cosmetic application, the emulsion ES is used to incorporate the essential oil. In some cases, surface modifications were performed on the fibrous mat in order to enhance the therapeutic properties.

Table 1.3. Properties and dermatological application of NFs.

Polymer	Active substance	Production technique	Application	Source
PCL-HA/Chitosan-Zein	Salicylic acid	ES, dual layer patch	Wound recovery	(Figueira et al., 2016)
PCL/Chitosan	Aloe Vera	ES, dual layer patch	Wound recovery	(Miguel et al., 2017)
Collagen-PLA-co-PCL	Stem cell	ES + surface cell culture	Wound recovery	(Jin et al., 2011)
PVA	Limonene oil	Emulsion ES	Fragrance release	(Camerlo et al., 2013)
Silk Fibroin	Vitamin E	Regular ES	Antioxidant	(Sheng et al., 2013)
Collagen	Vitamins A, C	Regular ES	Cosmetic	(Fathi-Azarbayjani et al., 2010)
Chitin	none	Regular ES	AD treatment.	(Izumi et al., 2016)
PLGA	Dexamethasone and green tea polyphenols	Regular ES	Keloid treatment	(Li et al., 2014)

PAN	Holmium isotope	Regular ES	Skin cancer	(Koneru et al., 2016; Munaweera et al., 2014)
PVA-PAA	Ketoprofen	ES and surface modification	Transdermal release	(Yun et al., 2011)
PCL	Vitamin B_{12}	Regular ES	Transdermal release	(Madhaiyan et al., 2013)
PVP-cellulose acetate	Ibuprofen	Regular ES	Transdermal release	(Shi et al., 2013)

1.6.2 Biofunctional Textiles by surface treatments

Biofunctional textiles have been defined as those medical textiles obtained by surface functionalization of fabrics with drug carriers. A wide range of carriers and active substances can be employed in biofunctional textile preparation. Therefore, the properties and application of such materials are various. The main driving force to integrate drug carriers in textiles is the fact that regardless of the improved efficacy of such nanoformulations they need to be topically applied as classical ointments and creams. Therefore, the therapy requires multiple applications and its success is intrinsically related to patient compliance. Biofunctional textiles make the therapy wearable and therefore require a single application overcoming the issue of scarce patient compliance (Amjadi et al., 2018; Lis Arias et al., 2018).

1.6.2.1 Production processes of biofunctional textiles.

The production of biofunctional textiles requires the application of the carrier to the fabrics which is done by a finishing treatment. The latter is an important unit operation of the textile supply chain whose scope is to impart the desired final properties to the material both from the aesthetic and technical point of view. It is generally performed at the end of the textile manufacturing process. Usually, the approach used to design biofunctional textiles is to employ some already known finishing technique using the drug carrier as a finishing agent. The rationality behind this approach is the easy scalability of the production by employing an industrially feasible process from the laboratory scale.

The most common finishing techniques include bath exhaustion, padding, layer by layer finishing and the spray method which are sketched in Figure 1.4.

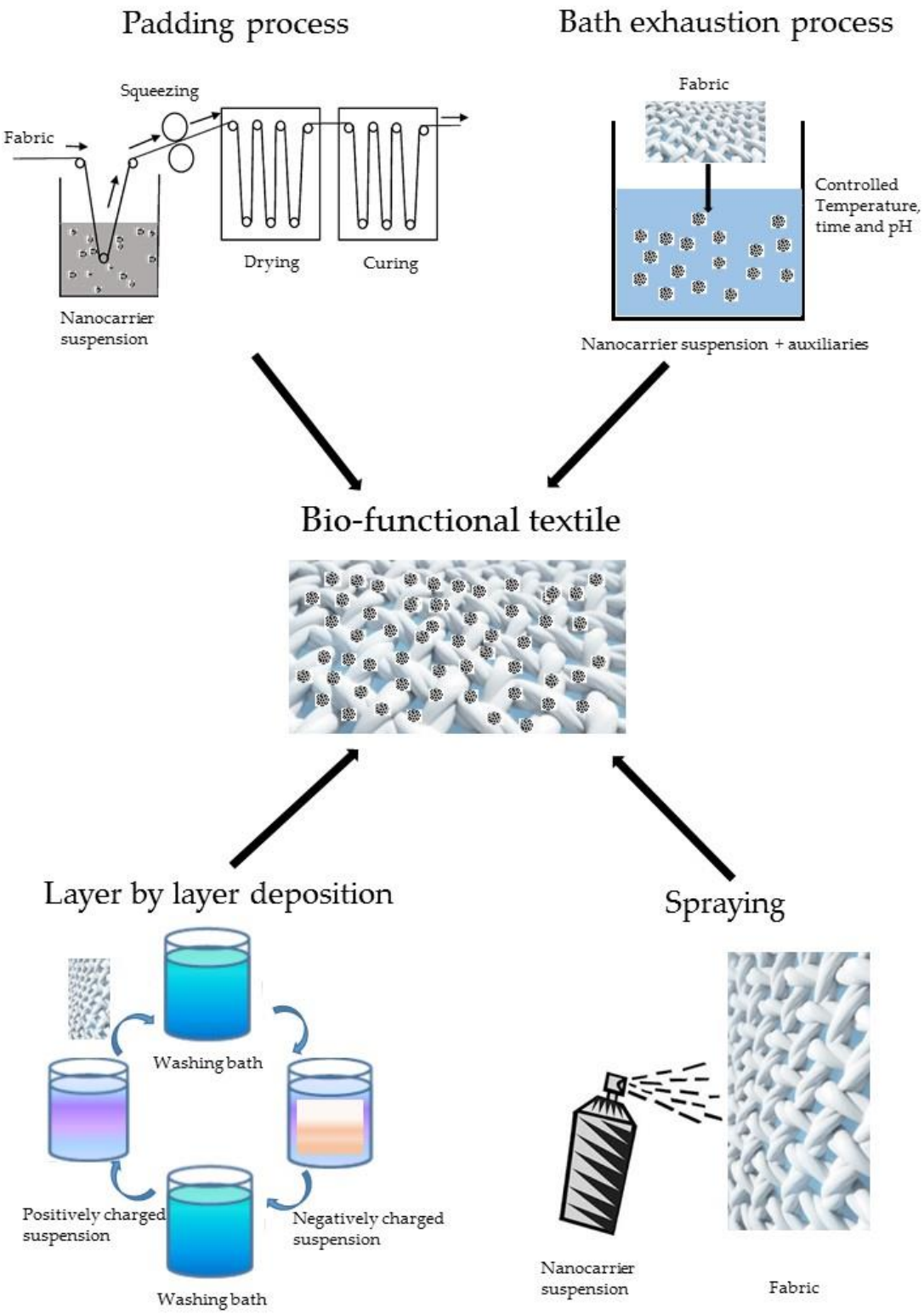

Figure 1.4. Graphical representation of finishing processes for biofunctional textile production.

These processes are often followed by drying and curing to effectively fix the carrier onto the textile surface (Yip and Luk, 2016). In most cases, the carrier is in the form of a liquid suspension so wet finishing processes are the most used ones (Hassan and Sunderland, 2015).

The bath exhaustion process is one of the first proposed finishing technologies. It mainly consists of immersing the fabric in the finishing liquor whose temperature and pH are controlled to achieve the highest affinity between the fibers and the finishes. Bath exhaustion can provide an excellent treatment uniformity; however, due to the high liquor ratios required it also implies a significant carrier and water consumption (Ali et al., 2011; Alonso et al., 2010).

On the contrary, padding is a continuous process that requires lower liquor ratios. This technology consists of quickly immersing the fabric in the finishing bath and then squeezing it between two rollers; by controlling the pressure applied by the rollers is possible to adjust the wet pick up. The finishing bath often contains a binding agent to improve the adhesion of the finish. In fact, for effective and uniform padding finish the affinity between fabric and carrier must be high (Nada et al., 2018; Souza et al., 2014).

Spray based finishing consists of the nebulization of the finishing solution and direct application to the textiles. The spray method can be easily implemented in a process line where it is usually followed by a fixation treatment that aims to enhance the finishing fastness. It is generally a water saving approach (De Falco et al., 2019).

Layer-by-layer (LbL) deposition is a surface engineering technique that has been widely exploited in recent years in for thin film assembling. The process consists in dipping alternatively the textile in oppositely charged electrolyte solutions, targeting a precise number of monolayers on the fiber surface. Indeed, such technique is quite versatile, given the large number of material combinations that could be deposited and is currently feasible at level of pilot scale plants (Junthip et al., 2016).

All of the described finishing processes are suitable for the application of drug carriers to the textile surface. The interactions between the drug carrier and fibers play a critical role in determining the properties of the biofunctional textiles in terms of fastness and release profiles. The use of binders and crosslinkers is a common strategy to promote the formation of physical and chemical interaction between the fabrics and the carrier. The use of a curing treatment after finishing one is also a commonly used strategy to increase the possible chemical reactions between the particles and the

textiles. Common curing treatments are thermo-curing, which exploits thermal activation, or photo-curing which employs UV irradiation (Hu et al., 2011; Junthip et al., 2016). In the context of bio-functional textiles, particular care must be taken to avoid drug degradation or carrier deterioration under the curing process conditions (Martí et al., 2012; Sharkawy et al., 2017).

1.6.2.2 Testing methodologies

Upon production, biofunctional textiles undergo a series of tests to asses their performance. From the literature, it is possible to observe some commonly employed experimental procedures which allow evaluating the performance of biofunctional textiles at a laboratory scale. A crucial point consists in assessing whether the finishing process had been effective in applying the nanocarriers. Usually, techniques like attenuated total reflectance Fourier transform infrared spectroscopy (ATR-FTIR), scanning electron microscopy (SEM) or data color analysis are employed. ATR-FTIR allows not only to assess the presence of the carrier onto the fabric but also to discriminate the kind of fabric-carrier chemical interactions. SEM permits to locally evaluate the material morphology allowing to assess also the carrier integrity. The data color oppositely allows globally to assess the carrier presence all over the fabric surface; however, it can only be applied to colored finishes. The durability of the treatment is generally assessed by making the material undergo several washing cycles. After each cycle, the already mentioned tests are repeated and this allows us to understand to which extent the carrier can stick to the fabric surface (Lam et al., 2013; Peila et al., 2017; Wijesirigunawardana and K. Perera, 2018). Upon having assessed the effectiveness of the finishing treatment, the performance of the biofunctional textiles is tested according to the specific application. These tests include biological and pharmaceutical assays. The drug transdermal penetration and release kinetic is generally evaluated using the Franz Cell release test which is recommended by the pharmacopeia for dermatological formulations and medical devices (Chien and Valia, 1984; European Pharmacopeia, 2001). The main body of the Franz Cell is constituted by a vessel divided into two compartments. The top one, where the formulation/device to be tested is placed, is named the donor compartment. The bottom one is the receptor compartment and is filled with a fluid that mimics the blood, usually kept under stirring. A capillary tube is connected to this chamber to collect solution samples. The cell is jacketed and a heating fluid is circulated to keep the temperature at physiological level. The donor and receptor chambers are separated by a membrane that mimics the skin. For in vitro testing the membrane is usually constituted by artificial materials such as cellulose acetate or mixed cellulose esters. In the case of the ex vivo permeation test, instead, the membrane consists of skin excised either from animals or human donors (Chien and Valia, 1984; Salamanca et al., 2018). The artificial

membranes allow having better repeatability of the experiments respect to excised skin ones which display different structures due to the physiological variability. However, the skin membrane can provide results much closer to clinical practice respect to artificial membranes that do not mimic the multilayered structure of the skin. Recently, the group of Martì introduced the use of novel artificial membranes enriched with SC mimicking lanolin which could combine the desirable low variability of artificial membranes while maintaining the diversified layer composition typical of real skin (Carrer et al., 2018). A complete review of the physical and chemical properties of excised skin was done by Todo, who also analyzed the possible effect on a transdermal penetration test (Todo, 2017).

Cell cultures are also a widely used tool to assess bio-functional textile in-vitro performance. Commonly, this practice is employed either for assessing the antimicrobial properties or to test the cytotoxicity of the material toward the human skin tissue. The microbial growth inhibition is conducted on model bacteria, such as the gram-positive *Staphylococcus aureus* and *Staphylococcus epidermis*, the gram-negative *Escherichia coli*, or on model fungi such as *Candida albicans.* The antimicrobial tests are realized according to several standard protocols, such as the EN ISO 20743, and AATCC 100-2004 (Haase et al., 2017). Concerning cytotoxicity tests, they are usually conducted on skin keratinocytes or corneocytes. The cell viability is inquired by standard protocols such as methyl-thiazolyl diphenyl-tetrazolium bromide (MTT) or Lactate dehydrogenase (LDH) assays. The cell viability test is generally performed on the HaCat skin keratinocytes cell line (Hui et al., 2013b, 2013a). Non-invasive in-vivo methodologies have also been proposed for biofunctional textile testing. They consist in applying the textile on the skin of human volunteers in the form of a patch test and subsequently obtain data on the skin condition by different methods such as tape stripping or transepidermal water loss measurement (TEWL) (Alonso et al., 2013; Mossotti et al., 2015). Such tests are of tremendous importance to develop the technology toward the market stage.

1.6.2.3 Regulation for biofunctional textile commercialization

To put biofunctional textiles on the market, all the requirements demanded by the regulatory agencies, such as European medicines agencies (EMA) and the FDA must be fulfilled. In the current regulatory status, the classification of a biofunctional textile may fall under different categories. A fabric containing a drug loaded carrier is classified either as a cosmetic product, a medical device or as a medicinal product based on the active substance and of its penetration profile. The drug should have only an ancillary function otherwise the regulation of medicinal products must be followed (Musazzi et al., 2017). Special attention must be also paid to the presence of nanomaterials. This issue is

particularly complicated in the European regulatory framework due to the lack of harmonization of the different norms.

Generally, the regulatory agencies require the producers to assess the safety, quality and efficacy profile of the nanotechnology based healthcare product (Rauscher et al., 2017). A clearer regulation of products containing nanomaterials was introduced by FDA the Nanotechnology Task Force in 2007. The task force introduced scientific and regulatory considerations regarding the effectiveness and safety of such products together with several guidance documents to industries to provide updated recommendations (FDA, 2007; Hamburg, 2012). For both EMA and FDA the key factor to be assessed is the safety of the product containing nanomaterials. In January 2015, the European Scientific Committee on Emerging and Newly Identified Health Risks (SCENIHR) adopted the "Guidance on the determination of potential health effects of nanomaterials used in medical devices". The latter provides information about the safety evaluation of nanomaterials, *i.e.*, the determination of hazards associated with the use of nanomaterials and risk assessment for their use in medical devices (SCHENIR, 2015). The basic tests to be carried out for medical devices, therefore including biofunctional textiles, are reported in the ISO guideline (EN ISO 10993) in which the necessary biological safety tests are listed. They include evaluation of cytotoxicity, tissue compatibility, sensitization and irritation potential (EN ISO, 2018). However, in the case of the presence of nanomaterial in the device, stricter classifications may apply due to the potential internal exposure to nanoparticles caused by the application of such a product.

In the FDA regulatory frame, the medical device must undergo a premarket approval application (PMA) if the inclusion of nanomaterial requires original clinical study data to ensure the safety of the nanoproduct. This approval process requires clinical trials or proofs about the safety and effectiveness of the device (Jones et al., 2019; Ventola, 2012). The application of nanomaterials in cosmetics is, instead, well defined and regulated. Regulation (CE) No 1223/2009 introduced specific requirements for marketing cosmetic products containing nanomaterials. It is required by the product manufacturer to register it in the cosmetic product notification portal (CPNP) by specifying the presence of nanomaterials together with their specification and possible exposure conditions. Thereafter the European commission may require the scientific committee on consumer safety (SCCS) to perform a risk assessment (EC, 2009). FDA provides guidelines to industry on the safety assessment of nanomaterials in cosmetic products. The guidance documents help to identify the potential safety issues of nanomaterials in cosmetic products and develop a framework for evaluating them. In particular, the safety of a cosmetic product containing nanomaterials should be evaluated by

analyzing the physicochemical properties and the relevant toxicological endpoints of each ingredient in relation to the expected exposure (FDA, 2014).

1.6.3 Examples and applications of biofunctional textiles

Over the last decade, significant efforts have been spent on the development of biofunctional textiles. In the production of such materials, different kinds of drug carriers have been applied to several fabrics by exploiting various finishing techniques. The different kinds of biofunctional textiles produced together with their main properties are summarized in Table 1.4.

Polymeric particles (either micro or nano) were widely employed in biofunctional textile finishing (Butstraen et al., 2016; Salaün, 2016). Mossotti et al. (2015) produced menthol loaded PCL nanoparticles by a solvent displacement method. The particles were applied to cotton fabrics and test on human volunteers in a double blind patch test. The work evidenced how these patches provided topical refreshment to the volunteer without damaging the skin as evidenced by the TEWL measurements. In the work of Ali (2011) an antimicrobial textile was developed by combining two antimicrobial agents i.e. silver and chitosan. Silver was loaded in a chitosan shell by an ionotropic gelation method. To apply the particles to the unreactive polyester fabrics their surface was activated by a NaOH treatment before proceeding with the bath exhaustion finishing. The antimicrobial assay evidenced an improved bactericidal activity of the composite material respect to one of every constituent, therefore synergistic antimicrobial mechanism was observed.
In the work of Yang et al. (2014), a spray drying method was employed to incorporate vanillin in a chitosan shell, the capsules were grafted on cotton fabrics by a bath exhaustion protocol in which citric acid was added to promote crosslinking. The obtained textile exhibited high washing fastness due to the chemical bonds between the chitosan shell and the cellulose fabric. In the work of Hassan and Sunderland (2015), encapsulated dodecyl-trimethyl-ammonium chloride was added to wool fabrics to impart both antimicrobial activity and insect repellency. Such an approach not only benefited and protect the user but also avoid degradation of the fabric by moths. The capsules where applied by a pad-dry-curing process which effectively imparted repellent activity.

In the work of Alonso (2013), gallic acid was incorporated in PCL microparticles by double emulsion method and applied onto polyamide fabrics. A novel noninvasive in vivo testing method for the antioxidant effect was proposed. The fabrics were applied to set of volunteers with different phototypes, thereafter the SC was removed by tape stripping. The tapes were tested for antioxidant

activity by UV irradiation and thiobarbituric acid assay. The work showed that PCL effectively vehiculared the drug in the SC, there the particles get stuck and act as reservoir systems. Ghayempour et al. (2017) have recently incorporated the hydrophilic chamomile extracts via a double emulsion method, the obtained capsules were mixed with an acrylic resin and applied to cotton fabric, the resin was crosslinked by UV curing. Such an approach led to the slow release and high washing fastness due to the presence of the capsules and the resins hindering the extract diffusion. Furtherly, the hindered diffusion did not compromise the antimicrobial activity of the extracts retained throughout several washing procedures.

According to Martí et al. (2012), the application of the capsules by resin finishing may cause considerable alteration on the transdermal release kinetics. The transdermal release occurs by diffusion phenomena, the driving forces depending on the concentration gradient, which is affected by the amount of drug contained in the fabric. For this reason, this study focuses on evaluating the effective drug loading of the fabric upon treatment with microcapsules and liposomes. The application was performed by padding process onto cotton, polyamide (PA), polyacrylic (PAC) and polyester (PES). The substance was extracted both by soxhlet extraction and ultrasound bath, and quantified by UV-vis spectroscopy and HPLC. The work proved that in the carrier loading onto different fabrics a significant role is played by surface interactions and chemical affinities between the carrier shell and the fiber.

The production of medical textiles utilizing inorganic and hybrid particles reported by Hassabo et al. (Hassabo et al., 2015) who incorporated different topical drugs, like diclofenac and linoleic acid in silica nanoparticle. The particles were produced by using TEOS as a precursor and following the Staber protocol. Thereafter, the particles were applied to cotton fabrics by spraying finishing. The release test proved the delivery of the active substance in dermal pH conditions and the antimicrobial activity against several species. A combination of organic and inorganic particles was proposed by Perelshtein *et al*., which employed a sonodynamic deposition method (Perelshtein et al., 2013). This approach allowed the direct assembly of the particles onto the cotton surface. The combination of zinc oxide (ZnO) and chitosan significantly improved the antimicrobial activity compared to the single agents and the use of ZnO particles imparted also UV protection properties to the garment.

Some studies reported the production of biofunctional textiles by exploiting liposomal carriers. Rubio et al. (2010) studied the transdermal release of caffeine loaded liposomes from functionalized cotton fabrics. The authors performed a series of release experiments on a Franz Cell by testing firstly

caffeine solution and liposome formulation, secondly the fabrics functionalized with the same solution and formulation. Each experiment was performed both on the synthetic membrane and excised porcine skin. In a successive work, the same textile substrate was functionalized liposomal carrier produced using either phosphatidylcholine and with internal wool lipids as shell material (Martí et al., 2011). The materials were tested on human volunteers by applying a non invasive in vivo methodology based on a patch test similar to the one previously described (Alonso et al., 2013).

Cyclodextrins have been extensively employed for textile finishes over the last years. Martel's group proposed methodologies for CDs chemical modification to produce cyclodextrins based polycationic and polyanionic species (Junthip et al., 2015). Upon imparting positive or negative charges, the CDs were loaded with 4-tert-butyl benzoic acid and used to finish polyester fabrics through a layer by layer deposition. Considered the nonreactive nature of the textile material, a preliminary surface activation by plasma treatment was performed. The biofunctional textile exhibited effective drug release properties and antibacterial (Junthip et al., 2016). Mihailiasa et al. (2016) synthesized cyclodextrin nanosponges by chemical crosslinking to better incorporate melatonin. The crosslinking was proven to improve drug loading since the drug was not only entrapped inside the CDs cavity but also in the inter-CDs network of the nanosponges. The loaded nanosponges were applied on cotton fabrics by a bath exhaustion process and the treatment exhibited fastness for two washing cycles; moreover, a controlled melatonin release was observed in the Franz diffusion cell test. Maestà Bezerra et al. (2018) produced similar crosslinked cyclodextrin systems that were employed for the incorporation of citronella oil. The CDs were applied on wool fabrics by padding method, the overall system presented an anomalous release kinetics according to the Korsmeyer and Peppas's model.

The use of hydrogels in the context of bio-functional textile preparation was proven to be an effective strategy to provide drug administration and moisture management simultaneously (Chatterjee et al., 2018). Some authors proposed a biofunctional textile for treating atopic dermatitis. The antioxidant gallic acid was extracted from a mixture of Chinese traditional herbs and incorporated in multilayer capsules of chitosan and sodium alginate. The carriers were applied to cotton fabrics by padding finish followed by oven curing. A resin binder was added to finish formulation to improve the fixation. The drug release test showed a continuous release for over 72 hours. Moreover, a cytotoxicity test, performed on the HaCaT cell line both by MTT and LDH protocols, proved that the proposed material is not toxic for human skin (Hui et al., 2013a, 2013b).

By observing the literature summarized in Table 1.4, it emerges that biofunctional textiles have been extensively studied in recent years for a wide range of applications. Cotton fabrics are the most exploited material for this technology. The choice of using cotton for biofunctional textiles production can be explained considering that it is made of cellulose which is an extremely biocompatible compound. Indeed, cotton was never reported to cause any skin allergy; moreover, it displays good breathability and moisture management properties. The last two features are indeed very important in wound healing applications. Lastly cotton is extremely hydrophilic and wettable, this is a tremendous advantage in the context of the wet finishing processes since easy pick-up of the carrier suspension into the textile material is obtained. The finishing treatments that have been employed for bio-functionalization are diverse, the choice of each author made based on the final application. Indeed, the kind of finishing treatment is strictly related to the final application. Several authors aimed to obtain the formation of chemical bonds to boost the fastness of the treatment. Some other designed the finishing treatment to bind the carrier only physically and therefore promote its release. Concerning the drug carrier used for biofunctional textiles preparation, it is noticeable that polymeric particles have been the most exploited ones. Such carriers have indeed aroused significant interest due to their versatility in incorporating different kinds of active substances. Moreover, the large availability of polymers which can be employed to encapsulate active principles allows designing carriers with proper surface affinity with the fibrous substrate.

Table 1.4. Characteristics and application of bio-functional textiles.

Carrier	Active Substance	Textile	Finishing technique	Application	Reference
Nanoparticles	Menthol	Cotton	Imbibition	Thermal regulation	(Mossotti et al ., 2015)
Microparticles	Silver	PES	Bath exhaustion	Antimicrobial	(Ali et al., 2011)
Nanoparticles	Iodine	Viscose	Padding	Antibacterial antioxidant	(Zemljič et al., 2018)
Microparticles	Vanillin	Cotton	Bath Exhaustion/ crosslinking	Antibacterial and aroma release	(Yang et al., 2014)
Microparticles	dodecyl trimethyl ammonium chloride	Wool	Pad-dry-cure	Bacterial and insect protection	(Hassan and Sunderland, 2015)
Nanoparticles	Gallic Acid	Polyamide	Bath exhaustion	Topical antioxidant	(Alonso et al., 2013)

Microparticles	Chamomile extracts	Cotton	Resin finishing/UV curing	Topical antibacterial	(Ghayempour and Montazer, 2017)
Microparticles	Berberine	Cotton	Spraying	Topical treatment	(Lam et al., 2013)
Polymeric Nanoparticles	Zinc Oxide	Cotton	Pad dry curing	UV protection	(AbdElhady, 2012)
Nanoparticles	Rose fragrance	Cotton	Dipping	Cosmetic	(Hu et al., 2011)
Nanoparticles	Aromas	Cotton	Chemical grafting	Cosmetic	(Sharkawy et al., 2017)
Silica nanoparticles	Diclofenac	Cotton	Spray	Topical treatment	(Hassabo et al., 2015)
ZnO nanoparticles	-	Cotton	Direct synthesis onto fabrics	UV protection	(Perelshtein et al., 2013)
Liposomes and Microcapsules	Sunscreen	Cotton, PA, PAC, PES.	Foulard	UV protection	(Martí et al., 2012)

Liposomes	Sunscreen	Cotton	Bath Exhaustion	UV Protection	(Martí et al., 2011)
Liposomes	Pyrazole	Cotton	Pad dry curing	Topical release	(Nada et al., 2018)
Liposomes	Caffeine	Cotton	Imbibition	Transdermal administration	(Rubio et al., 2010)
Cyclodextrins	TBBA	PES	Layer by layer deposition	Topical infections treatment	(Junthip et al., 2016, 2015)
Cyclodextrin nanosponges	Melatonin	Cotton	Bath exhaustion	Transdermal release	(Mihailiasa et al., 2016)
Cyclodextrin	Citronella oil	Wool	Padding	Insect repellency	(Maestá Bezerra et al., 2018)
Hydrogels	Chinese Herbal extract	Cotton	Pad-dry curing	Topical treatment	(Hui et al., 2013a, 2013b)

Chapter 2. Encapsulation processes and technologies

Micro- and nanoparticles are the most exploited carriers for medical and biofunctional textile functionalization. The large availability of biocompatible polymers provides a wide range of possibilities in the design of such carriers. Furtherly, the technological maturity of the encapsulation processes makes possible to easily adjust production to achieve the desired product characteristics. In the context of transdermal delivery, it is necessary to produce particles respecting quality and quantity constraints. In terms of quality, it is necessary to produce particles with a characteristic size sufficiently low to allow the permeation through the skin. A particle size of 500 nm was reported as the threshold for polymeric particles to overcome the skin barrier (Kohli and Alpar, 2004; Schneider et al., 2009). Therefore, the nano-sized carriers must be employed for skin delivery applications. Considering the chemical selectivity of the epidermis, particles owning a lipophilic and polar surface are considered to be more effective in permeating the SC. The latter surface properties mostly depend on the polymer used as shell material. The polymer used for drug encapsulation is strictly required to be biocompatible, moreover, the use of a biodegradable polymer is considered as a plus for the drug delivery applications (Abdel-Mottaleb et al., 2012). Considering that the produced carriers have to be used as a textile finishing agent, it is also of crucial importance to select an encapsulation process that assures levels of productivity consistent with the needs of textile finishing.

Encapsulation processes are mostly classified according to physicochemical principles and phenomena that induce the particle formations. A list of the encapsulation processes considered of interest for the present application is summarized in Table 2.1. These process mainly consists of two fundamental steps i.e, i) the formation of an interphase that leads to the production of the droplets and ii) the shell formation and hardening of droplets to form the carriers (Trojanowska et al., 2017).

Regarding the first step, liquid-gas or liquid-liquid interphases can be exploited for droplets generation. The liquid-gas dispersion is formed in spray based processes such as the spray-drying or the electrospray. In such processes, the polymer solution is atomized in the air to form the droplets. The shell formation is generally achieved by the evaporation of the solvent during the travel from the atomizer to the collector. The morphology of the particles obtained is either of capsule or sphere depending on the substance encapsulated.

Table 2.1. Comparison of different transdermal technologies.

Encapsulation method	Interface	Size	Polymer used	Morphologies	Sources
Spray drying	Liquid-Gas	0.2-10 µm	PLGA, Arabic gum, chitosan, PVA, Sodium alginate	Spheres and capsules.	(Arpagaus et al., 2017)
Electrospray	Liquid-Gas	0.2-25 µm	Chitosan, PCL, PLGA, PLA, Silk Fibroin, Gelatin, cellulose acetate.	Spheres and capsules.	(Pawar et al., 2018)
Solvent evaporation	Liquid-Liquid (Emulsion)	0.5-200 µm	PLGA, PLA, PEG EC, PMMA	Capsules	(Li et al., 2008)
Chemical crosslinking	Liquid-Liquid (Emulsion)	0.1-230 µm	Chitosan, PMMA, Gelatin, Arabic gum	Capsules	(Agnihotri et al., 2004; Taban et al., 2020)
Photopolymerization	Liquid-Liquid (Emulsion)	50-500 nm	Photo-reacting monomer: Thiol-ethers, divinyl-ethers, acrylates, meta-acrylates.	Capsules	(Sangermano and Bazzano, 2018)
Simple coacervation	Liquid-Liquid (Emulsion)	0.1-50 µm	Gum arabic, gelatin, chitosan, alginate, pectin.	Spheres and capsules	(Mohanty et al., 2007; Salehiabar et al., 2018)
Complex coacervation	Liquid-Liquid (Emulsion)	0.1-50 µm	Polyanions and polycations couples: gum arabic, gelatin, chitosan, alginate, pectin.	Spheres and capsules	(Li et al., 2018; Timilsena et al., 2019)

Solvent displacement	Liquid-Liquid (Miscible)	100-5000 nm	PLA, PCL, PLGA, PEG, Chitosan, Gelatin	Spheres and capsules	(Martínez Rivas et al., 2017)
Flash nanoprecipitation	Liquid-Liquid (Miscible)	50-5000 nm	PEG-b-PLA, PEG-b-PLGA, PCL, Lecithin, Zein	Spheres and capsules	(Tao et al., 2019)

Several encapsulation techniques exploit the liquid-liquid dispersions for the droplet formation. The liquid substances involved can be either miscible or not miscible among them. When two not miscible liquids are employed emulsions are formed. The emulsion technologies are a very popular and versatile approach for the formation of the droplets. Numerous approaches such as solvent evaporation, chemical crosslinking, photopolymerization and coacervation have been proposed to promote membrane hardening. These techniques lead to the production of liquid core capsules (Tan and Danquah, 2012).

When miscible liquids are used instead, the droplets are formed because of a lack of solubility of the polymer in the new liquid environment. This approach, typical of the solvent displacement method leads to the formation of spheres or capsules depending on the substances employed (Martínez Rivas et al., 2017).

Observing the encapsulation techniques summarized in Table 2.1 it is evident that the proposed techniques have been reported to exploit different kinds of polymers such as natural polymers (chitosan, gelatin, alginate) and synthetic ones (PLA, PCL, PLGA). The morphology of the products obtained mostly consists of capsules and spheres. Most of the proposed techniques lead to the production of carriers with size ranging from a few hundreds of nanometers to several micrometers. Being particle size a fundamental property in determining the skin permeation, the mentioned processes were deeply analyzed to understand which one allows to obtain nanosized particles while matching other desired properties both from material and process point of view.

2.1 Liquid-gas dispersion: spray based methods

Spray based technologies employ liquid-gas dispersions. The droplets are formed as aerosols and dried inside the appositively designed device. Therefore, the main peculiarity of these techniques

consists in the production of dried particles powders. These products are generally easier to handle, store and transport, moreover, the lower water activity makes dried particles less sensible to microbial attacks compared to particle suspensions (Gouin, 2004). Indeed, spray methods can be used both for particle formation or for the drying of particle suspensions produced through other technologies. The main technologies in this contest are the spray drying and the electrospray.

2.1.1 Spray drying

The spray drying process exploits the atomization of a polymer solution to form an aerosol. High-temperature gas is required to dry the aerosol and form dry particles. Spray drying equipments are nowadays commercially available at industrial scale and can operate in continuous mode (Arpagaus et al., 2017). The flow diagram of a spray drying apparatus is sketched in Figure 2.1.

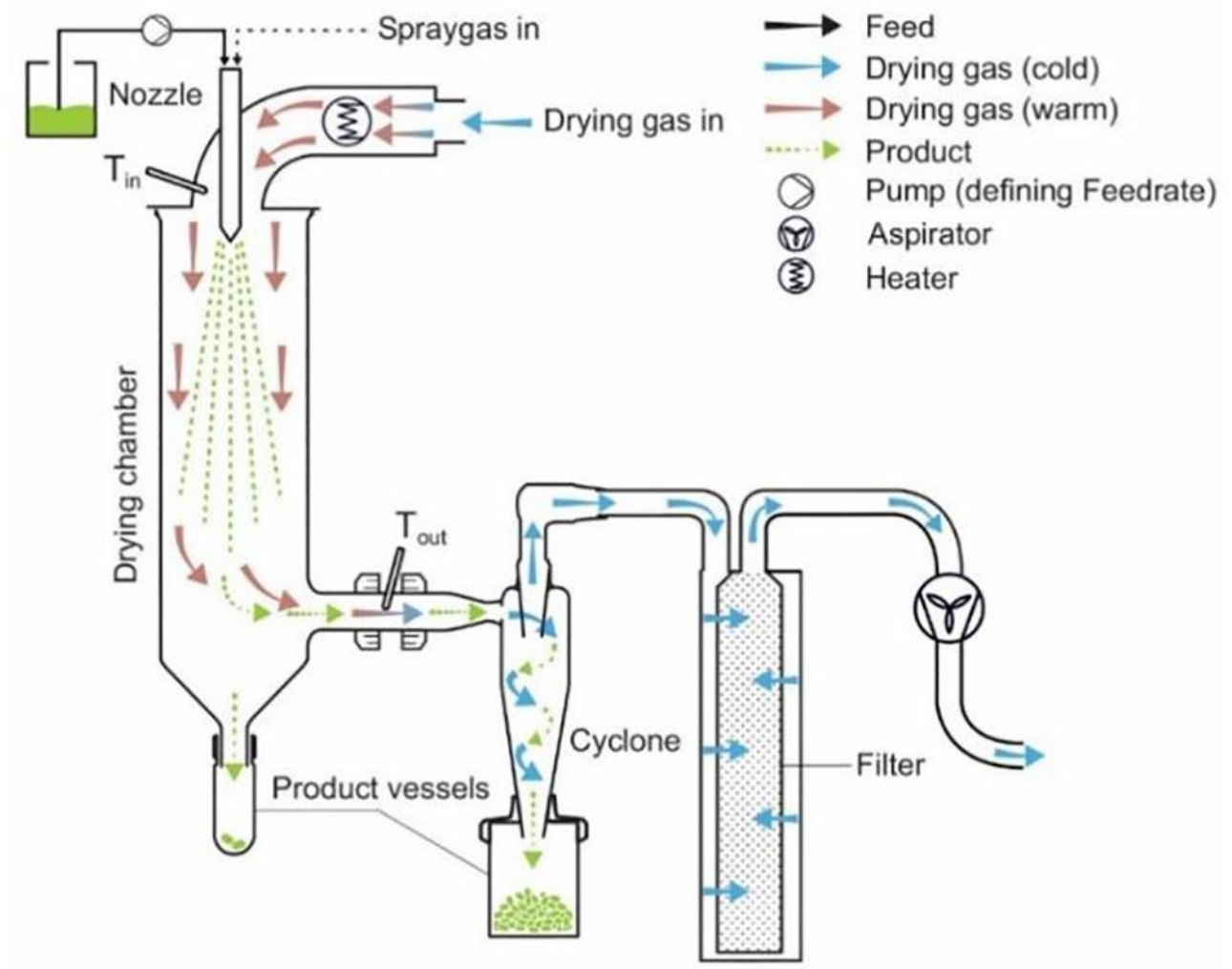

Figure 2. 1. Representation of the spray drying process reprinted from (Arpagaus et al., 2017).

As shown in Figure 2.1, the liquid solution is pumped through a nozzle which promotes the atomization of the stream and the production of tiny droplets. The droplets are sprayed inside a drying chamber where a heated gas is flown, this promotes the solvent evaporation. The low size of the droplets results in significant surface area and fast solvent evaporation. Moreover, due to the latent heat of evaporation of the solvent, the temperature of the droplet is kept low and this prevents the damaging of the core substance. Thereafter, the dried product is separated by the gas stream by a cyclone and collected (Wong and John, 2015). The liquid phase fed to the nozzle contains both the polymer and the active substance. It can be either a solution in the case of solid core particles or an emulsion in the case of liquid core capsule production (Assadpour and Jafari, 2017).

In the design of the spray drying process, several parameters can be adjusted to control the particle properties. The solution properties can be adjusted to obtain a small droplet size. This objective is generally achieved by increasing the solution viscosity and lowering its surface tension. These properties are controlled by adjusting the polymer concentration and by adding surfactants to the formulation (Littringer et al., 2013). The characteristics of the gaseous stream i.e. temperature and flow rate can also impact the process productivity. Generally, increasing the gas flow rate and temperature allows increasing productivity. However, attention must be taken to avoid the local temperature of the particles to be increased above the threshold at which the active substance is damaged (Cal and Sollohub, 2010).

The solution can be water-based, organic solvent-based or a mixture of the two. The common organic solvents used in spray drying include dichloromethane, ethanol, acetone, ethyl acetate, methanol and acetonitrile. Organic solvents are required when hydrophobic polymers or drugs are processed. Moreover, organic solvents allow the generation of finer droplets due to their lower surface tension respect to water. Due to their high volatility, the processing time and the fed temperature are low but, particular attention must be paid to their toxicity and flammability (Fontana et al., 2014).

Spray drying technology has been proven to be advantageous under many points of view, firstly it is a quite versatile technique suitable for many materials. Indeed, the possibility of employing both water and organic solvents permits to encapsulate both hydrophilic and hydrophobic substances. Secondly, it allows having good control over the particle size and structure by adjusting the different process parameters that come into play. However, industrial spray drying systems are generally reported to produce particles with size above 1 micrometer which may not be suitable for transdermal delivery applications (Arpagaus et al., 2018).

2.1.2 Electrospray

Electrospray (ES) is an electrohydrodynamic deposition process conceptually similar to the electrospinning one, it is used to produce polymer particles in dried powder form instead of nanofibers (Anu Bhushani and Anandharamakrishnan, 2014). The representation of an electrospray process is sketched in Figure 2.2.

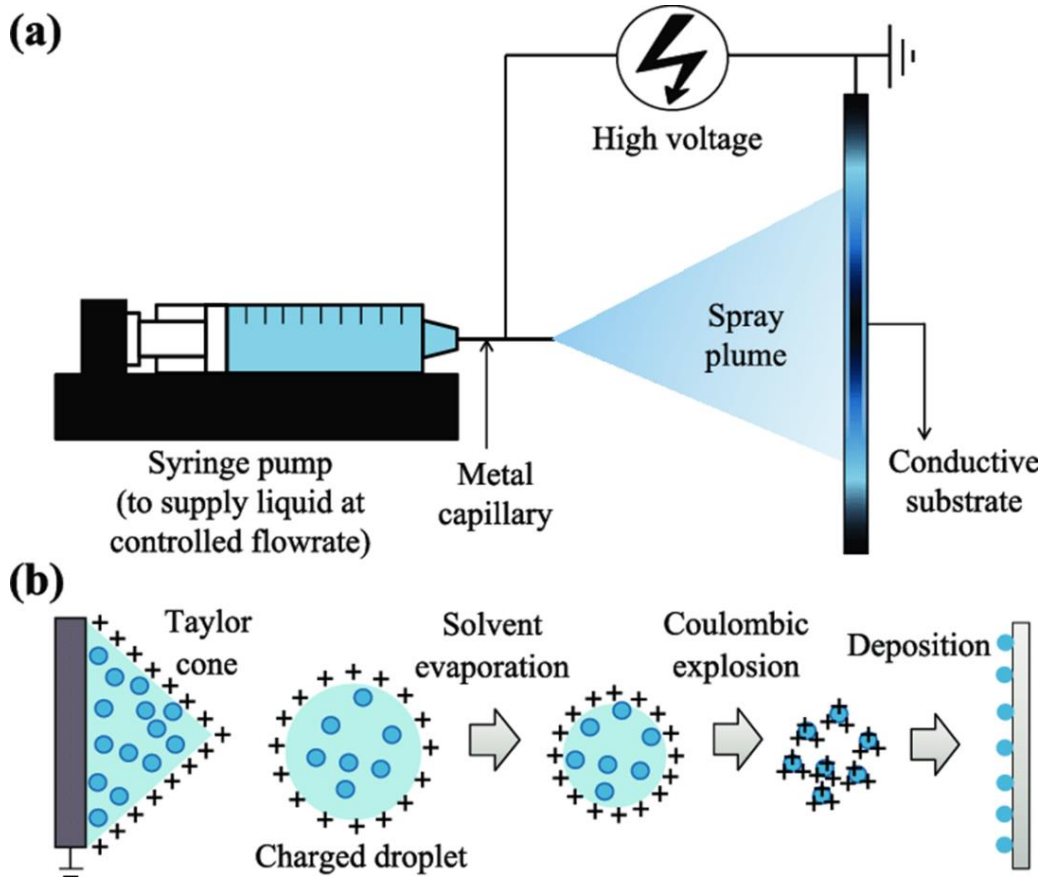

Figure 2.2. Representation of the electrospray process (Haider et al., 2019).

The electrospray apparatus consists of a syringe pump which pumps the polymer solution through a tiny nozzle spinneret. The nozzle is connected to an electric power supply which is grounded to a metal collector. The application of an electrical potential causes the polymeric solution to be stretched in a Taylor cone at the end of the nozzle tip. This conical shape is due to the forces acting at the nozzle tip, these forces are surface tension, viscosity, gravity, applied pressure and applied electrical force. From the Taylor cone, small charged droplets are atomized and travel toward the collector. The formation of a stable Taylor cone is a necessary condition to achieve uniform particle production (Pawar et al., 2018). Once the droplets have been detached from the Taylor cone, two main forces

act on them, these forces are the coulombic and the cohesive ones. Coulombic forces promote the repulsion among the charged polymer chains while the cohesive forces held the droplet size stable. Upon solvent evaporation, the size of the droplets lowers causing an increase in the surface charge density. This makes the coulombic forces overcome the cohesive ones leading to the scission of the droplet in smaller ones by the coulombic explosion phenomenon. Thereafter, the particles are collected on the oppositely charged collector (Tapia-Hernández et al., 2015).

The size of the particles obtained from the electrospray process depends both on the properties of the sprayed solution and on the process parameters. The solution properties that play a major in the electrospray process are the viscosity, the electrical conductivity and the surface tension. The increase of viscosity causes an increase in the particle size since the viscous force opposes the atomization and coulombic explosion phenomena. Moreover, high viscosities cause the product to have fibrous shape instead of a particular one (Ardila et al., 2018). The increase in electrical conductivity favors both the atomization and the coulombic explosion phenomena, thus it leads to the formation of finer particles (Rascón-Chu et al., 2018). Low surface tension is required to obtain finer particles, indeed, high surface tension increases the energy required for atomization. All these solution properties are tuned by adjusting the formulation (Moreno et al., 2018; Pawar et al., 2018).

The process parameters also play a significant role in determining both the feasibility of the electrospray process and the particle size. Many authors evidenced that decreasing the process flow rate (FR) leads to the formation of smaller particles. Furtherly above a certain FR the dripping jet phenomenon occurs, this hinders the solvent evaporation and the formation of the particles (Sreekumar et al., 2017; Zhang and Kawakami, 2010). Increasing the applied electrical field promotes the coulombic explosion leading to finer particle formation. It is necessary to keep the applied voltage in a proper range to ensure the Taylor cone stability (Hu et al., 2012; Omidi et al., 2010). The tip-to-collector distance determines the time of travel between the nozzle and the collector, therefore increasing it promotes coulombic explosion and finer particle formation (Ardila et al., 2018).

In the electrospray process, dry particles are formed without the need of employing chemical cross-linkers (Gómez-Mascaraque et al., 2016). Moreover, the process is normally carried out at ambient temperature, thus reducing the risks of drug denaturation and the safety concerns connected to the use of flammable solvent. Compared to the spray drying, ES is a less versatile technique in terms of processable substances. In fact, the polymeric solution must be electrically conductive to be electrosprayed. The ES technique was reported to produce nanoparticles of a few hundreds of nanometers. However, to achieve such low particle size high electrical potential (in the order of KV) must be employed, making the process demanding under the energetic point of view. Moreover, to

achieve nanometric size particles it is necessary to work with low flow rates (in the order mL/h). This makes this necessary to compromise between process productivity and particle quality (Zhang and Kawakami, 2010).

2.2 Liquid-liquid dispersion: Formation of the emulsions

Emulsion based processes are the first encapsulation technologies to be proposed. The concept behind this technology is to mix an aqueous and an oily substance to create a heterogeneous liquid system. The main principles and process schemes of an emulsion based encapsulation process are sketched in Figure 2.3. An emulsion based encapsulation method occurs in three steps, i.e. i) the solution preparation, ii) the emulsion formation and iii) the hardening of the droplets.

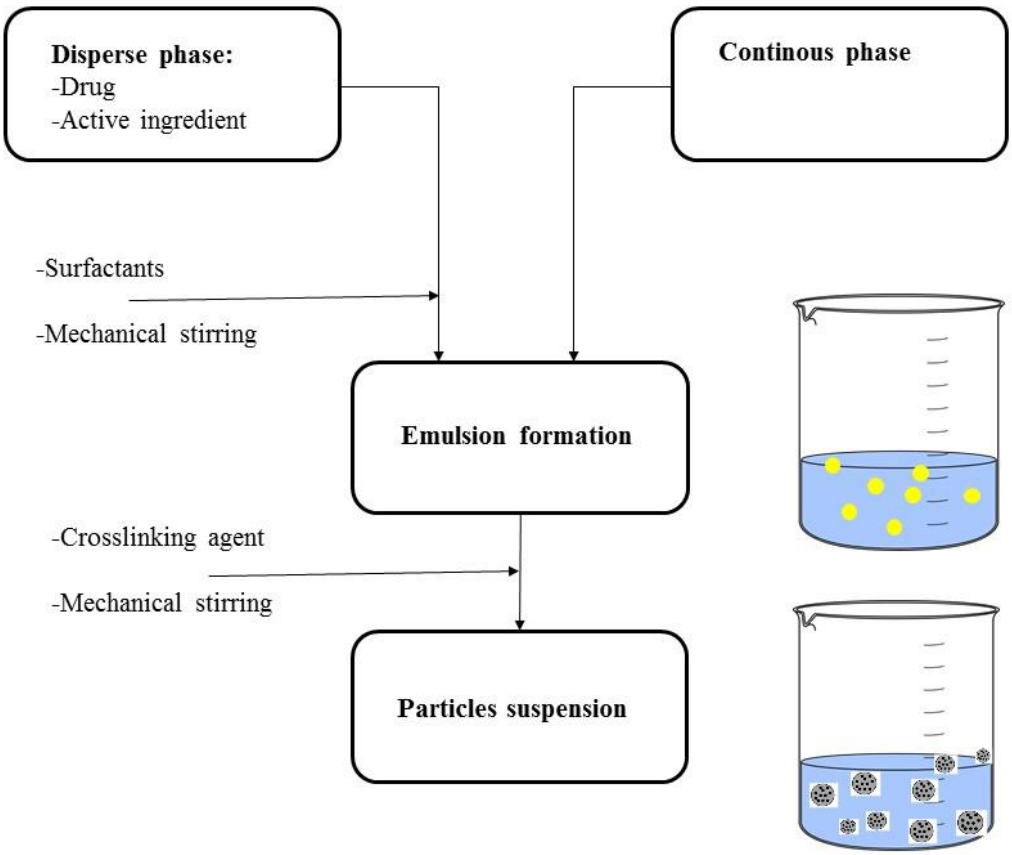

Figure 2.3. Emulsion based encapsulation process scheme.

The emulsification step is the one that mostly affects the particle size and the particle size distribution (PSD) as well as the other particle properties. Then several emulsification strategies have been proposed to obtain the desired product quality. Above all different kinds of emulsions have been

proposed to produce different capsules morphologies and incorporate different active ingredients. Moreover, particular focus has been paid on achieving emulsion droplets with small size and good colloidal stability to obtain particles with lower diameter. To produce fine and stable emulsions mechanical energy is supplied to the system. Moreover, surfactants are conventionally employed to obtain smaller and more stable droplets. (Jenjob et al., 2019).

To effectively encapsulate a wide range of active ingredients and achieve different capsules structure, several kinds of emulsion have been employed. The oil-in-water emulsion (O/W) uses oils as the disperse phase and water as the continuous one. This technique is generally exploited to produced capsules whose core is hydrophobic drugs or oily substances such as essential oils. Oppositely, water-in-oil emulsions (W/O), water constitutes the disperse phase and oil the continuous one. Such a technique permits to effectively incorporate hydrophilic substances. Double emulsions ($W_1/O/W_2$) have been proposed to produce multinuclear capsules. They are produced in multiple steps. Firstly, the active is dissolved in the primary water phase. Then the solution is added to the oil to produce a small volume of W/O emulsion. Finally, the W/O emulsion is poured inside a larger amount of water to produce the double emulsion. Similarly, oil-in-water-in-oil double emulsions ($O_1/W/O_2$) are prepared (Ding et al., 2019).

The quality of the emulsion plays a significant role in determining the quality of the final products. Achieving the formation of small droplets in the emulsion is necessary to achieve the formation of nanoparticles. This task is performed by supplying mechanical energy to liquid-liquid system (Li et al., 2008). Conventional apparati employed to supply this energy include ultrasounds probes, high pressure valves or rotor-stator mixers. The latter devices present the advantage of being easy to operate and available at the industrial scale. However, they apply energy locally causing a gradient of shear stress to be present over the volume of the batch. This causes the production of droplets with broad size distribution. Moreover, the high amount of energy supplied in proximity of the mixing devices can cause a local temperature increase which may damage the active ingredients. To overcome the drawbacks of classical mixing devices alternative emulsification processes have been proposed (Vladisavljević, 2019).

2.2.1 Membrane emulsification

Membrane emulsification processes (ME) refers to a particular technique for emulsion preparation in which the liquid is pressed through a microporous membrane under controlled shear conditions and injection rates (Pradhan et al., 2013). The ME process can be direct or premixed. The direct membrane

emulsification (DME) consists in the pumping of the dispersed phase in the continuous phase, the droplet formation occurs at the membrane/continuous phase interphase. In premix membrane emulsification (PME) a coarse emulsion is pressed through the membrane, the pressure gradient causes the emulsion to break down in finer droplets (Nakashima et al., 2000). Both techniques are suitable to produce different kinds of emulsions (direct, indirect or double) upon selection of the proper membrane, as shown in Figure 2.4. Hydrophilic membranes are suitable for the preparation of O/W, W/O/W emulsions while hydrophobic membranes are used for W/O and O/W/O ones. It is indeed required to have scarce affinity between the membrane and the liquid pumped through it to promote droplet formation and detachment (Vladisavljević, 2019).

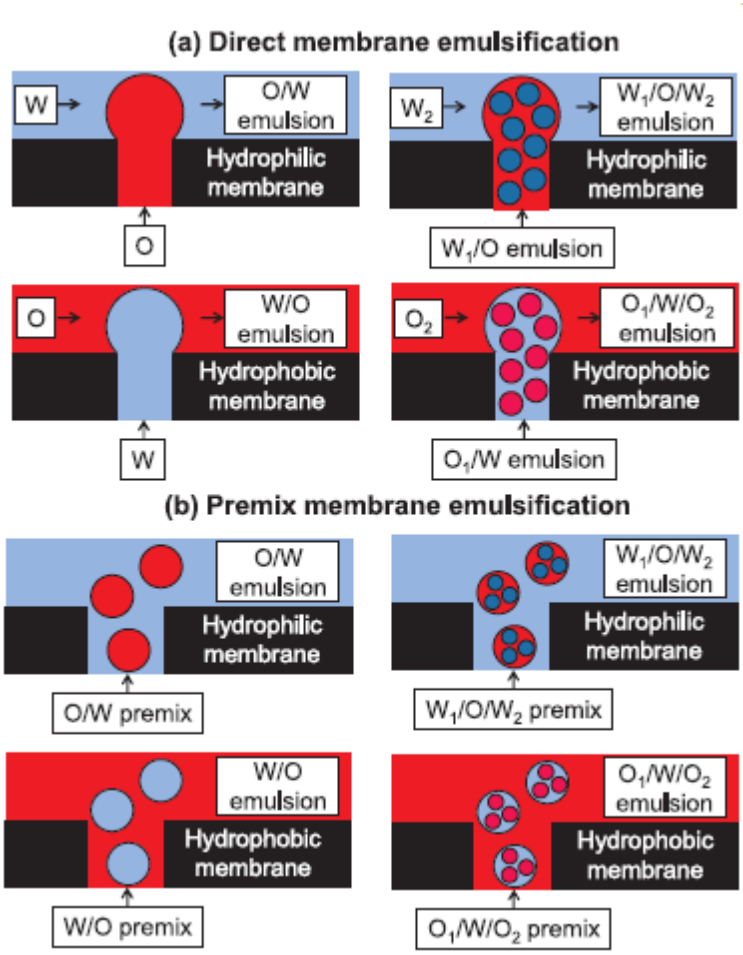

Figure 2.4. Production of the different emulsion by ME and required membrane (Vladisavljević, 2019).

In ME processes the membrane properties play a key role in determining the final characteristic of the obtained product. The used membranes are required to have a high number of pores and uniform pore size distribution, moreover, they have to be own good mechanical and chemical resistance. Materials employed in membrane production are ceramics, such as the Shirasu Porous Glass, metals

such as nickel and aluminum alloys, or polymers such as polycarbonate (PC) or poly-vinylidene-fluoride (PVDF). All these materials can undergo surface modifications to impart the desired wettability demanded by the specific process (Vladisavljević, 2019).

Concerning the emulsion preparation, ME was proved to display some advantages compared to other mechanical techniques such as high-pressure valves, rotor-stator mixers and ultrasounds. Indeed, the ME is a spatially uniform process where the shear stress is equally distributed over the membrane. Thus it overcomes the limitations of rotor-stator that cannot apply energy uniformly over the reactor volume, leading to dead zones and polydispersed droplets size. Moreover, concerning energy consumption, ME requires much lower energy inputs. The fact that conventional mixing requires higher energy makes the process less sustainable and decreases the quality of the product. The high energy input leads to a temperature rise which can alter or damage the active principle (Vladisavljević, 2015). Currently, the main limitation in the scale-up of the ME process is the low emulsion productivity and the membrane damages which require the process to be stopped and membrane to be substituted regularly. This makes still challenging to employ the ME method in continuous production (Piacentini et al., 2014).

2.3 Liquid-liquid dispersion: hardening of the droplets

The hardening of the droplets is the final step of the emulsion based encapsulation techniques (Figure 2.3). In this step, the emulsion droplets are turned into solid nanoparticles by the formation of the polymeric membrane. The formation of the polymeric shell can be induced by several approaches such as the physical, the chemical and the physical-chemical ones. The methods employed to promote the rigidification of the droplets critically affects not only the product quality but also the overall sustainability of the process from the economic and environmental point of view. Given the importance of this step, the encapsulation processes are often classified and named according to the method used to promote the hardening of the emulsion droplets (Wu et al., 2008).

2.3.1 Solvent Evaporation

The solvent evaporation was one of the oldest methodologies to promote the hardening of the droplets to solid particles. In the most classic setups, the encapsulation procedure consisted of three steps which are summarized in Figure 2.4.

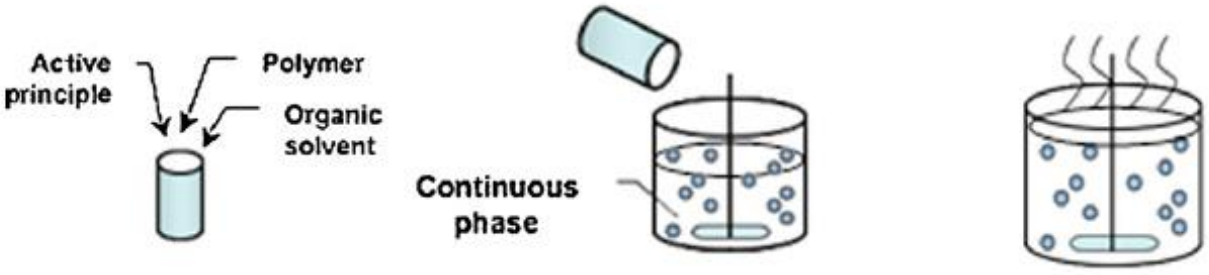

Figure 2.5. Production of particles by solvent evaporation method modified by (Li et al., 2008).

Firstly, the drug and the polymer are dissolved in an organic solvent which will constitute the disperse phase. Secondly, the solution is added to the water continuous phase and the emulsification is promoted. Finally, the evaporation of the solvent is promoted causing the precipitation of the polymer and hardening of the capsule shell (Li et al., 2008). This method was initially developed to incorporate hydrophobic active principles employing O/W emulsions. Subsequently, the encapsulation of hydrophilic substances was also achieved by changing the kind of emulsion. Such modified approaches included the W/O/W emulsion, the O/W co-solvent method and the O/O non aqueous solvent evaporation method (Herrmann and Bodmeier, 1998).

The evaporation step is the crucial one as it has the greatest influence on the particle characteristics. The solvent evaporation can be promoted by heating and/or depressurization. Heating is the simplest approach, it leads to the production of particles with a bigger size. It is necessary to not exceed the temperature threshold which could cause solvent boiling or drug denaturation (Freitas et al., 2005). Reducing pressure effectively promote solvent evaporation. Such an approach indeed can reduce the overall process time and in some studies, it has also been reported to improve the encapsulation efficiency (Meng et al., 2004). Furtherly, the reduced pressure configuration allows the production of particles with a smoother surface and smaller size if compared to atmospheric pressure configuration. In tuning the process conditions, pressure must be kept greater than the vapor pressure at the process temperature to avoid boiling.

The solvent evaporation method presents the advantages of not requiring chemical crosslinkers to harden the particle surface. However, a high amount of solvent must be removed and the complexity of working under reduced pressure must be considered. The main concerns on the solvent evaporation processes consist in the fact that it requires significant amounts of solvent to be removed and released in the environment. In case toxic solvents are used this procedure arises several concerns from the operator safety and environmental compliance point of view (Li et al., 2008).

2.3.2 Chemical crosslinking

In the emulsion-chemical crosslinking method, specific chemicals react with the polymer chains reticulating and crosslinking them. Such an approach presents the advantages of exerting a good control of the particle size. The nature of the cross-linker affects the overall quality of the process. Many authors employed aldehyde based cross-linkers such as glutaraldehyde due to their effectiveness in promoting cross-linking reaction at mild temperature conditions (Agnihotri et al., 2004). Due to the toxicity of such reactants, green crosslinkers have been arising significant interest. These crosslinkers are mainly organic acids such as butane tetracarboxylic acid (BTCA). In the choice of the cross-linker, particular attention should be taken to avoid substances that do chemically interact with the active substance (Yang et al., 2014).

2.3.3 Photopolymerization

The emulsion photopolymerization employs photochemical principles to crosslink and harden the particles, as represented in Figure 2.5.

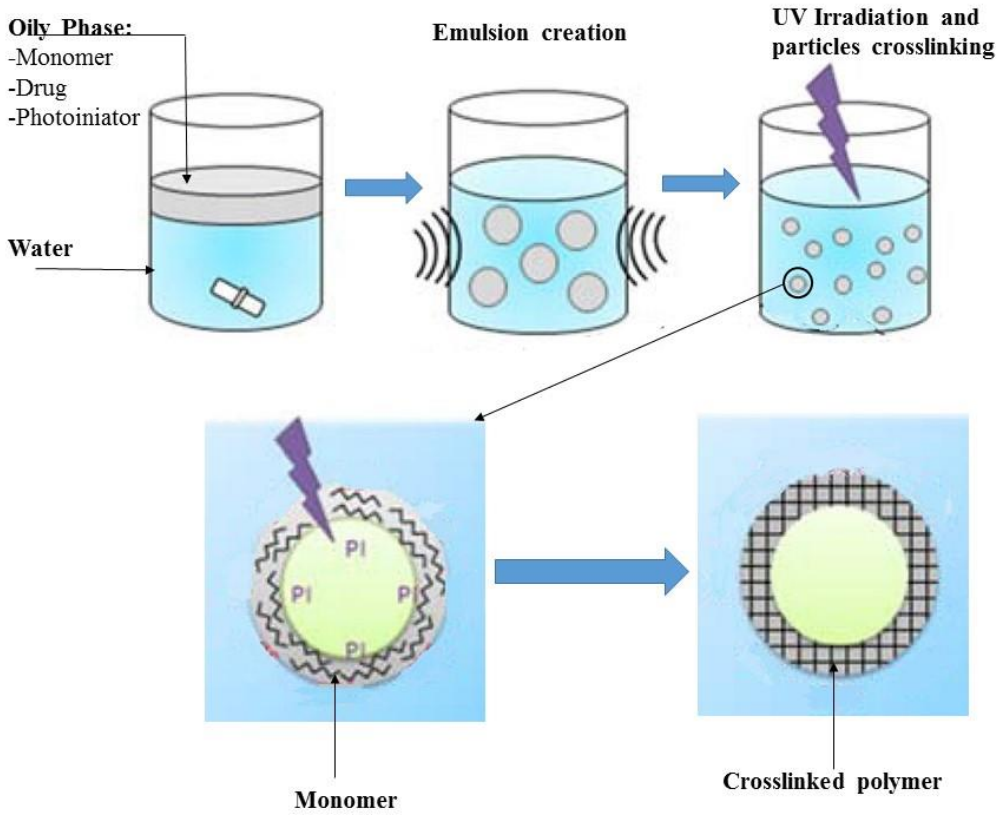

Figure 2.6. Schematic representation of an emulsion photopolymerization process.

In this technique, the emulsion is prepared by adding to the disperse phase the active substance, a monomer, and a photoinitiator (PI). The photoinitiators are molecules which undergo structural changes upon light irradiation, UV light is mostly used to excite the PI. This UV excitation leads to the formation of molecular forms that display either radical or cationic configurations (Artusio et al., 2018). Upon preparation of stable emulsion by mixing and surfactant addition, the system is photo irradiated. Therefore, the exited photoinitiator reacts with the monomer and starts the polymerization reaction. The polymerization mechanism can be either radical or cationic chain propagation, and the emulsions can be either W/O or O/W (Sangermano and Bazzano, 2018).

The emulsion photopolymerization permits to promote the hardening of the droplets at mild temperature. Moreover, given that the active substance is not soluble in the continuous phase, photopolymerization guarantees high encapsulation efficiencies. The main drawback of this technique is that the photochemical processes are inhibited by oxygen (oxygen quenching phenomenon) and therefore the process must be carried out under an inert atmosphere. These conditions indeed complicate significantly the scale-up toward industrial production. The materials employed in such processes also arise some concerns; first of all, the molecules used as photoinitiators can display toxicity. Moreover, this technique requires the use of photo reticulating monomers. The polymeric structure obtained, as reported in Table 2.1 are biocompatible polymer such as polyacrylates, however, they are not biodegradable thus are not the optimal choice for drug delivery devices (Bazzano et al., 2016).

2.3.4 Coacervation methods

The phase coacervation is a physical-chemical phenomenon that occurs in macromolecular solutions or dispersions which are not in thermodynamic equilibrium. It mainly consists of phase separation where a colloid-rich phase called coacervate is produced while the remaining phase is defined as the equilibrium phase. The coacervation process is initiated by a change in the properties of the solution, such as temperature, ionic strength, pH or by addition of chemicals (Nairm, 1995). Such a colloidal formation process can be tailored to produce polymeric micro- and nanoparticles. Two methods have been proposed i.e. simple and complex coacervation.

In simple coacervation, a unique macromolecular species is precipitated either by adjusting solution properties or by adding a coacervation agent which can be either a desolvation liquid or a salt. Examples of simple coacervation processes can be the induction of phase separation in gelatin solution by sodium sulfate or ethanol (Madan, 1978).

The complex coacervation method, instead, requires two oppositely charged molecular species. Once the coacervation is initiated the colloids are formed thanks to electrostatic forces, hydrogen bonding and Van der Walls interactions among the two polymers (Xiao et al., 2014). Therefore, in the complex coacervation process, the combination of proteins and polysaccharides has been extensively proposed. Proteins such as gelatin, silk fibroin, egg albumin, soy proteins, and polysaccharides such as chitosan, Arabic gum, pectin and carboxymethyl cellulose have been studied. The possibility of coupling such a wide range of materials allows designing a complex shell to impart multifunctional properties to the capsules (Schmitt and Turgeon, 2011). In these methods the effective encapsulation of the active substance occurs because the coacervated polymer tends to deposit around the drug, resulting in its incorporation in the core of the colloid (Espinosa-Andrews et al., 2007).

The complex coacervation process generally consists of four step procedure which is sketched in Figure 2.7. Firstly, an aqueous solution of one polymer is prepared. Secondly, a solution of the second polymer is prepared and added to the first one allowing interactions among the two oppositely charged polyelectrolytes. Thereafter, a change of the temperature or pH is exploited to induce the polymer coacervation. Lastly, the hardening of the particles is furtherly promoted by adding a proper crosslinker (Timilsena et al., 2019).

Considering the different physical and chemical phenomena occurring during the complex coacervation process, it is possible to identify several parameters that influence the process. The pH of medium displays a strong effect both on particle size and encapsulation efficiency. The complex coacervation occurs because of the electrostatic interactions between the macromolecules, whose ionization state depends on pH. Polysaccharides structures are rich in carboxylic groups which normally undergo deprotonation and display negative charges unless they are dissolved in very low pH media. Proteins, instead, have amphiphilic behavior due to the presence of both amino and carboxylic groups. If the pH is below the isoelectric point (pI) the protonation of the amino groups prevails imparting the molecule positive charge, in the opposite case, the deprotonation of the carboxylic group makes the molecule to have anionic character. Therefore, the pH can be easily used to induce coacervation. Firstly, the two solutions are mixed above the pI, making both the species to be negatively charged. Secondly, the pH is lowered below the pI, in this condition the protein becomes positively charged and coacervates with the polysaccharide.

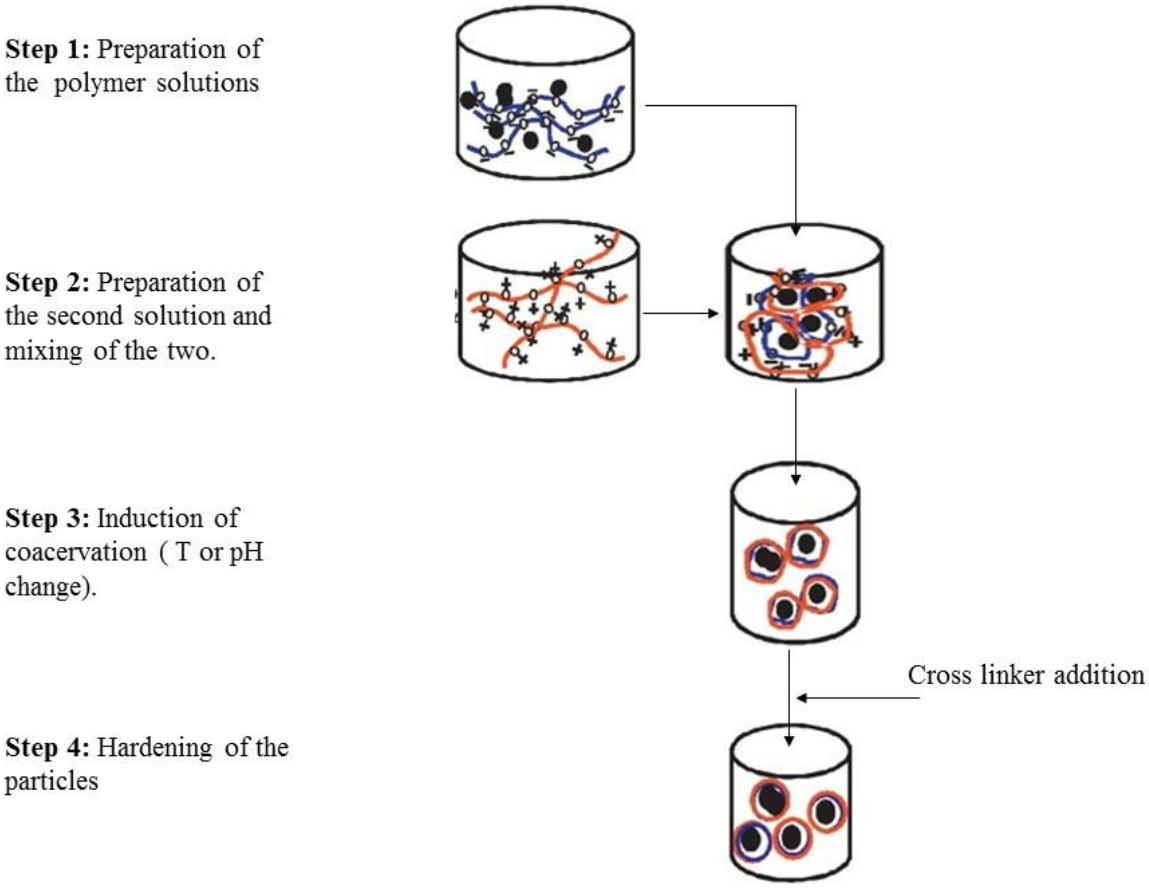

Figure 2.7. Scheme of a complex coacervation based encapsulation process.

Besides inducing coacervation, the change of pH and the mode in which is induced (kind of acid substance, quantity, speed of pH adjustment) affect the particle formation mechanism and the properties of the particles (Siow, 2012). The quantity of electrolytes present in the solution also influences the coacervation phenomena since the added ionic species interacts with the charged polymers. Several authors reported that high salt concentration can suppress the complexation of the polyelectrolytes hindering the encapsulation phenomenon. The effect of salt concentration is different depending on the polymer and salts (Ru et al., 2012). The polymer concentration should be adjusted carefully since high concentration hinders the free movement of the macromolecular chains and prevents them to interact. The polymer molecular weight (MW) also influences the coacervation phenomenon, low MW polymers tend to interact with each other by ion pairing and this hinders the coacervation. Oppositely, high MW increases the tendency of the polymer to gel and precipitate (Burgess, 1994).

It can, therefore, be concluded that the formation and properties of the particles can be controlled by adjusting such parameters and this makes complex coacervation a tunable and versatile technique. Moreover, this method allows good results in terms of reproducibility and high payload of the drug. The possibility of working at low temperatures makes it suitable also for the incorporation of thermally sensible active ingredients. Oppositely, since the pH below the proteins isoelectric point is required it may not be suitable for the incorporation of pH sensible substances.

The coacervation process can produce particles with characteristic size from hundreds of nanometers to several micrometers. Achieving nanosized particles often requires significant efforts since these processes are very sensitive to the presence of salts or ionic species. Ensuring the absence of such species makes complex to carry out these processes at an industrial scale ensuring productivity while keeping the production cost sustainable (Timilsena et al., 2019).

2.4 Liquid-liquid dispersion: the solvent displacement method

The solvent displacement or "nanoprecipitation" methods was reported for the first time by Fessi in 1989. This technique exploits the formation of a liquid-liquid interphase between two miscible fluids upon moderate stirring. The first fluid is a good solvent of the polymer and is therefore used to prepare a solution of the polymer and the drug to be incorporated. This solution is mixed with a volume of the second fluid which is a bad solvent of the polymer and therefore commonly defined as antisolvent. Being solvent and antisolvent two miscible liquids, the solvent diffuses in the antisolvent causing the polymer to precipitate forming a particulate suspension. The solvent can thereafter be removed by evaporation and the particles could be collected by centrifugation or filtration (Fessi et al., 1989). A schematic representation of the nanoprecipitation method is reported in Figure 2.8.

The solvents used in this method are generally organic solvents such as acetone, ethanol, methylene chloride and hexane. Oppositely, the antisolvent is either water or an aqueous solution. In this aqueous solution, some chemicals can be added to achieve specific properties. For example, surfactants are commonly added to the antisolvent to prevent particle aggregation (Mora-Huertas et al., 2011). This technique is generally used to produce nanospheres, however, the addition of oils in the solvent stream allows for the production of nanocapsules (Miladi et al., 2016).

The nanoprecipitation method is generally exploited to incorporate poorly water soluble drugs; oppositely it has not been significantly exploited for the encapsulation of hydrophilic substances. This is because hydrophobic substances tend to precipitate together with the polymer upon solvent

displacement. Instead, the hydrophilic molecules easily diffuse in the antisolvent rather than being incorporated into the polymer particles (Arpicco et al., 2016).

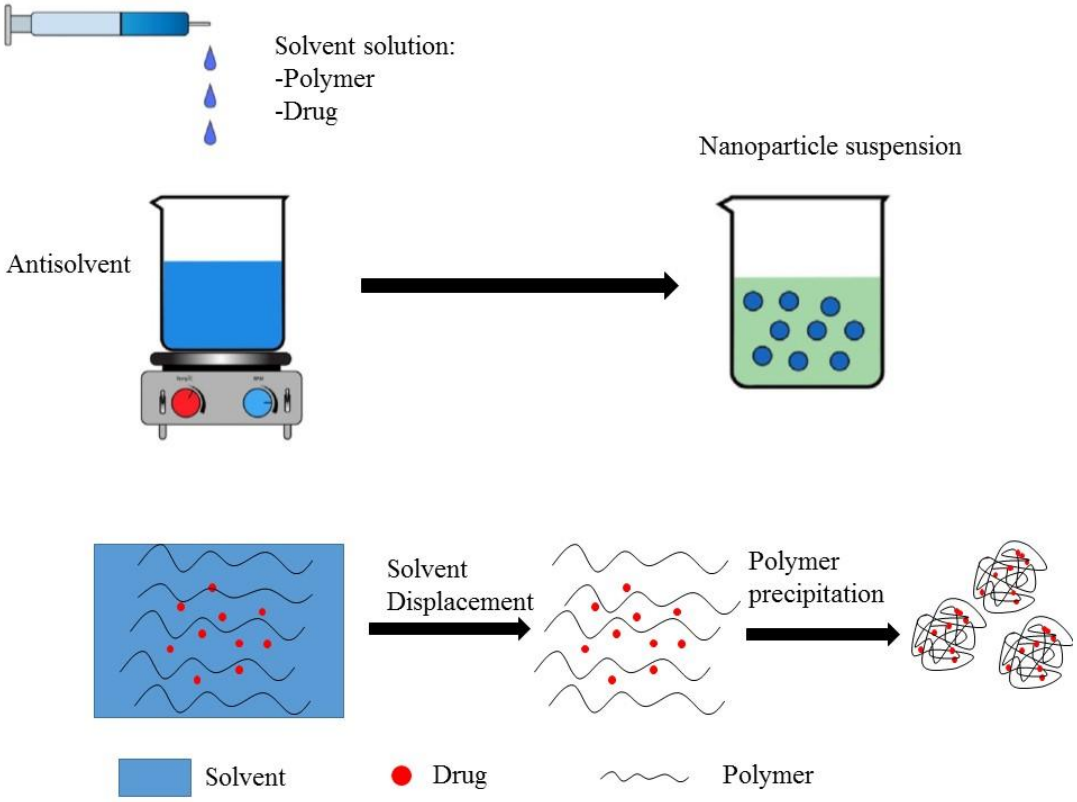

Figure 2.8. Formation of nanoparticles by solvent displacement.

Several polymers have been successfully employed for particle production by solvent displacement. They include carbohydrates such as starch and chitosan (Luque-Alcaraz et al., 2016; Qin et al., 2016), proteins such as gelatin (Quiroz-Reyes et al., 2014), polyesters such as PCL and PLA (Bazylińska et al., 2014; Mazzarino et al., 2012), polyethers such as PEG, polyacrylates such as Eudargit (Averina and Allémann, 2013) and block copolymers (Şimşek et al., 2013).

The overall precipitation process can be divided into three steps i.e. supersaturation, nucleation, and growth (Joye and McClements, 2013). The supersaturation condition occurs when the polymer concentration is above the saturation one for the given solvent; the addition of a bad solvent indeed sharply decreases the solvent potency of the solvent to dissolve the polymer. Being supersaturation a non-equilibrium condition, the nucleation phenomenon occurs for the system to gain stability. Thereafter, primary nuclei are formed and their size increase through a growth step until the solution is depleted from the polymer molecules and a new equilibrium condition is reached. The extent of nucleation and growth phenomena determines the particle size. In facts, if the nucleation mechanism dominates over the growth one, a large number of particles with small size are formed. Oppositely,

in the case of the dominant growth mechanism, the formation of a small number of large particles is observed (Joye and McClements, 2013; Miladi et al., 2014).

The extent of the two phenomena depends both on solution properties and operational parameters. The diffusion rate of the solvent in the antisolvent influences the precipitation time; for high diffusion rates, the precipitation of the fast particles hinders the growth leading to small particle size (Asadi et al., 2011; Budhian et al., 2007). The addition of a surfactant to the antisolvent was already mentioned as a strategy to prevent particle aggregation. It was also evidenced that increasing the surfactant concentration in the proper range allows having fine particles due to the hindering of particle growth exerted by surfactant molecules (Contado et al., 2013). The increase in polymer concentration is associated with the increase of the particle size. In fact, the high viscosity of the concentrated polymer solution causes the mixing to be less efficient and reduces the extent of nucleation (Badri et al., 2017). For the same reason, the increase in the polymer MW is commonly related to higher solution viscosity and coarser particle size (Holgado et al., 2012).

The extent of encapsulation is mostly affected by both the drug and polymer concentration in the organic solvent stream. Increasing polymer concentration improves the polymer capability to incorporate the active substance. Oppositely, increasing the drug concentration may cause to overcome the polymer incorporation capability and to cause the drug migration in the bath (Dong and Feng, 2004). Similarly, the increase of the antisolvent volume increases the amount of drug that can be solubilized causing losses inside the aqueous bath (Budhian et al., 2007; Limayem Blouza et al., 2006).

Compared to other encapsulation methods, the solvent displacement method displays considerable advantages. Firstly, it is operatively simple and displays good results reproducibility; these features significantly ease the scale up. In terms of product quality, it allows to produce particles with low diameter, narrow size distribution and high encapsulation efficiencies. Finally, nanoprecipitation has good environmental compliance since neither significant amounts of organic solvent nor high energy consumption are required (Lassalle and Ferreira, 2007). Nanoprecipitation has been identified as a simple and effective technique for encapsulation of poorly water soluble drugs.

The nanoparticles obtained by the nanoprecipitation method have been tested in vivo and underwent preclinical and clinical trials for the treatment of different diseases. As reported in Figure 2.9 such formulations have been administered by different routes to treat various organs.

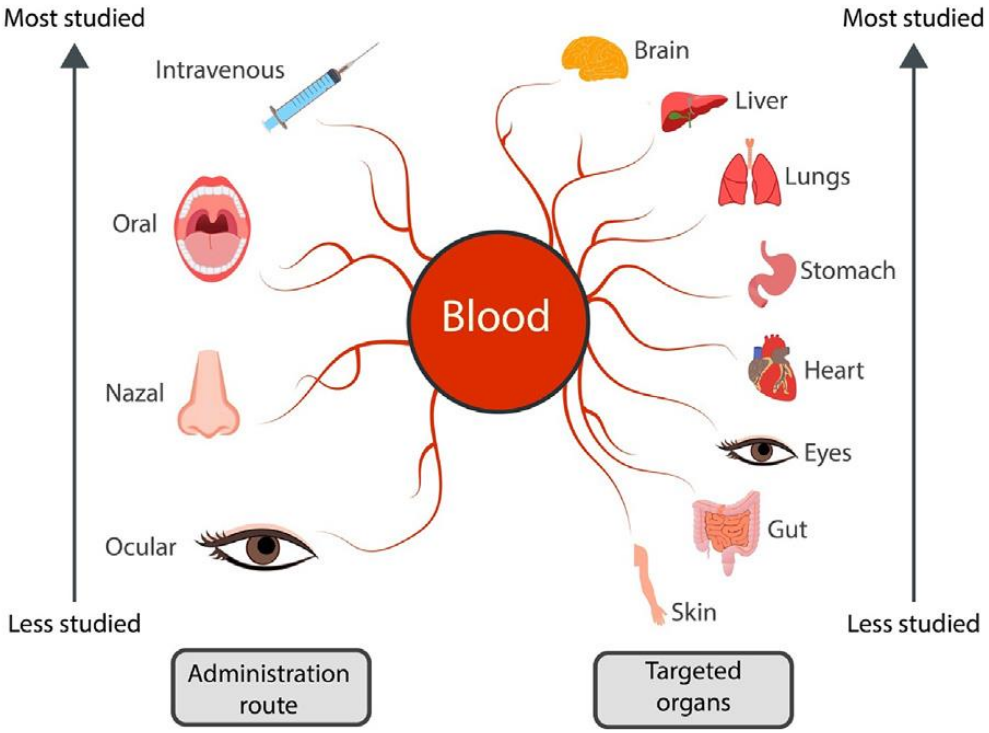

Figure 2.9. In vivo and clinical application of nanoparticles produced by Nanoprecipitation reprinted from (Martínez Rivas et al., 2017).

Among the various tissues, the skin is the least studied therapeutic target of particles produced by nanoprecipitation methods. Moreover, among the different administration routes, the transdermal one is still unexplored. This fact together with already mentioned advantages of the solvent displacement method makes it a novel good candidate for the production of nanoparticles for transdermal release and biofunctional textile production. In particular, in recent years, a novel approach to the solvent displacement method called Flash Nanoprecipitation was proposed (Johnson and Prud'homme, 2003).

2.5 The Flash Nanoprecipitation technique

The flash nanoprecipitation technique is a modified version of the classical solvent displacement method previously presented. In this method, the solvent and the antisolvent are mixed in small appositively designed mixers as sketched in Figure 2.10 (Martínez Rivas et al., 2017).

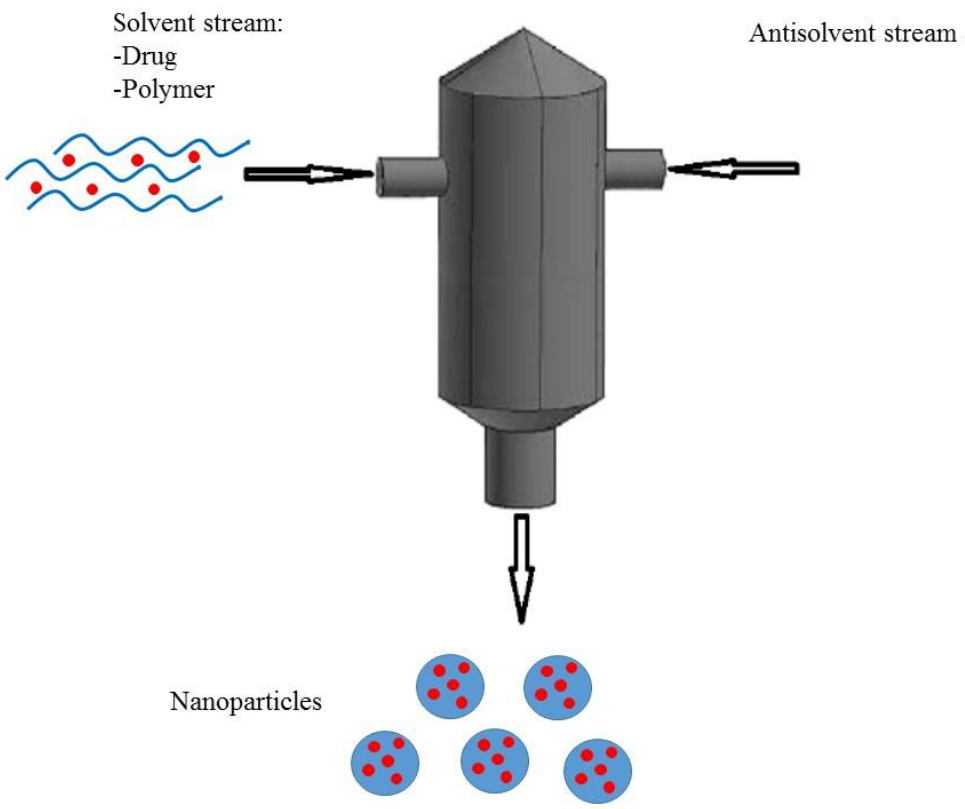

Figure 2. 10. Schematic representation of a particle production process by Flash Nanoprecipitation.

Upon mixing the polymer solution with the antisolvent, the nanoparticles are formed and ejected from the mixing device. Such an approach preserves all the mentioned advantages of nanoprecipitation while displaying further advantages. FNP allows to significantly reduce the mixing time to the order of milliseconds. Moreover, the mixing efficiency in the microreactors is generally superior to that occurring in mechanically agitated beakers or tanks (Gindy and Prud'homme, 2009).

The particle formation mechanism is represented in Figure 2.11, the polymer concentration is described as a function of time over the fundamental steps of the FNP. At the beginning of the process, the two streams are mixed, causing the polymer concentration to quickly rise and supersaturation to occur. This supersaturation is a necessary condition for the precipitation. The degree of supersaturation is defined as the ratio of the actual concentration of the polymer and its bulk solubility in the solvent (Di Pasquale et al., 2012).

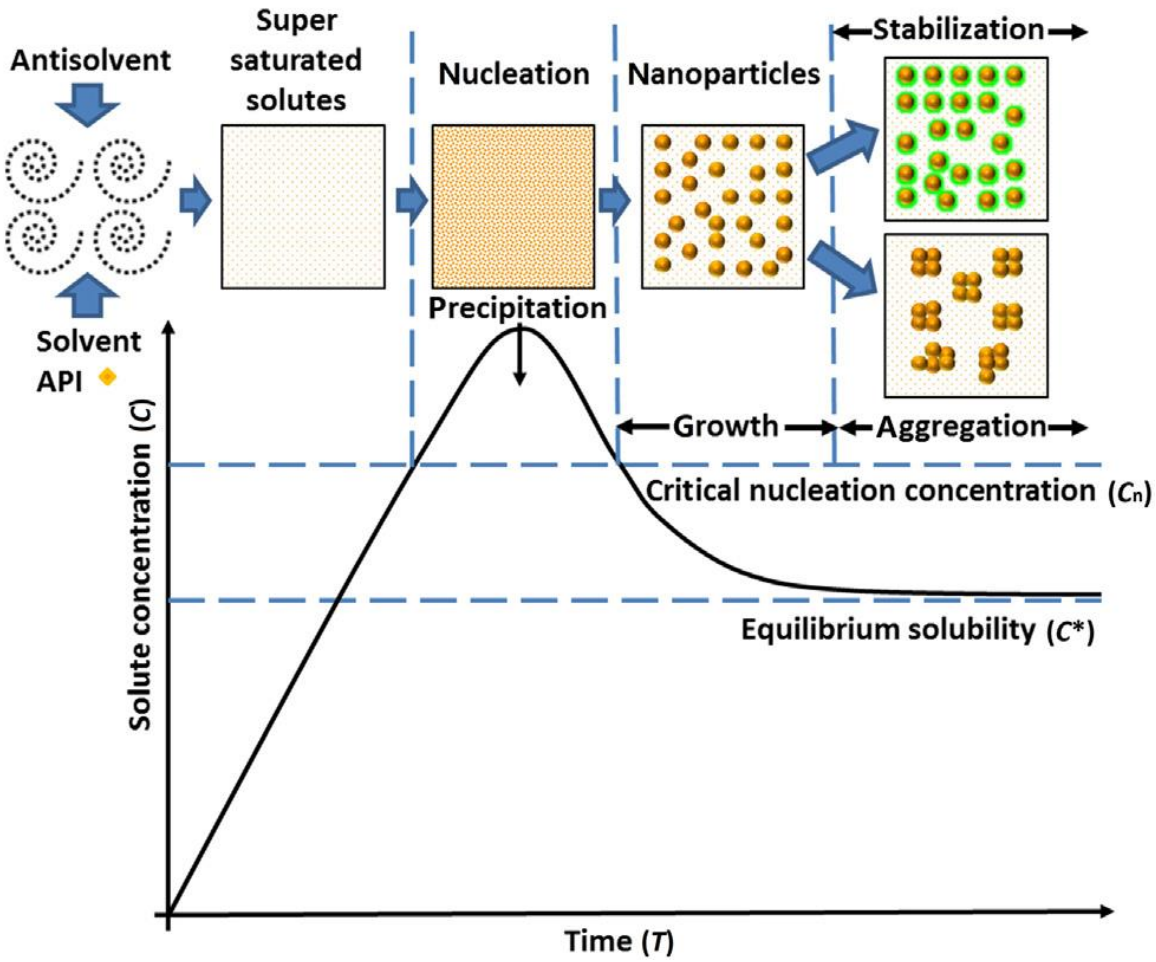

Figure 2. 11. Particle formation by FNP seen as a function of concentration over time (Tao et al., 2019).

The supersaturation induces the formation of polymer nuclei. The nucleation rate was correlated with several properties of the system such as the diffusivity of the organic solvent in the antisolvent, the temperature, the surface tension between the solid and the liquid and the supersaturation degree (D'Addio and Prud'homme, 2011; Mersmann, 1999). The formation of the nanoparticles was also explained to occur because of the self-assembly of the polymer upon decreasing the solvent quality. This phenomenon leads to the formation of very fine particles and it occurs in competition with the particle nucleation(Johnson and Prud'homme, 2003).

Upon nuclei formation, the polymer concentration in the solution decreases below the critical saturation concentration freezing the nucleation phenomenon. However, the polymer molecules are still present in the solution at a concentration greater than the equilibrium saturation. Therefore, the polymer molecules tend to migrate to the surface of the freshly formed nuclei. Such a phenomenon is defined as molecular growth and is often a diffusion-limited stepwise process. Factors affecting the growth rate are polymer concentration and molecular weight. Saad inquired about the effects of precipitating PCL of different molecular weights while keeping constant concentration. He observed

an increase in particle size upon increasing the polymer MW (D'Addio and Prud'homme, 2011; Saad, 2007).

Simultaneously to molecular growth, particle aggregation occurs. The aggregation phenomena sensibly occur in the particles whose are not stabilized either sterically or electrostatically and is correlated to the frequency of collisions among the particles (Saad and Prud'homme, 2016). An increase in the supersaturation level causes a significant increase in the nucleation rate while it scarcely affects the growth rate. As for nanoprecipitation, a high nucleation rate results in small size nanoparticles, modulating the supersaturation level is the primary strategy to achieve control over the particle size.

A second critical factor is the mixing efficiency (Ferri et al., 2017). Indeed, the processes of mixing, nucleation and growth occur in series and the overall process outcomes are dictated by the slowest one. Being the mixing process slower than the nucleation one, the generation of nuclei is governed by the mixing step. Poor mixing results in the scarce generation of nuclei leading to coarser particle production. However, mixing also exerts a dilution effect which decreases the supersaturation, therefore it displays two conflicting effects.

The interactions between the polymer and the solvent are of significant importance in the initial particle formation steps when strong concentration gradients are imposed by the fast and intensive mixing. In the case of acetone and water mixtures, it was evidenced how the nanoclustering phenomenon occurs and that the organic solvent tends to locate itself close to the polymer chain (Di Pasquale et al., 2014).

Several studies explained the formation of the particles as a consequence of the mechanical instability induced by the turbulence at the interface between solvent and antisolvent. According to this theory, the solvent flux is broken down in fine droplets that keep breaking down in smaller ones. This chain breakage process goes on until solvent microdroplets surrounded by the antisolvent are formed. Thereafter, the solvent diffuses away inducing polymer precipitation (Quintanar-Guerrero et al., 1997; Thioune et al., 1997).

When oils are dissolved in the organic solvent the formation of the particles can be attributed to a self-emulsification phenomenon denominated Ouzo or Louche effect. In this case, the hydrophobic solute is brought in the metastable region of the phase diagram between the bimodal and spinodal curve (Solans et al., 2016). The nanocapsules production is achieved by the formation of oil droplets by the Ouzo effect followed by their coverage by the polymer molecules (Ganachaud and Katz, 2005).

2.5.1 Factors influencing particle properties

The inlet flow rate (FR) is found to be a crucial parameter in affecting particle size. Several authors reported that increasing flow rate the average particle diameter decreases (Chow et al., 2015; Ferri et al., 2017; Zelenková et al., 2014). Such trends are generally explained by considering that increasing the inlet flow rate makes the mixing to be more efficient. As previously stated, mixing is the rate determining step in the process series. Therefore, effective mixing velocity promotes high nucleation rates, leading to fine particles (Di Pasquale et al., 2014).

As observed for the regular nanoprecipitation process, the increase of polymer concentration generally leads to higher particle size. Higher polymer concentration increases the solution viscosity, lowering the mixing efficacy and hindering nucleation. The polymer molecular weight displays a significant role in particle size (Zhang et al., 2012). Indeed, it increases the growth rate. Moreover, Saad proved experimentally that it increases the particle size (D'Addio and Prud'homme, 2011; Saad, 2007). Block copolymers have been widely exploited in the context of FNP technology. For such materials, the effect of molecular weight on particle size has been assessed taking into account both the chain length and polarity of every single block (Chow et al., 2015).

Concerning the addition of surfactants to the formulation, several effects have been observed. Some authors reported that the surfactant addition caused a reduction of particle size. Moreover, a decrease in particle size was observed by increasing surfactant concentration from 0 to 1% by weight (Goodman et al., 2018). Such results are easily explainable as the surfactant can exert a stabilizing effect over the particles and thus reduce aggregation phenomena. However, some authors also reported no significant correlation between surfactant concentration and particle size (Ferri et al., 2017; Zelenková et al., 2018). Indeed, the effect of surfactants is strongly correlated to the nature of surfactant as it chemically interacts with the polymer species. Other particle properties that are affected by surfactant concentration are the Zeta potential and encapsulation efficiency. The Zp tends to change acquiring the polarity of the surfactant itself (Chow et al., 2015; Zelenková et al., 2018). It was observed that the addition of a surfactant caused the decrease of EE for poorly water soluble drug encapsulation. This is because the surfactant enhances the water solubility of the drug causing it to partition more toward the liquor than the particles.

A common strategy to limit the excessive growth and aggregation of nanoparticles consists of quenching the particles exiting the mixer by collecting them in a vial filled with a precise volume of antisolvent. It was reported that increasing the volume of quenching water the average particle size decreases. (Zelenková et al., 2015, 2014). This trend can be explained taking into account that the

particle growth and aggregation occur in a given window of solute concentration (Figure 2.11). The quenching sharply decreases the solute concentration below the values for which molecular growth occurs, therefore not enough time is allowed for polymer chains to grow on the formed nuclei. Moreover, aggregation is also hindered by dilution which limits the particle frequency of collision necessary for aggregation.

2.5.2 Reactors and Mixers for Flash Nanoprecipitation technology

Since mixing efficiency is a crucial factor in determining the properties of the particles, several reactor designs have been proposed over the years. The different mixer shapes and designs are summarized in Figure 2.12.

Mixing at the microscale can be obtained by two approaches i.e. passive and active mixing. In the first case, the mixing flow energy is provided by the hydrostatic pump action. Differently, in active mixing, an external source of energy such as ultrasound and magnetohydrodynamic action induces a periodic variation of flow rate.

For FNP technology passive mixing is preferred since it allows precise regulation of the solvent and antisolvent flow rates (Lince et al., 2008). To achieve high turbulence levels and short mixing times, special microdevices such as the confined impinging jet mixer (CIJM), the multi inlet vortex mixer (MIVM), the T mixer and Y mixer have been proposed. The T mixer is the simplest design, it consists of two inlet pipes and an outlet pipe perpendicular to the inlet ones, no mixing chamber is present. The performances of the T mixers of different size and the characteristic mixing times have been investigated both experimentally and numerically (Schwarzer et al., 2006). The Y mixer has very similar to the T one. The main difference between the two is that in the Y mixer the angle between the inlet tubes is 160° instead of 180° (Choi et al., 2005).

The Multi inlet vortex mixer is characterized by a mixing chamber where the inlet pipes are connected tangentially. The pipes can be either 2 (MIVM-2) or 4 (MIVM-4). The main advantage of the 4 inlet vortex consists of its versatility. Indeed, it is possible to mix in the reactor chamber several inlet streams with different compositions and also feed different fluids with different flow rates. Such an approach was mainly exploited to tune particle properties and obtain the desired surface decorations; moreover, it allows to increase the supersaturation level by increasing the antisolvent/solvent ratio (Liu et al., 2008; Saad and Prud'homme, 2016).

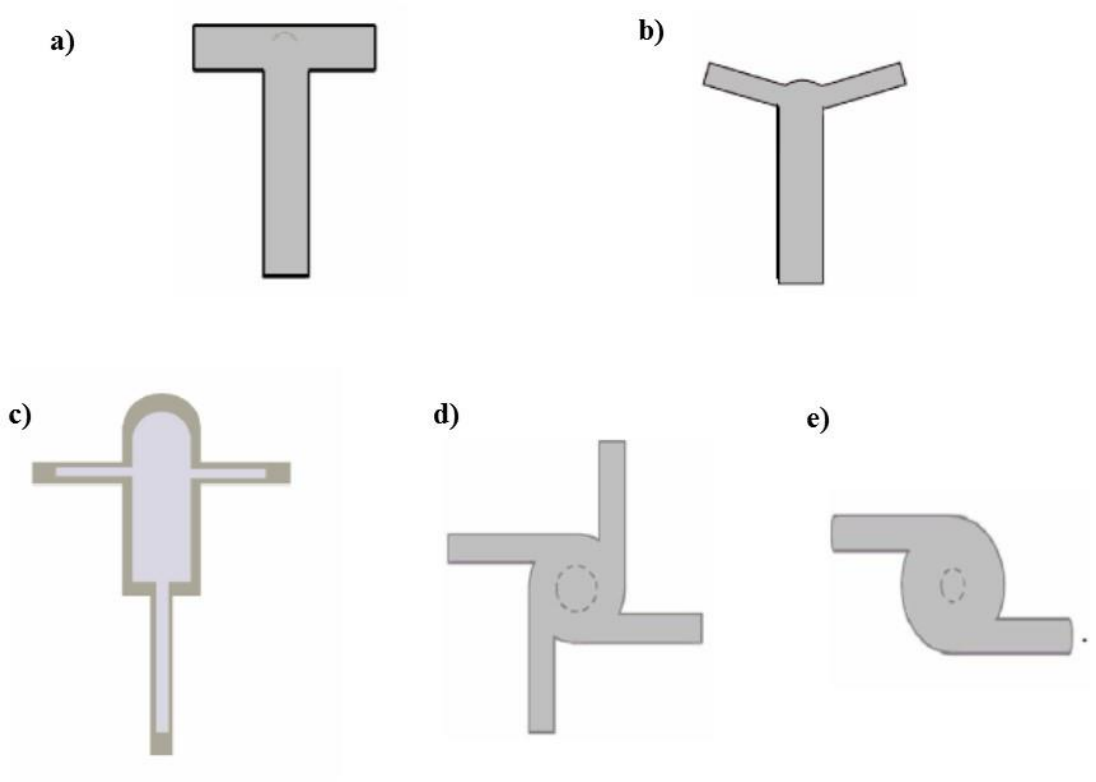

Figure 2. 12. Scheme of the mixer employed in FNP technology: a) Side view of T mixer b) Side view of Y mixer c) section view of CIJM d) Upper view MIVM 4 inlets e) Upper view MIVM 2 inlets.

The confined impinging jet mixer consists of two inlet tubes who directly inject the streams in the reactor chamber where the jet collision occurs. The reaction chamber generally has a 5 mm diameter and its height is greater than the one of the MIVM one. The CIJM provides the highest mixing efficiency among the presented devices, this is due to the high degree of turbulence generated when the two jets collide. Indeed, CDF studied proved that the mixing time is of the order of milliseconds (Gavi et al., 2007; Valente et al., 2012). Several modifications of CIJM have been proposed in the literature.

The Roughton mixer is characterized by a vertically extended mixing chamber typical of the CIJM with tangential inlet tubes (Lindenberg et al., 2008). Unger et al (1999) proposed a modification of CIJM with V entering tangential streams. Such geometry allows achieving efficient mixing while eliminating the dead regions at the bottom of the mixer for better mixing homogeneity. Recently a hand operated CIJM was proposed by Han et al. (2012) such a device presents the advantage of operating with small volumes and therefore is particularly suitable for laboratory formulation studies.

2.5.3 Nanoparticles produced by Flash nanoprecipitation

In the last decade, the significant interest aroused in the production of drug loaded nanoparticles by the FNP technique. A partial summary of experimentation conducted is reported in Table 2.2 where the polymer, the encapsulated drug and the smallest achieved particle size are reported.

Table 2.2. Characteristics of the nanoparticles produced by FNP.

Polymer	Drug	LogP	Size (nm)	Reference
PEG-PLA	β-Carotene	15.2	55	(Han et al., 2012)
PEG-PLA	Curcumin	4.1	70	(Chow et al., 2014)
PEG-PLA	Vitamin D3	7.1	100	(Lalloz et al., 2019)
PEG-PLA	Doxorubicin	1.3	100	(Tam et al., 2016)
PEG-PLA	Itraconazole	6.2	120	(Wan et al., 2018)
PEG-PLGA	Schisanterin	4.9	70	(T. Chen et al., 2017)
PEG-PLGA	Paclitaxel	4.7	122	(Zhu, 2014)
PEG-PLGA	β-Carotene	15.2	110	(D'Addio et al., 2010)
PLGA	Curcumin	4.1	250	(Shen et al., 2013)
PLGA	Florfenicol	2.8	100	(Turino et al., 2018)
PCL	Florfenicol	2.8	230	(Turino et al., 2018)
PCL	Menthol	3.2	200	(Ferri et al., 2017)
Soy Lecithin	Cyclosporine A	3.0	180	(Chiou et al., 2008)
Lecithin	Clofazimine	7.7	170	(Zhang et al., 2017)
Zein	Clofazimine	7.7	240	(Zhang et al., 2017)

Several authors employed block co-polymers in the production of NPs. However, some experiments in which homo-polymers and naturally sourced polymers were precipitated have also been reported.

By employing block co-polymer very fine particles were produced. Since many articles reported the production of nanoparticles as carriers for anticancer drugs administered parenterally, it is of primary importance to keep the particle diameter below 200 nm to avoid the risk of embolization (Hickey et al., 2015). Homopolymers, either of natural and synthetic origin have been reported to produce particles with a slightly bigger size, i.e between 200-300. Such materials have therefore been proved to make possible the production of nanocarriers that satisfy the size constraint of transdermal release. The bigger diameter obtained with these homopolymers is counterbalanced by their higher availability and lower commercial price.

The LogP is used as an index as drug polarity. By observing the high values of LogP for the drug incorporated by FNP, it can be concluded that this technique has mostly been employed for the incorporation of lipophilic and poorly water soluble drugs. Such fact is indeed not surprising taking into account that the drug should not diffuse easily in water used as antisolvent to achieve high encapsulation efficiencies. Oppositely not extensive research has been conducted on the encapsulation of hydrophilic substances by FNP.

Among the presented encapsulations techniques, FNP has been proven to be of significant interest. Indeed, it allows fast and simple production of nanoparticles. It has high scalability potential given the possibility of implementing significant production by making several reactors run in parallel. Moreover, a good understanding of the precipitation mechanism achieved both using experimental and numerical studies allows to finely control the process to achieve the desired nanoparticle properties.

Part I Final remarks

The literature analysis conducted in the state of the art clarified the current issues in the context of textile materials for dermatological applications. The discussion about the advantages of transdermal delivery together with the identification of the current limitations of the transdermal delivery technologies highlighted the interest in the development of a textile based skin delivery device. The literature review about the nanocarriers developed for transdermal applications evidenced the suitability of this nanotechnology based approach to effectively promote the skin permeation of the drug. Moreover, such a discussion pointed out the main requirements that the nanocarriers for transdermal release need to fulfill in terms of size and polarity.

The presentation of the biofunctional textile technology highlighted the previous efforts of the scientific community in integrating pharmaceutical carriers with textile fabrics. It emerged that carriers employed in such technology not only need to be suitable to be employed in finishing treatment but also have to be producible by a cost effective method in quite large batches to meet the requirements of the textile industry.

To achieve the desired nanocarriers properties while meeting the productivity required for textile finishing applications, the encapsulation processes of potential interest were critically evaluated. The flash nanoprecipitation process aroused significant interest due to its simplicity and scalability combined with its capability of fastly producing nanoparticles with nanometric size. The possibility of using the FNP technique to prepare nanocarrier to be employed in a textile mediated transdermal delivery was however never reported.

The present thesis tested this possibility with an experimental approach. Nanoparticles synthesis methods as well as textile finishing approaches were developed and evaluated in terms of efficacy in producing biofunctional textiles which own the potential of benefiting the user's health.

Part II The materials and the methodologies employed

Chapter 3: Materials and methods

3.1 Materials and chemicals

The principal materials employed in the present work consisted of Polycaprolactone, used as shell material for the nanoparticle production and the three drugs to be encapsulated i.e. melatonin, caffeine and curcumin.

The PCL was selected as a hydrophobic and biodegradable polymer for the nanoparticle production and the encapsulation of the active principles. The PCL employed in the experiments was supplied in the form of flakes by Sigma Aldrich. As declared by the producer it owned a Molecular Weight of 14000 Da assed by gel permeation chromatography (GPC).

Melatonin was employed for preliminary studies about drug encapsulation and release; it was identified as the model substance for medium hydrophilicity drugs. The melatonin used in the present study was purchased by Sigma Aldrich. The chemical was supplied in the form of white powder with a purity ≥ 98% assessed by thin layer chromatography (TLC) as specified by the supplier.

Caffeine was chosen as the model for hydrophilic active principles and used to investigate the performances of the proposed system to incorporate this kind of actives. For the experimental trials, caffeine in the form of anhydrous powder was used. The reagent was obtained from Sigma Aldrich and had a purity grade >95%.

Curcumin was selected as the model substance for hydrophobic drugs. This substance was acquired from Sigma Aldrich in the form of powder from the Curcuma Longa plant. As declared by the supplier the reagent had a purity ≥ 65% assessed by high performance liquid chromatography HPLC.

The other materials employed for the manufacturing and analysis of the nanoparticles produced in the thesis have been listed in the next lines. All chemicals were purchased from Sigma Aldrich and used as received unless otherwise specified.

The following chemicals were used:

- Sodium chloride anhydrous ≥ 99%, potassium chloride ACS grade ≥ 99.5%, sodium phosphate dibasic dehydrate ≥ 99%, and potassium dihydrogen phosphate ACS reagent ≥ 99% for buffer preparations
- Porcine ears for transdermal penetration test supplied by a local butcher;
- Acetone (purity ≥ than 99.5% in compliance with European Pharmacopeia standard);
- Acetonitrile (HPLC grade purity ≥ 99.9%);

- Tetrahydrofuran (THF) (reagent grade purity ≥ 99%);
- Absolute ethanol ACS grade purity ≥ 99.5%;
- Ultrapure produced using a Milli-Q RG system by Millipore R (Billerica, MA, USA).
- For spin trapping reactions, 5,5-dimethyl-1-pyrroline N-oxide (DMPO) with assay ≥ 97%, dimethyl sulfoxide with purity ≥ 99%, hydrogen peroxide 30% in H_2O ACS reagent and iron (II) sulfate with purity > 97%.
- Technical grade Nile red was used for fluorescent marking.
- Potassium Iodine was employed for zeta cad analysis.
- Knitted cotton fabrics (100% cotton, Nm 30/1, single jersey) were kindly gifted by Eusebio S.p.A (Italy).

3.2 Materials preparation and manipulation

3.2.1 Particle production

PCL particles were produced by flash nanoprecipitation in a confined impinging jet mixer (CIJM). The CIJM has the following geometrical characteristics: 1-mm diameter inlet tube, 5-mm diameter chamber, 11.2-mm chamber height, and a 2-mm diameter exit tube, 40-mm length exit tube. The solvent and antisolvent solution were prepared by dissolving the proper amount of substances either in the organic solvent or in water respectively. Acetone was mainly used as the solvent for PCL, few preliminary tests were also run by using acetonitrile and THF. All the drugs were dissolved in the organic solvent. For caffeine, as it has a hydrophilic nature, some formulations were prepared by dissolving it in water. The solvent and antisolvent solutions were placed into 100-ml syringes. The syringes were placed on a KDS200 syringe pump (KD Scientific, Holliston, MA, USA) and connected to the mixer through plastic tubes. The syringe pump controlled the inlet flow rate of the streams and the volume of injected solutions. A vial containing water, placed under the reactor exit tube, collected the exit stream to quench the freshly formed particles. The amount of water in the collecting vial was adjusted to achieve the proper quenching ratios QR defined in Equation 3.1.

$$QR = \frac{V_S}{V_Q} \tag{3.1}$$

Where V_s is the volume of solutions fed to the reactor and V_Q is the volume of quenching water, both expressed in mL. The overall particle production system is shown in Figure 3.1.

Figure 3.1. Nanoparticle production set up. The main elements highlighted are a) the syringe pump, b) the CIJM mixer and c) the collecting vial with quenching water and magnetic stirrer.

The collecting vial was kept under magnetic stirring to limit particle aggregation. Once produced, the prepared nanoparticles were processed for different analyses.

3.2.2 Particles manipulation

The nanoparticles underwent different post-processing procedures to be properly analyzed. Solvent removal was performed in a rotary evaporator RE 300 (Buchi, Switzerland). The NP suspension was weighted to roughly estimate the weight of the solvent to remove. The formulation was then processed under vacuum at 45 °C to ensure solvent evaporation. The operation was monitored by weighing the suspension periodically until the solvent was completely evaporated. After solvent removal, the suspension initial volume was restored by adding water.

NP separation from the liquid phase was achieved either by centrifugation or filtration. Centrifugation was performed in an SL 16 centrifuge by Thermo Scientific (Langenselbold, Germany). Screw sealed falcon tubes of 12 mL volumes were used. Centrifugation time and speed were adjusted to achieve effective particle separation. After centrifugation, the supernatant was removed by a pipette. Particle filtration was performed by using a syringe driven cellulose filter with a porosity of 0.2 µm. The particles separated by centrifugation were dried overnight at 40 °C.

3.2.3 Textile functionalization

Textile functionalization was done either by imbibition or cold impregnation protocols. The main objective was to apply the NPs suspensions onto the fiber surface by employing easily scalable methods. The interaction between the NPs and the fibers was desired to be weak to allow the particle release when in contact with the skin.

Imbibition consisted of a drop-by-drop deposition of a controlled volume of particles suspension onto the textile surface by using a micropipette. The fabric was dried between each drop deposition to ensure complete pick up of the finishing agent and precise control of the deposited dosage.

In the impregnation method, instead, the fabrics were dipped in the particle suspension until uniformly wet. Thereafter, they were fast rinsed with ultrapure water to avoid aggregation of particles on the fabric surface. The procedure for textile imbibition and impregnation are graphically sketched in Figure 3.2.

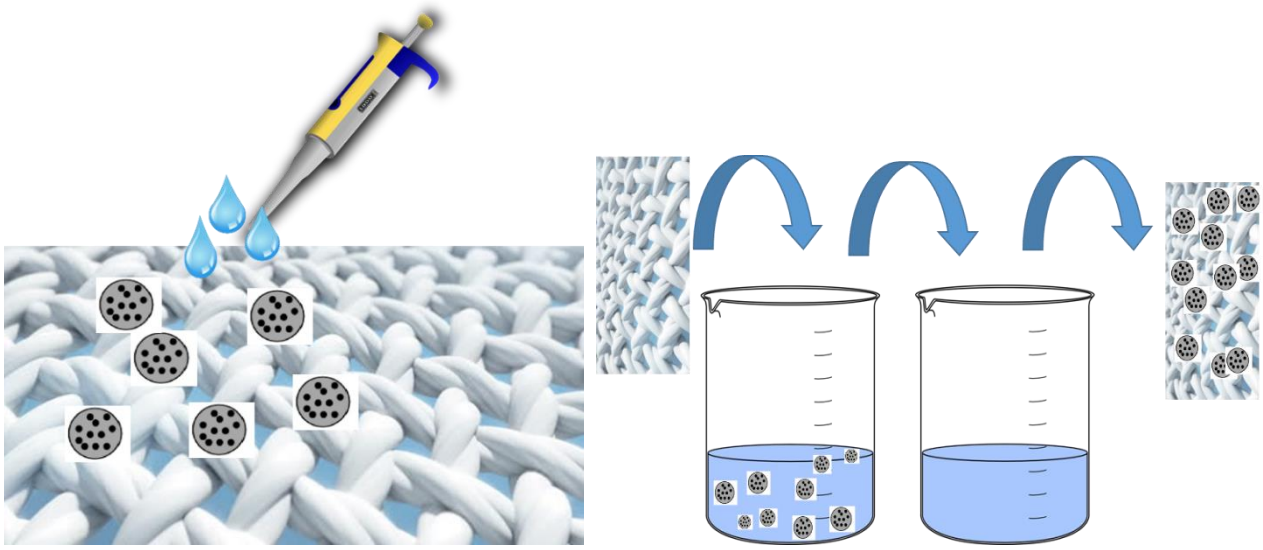

Figure 3.2. Textile functionalization methods: imbibition (right) and impregnation (left).

3.3 Materials characterization and analytical techniques

3.3.1 Particles size and zeta potential

Particle size distribution (PSD) was measured by Dynamic light scattering (DLS) technique. This property is of significant importance in the design of a transdermal release system. Indeed, particles

are required to have small siameter to successfully cross the skin barrier. The measurements were performed on a DLS Zetasizer Nanoseries ZS90, Malvern Instruments (Malvern, UK). For particle size analysis, disposable 3 mL polycarbonate cuvettes were employed. The Malvern General Purpose non-negative least squares analysis was selected as the algorithm for the calculation of PSD since it is known to suit the majority of samples whose size is not known a priori.

Zp is defined as the electrical potential at the slipping/shear plane of a colloid particle moving under the electric field and is commonly used as a measure of particle surface charge (Kaszuba et al., 2010). Moreover, Zp is commonly used as an index of colloidal stability. Low absolute values of the Zp hint scarce colloidal stability of the system, for absolute values of zeta potential above 30 mV the system is considered to be highly stable (Bhattacharjee, 2016).

Moreover, in the context of transdermal delivery, the surface charge of the carrier is known to impact skin penetration; therefore, Zp is a crucial parameter. The same DLS machine used for PDS analysis was used for the Zp measurement, the. U-shaped capillary cuvettes equipped with copper electrodes were employed for the measurement. The Henry equation, with Smoluchowski approximation, was used to get the zeta potential from the measurement of the electrophoretic mobility (Ohshima, 2013). For both PDS and Zp analyses, the particle suspensions were diluted with water in a 1:10 ratio. The temperature of the sample was kept steady by the DLS machine, the temperature setpoint was 25°C.

3.3.2 Drug quantification: Loading Capacity and Encapsulation Efficiency

In drug loaded nanoparticle production it is of primary importance to assess the amount of active principle incorporated in the polymer system. To assess the quality of the nanoparticle production two main properties are defined: the loading capacity (LC) and the encapsulation efficiency (EE). LC is the parameter that describes the percentage of loaded drugs respect to the overall mass of the nanoparticle system as reported in Equation 3.2.

$$LC = \frac{m_{en}}{m_{tot}} \times 100 \qquad (3.2)$$

Where m_{en} is the mass of encapsulated drug while m_{tot} is the total mass of the particle system (drug plus polymer). Knowing and controlling the LC is necessary to administer an effective therapeutic dosage of the active principle. The LC values should indeed be as tunable as possible to achieve correct dosage administration.

EE is instead defined as the amount of drug encapsulated respect to the amount of drug fed in the encapsulation process (Equation 3.3).

$$EE = \frac{m_{en}}{m_{in}} \times 100 \quad (3.3)$$

Where m_{in} is the mass of drug fed to the encapsulation process. In Equation 3.2 and 3.3, the values of masses are expressed in mg while the EE and LC values are expressed in percentages. The value of EE is an important parameter to assess the efficiency of the encapsulation process and therefore it should be as high as possible.

To quantify the amount of drug incorporated and calculate the values of EE and LC, two approaches where proposed i.e. the direct and the indirect ones. The direct analysis was conducted on dried NPs: a sample was weighted and thereafter dissolved in a proper solvent. The amount of drug in the obtained solution was quantified by spectroscopic methods. The indirect method consisted in separating the supernatant from the nanoparticles, then, the amount of drug in the supernatant was quantified by a proper analytical technique to measure the amount of not encapsulated drug. The incorporated drug was therefore calculated by difference and so were the EE and LC values. Concerning the quantification of the active principles in the solution, it was achieved either using UV-Visible spectroscopy or Fluorescence spectroscopy.

UV-visible spectroscopy was employed to measure the concentration of all three drugs. The analyses were performed on a spectrophotometer 6850 UV/Vis Jenway (Stone, Staffordshire, UK). The type of cuvette (PMMA or quartz) was selected on the base on the absorbance peak wavelength of the analyte and solvent nature. Even though UV-Vis spectroscopy is a fast and simple analytical tool, it may display some drawbacks. Indeed, for a colloidal system, it is known that the particles may absorb light at wavelengths similar to the ones of the particle diameter. Such a phenomenon, named Tyndall effect, may bias the spectrophotometric measurement (Heller et al., 1946). This bias on drug quantification due to the Tyndall effect is more significant when particle size is close to the absorbance peak wavelength of the analyte. Therefore, the quantification protocols based on spectrophotometric measurements were adjusted on the basis of the particle size and of the analyzed drug.

Fluorescence spectroscopy was employed for curcumin quantification. Such a technique permits to collect the emission spectrum of a fluorophore and correlate it with its concentration. Being the fluorescence emission a peculiar phenomenon of the analyte, the colloidal nature of the sample does not interfere with the measurement. Therefore, the analysis is not biased by the Tyndall effect. An

RF-551 Spectrofluorometer (Shimadzu, Kyoto, Japan) was employed. the analysis was performed using a quartz cuvette, a fixed wavelength of 422 nm was used for excitation.

3.3.3 X-ray photoelectron spectroscopy

X-ray photoelectron spectroscopy (XPS) was used for the compositional analysis of the material surface. Such a technique provides information about the elements present in the material surface and their binding state. By detecting the binding energy, it is possible to identify the chemical element and the chemical bond to which it took part. The photon penetration regards the first atomic layer of the materials. The analysis was conducted on the caffeine loaded nanoparticles using an XPS Versa Probe 5000, PHI Electronic (Chanhassen, MN, USA) instrument.

The system was equipped with a dual charging neutralization guns. They consist of an electron gun combined with and argon ion gun, at low energy, to minimize the charging effect during data acquisition. The same Argon gun was employed during the depth profile analyses. Particularly it was employed to perform the surface etching of the sample, with a rate of 5.9 nm/min. The etching procedure was performed simultaneously with the scanning to obtain a real time compositional analysis of the first atomic layers of the samples.

3.3.4 Attenuated total reflectance Fourier transform infrared spectroscopy

Infrared spectroscopy was performed to obtain information about the chemical composition of the samples in terms of functional groups. The Fourier transform infrared spectroscopy was conducted in attenuated total reflectance mode (ATR-FTIR) to minimize the signal to noise ratio and simplify sample handlings. The analysis was performed both on the NPs, upon separation and drying, and on the textile samples. The penetration thickness of infrared radiation for the ATR set up was of 0.5-2 μm. Therefore, this analysis was used to investigate the bulk composition of the materials. A Nicolet Nexus (Thermo Fisher Scientific, Villebon Sur Yvette, France), infrared spectrometer, connected to a PC was employed. Samples were placed on a ZnSe crystal for the analysis, particular care was taken to assure the full contact between the sample and the crystal to minimize biases due to air in the measurement. The spectra were collected in absorbance mode, using a 254 scan for each sample, the resolution was 1 cm^{-1}.

3.3.5 Electron paramagnetic resonance spectroscopy

The electron paramagnetic resonance spectroscopy (EPR) is a spectroscopic technique used to analyze paramagnetic species i.e. chemical substances in which an unpaired electron is present. The working principle of EPR is analogous to the one on H-NMR spectroscopy apart that the exited subatomic species are the electron spins instead of the nuclei. The spin excitation is obtained by applying a magnetic field to the sample. The applied magnetic field increases the energy gap between the positive and negative spin states. Since unpaired electron transit between the positive and negative spin state by absorbing or emitting an amount of energy equal to the gap between the states, the increase of the energy gap due to the magnetic field application records this electronic transition and detect the paramagnetic species. In the context of this thesis, the EPR spectroscopy was used for the analysis of radical oxygen species which are known to be the cause of several skin illnesses. Indeed, an EPR based method was developed to investigate the interaction of the produced NPs and functionalized fabrics with ROS. The aim was to observe whether NPs and functionalized fabrics were able to bind ROS acting as a shield for the skin and therefore exerting antioxidant activity.

The capability of the materials to scavenge ROS species was evaluated by exploiting the EPR method. Since the radical species have a short half-life, a spin trapping method was employed. Firstly, free radical species were generated by using different chemical reactions tailored to the drug under analysis. The radical species reacted with DMPO which was used as a model spin trap. The oxidation reaction of DMPO in presence of hydroxyl radicals is reported in Figure 3.3.

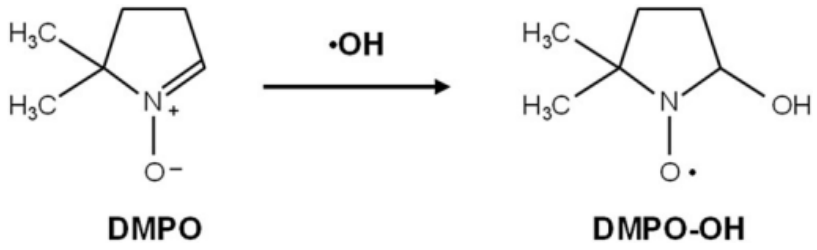

Figure 3.3. Oxidation of DMPO in presence of hydroxyl radicals.

The reaction leads to the formation of the stable radical species DMPO-OH, whose concentration could be quantified by EPR spectroscopy. During the antioxidant assay, a given amount of the NP formulation or functionalized fabric was added to the reaction medium. The antioxidant activity was characterized based on the capability of the sample to preferentially react with the radical hydroxyl species compared to the model spin trap. This was quantified by observing the reduction of DMPO-

OH concentration respect to the control medium (without sample). The antioxidant efficiency, expressed in percentage, was thereafter calculated according to Equation 3.4.

$$AE = \frac{[DMPO-OH]_{Control} - [DMPO-OH]_{Sample}}{[DMPO-OH]_{Control}} \times 100 \quad (3.4)$$

Where $[DMPO-OH]_{Control}$ is the molar concentration of oxidized DMPO obtained in the control trial using water and $[DMPO-OH]_{Sample}$ is the molar concentration of the oxidized DMPO obtained by adding the investigated material in the reaction medium.

Specific chemical reactions were employed to generate free radicals. All the necessary reactants were mixed and homogenized in an Eppendorf tube, the solution was transferred to a quartz microcapillary tube and placed in the EPR cavity for measurement. The spectra were recorded after 15 minutes from the mixing of the reactants. A Bruker EMXnano X-Band spectrometer (Bruker, Billerica, MA, USA). The EPR measurement conditions were as follows: Frequency, 9.74 GHz; scan width, 100 G; receiver gain, 60 dB; time constant, 1.28 ms; sweep time, 80 s; scan, 1. The test was of particular interest for evaluating the biofunctional activity of the NP formulation and of the functionalized textile given the high number and variety of skin illnesses, which are correlated to ROS.

3.3.6 Fluorescence Microscopy

Fluorescence microscopy is widely employed in biological and pharmaceutical research. It is used to investigate the traceability of fluorophore loaded nanoparticles. Indeed, traceability is considered an advantageous feature for biomedical applications. The NP samples were observed with a fully motorized wide-field inverted fluorescence microscope (Eclipse TiE Nikon USA) equipped with a high resolution sCMOS camera (Zyla 4.2 Plus from Andor). The diluted particle suspensions were dropped on a glass slide and observed with immersion oil 60 X objective. Specific excitation wavelengths were selected to observe the different species.

3.3.7 Scanning electron microscopy

Scanning electron microscopy (SEM) analysis was used to observe the morphology of the sample of the nanoparticles and the fabric samples. The samples were mounted on aluminum stubs using carbon tapes. For the NP samples, the suspensions were dropped on the stub and dried overnight. Before the

observation, the samples were metalized by sputter coating with chromium. Different SEM instruments, available in the partner universities, were used for the analysis.

3.3.8 Thermogravimetric analysis

Thermogravimetric analysis (TGA) was employed to investigate the thermal behavior of the nanoparticles. Furtherly TGA provides information about the structural and chemical properties of the material (Groenewoud, 2001a). The analyses were performed on dried nanoparticle samples under a nitrogen atmosphere using a TGA 3+ (Mettler Toledo, Columbus, OH, USA). The samples were heated from 25 to 700°C with a heating rate of 10 °C/min; the weight of the samples was between 6-12 mg.

3.3.9 Differential scanning calorimetry

Differential scanning calorimetry (DSC) analysis was employed to gain insights about the thermal properties and the phase transitions of the material in the operating conditions. Moreover, such analysis was also run to investigate whether polymer are in the amorphous state, a condition that eases the release of the drug (Groenewoud, 2001b). DSC was conducted on the dried nanoparticle samples using a DSC 3+ apparatus (Mettler Toledo, Viroflay, France). All samples, of weight between 6-12 mg, were placed and sealed in aluminum pan crucibles. The analysis was conducted under a nitrogen atmosphere. Samples were heated from -20 to 200°C, stabilized by a 3 minutes isotherm and then cooled down to -20 °C. The heating and cooling cycle was repeated twice, the temperature ramp was 10°C/min. From the DSC data, the degree of crystallinity of the polymer was calculated employing Equation 3.5.

$$X_c = \frac{\Delta H_{fus}}{\Delta H^0_{fus}\ (1-W_d)} \tag{3.5}$$

Where X_c is the polymer crystallinity degree expressed as a percentage, ΔH_{fus} is the fusion enthalpy measured during the DSC experiment expressed in (J/g). ΔH^0_{fus} is the fusion enthalpy of purely crystalline PCL which as a value of 140 J/g (Keroack et al., 1999) and W_d is the weight fraction of the drug in the nanoparticle formulation.

3.3.10 Contact angle

The contact angle measurement was employed to gain insights about the hydrophilic or hydrophobic nature of the functionalized textiles. The good characteristics in terms of hand and comfort of cotton fabrics are connected with its hydrophilicity. It was then considered important to inquire whether the functionalization of cotton fabrics with a hydrophobic polymer compromised the material hydrophilicity. Furtherly, contact angle measurement provides hints on the surface roughness of the material (Seo et al., 2015). To assess whether the cotton hydrophilic nature was affected by the surface treatment, the water contact angle was measured by a sessile drop method. A Digidrop apparatus from GBX instrument (France) was employed for the measurement. The samples were fixed on an optical microscope glass slide and placed under the Digidrop camera. 5 µL of water were poured on the sample and the droplet shape deposited on the textile was observed to calculate the contact angle by employing the GBX software. Water surface tension was measured by the Wilhelmy plate method. Water surface tension values of 70-75 mN/m were considered acceptable to conduct the sessile water test.

3.3.11 Textile Zeta potential

The Zeta potential of textile samples was measured by using the streaming potential technique. In this method, the textile sample is placed in a cylinder sealed at the extremities where two measurement electrodes are placed. An electrolyte solution is pumped through the sample holding cylinder by applying a controlled pressure gradient. The excess charges around the fabric are carried along with the liquid and accumulated at the tube downstream where an electric field is built, having an electrical potential which is defined as streaming potential. From the measurement of the streaming potential, the Zp, expressed in V, can be calculated by the mean of the Helmholtz-Smoluchowski equation (Equation 3.6).

$$Z_p = \frac{U_{str}}{\Delta P} \times \frac{\nu C_L}{\varepsilon \varepsilon_0} \qquad (3.6)$$

Where U_{str} is the streaming potential expressed in V, ΔP it the applied pressure expressed in Pa, C_L is the electrical conductivity of the electrolyte solution which is expressed in S/m. The term $\varepsilon_0 \varepsilon$ accounts for electrical permittivity of the solution and is expressed in F/m. In the experimental setup, textile pieces of square shape and size of 5x5 cm were where analyzed. The electrolyte solution was a 0.0745 mg/mL solution of KCl. Each textile sample was soaked in 1 L of KCl solution for 24 hours before

the analysis to achieve equilibrium conditions. The samples were then tested utilizing a Zetacad equipment (France). Such analysis was mainly conducted to understand the surface polarity of the samples and investigate whether such property affects the biofunctional properties of the developed material.

3.3.12 Color intensity

Color analysis is a widely exploited tool in the field of textile chemistry. The working principle consists in testing the textile material by data color spectroscopy. The samples are scanned for wavelengths between 360 and 700 nm in reflectance mode. The color intensity K/S is then calculated according to the Kubelka-Munk theory (Equation 3.7).

$$\frac{K}{S} = \frac{(1-R)^2}{R^2} \tag{3.7}$$

Where *K* is the spectral absorption, *S* is the scattered light and *R* is the minimum spectral reflectance ratio expressed as dimensionless numbers. Such analysis was employed to the curcumin functionalized textiles to achieve information on the effectiveness of the functionalization. Moreover, given the simplicity and the fastness of this analytical method, it was possible to process multiple samples and gain insights about the repeatability and evenness of the functionalization process. The measurement was performed by using a Konica-Minolta CM3610A spectrophotometer (illuminant D65, 10° standard observer).

3.3.13 UV protection factor

UV radiation is well known to be a source of potential harm for skin and responsible for the arise of premature skin aging and cancer. It was therefore interesting to inquire whether the finishing with the NPs system could improve the UV protective properties of the fabric. The UV protection factor (UPF) was investigated according to the Australian Standard/New Zealand Standard AS/NZS4399:2017. The fabric samples were investigated by employing a Labsphere UV-1000F ultraviolet transmittance analyzer (Labsphere Inc., USA). The scanning was performed between 250 and 450 nm to fully cover all the UV region (UV-A and UV-B). Upon collecting the UV transmission spectrum, the UPF (dimensionless number) is calculated according to Equation 3.8 as reported by the norm (AS/NZS, 2017).

$$UPF = \frac{\sum_{\lambda=250}^{450} E_\lambda S_\lambda \Delta_\lambda}{\sum_{\lambda=250}^{450} E_\lambda S_\lambda T_\lambda \Delta_\lambda} \tag{3.8}$$

Where E_λ is the relative erythemal spectral effectiveness expressed in $\frac{W}{m^2 nm}$. S_λ is the solar spectral irradiance, a dimensionless number whose values were reported by the World health organization (1992). T_λ is the spectral transmittance at a given wavelength expressed as dimensionless number and Δ_λ is the wavelength step expressed in nm.

3.3.15 Drug release test

The drug release tests were run to the performances of the proposed controlled delivery system. Several in vitro drug release experiments have been proposed in the literature depending on the kind of delivery device employed, and the administration route. In the present work, the dialysis method and the Franz Cell experiment were used. These two methodologies display some common features in terms of experimental setup and protocols. Both the systems are divided into a donor and an acceptor compartment. The drug formulation is placed in the donor compartment while the acceptor compartment consists of a solution that mimics the body fluid in which the drug is released in real applications. During the release test given aliquots of the acceptor fluid were withdrawn and analyzed to quantify the amount of drug released at that specific time. The initial volume of the acceptor phase was restored by adding a volume of fresh acceptor fluid equal to the withdrawn one. From such a test, it is possible to assess the drug release kinetic curve. Such curve reports on the X-axis the time over which the experiment was run and in the Y-axis the cumulative mass of drug released. The cumulative mass of drug released at the time released upon n samplings, m_n, expressed in mg, is calculated from Equation 3.9.

$$m_n = C_n V + \sum_{i=1}^{n-1} C_i V_i \qquad (3.9)$$

Where C_n is the concentration of drug the n-th withdrawal, V is the total volume of the acceptor fluid, the summation term serves to compensate for the effect of previous withdrawals. Therefore, C_i is the concentration of the drug at the i-th withdrawal and V_i the withdrawn volume, concentrations are expressed in mg/mL while volumes are expressed in mL.

The dialysis test simulates the release of the drug from the carrier system directly to a body fluid. The experimental set up consists of incorporating the drug formulation inside a dialysis bag as shown in Figure 3.4.

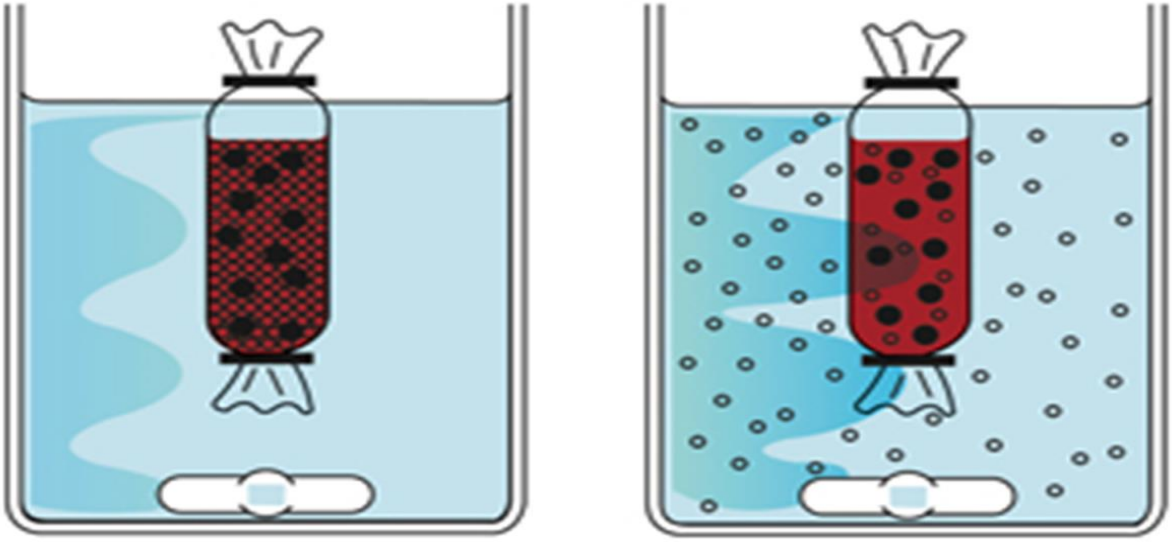

Figure 3.4. Experimental set up to the dialysis release test.

The latter consists of a membrane with a low molecular weight cut off to selective allow the drug to diffuse to the acceptor compartment while hindering the carrier system to pass. The dialysis bag filled with the formulation is sealed at the ends and sink in the acceptor fluid.

The sinking condition is of particular importance to properly allow the dialysis phenomenon i.e. the exchange of solvent between the donor and the acceptor compartment to occur. The drug transport among the donor and acceptor compartment is driven by the concentration gradient between the donor and acceptor fluid and goes on until equilibrium is reached. The acceptor fluid was a phosphate buffer solution of pH=7.4 prepared according to the recipe reported in Table 3.1.

Table 3. 1. Composition of the Phosphate Buffer solution with pH 7.4.

Substance	**Concentration (mg/mL)**
NaCl	8.00
KCl	0.20
$Na_2HPO_4 \bullet 2\ H_2O$	1.44
KH_2PO_4	0.24

The dialysis test is quite well known and robust, indeed it allows to perform a release test with quite large volumes of receptor fluid and therefore it is less sensitive to solvent evaporation phenomena and other possible disturbance.

The Franz cell release test is the most used preclinical test to inquire about the efficacy of skin topical and transdermal formulations. The Franz Cell device is built in different models and geometries to provide more reliable and close to biological reality results. In Figure 3.5 the two models of Franz Cell employed are sketched i.e. a single port (Figure 3.5 left) and a double port (Figure 3.5 right). Both apparatuses consist of a vertical shaped cell composed of a donor and acceptor compartments clamped together and separated by the skin mimicking membrane. Both models are jacketed to circulate the heating fluid and control the temperature of the receptor fluid.

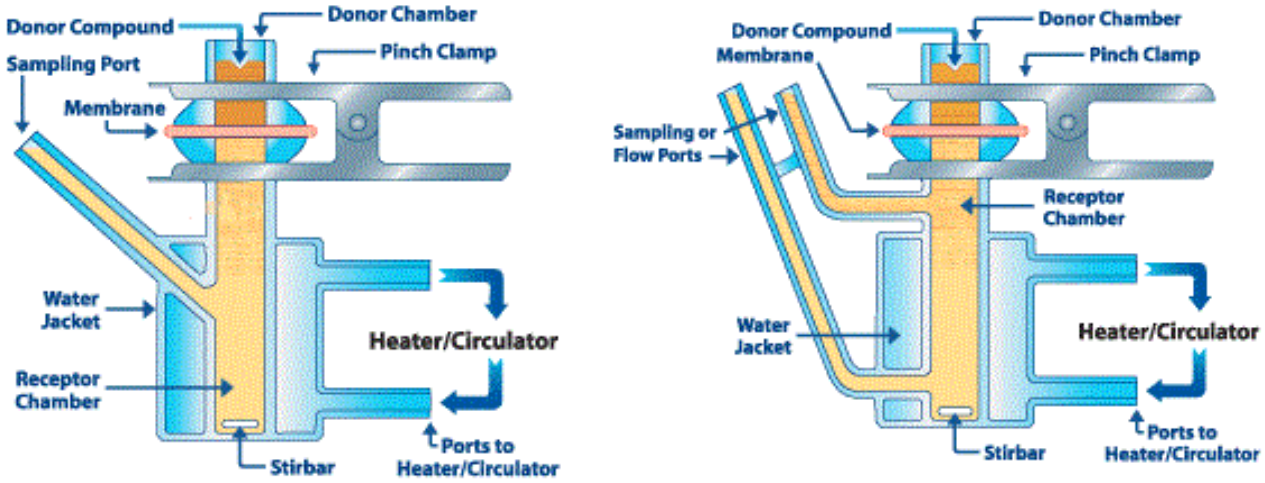

Figure 3.5. Scheme of the Franz Cell used: single port (left) double port (right).

Therefore, the main difference between the two models is the geometry of the sampling port. In the single port model, the withdrawing and the refilling of the receptor fluid are done from a unique port placed in the middle of the receptor chamber. Instead in the double port model, it is possible to collect the receptor fluid from the bottom port while simultaneously injecting the fresh fluid in the top port.

In order for the drug transport across the membrane to occur, it is necessary to have good contact between the formulation and the membrane and between the membrane and the acceptor fluid. In the experimental practice achieving good contact between the membrane and acceptor fluid can be tricky. This can be due to solvent evaporation or the formation of air bubbles during sampling and refilling. Concerning this issue, the double port Franz Cell model displays the advantage of allowing simultaneous sampling and refilling avoiding the formation of air bubbles. With the single port system, it was instead necessary to reverse the cell for avoiding the formation of air bubbles. This makes the usage of the single port cell limited to solid and semisolid formulations while for the liquid formulation the double port is considered more suitable. For this reason, the single port model was used to perform preliminary studies on the release from the melatonin functionalized fabrics. Instead,

a double port model was used to study dermal permeation of the caffeine and curcumin loaded nanoparticles and the fabrics functionalized with them.

The skin mimicking membrane used in the Franz cell was either an artificial membrane or excised skin membranes. In the first case, it is said to be in vitro while in the second case is defined as ex vivo. In the first case, a cellulose acetate membrane with a pore size of 0.45 µm was used. For the ex vivo testing, the skin was excised from butchered pig ears. The in vitro test is indeed a good screening method which allows obtaining more replicable results thank the homogenous chemical structure of the membrane with determining pore size. On the contrary, the ex vivo methods allow obtaining results closer to the real systems even if the handling is more complicated and the results less replicable due to the biological variability of the excised skin samples.

3.3.16 Modeling of the release kinetics

To understand the mechanism controlling the kinetics of drug release the results of the release test were interpreted by fitting different empirical mathematical models such as the Zero-Order kinetic, the First-Order order kinetic, the Higuchi model, the Hixon-Crowell model and the Baker- Lonsdale model. Such models describe different drug mechanisms release and, by comparing the experimental data fitting of the different models, it is possible to ascribe the drug release to different phenomena (Costa and Sousa Lobo, 2001). The zero order kinetic also defined as linear kinetics describes the release of the drug under the assumption that the release rate does not depend on the concentration of the active substance in the acceptor compartment. It is described by Equation 3.10.

$$Q - Q_0 = K_0 t \tag{3.10}$$

where t is the release time expressed in s. Q_o and Q, both expressed in mg, are the amount of drug released at the beginning of the test and at the time t respectively.K_0 is the kinetic constant of the zero order model expressed in $\frac{mg}{s}$. The first order kinetics describes the drug release in the case where the release rate depends on the substance concentration. The first order model is expressed in Equation 3.11.

$$\log Q = \log Q_0 - \frac{Kt}{2.303} \tag{3.11}$$

where K is the first-order rate constant expressed in $\frac{1}{s}$. Higuchi model was derived from the Fick laws to describe the drug release from porous matrices by a diffusion mechanism. As reported in Equation 3.12 the amount of drug released is proportional to the square root of the mass.

$$Q = K_H\sqrt{t} \tag{3.12}$$

where K_H is the release constant of Higuchi's model expressed in $\frac{mg}{\sqrt{s}}$. Baker and Lonsdale's model was derived from the Higuchi one by applying geometrical constraints. It describes the diffusion controlled Fickian release occurring from a spherical matrix (Equation 3.13).

$$\frac{3}{2}\left[1-(1-\frac{Q}{Q_\infty})^{\frac{2}{3}}\right]\times\frac{Q}{Q_\infty}=K_{BL}t \tag{3.13}$$

where K_{BL} is the release constant expressed in $\frac{1}{s}$. Q_∞ is the cumulative released at the plateau expressed in mg. Therefore, the quantity $\frac{Q}{Q_\infty}$ is a dimensionless number indicating the fraction of the drug released at time respect to the total. Lastly, the Hixson-Crowell kinetics describes the release from a matrix whose size is changing over time (Equation 3.14).

$$\sqrt[3]{Q_0}-\sqrt[3]{Q}=K_{hc}t \tag{3.14}$$

where K_{hc} is the release constant of the model expressed in $\frac{\sqrt[3]{mg}}{s}$. The Hixon-Crowell model is used to describe the release phenomena controlled by erosion, dissolution or degradation of the matrix. For all the models the data were fitted by linear regression. The correlation coefficients R^2 of the different models were compared to evaluate the best fitting one and obtain insights on the release mechanisms as proposed in the literature (Rodrigues et al., 2011).

3.3.17 Statistical analysis

Statistical analysis was conducted to better evaluate the effects of the different factors over the properties of the produced materials. One-way ANOVA analysis was carried out to check data statistical significance by means of Minitab 17. Conventionally, it was assumed p-values < 0.05 as the threshold to assess whether the factor had a significant effect on the material properties. The main effect function was employed to evaluate which factors had a more significant impact on the response. The interaction plots were employed to evaluate possible synergic effects of the factors over the response.

Chapter 4. Properties and characterization of the raw materials

The main materials employed were PCL and cotton as well as the three model drugs. The main properties and applications of these substances are reviewed in this section. Furtherly the preliminary ATR-FTIR spectra of the mainly investigated substances were collected, discussed and compared to ones found in the literature. This allowed to preliminarily assess the quality of the raw materials employed in the study.

4.1 Poly-ε-caprolactone

Poly-ε-caprolactone is an aliphatic synthetic polyester which was synthesized for the first time by Carothers in the 1930s. Its chemical structure is depicted in Figure 4.1 (Natta et al., 1934). PCL became commercially available thanks to the fact that significant efforts were made in those times to develop polymers that could be degraded by microorganisms. It is indeed its biodegradability that made PCL extremely popular for biomedical applications (Hayashi, 1994).

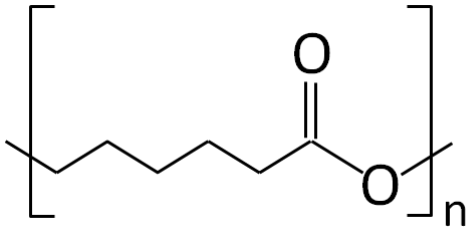

Figure 4.1. PCL chemical structure.

The synthesis of PCL is obtained by exploiting the ring opening polymerization of the cyclic monomer ε-caprolactone as depicted in Figure 4.2. Such a reaction is conducted by employing catalysts such as Stannous Octoate while alcohols are generally used to control the molecular weight of the obtained polymer. The PCL polymerization can be affected by several mechanisms, such as cationic, anionic and radical ones. Each method has an impact on the obtained polymer molecular weight and molecular weight distribution. The same synthesis approaches are used to prepare PCL based co-polymers, either random or block. In this case, several monomers, such as ethylene oxide, vinyl chloride, ethylene glycol, styrene, glycolide, lactide and methyl methacrylate can be employed in the synthesis. The synthesis method also determines the functional groups, the chain length of each block and the overall characteristics of the macromolecule (Okada, 2002).

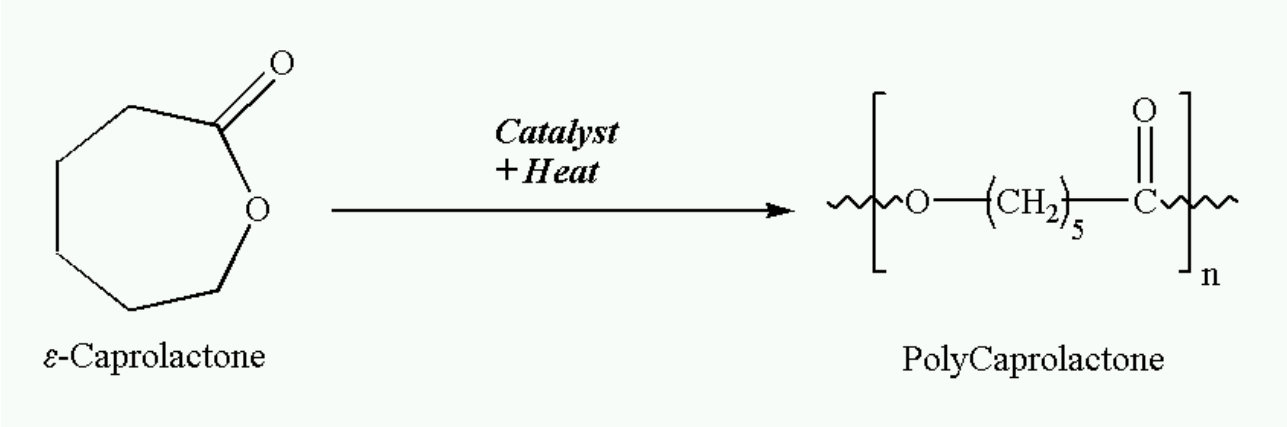

Figure 4.2. PCL synthesis by ring opening polymerization.

The PCL molecular weight ranges between 3000 and 80000 Da; according to this characteristic, PCL is classified and commercialized in high, medium and low MW. PCL is a hydrophobic semi-crystalline polymer, its melting temperature is around 60°. PCL is soluble in chloroform, dichloromethane, benzene, toluene, ethyl acetate, acetone, acetonitrile and tetrahydrofuran. Oppositely, it is not soluble in ethanol, diethyl ether and water (Coulembier et al., 2006; Zhang et al., 2019). PCL can be totally degraded by outdoor leaving microorganisms in a short time (e.g.few weeks) (Ohtaki et al., 1998). Oppositely, its biodegradation in animal bodies takes a long time. Indeed, depending on the molecular weight of the homopolymer, a PCL implant can take up to 2-4 years to be fully biodegraded (Pitt et al., 1981). The biodegradation mechanism of PCL has been extensively studied and it was proved to occur in two stages. A first step consists of the degradation by cleavage of the ester bond which causes the molecular chain to be degraded and the amorphous domain to be significantly reduced (Sun et al., 2006). The remaining macromolecules have low molecular weight and high crystallinity, therefore they are uptaken by the cells and be degraded inside their membrane (Woodward et al., 1985). The biodegradation time of PCL based materials can be tailored for by copolymerization an, blends. For these reasons, PCL has been widely employed for the production of biomedical devices, which include particulate drug carriers, suture yarns, wound dressings, scaffolds and stents. In the context of drug delivery applications, it is considered to be an optimal polymer when long lasting releases are required (Woodruff and Hutmacher, 2010). In fact, the drug carriers made with PCL showed a slow and prolonged release; their release kinetics was observed to be mainly dominated by diffusion phenomena. Nevertheless, contribution to the drug release due to surface erosion and depolymerization phenomena were observed (Kumari et al., 2010). Due to its hydrophobic nature, PCL is a good candidate for transdermal delivery applications. It could

be exploited to enhance the permeation through the lipophilic epidermis and deliver the drug in the dermal layer.

The chemical structure of the raw PCL employed in the nanoparticles production was investigated by infrared spectroscopy. The ATR-FTIR spectrum of the PCL is reported in Figure 4.3 while the characteristic absorption bands are reported in Table 3.2.

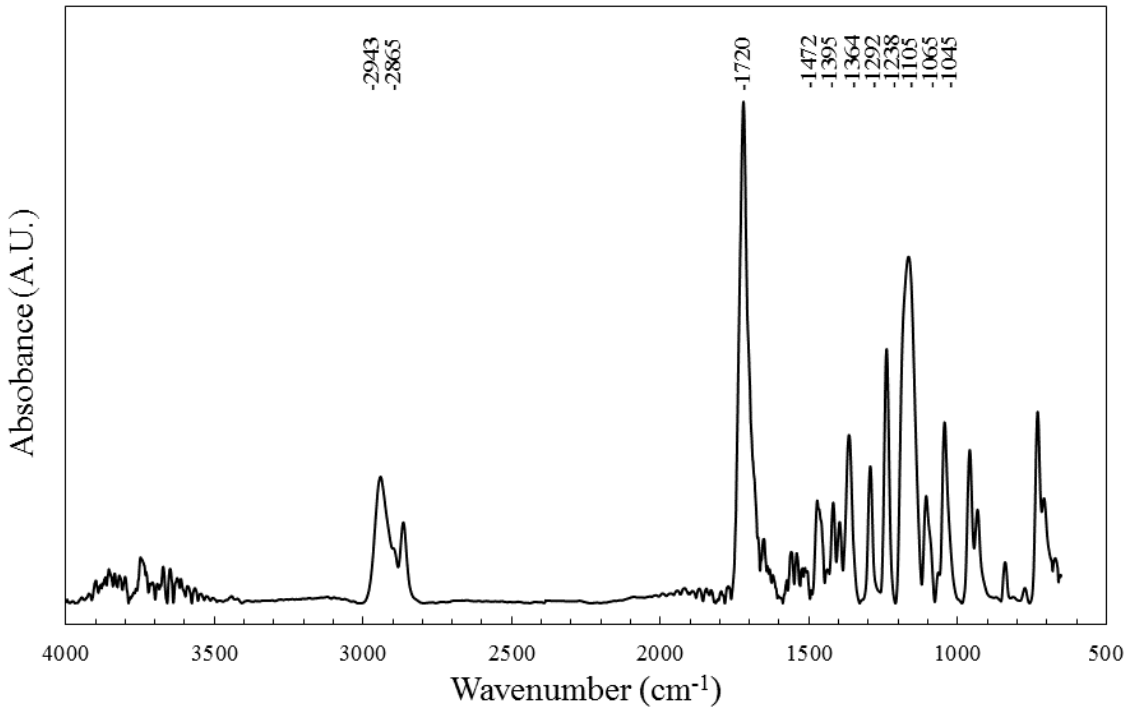

Figure 4.3. Infrared spectrum of the raw PCL.

The PCL spectrum is characterized by the typical absorption bands of an aliphatic polyester. Two medium intensity peaks are present at 2941 and 2865 cm^{-1} which correspond to the asymmetric and the symmetric stretching vibration of the C-H bonds in the macromolecule skeleton. A strong absorbance peak is observed at 1720 cm^{-1} where the stretching vibration of the C=O bond in the ester group is commonly observed. Peaks connected to the bending vibration of the C-H bonds were observed at 1470, 1395, 1364 cm^{-1}. The absorption peaks peculiar of the stretching of C-O bonds were observed at 1292, 1238, 1171, 1105, 1042 cm^{-1}. The observed absorption bands were analogous to one reported in the literature (Elzein et al., 2004).

Table 4.1. Characteristic IR absorption bands of the raw PCL used in the study.

Wavenumber (cm^{-1})	Attribution
2943	Asymmetric C-H stretching vibration
2865	Symmetric C-H stretching vibration
1720	Stretching vibrations of C=O bond in esters groups
1472, 1395, 1364	Bending vibrations of C-H
1292, 1238, 1105, 1065, 1045	Stretching vibrations of C-O

The thermal properties of the PCL used in the present study were inquired by DSC and TGA analyses. The DSC thermogram of the raw polymer is depicted in Figure 4.4 while the main thermal events observed are listed in Table 4.2.

The main thermal event evidenced by DSC analysis is a sharp endothermic peak occurring between 50 and 60 °C. The peak was attributed to the fusion of the polymer which was found to occur in the same temperature range reported in the literature (Gurarslan et al., 2013)**.** The fusion enthalpy was observed to be of -60.8 J/g; from such a result the degree of crystallinity of the polymer was calculated to be 43.7 %. Thus the polymer was proved to be in a semicrystalline form as declared by the producer.

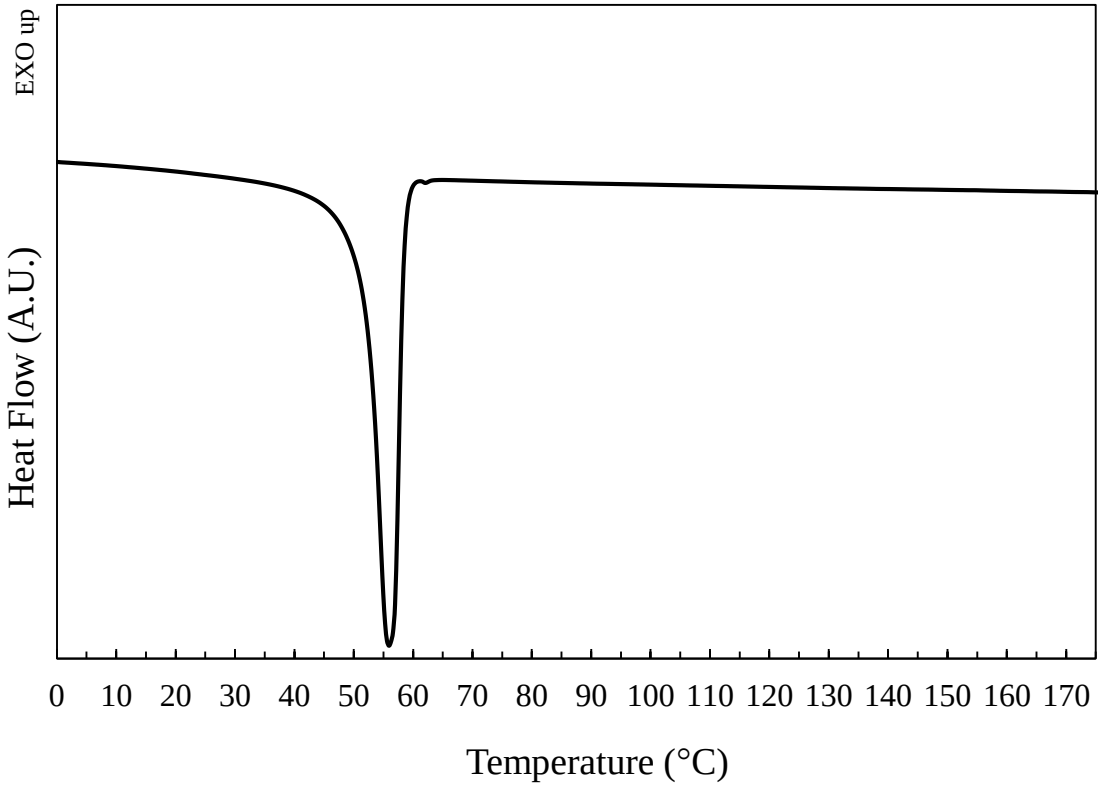

Figure 4.4. DSC thermogram of PCL for the second heating ramp.

Table 4.2. List of the thermal events observed during the DSC analysis of PCL.

Sample	**PCL**
ΔH_{fus} (J/g)	-60.8
$T_{fus,\ onset}$ (°C)	51.8
$T_{fus,\ peak}$ (°C)	55.9
X_c (%)	43.7

In Figure 4.5 the results of the TGA analysis of PCL are reported, the main data obtained from the analysis are listed in Table 4.3.

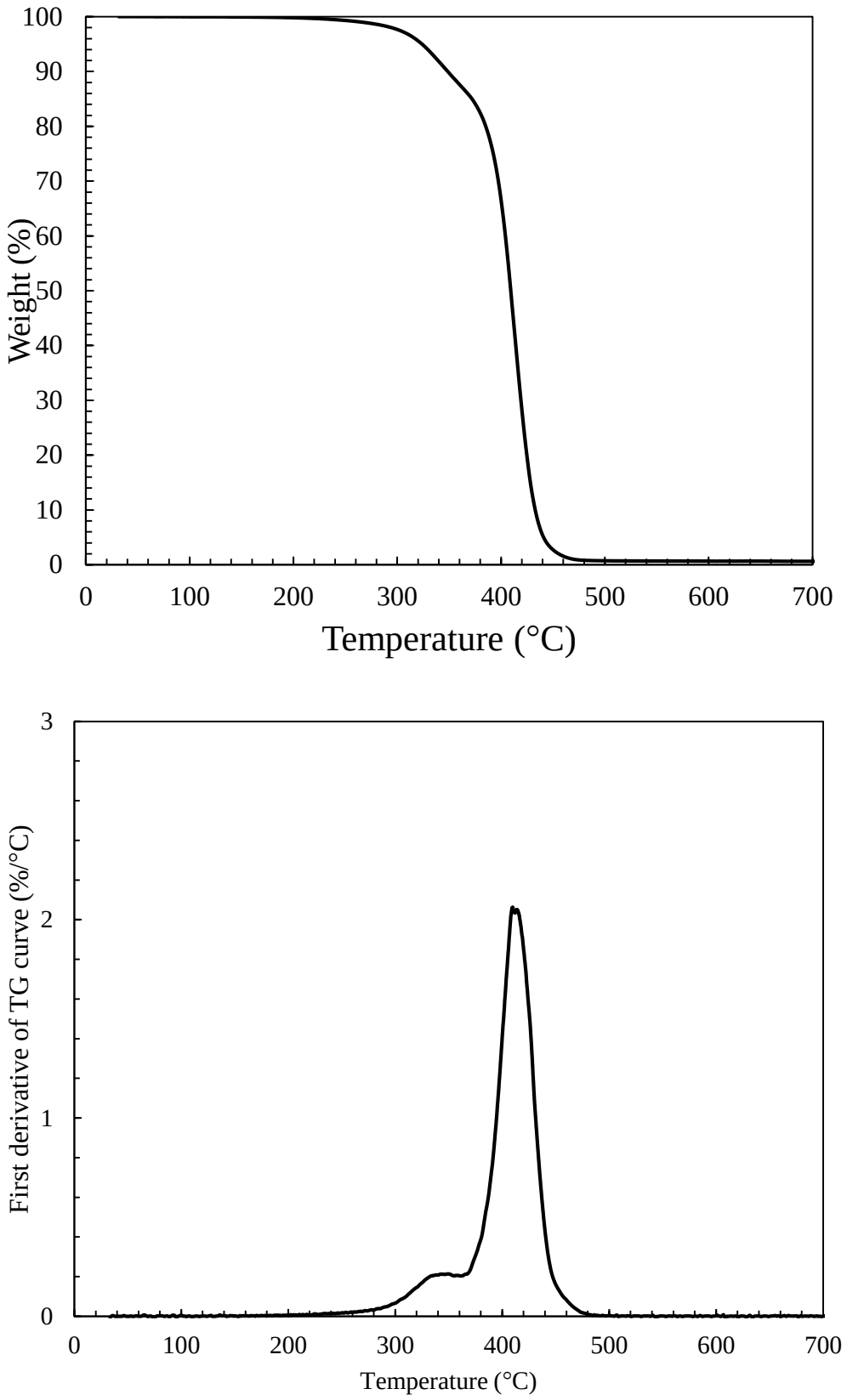

Figure 4.5. TGA analysis of PCL. TG curve (top) and the first derivative of the TG curve (bottom).

The TGA analysis evidenced PCL to be thermally stable until 300°C. Thereafter, the thermal degradation was initiated around 324°C, where the 5% by weight of the sample was degraded. From

that point, the rate of mass loss was observed to be increased up to its maximum at 409 °C. The degradation went on until 500°C, where the sample was completely degraded. The DTG curve was characterized by a main peak at 409 °C where the maximum degradation occurs and by a side shoulder around 340°C. This indicates that PCL thermal degradation occurs in two consecutive steps, consistently with what reported in the literature (Persenaire et al., 2001). A first degradation step was reported to occur around between 320 and 340°C and involved the pyrolysis of the polyester with the production of CO_2 and hexenoic acid. Then, above 400°C, the depolymerization reaction occurred leading to the formation of the caprolactone monomer.

Table 4.3. List of the thermal data obtained from the TGA analysis of PCL.

Sample	$T_{5\%}$ (°C)	T_{max} (°C)	MMLR (%/°C)	Residue at 700 °C (%)
PCL	324	409	2.1	1

4.2 Cotton

Cotton is a natural fiber of plant origin whose staples are harvested from the seed of cotton plants. The chemical composition of cotton fibers is mainly consisting of cellulose (90-95%). The remaining part is constituted by waxes, proteins and organic substances that are partially removed during the textiles processing operations. Cellulose is a linear polysaccharide whose brute formula is $(C_6H_{10}O_5)_n$. By observing the cellulose structure depicted in Figure 4.4 the monomeric unit of cellulose consists of two glucose units linked in positions 1 and 4 by the β-glucosidic bond.

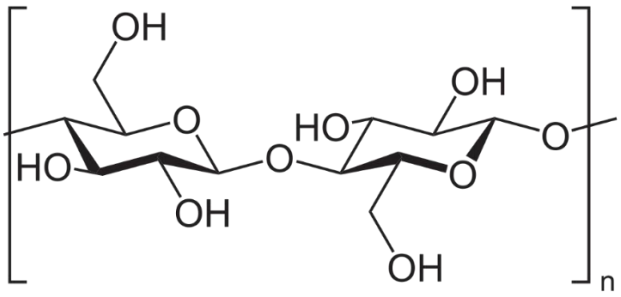

Figure 4.6. Cellulose chemical structure.

The degree of polymerization of cellulose is reported to be as high as 10000 (Klemm et al., 2005). The hydroxyl groups bonded to the carbon chain are mainly responsible for the supramolecular arrangement of cellulose polymer chains. The hydrogen bonding among the cellulose macromolecules causes the arrangement in microfibrils which constitute the building blocks of the fiber. Moreover, -OH groups impart the cotton fiber a strongly hydrophilic behavior. The degree of crystallinity of cotton fibers is normally between 70 and 80% (Dochia et al., 2012). The cotton fiber cross-section is characterized by a bean like shape which is composed of several layers. An internal hollow structure, called the lumen, constituted of the remaining nuclei and protoplasm of the plant cell. An intermediate layer constituted of microfibrils that arrange in a spiral network around the fiber center, this layer is constituted by the plant cell membrane. Finally, the outermost layer in a cuticle thin layer is constituted primarily by cell walls. Overall, the cotton fiber morphology depicted in Figure 4.5 is characterized by a typical twisted structure (Dochia et al., 2012).

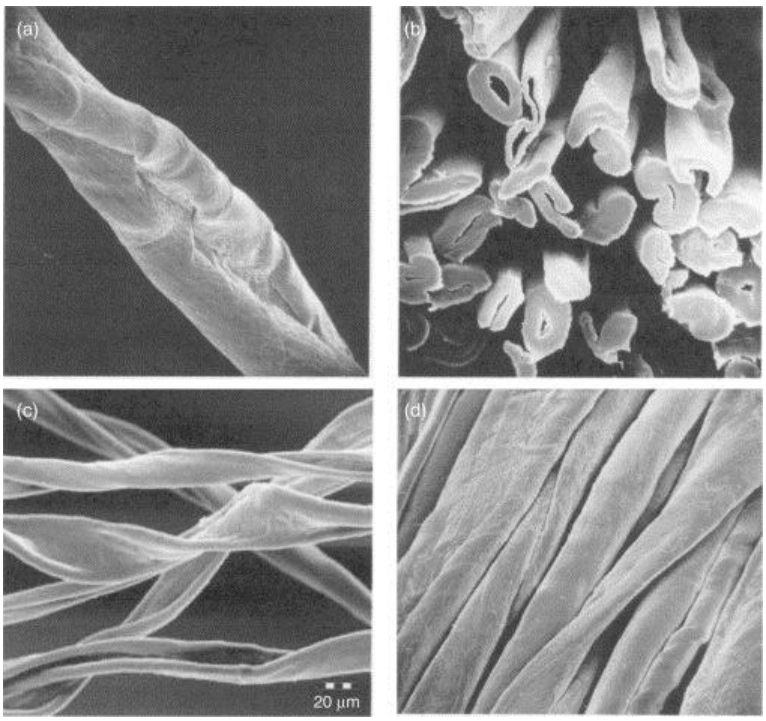

Figure 4.7. Morphology of cotton fibers observed by SEM (Dochia et al., 2012).

Being the cotton fiber mostly constituted by the plant cell residues, it is possible to observe the variation of the fiber properties depending on the botanical variety of the plants. The cotton fibers employed in the apparel industry commonly have the following properties: fiber length 20-32 mm and fiber diameter 12-22 µm. In standard textile laboratory conditions, its moisture regain is 7.5%.

The hydrophilicity is an advantageous characteristic that makes cotton to be easily dyed and finished by mean of water based processes (Grishanov, 2011). Being the most used fiber in garment production, cotton has been intrinsically proven to not cause any undesired effect on human skin. For this reason, cotton has been chosen to produce a transdermal delivery system and overcome the current limitation of adhesive patches which have been reported to cause skin irritations.

The chemical structure of the cotton fabrics employed in the nanoparticles production was investigated by infrared spectroscopy. The ATR-FTIR spectrum of the PCL is reported in Figure 4.6 while the characteristic absorption bands are reported in Table 3.3.

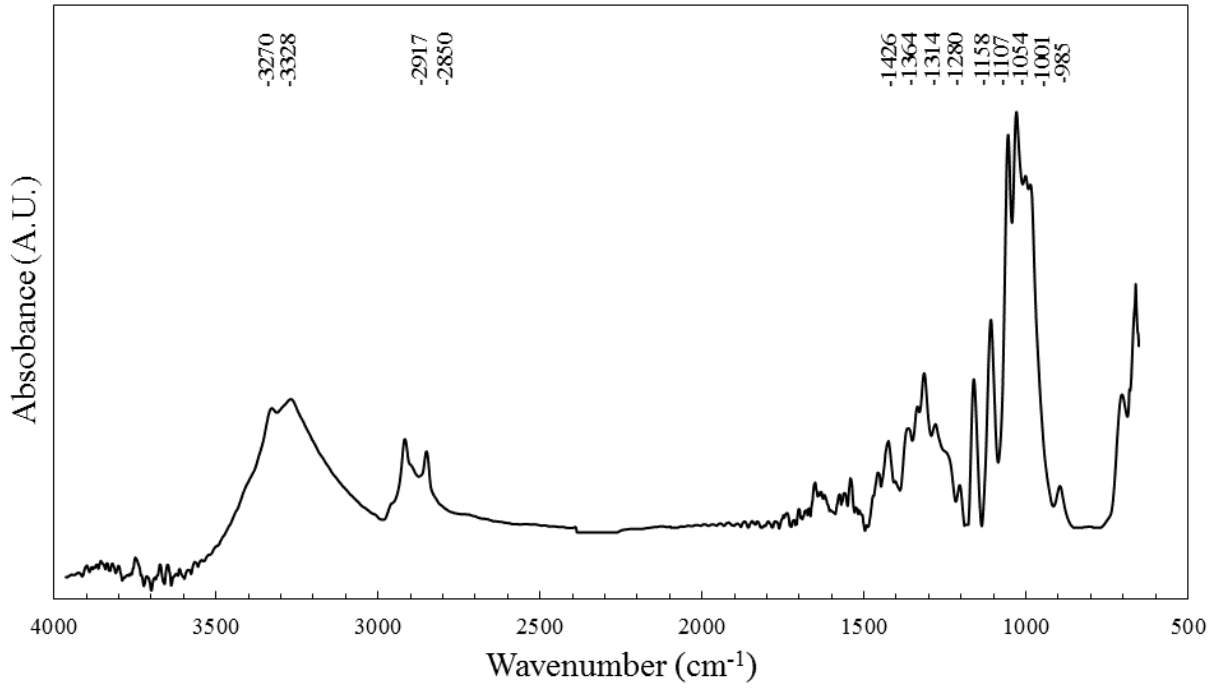

Figure 4.8. Infrared spectrum of pristine cotton fabrics.

The infrared spectrum of the pristine cotton fabrics exhibits the typical absorptions bands of the cellulose molecule. As reported in the literature (Cintrón and Hinchliffe, 2015) the cotton IR spectrum can be divided into 4 main regions. The first one ranges between 3700 and 3000 cm^{-1} and is characterized by wide absorption bands with peaks at 3270, 3328 cm^{-1} which are ascribed to the stretching vibration of the hydroxyl groups. The C-H stretching region is located between 3000 and 2700 cm^{-1}, in this zone of the spectrum, two weak peaks were observed at 2917, 2850 cm^{-1}. The third region is observable between 2700 and 1150 cm^{-1}. This zone is rich of weak peaks due to the bending vibrations of the O-H bond found precisely at 1465, 1426, 1364, 1335, 1314, 1280, 1200, 1158 cm^{-1}. Lastly, the lower region of the spectrum is mostly characterized by the sharp and strong peaks of the C-O bond at 1107, 1054, 1029, 1001, 985 cm^{-1}.

Table 4.4. Characteristic absorption bands of the cotton used in the study.

Wavenumber (cm^{-1})	Attribution
3270, 3328	Stretching O-H
2917,2850	C-H stretching vibration
1465, 1426, 1364, 1335, 1314, 1280, 1200, 1158	Bending of OH group
1107, 1054, 1029, 1001, 985	Stretching vibrations of C-O

4.3 Melatonin

Melatonin, (IUPAC name N-[2-(5-methoxy-1H-indol-3-il) ethyl]etanammide is a hormone produced by the pineal gland of mammals. It was isolated for the first time by the Lerner group in 1958. Its chemical structure consists of an amide bounded to an indol group that is bonded to a methoxy group, as sketched in Figure 4.7 It has a molecular weight of 232.3 Da.

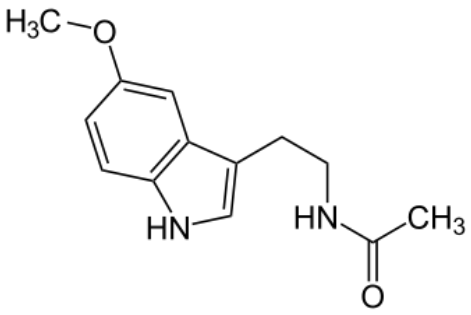

Figure 4.9. Chemical structure of melatonin.

Melatonin is slightly hydrophobic with LogP=1.15 and low water solubility (Brainard, 1978; López-Muñoz et al., 2016). It is highly soluble in acetone (up to 40 mg/mL); moreover, it was also reported to be slightly soluble in water (up to 2.5 mg/mL) (Kandimalla et al., 1999; Li et al., 2017). Such

intermediate properties make melatonin a potentially good candidate for transdermal release. In facts, its slight hydrophobicity permits diffusion in the epidermis and the non zero water solubility allows uptake in the systemic circulation. Therefore, it was selected as the first drug to be tested in the preliminary studies about drug encapsulation and transdermal release.

In the human body, melatonin is naturally synthesized by the pineal gland during evening hours, it accumulates reaching its maximum during the night and finally gets eliminated with sunrise. Its bodily function consists in regulating the circadian rhythm and controlling the sleep and wake cycles (Utiger, 1992). The biosynthesis of melatonin starts from the tryptophan amino acid which undergoes a series of reactions to produce melatonin. These reactions are normally inhibited by light, which is the reason why the synthesis of melatonin starts at sunset.

Melatonin exerts its effects by interacting with specific membrane receptors (MT1 and MT2) present in different brain areas, it promotes sleep using neuronal firing. For these reasons, the main medical use of melatonin consists of the treatments of sleep disorder (Mor et al., 1999; Zlotos et al., 2014). The production of melatonin changes sensitively with age making the amount of melatonin produced by the pineal gland to lower in old people (Diss et al., 2013).

Melatonin was also proved to exert an antioxidant activity against ROS being extremely reactive with the $OH^{\cdot}$ radical, moreover, melatonin promotes the synthesis of enzymes which promotes radical scavenging such as glutathione peroxidase, superoxide dismutase, catalase, and glutathione reductase (Poeggeler et al., 1993; Reiter et al., 2017).

Regarding melatonin pharmacokinetics, it was observed that, upon enteral administration, the drug reaches the maximum concentration in plasma in one hour. Thereafter it is metabolized in the liver and the kidneys; the main metabolite is the inert 6-sulfatoxymelatonin, which is excreted in the urines (Claustrat et al., 2005; Tordjman et al., 2017).

In the context of skin applications, melatonin has been receiving significant attention in the last years. Indeed, the membrane receptors MT1 and MT2 are significantly present in skin cells, therefore melatonin molecule can provide interesting biochemical interactions within the skin tissue (Slominski et al., 2005). Significant studies showed how melatonin can be a significant ally in skin cancer therapy by several mechanisms. These mechanisms include anti-inflammatory action, induction of tumor cell apoptosis by ROS mediation and synergistic effects with chemo and radiotherapy (Pourhanifeh et al., 2019).

Melatonin was also employed in studies regarding wound healing and tissue regenerations, in this context the drug was observed to promote re-epithelialization, granulation and wound closure. Such action was due to knockdown of MT2 receptors which promoted the synthesis of proteins involved in cytoskeletal reorganization such as F-actin, cofilin-1, profilin-1 (Lee et al., 2014; Majidinia et al., 2018).

4.4 Caffeine

Caffeine, (IUPAC name 1,3,7-trimethylpurine-2,6-dione) is a naturally occurring alkaloid found in a wide variety of plants, beans and leaves (Heckman et al., 2010). It was firstly isolated from the coffee beans by Friedlieb Ferdinand Runge in 1819. From the chemical point of view, caffeine is a derivative of Xanthine which has three methyl groups substituted in position 1,3,7. Its molecular weight is 194.2 Da. The caffeine chemical structure is represented in Figure 4.8. Caffeine is a hydrophilic compound, with a LogP of -0.55. Its solubility in water and acetone was reported to be about 22 mg/mL and 12 mg/mL respectively (Shalmashi and Golmohammad, 2010). The pure product is obtained by solvent extraction from the coffee beans, thereafter other purification steps are done to obtain the pure product in the form of dried powder (Mottram and Chester, 2018).

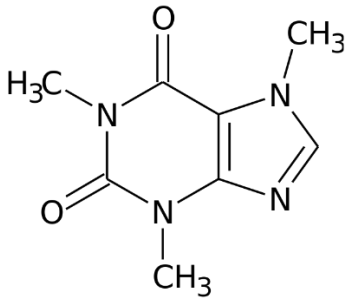

Figure 4.10. Caffeine chemical structure.

The human consumption of caffeine mainly consists of drinking the infusion obtained from coffee beans and tea leaves. However, caffeine has wide applications in pharmaceuticals, cosmetics and supplements making caffeine the most consumed drug worldwide (Harpaz et al., 2017). Caffeine is commonly present in the diet of several population segments due to its well known properties of increasing mental alertness and concentration and reducing mental fatigue (Barone and Roberts, 1996), it is used as a dietary supplement in sports activities to promote physical performance and ease weight loss (Goldstein et al., 2010; Heckman et al., 2010). Being structurally similar to adenine, caffeine binds to the adenosine receptors onto the cellular membranes, therefore it influences the

nerve regulation processes (Jandova et al., 2019). This leads to an increase of the adrenaline levels which in turn lead to an increase of cardiac rhythm and the blood delivered to the muscles. Moreover, caffeine facilitates the transmission of dopamine and glutamate, which are the neurotransmitter linked to motivation and memory (Nehlig et al., 1992).

Caffeine was also proved to be a powerful antioxidant given its high reactivity with radical oxygen species (ROS) (Devasagayam et al., 1996). Upon oral administration, caffeine is absorbed quickly into the bloodstream, the clearance of caffeine into the stomach takes only 20 minutes and the caffeine concentration peak in the blood occurs in about 1 hour (Nawrot et al., 2003). The velocity at which caffeine reaches the circulatory system is mainly due to its marked hydrophilicity, thanks to which it easily diffuses in an aqueous medium such as human blood (Ginsberg et al., 2004). Once it reaches the liver, caffeine is degraded in three different metabolites with a dimethyl xanthine structure: paraxanthine, theobromine and theophylline. Each one of these metabolites furtherly has a stimulant effect, leading to the overall empowerment of caffeine stimulant properties (Jandova et al., 2019; Nawrot et al., 2003).

Caffeine has been also applied dermally to achieve either a topical or a systemic effect. Caffeine can reduce skin aging caused either by endogenous and exogenous factors. It displays hyaluronidase inhibition and, thanks to its antioxidant activity, prevents ROS related aging effects (Furusawa et al., 2011). Being a UV absorbing compound, caffeine protects the skin from damages caused by UV light showing that this molecule plays a key role in the prevention and cure of skin cancer (Koo et al., 2007; Lu et al., 2007). A study conducted on mices proved a positive effect against UVB induced skin cancer development. A daily application of caffeine for 18 weeks allowed the decrease in the number of benignant and malignant tumors of 44% and 72% in each mouse (Lu et al., 2002). Caffeine topical administration is also gaining significant interest given its anti cellulite and anti hair loss effects. The anti cellulite activity arises from the inhibition of the phosphodiesterase enzyme in adipocytes cells which promotes the formation of cyclic adenosine monophosphate; the latter accumulates causing the activation of hormone sensitive lipase which degrades the subcutaneous fats (Herman and Herman, 2013; Rawlings, 2006). The anti hair loss activity is mainly ascribed to caffeine 5-α-reductase inhibition activity. This enzyme is normally responsible for the conversion of testosterone in dihydrotestosterone which attacks hair follicles and induces hair loss. The inhibition of 5-α-reductase leads to prevention of hair loss and improves the hair renewal (Fischer et al., 2007). This highly hydrophilic nature makes caffeine administration to be uncontrolled in the oral route and not very effective at topical and transdermal level (Dias, 1999). Therefore, the main interest in developing an encapsulation system for this drug is to control over time its release kinetics.

The chemical structure of the pure caffeine employed in the nanoparticles production was investigated by infrared spectroscopy. The ATR-FTIR spectrum of the PCL is reported in Figure 4.9 while the characteristic absorption bands are reported in Table 3.4.

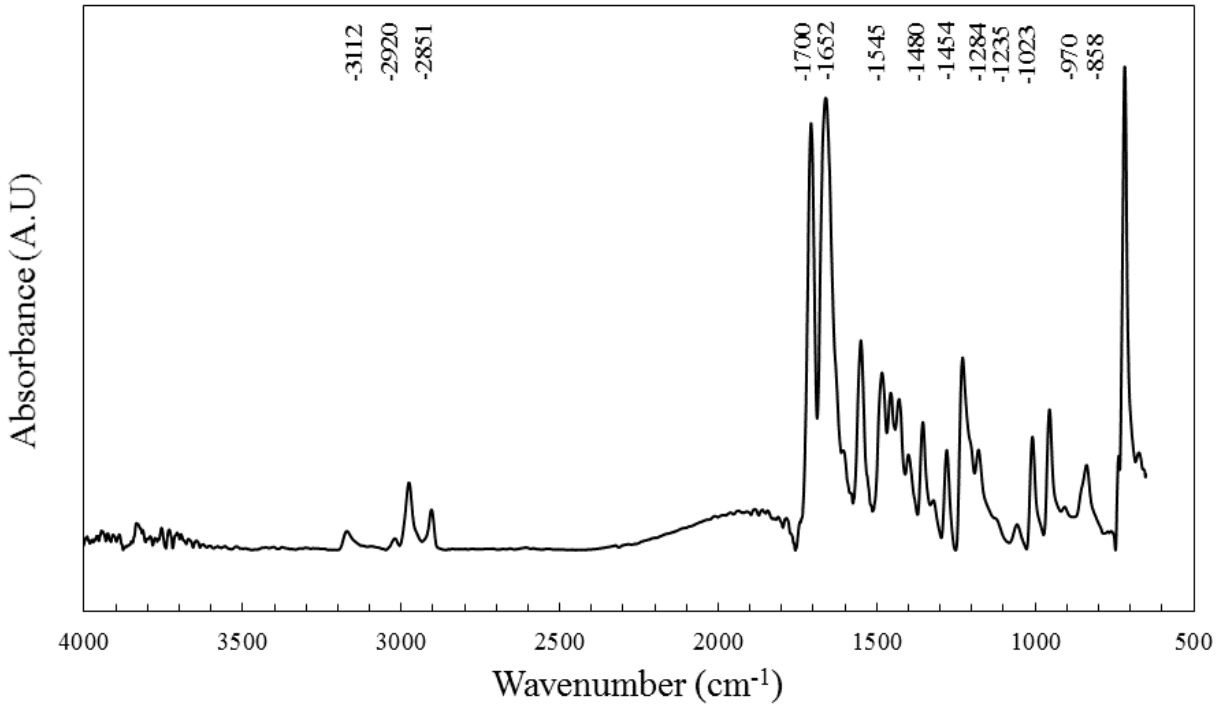

Figure 4.11. The infrared spectrum of pure caffeine

The pure caffeine IR spectrum was found to be analogous to the ones reported in the literature (Butt et al., 2019; Paradkar and Irudayaraj, 2002). Weak absorption peaks were observed at 3112, 2920, 2851 cm^{-1} and correlated with the stretching vibrations of the C-H bonds. The strong absorption of the C=O bond was observed at 1700 cm^{-1}. The presence of two sharp peaks at 1652 and 1545 cm^{-1} was associated with the C=N double bonds in the caffeine structure. The region between 1500 and 1400 cm^{-1} was mainly characterized by the peaks of the C=C stretching at 1480, 1454 and1428. The C-N bond stretching vibrations were observed in the fingerprint where peaks at 1354, 1284, 1235, 1023 cm^{-1} are found. The lower frequency region was characterized by the peaks 970, 858 cm^{-1} due to the bending of the C=C bond.

Table 4.5. Characteristic absorption bands of the pure caffeine used in the study.

Wavenumber (cm^{-1})	Attribution
3112, 2920, 2851	C-H stretching vibration
1700	C=O stretching vibration
1652, 1545	C=N stretching vibration
1480, 1454, 1428	C=C stretching vibration
1354, 1284, 1235, 1023	C-N stretching vibration
970, 858	Bending of the C=C bond

The thermal properties of the caffeine powder were inquired by DSC and TGA analyses. The DSC thermogram of the drug is depicted in Figure 4.12 while the main thermal events observed are listed in Table 4.6.

The DSC thermogram of caffeine is mainly characterized by an endothermic event occurring between 145 and 160 °C. According to the literature, caffeine molecule presents two crystalline polymorphs. The first one conventionally referred to as phase II is stable up 146 °C while the other, called phase I is usually observed above that temperature (Pinto and Diogo, 2006). Therefore, the observed endothermic peak was ascribed to the crystalline phase II to phase I transition. Not any other thermal events were observed during the cooling and the second heating ramp. Therefore, for the caffeine containing samples only the first heating ramp was plotted throughout the present manuscript.

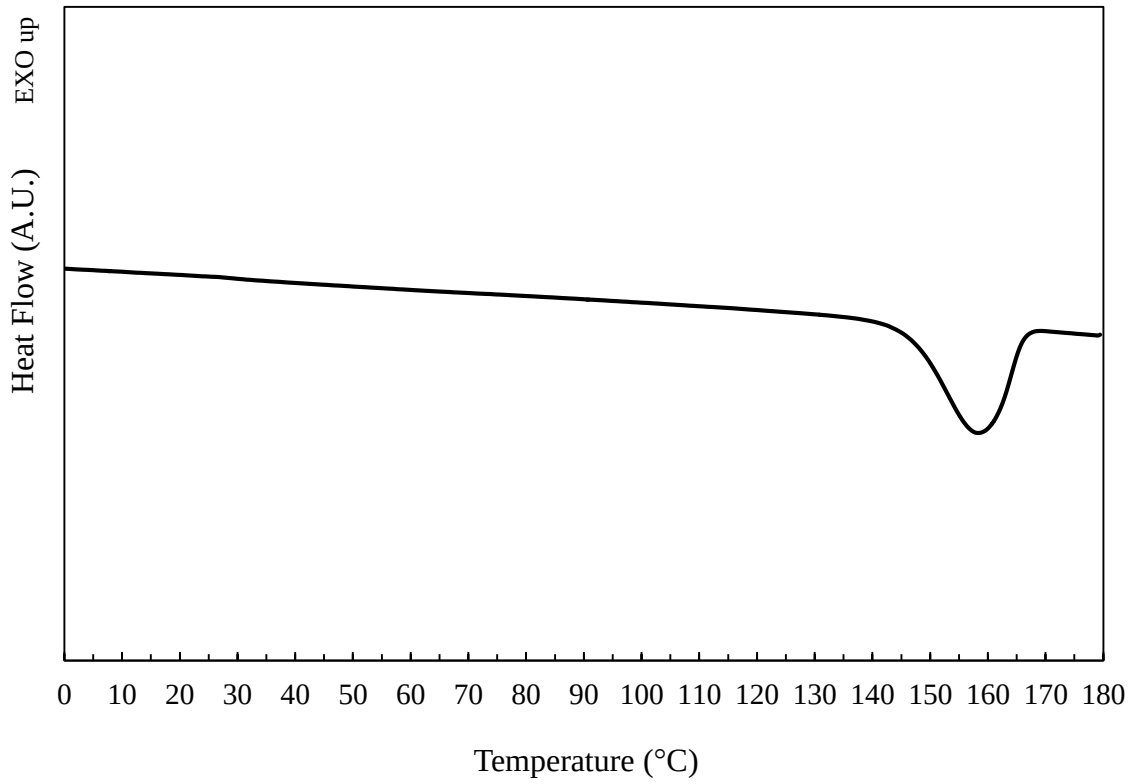

Figure 4.12. DSC thermogram of caffeine for the first heating ramp.

Table 4.6. List of the thermal events observed during the DSC analysis of caffeine.

Sample	**Caffeine**
ΔH_{trans} (J/g)	-20.3
$T_{trans,\ onset}$ (°C)	146.3
$T_{trans,\ peak}$ (°C)	158.2

In Figure 4.13 the results of the TGA analysis of caffeine are reported, the main data obtained from the analysis are listed in Table 4.7.

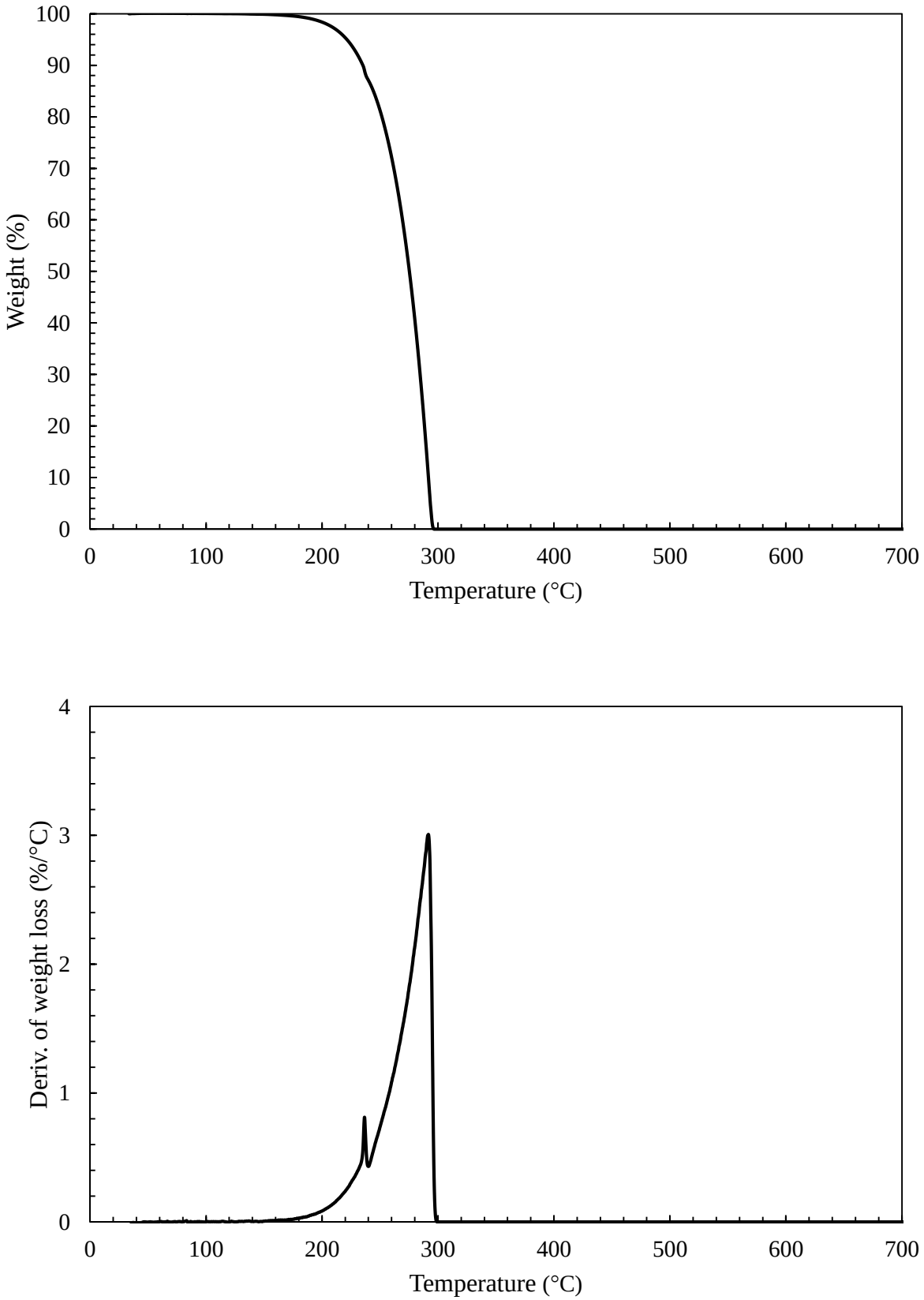

Figure 4.13. TGA analysis of caffeine. TG curve (top) and the first derivative of the TG curve (bottom).

The caffeine molecule was observed to be thermally stable until 221 °C, the temperature at which the 5% by weight of the sample was observed to be degraded. Thereafter, the degradation proceeded in the main step, with the maximum weight loss rate was observed at 291°C. By observing the DTG curve it is observable a small peak around 230°C. According to the literature, the crystalline caffeine molecules undergo fusion around 235°C (Hubert et al., 2011). Therefore, the peak of DTG in that temperature range was ascribed to the release of volatile compounds occurring during the simultaneous melting and degradation of caffeine. Regarding the melting of the caffeine molecule it was not possible to collect further data by DSC analysis, indeed raising the temperature above 200 °C during caffeine analysis caused problems and risks of damaging the employed DSC equipment. Therefore, the phase transition peak at 146°C was selected to gain information about caffeine crystalline state. This choice was also motivated by the fact that some thermal degradation phenomena were observed below the melting temperature and therefore it was preferred to keep the temperature range for DSC analysis below the onset of thermal degradation.

Table 4.7. List of the thermal data obtained from the TGA analysis of caffeine.

Sample	$T_{5\%}$ (°C)	T_{max} (°C)	MMLR (%/°C)	Residue at 700 °C (%)
Caffeine	221	291	3.0	0

4.5 Curcumin

Curcumin, (IUPAC name (1E,6E)-1,7-bis-(4-idrossi-3-metossifenil)-epta-1,6-dien-3,5-dione) is a yellow colored substance found abundantly in the *Curcuma Longa* plant. It was first isolated in 1842 by Vogel, however, the chemical formula was not identified until 1910 by Milobedzka and Lampe (Gupta et al., 2012). It is an alkaloid compound that belongs to the family of polyphenols. Curcumin chemical structure (represented in Figure 4.10) has three chemical entities: two aromatic ring systems containing o-methoxy phenolic groups, linked by a seven carbon skeleton which consists of an α,β-unsaturated β-diketone moiety (Esatbeyoglu et al., 2012). It is important to notice that curcumin exists in two forms exhibiting a keto-enol tautomery on the di-keto group. In aqueous solution the

prevalence of one or the other tautomers can be controlled by pH; the keto form is mostly present for pH < 8, this imparts curcumin yellow color and fluorescence properties. Oppositely, for pH > 8 the enol form prevails, the color shifts to orange-brown and no fluorescence are observable (Kaur et al., 2018).

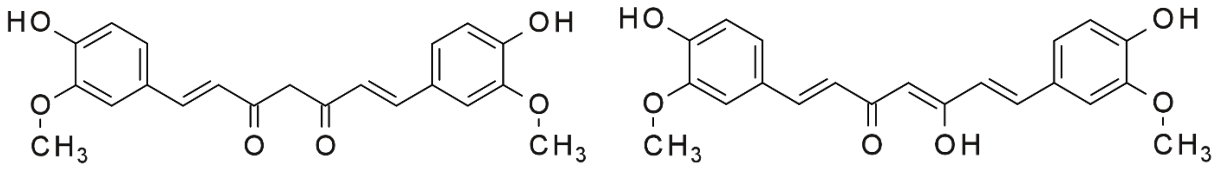

Figure 4.14. Representation of Curcumin chemical structure with keto form (left) and enol form (right)

It has a molecular weight of 368.4 Da. Curcumin has markedly hydrophobic behavior, with LogP of 4.12, it is not soluble in water at neutral pH. Its solubility in acetone was reported to be 6.5 mg/mL (Bazzano, 2018). Commercial curcumin powders are constituted by a mixture of curcuminoids, which are chemically similar among them. Average composition contains curcumin (66-85% b.w.), demetoxycurcumin (12-25% b.w.) and bisdemetoxycurcumin (1-10% b.w.) (Yadav et al., 2017). The chemical structure of these other curcuminoids is reported in Figure 4.15.

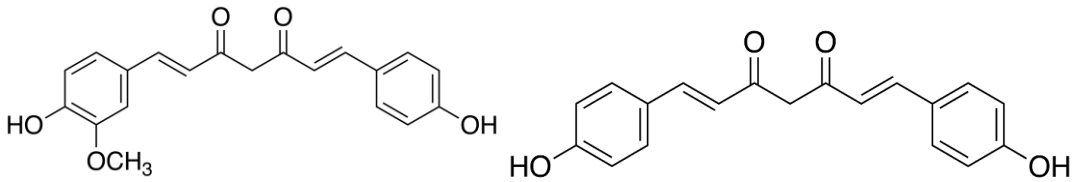

Figure 4.15. Curcuminoids chemical structure: demetoxycurcumin (left) and bisdemetoxycurcumin (right).

Curcumin has been historically used for centuries in the form of turmeric powders. It has been used as a spice in cooking, as a culinary dye and as a drug in the traditional medicine of eastern countries. Such traditional medicine applications arose the interest of the world scientific community toward this molecule (Aggarwal et al., 2007). In its chemical structure, the di-keto and the two phenol groups play important roles in promoting the biological reactions, which make this molecule of interest for pharmaceutical applications (Priyadarsini, 2014). In the first set of reactions in ROS scavenging, all the three functional groups of curcumin react with radical species by hydrogen abstraction and electron transfer reactions. In particular, the two phenyl groups are particularly reactive with ROS forming the phenoxyl radical, whose resonance is stabilized by the keto-enol structure. Thereafter, this more stable radical form of curcumin can be reconverted in molecular form by reaction with

proton donors, such as ascorbic acid. These reactivity properties are mainly responsible for the well known antioxidant properties of curcumin (Priyadarsini, 1997; Sun et al., 2002).

Of significant importance for the biological activity of curcumin is the reactivity of the di-keto groups, which undergo nucleophilic addition with –SH in proteins and enzymes. Such a reaction is mainly responsible for curcumin capability to conjugate to glutathione and to inhibit the thioredoxin reductase enzyme. These reactions are of significant importance in imparting curcumin anticancer properties (Awasthi et al., 2000; Fang et al., 2005).

Another important reaction of curcumin is the chelation of metal ions. The di-keto moiety shows very good chelating properties toward transition metals ions, who substitute the enol proton in the drug structure. Therefore, it can easily chelate different metal and metal oxide ions such as Fe^{3+}, Mn^{2+}, Ni^{2+}, Cu^{2+}, Zn^{2+}, Al^{3+} and VO^{2+} (Ferrari et al., 2013; Priyadarsini, 2014). Such metal-curcumin interaction is of crucial importance, indeed it not only modifies the chemical structure of curcumin but also changes the biological activity of metal. This can lead for example to a reduction of some metal toxicity in the biological environment (Oguzturk et al., 2012). Moreover, the complex formed between curcumin and copper and manganese ions can mimic the activity of superoxide dismutase enzyme creating a metal-organic antioxidant (Vajragupta et al., 2004). The capability of chelating metals is what makes curcumin a drug of potential impact in the treatment of Alzheimer's disease. In fact, the hydrophobic nature of curcumin helps to cross the blood brain barrier, thereafter its chelating properties allow to counteract the metals which are toxic to neurons (Baum and Ng, 2004).

Regarding curcumin stability, several studies highlighted its tendency to quickly degrade in biological environments (Anand et al., 2007). It has an half-life of 10 minutes at 37° C and neutral pH. Moreover, having several reactive moieties, it can be easily biodegraded generating ferulic acid, vanillin and ferulic aldehyde (Nelson et al., 2017). Curcumin is sensitive to light and easily undergoes

photodegradation both in solution and in powder forms. Care must be taken in product storage to preserve the efficacy of the drug (Priyadarsini, 2009).

Among the various therapeutic applications of curcumin, it is important to mention the dermatological ones, given the fact that this molecule has been recent studies for the treatment of several skin pathologies (Panahi et al., 2019). In the skin tissue, curcumin displays an antioxidant effect, indeed it not only exerts the radical scavenging effects by itself but also mediates the regulation of genes that codify the antioxidant properties at intracellular level (Kou et al., 2013). The antioxidant properties together with light absorbance make curcumin effective in protection from light radiations. It was shown that topical application of curcumin delays the appearance of dermal inflammations, tumors and skin aging (Li et al., 2016).

Besides the great potential for skin cancer prevention, curcumin can also be applied in the treatment of developed melanomas. Indeed, it was demonstrated that curcumin can induce the apoptosis of melanoma cell lines by regulating cytokine expression (Jiang et al., 2015). Through the inhibition of cytokine expression, curcumin exerts anti-inflammatory properties (Panahi et al., 2019). Moreover, this molecule interferes with the bacterial cell wall and inhibits the cell division of these microorganisms acting therefore as a natural antibiotic (Krausz et al., 2015). The anti-inflammatory and anti-bacterial effects make curcumin a useful drug in wound healing applications. It was indeed demonstrated by *in vivo* studies that curcumin can promote re-epithelialization and accelerating the healing rate on rats (Kulac et al., 2013). According to some authors, the anti-inflammatory and anti-bacterial properties of curcumin can be exploited for acne treatment. Indeed, it represents a valid alternative to traditional antibiotics to which the pathogens involved in acne (such as *Staphylococcus Epidermis*) are growing resistance (Liu and Huang, 2012; Panahi et al., 2019). Moreover, by the exploitation of anti-inflammatory action curcumin formulations can be employed in the treatment of psoriasis. Indeed, the anti-psoriasis action was proved both for topical and for oral formulations by *in vivo* testing in mice (Kang et al., 2016; Sun et al., 2017).

Notwithstanding the multiple therapeutic properties of curcumin, the effective applications of this substance are nowadays limited. This occurs because this molecule suffers several limitations such as low water solubility, poor cellular uptake, low chemical stability and fast systemic elimination (Rafiee et al., 2019). The incorporation of curcumin into nanostructured carriers has been proposed as an approach to overcome these issues (Moballegh Nasery et al., 2020).

The chemical structure of the pure curcumin employed in the nanoparticles production was investigated by infrared spectroscopy. The ATR-FTIR spectrum of the PCL is reported in Figure 4.12 while the characteristic absorption bands are reported in Table 3.5.

The used curcumin powder has an infrared spectrum analogous to the ones reported in the literature (Siregar et al., 2018). A weak absorption peak was observed in 3501 cm^{-1} and correlated with the stretching vibrations of the O-H bond in the phenol group. A strong absorption signal due to the C=O bond in the keto-enol group was observed at 1626 cm^{-1}. The presence of sharp peaks at 1602, 1507, and 1456 cm^{-1} was associated to the C=C double bonds in the curcumin aromatic rings. The peak at 1427 cm^{-1} was ascribed to the bending of the olefinic C-H. The absorption band between 1300 and 1000 cm^{-1} was mainly characterized by the peaks of the C-O stretching at 1274, 1232, 1152, 1114 and 1026.

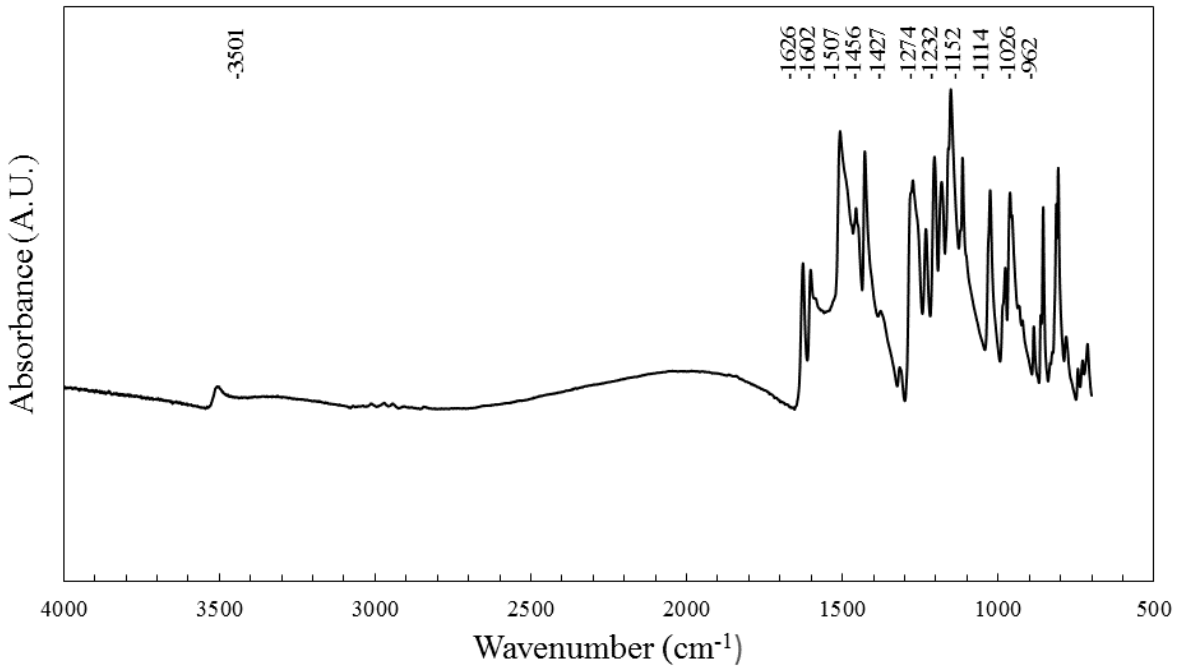

Figure 4.16. Infrared spectrum of curcumin powder.

Table 4.8. Characteristic absorption bands of the curcumin used in the study.

Wavenumber (cm^{-1})	Attribution
3501	Streching O-H in phenol group

1626	Stretching C=O in the keto-enol
1602, 1507, 1456	Stretching vibration C=C aromatic
1427	Bending C-H olefinic
1274, 1232, 1152, 1114, 1026	Stretching vibration C-O
962	Stretching vibration C-H aromatic

The thermal properties of the curcumin powder used in the present study were inquired by DSC and TGA analyses. The DSC thermogram of the for curcumin is depicted in Figure 4.17 while the main thermal events observed are listed in Table 4.9.

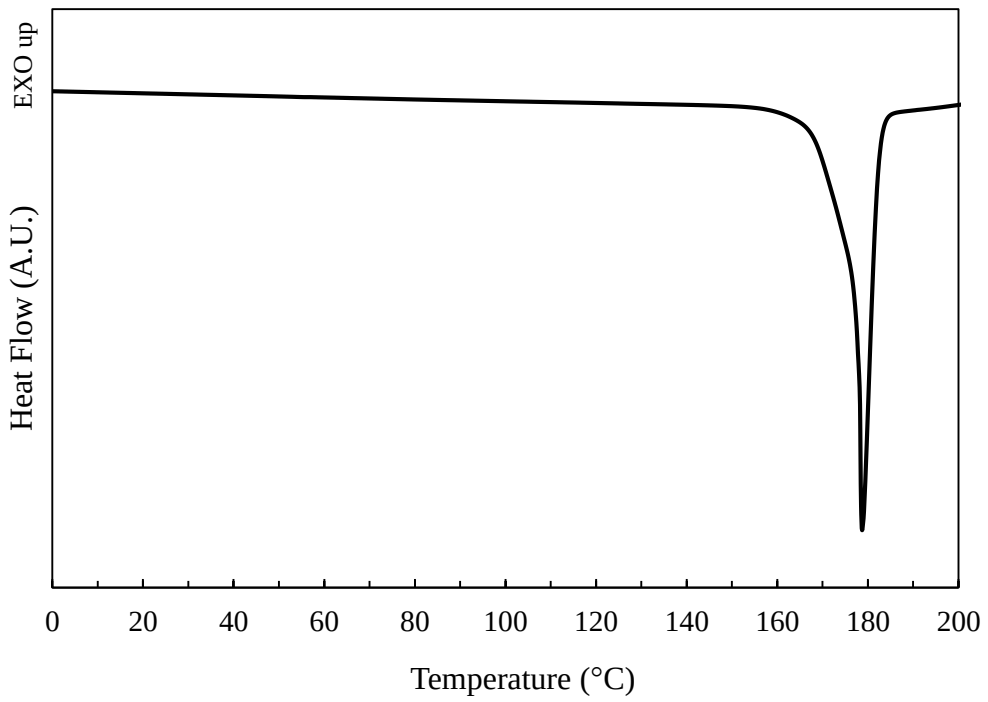

Figure 4.17. DSC thermogram of curcumin for the first heating ramp.

Table 4.9. List of the thermal events observed during the DSC analysis of curcumin.

Sample	**Curcumin**
ΔH_{fus} (J/g)	-129.0

$T_{fus,\ onset}$ (°C)	177.3
$T_{fus,peak}$ (°C)	178.7

The DSC analysis highlighted a single endothermic peak between 175 and 180 °C. The presence of this peak was attributed to the curcumin melting which is known to occur around 180°C. No other thermal events were observed during the second heating and the cooling scans, therefore for the curcumin containing samples only the first heating ramp was plotted throughout the present manuscript. Such observations were consistent with the one observed in the literature for the DSC analysis of curcumin (Souguir et al., 2013).

In Figure 4.18 the results of the TGA analysis of curcumin are reported, the main data obtained from the analysis are listed in Table 4.10.

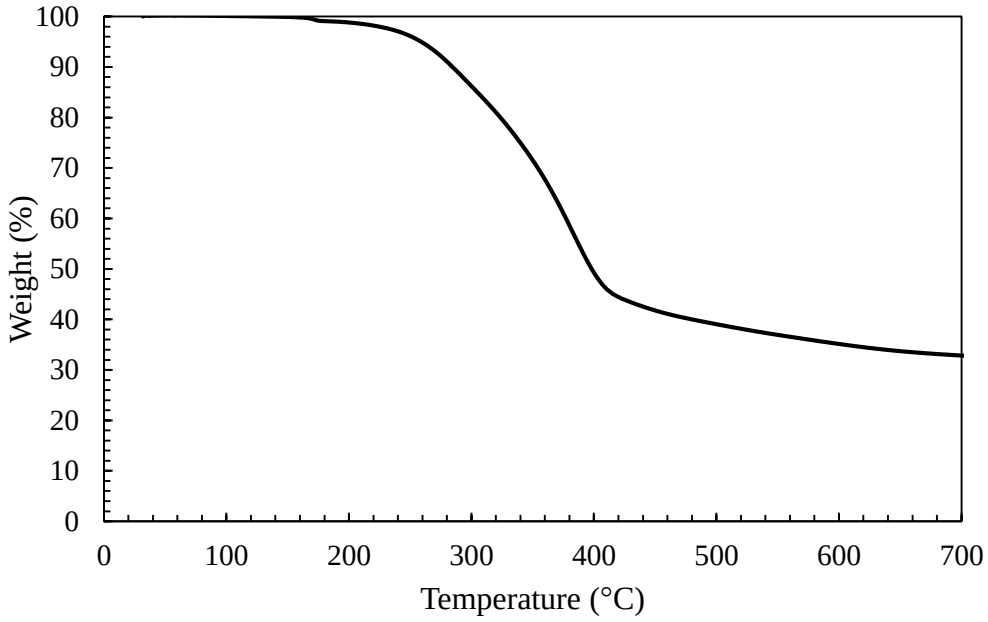

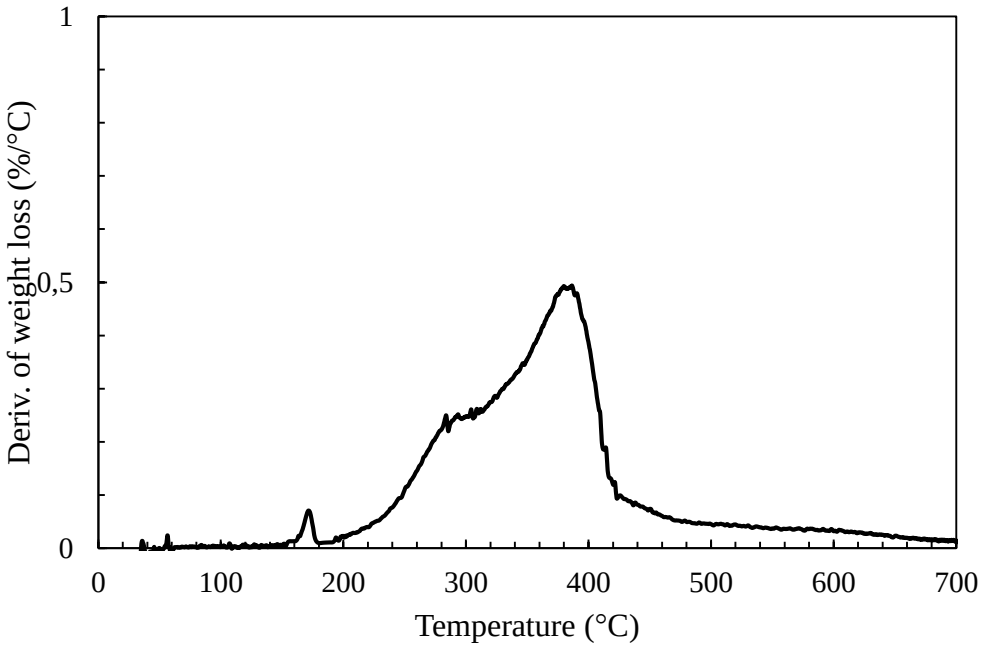

Figure 4.18. TGA analysis of curcumin. TG curve (top) and the first derivative of the TG curve (bottom).

The analysis evidenced that the curcumin molecule was fully stable until 180°C. The peak observed on the derivative curve in this temperature range was due to the release of volatile substances during the melting process. More marked degradation phenomena were observed from 259 °C where the 5% by weight of the sample was observed. From that temperature on, the sample degradation proceeded with a mechanism similar to one observed in the literature (Jasim and Talib, 1992). The degradation proceeded with two consecutive overlapped steps as observable from the DTG curve where the main peak and a side shoulder were observed. The maximum degradation rate was observed at 386 °C. A char residue of 33% of the initial sample weight was found at 700°C.

Table 4.10. List of the thermal data obtained from the TGA analysis of the curcumin powder.

Sample	$T_{5\%}$ (°C)	T_{max} (°C)	MMLR (%/°C)	Residue at 700 °C (%)
Curcumin	259	386	0.5	33

Overall, in the present chapters the properties of the main raw materials employed in the present research were reported. The preliminary characterization conducted on the raw materials highlighted

that they own physical and chemical properties consistent with the ones reported in the literature, thus they were considered to be suitable to be employed in the experimental procedures.

Part III The preliminary results

Chapter 5. Production of PCL nanoparticles

5.1 Scope of the study

In the development of a nanoencapsulation process, the first issue to be tackled is the formation of the polymeric nanoparticles. Therefore, the first set of experiments was focused on the preparation of PCL nanoparticles by exploiting the flash nanoprecipitation protocol. These preliminary experiments aimed to firstly confirm the suitability of the FNP method to produce polymeric particles with proper size for transdermal delivery, and thereafter to investigate the most suitable process condition to run the particle production process.

To tune the particle formation process, the results reported in the literature about the nanoprecipitation of PCL in a confined impinging jet mixer were carefully analyzed. Furtherly some of these experiments were replicated to assure their replicability in the used experimental setup. Particular attention was paid to the works investigating the effects of process conditions on the particle size when acetone was used as solvent (Lince et al., 2008; Zelenková et al., 2014).

Furtherly, the potential use of other organic solvents such as acetonitrile and tetrahydrofuran was inquired. Indeed, it was considered of potential interest to increase the spectrum of solvents which allows to run the FNP process without compromising the properties of the particles. Such finding can indeed open new possibilities in terms of drugs which can be incorporated.

The FNP process was run under different process conditions, mainly investigating the effect of inlet flow rate and quenching ratio. The known property of the FNP process to decrease the particle size while increasing the FR, and so the productivity was one of the reasons for which this encapsulation method was selected. Then it was crucial to confirm the validity of such property before proceeding to drug loading experiments.

Upon having identified suitable solvent and process conditions, the produced particles were characterized with the scope of highlighting both the particle properties and formation mechanisms. The specific experiments conducted for the synthesis and analysis of the PCL nanoparticles are reported in the following lines.

5.1.1 Nanoparticles preparation

The nanoparticles were prepared by flash nanoprecipitation in a confined impinging jet mixer. The process scheme is illustrated in Figure 5.1. Stream 1 was constituted of water. The pumped volume

was the same for each stream and equal to 3 mL. The inlet flow rate was varied between 10 and 80 mL/min. In the case of production of PCL nanospheres, Stream 2 was constituted of a PCL solution of 6 mg/ml; the solvents were acetone, acetonitrile and THF alternatively. The NPs were collected in a vial in which a given amount of water was placed to achieve quenching ratios of 0.12, 0.5, and 1.

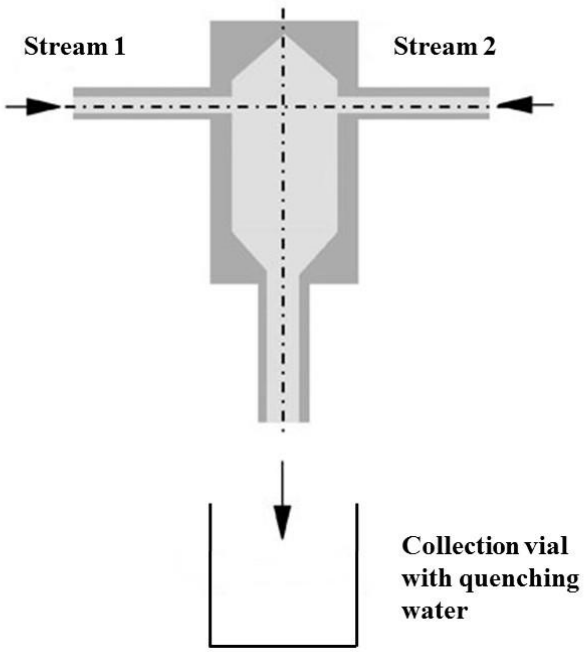

Figure 5.1. Scheme of the process of nanoparticle production by FNP.

5.1.2 PCL Nanoparticle characterization

The size of the PCL nanospheres produced with the different solvents was measured by the DLS technique. From the study of particle size, the best solvent and operative conditions were selected. Further characterization was conducted on the PCL nanospheres produced in the selected conditions.

The SEM analysis was conducted to observe the morphology and shape of the produced species. The samples were prepared by dropping the NP suspension on an aluminum stub and letting it dry overnight. Upon drying, the samples were metalized with chromium and observed by mean of field emission scanning electron microscope (FESEM) Zeiss Merlin (Oberkochen, Germany).

The ATR-FTIR analysis was conducted on the nanoparticles to test whether the process induces modification in the chemical structure of PCL. The thermal properties of the nanoparticles were studied by trough TGA and DSC analyses.

5.2 Production of PCL nanospheres in different solvents

The formation of polymeric nanoparticles by flash nanoprecipitation occurs as a consequence of several phenomena that are influenced by the different operating parameters. The particle formation mechanism was studied by running some preliminary experiments on the production of plain PCL particles. The effect of the process conditions on the particle size was evaluated. Three different solvents, i.e. acetone, acetonitrile, and THF were employed.

5.2.1 Production of particles in acetone

The effect of the inlet flow rate on the particle size for the initial concentration of PCL of 6 mg/ml and QR=1 is shown in Figure 5.2.

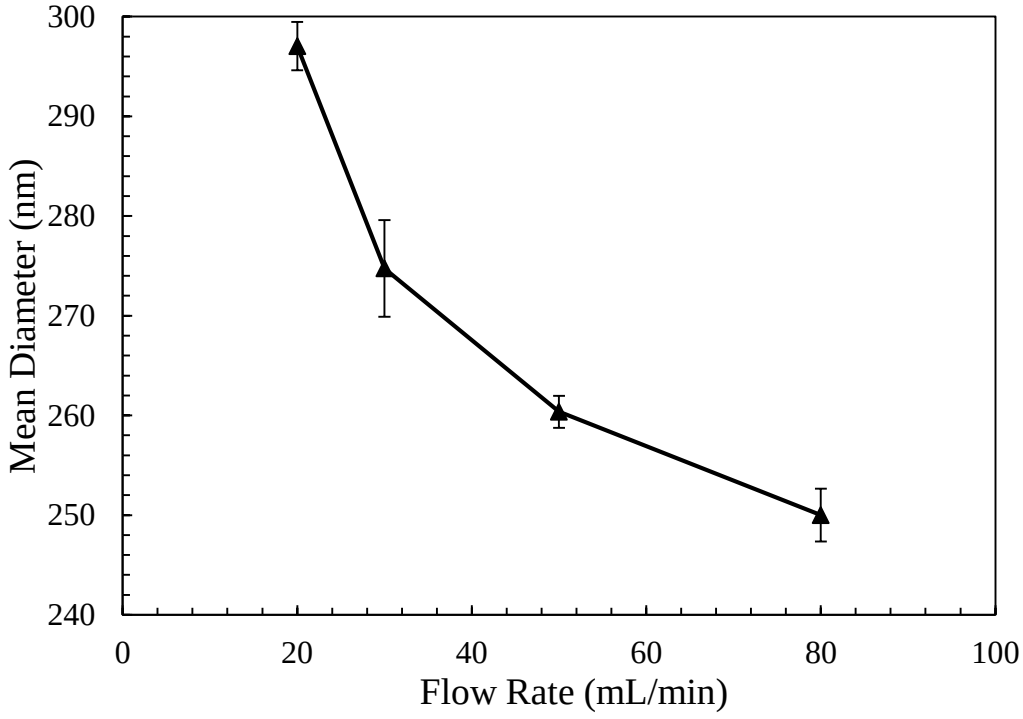

Figure 5.2. Effect of inlet flow rate on the particle size for C_{PCL}= 6 mg/ml and QR=1.

The average diameter of the particles decreased as the flow rate increased. This is mainly due to the fact that turbulence inside the reactor increased at higher flow rates. Therefore, mixing was more efficient at a higher flow rate allowing a higher extent of nucleation and limiting the growth. Although

such a trend is well known from the literature (Lince et al., 2008; Zelenková et al., 2014), it was of significant importance to confirm it experimentally. Indeed, the tuning of particle size with flow rate is a promising feature to match the gap between pharmaceutical carrier production and textile functionalization. The particle size was found to be smaller than the skin pores for all the tested flow rates, this makes the necessary quality parameters to be satisfied. Moreover, the possibility of increasing FR and, as a consequence, the process productivity (while keeping the particle size low and so furtherly improving the product quality) makes this technology worth of further investigation for application in dermatological delivery.

5.2.2 Production of particles in acetonitrile

Although acetone has proved to be a good solvent for PCL NP production, some experiments were run with other solvents to evaluate if interesting performances in terms of particle size control were achievable and furtherly increase the versatility of the proposed process. In Figure 5.3, the plots of the particle mean diameter as a function of inlet flow rate are reported for formulations with the same initial concentration of PCL (6 mg/ml) at varying quenching ratios.

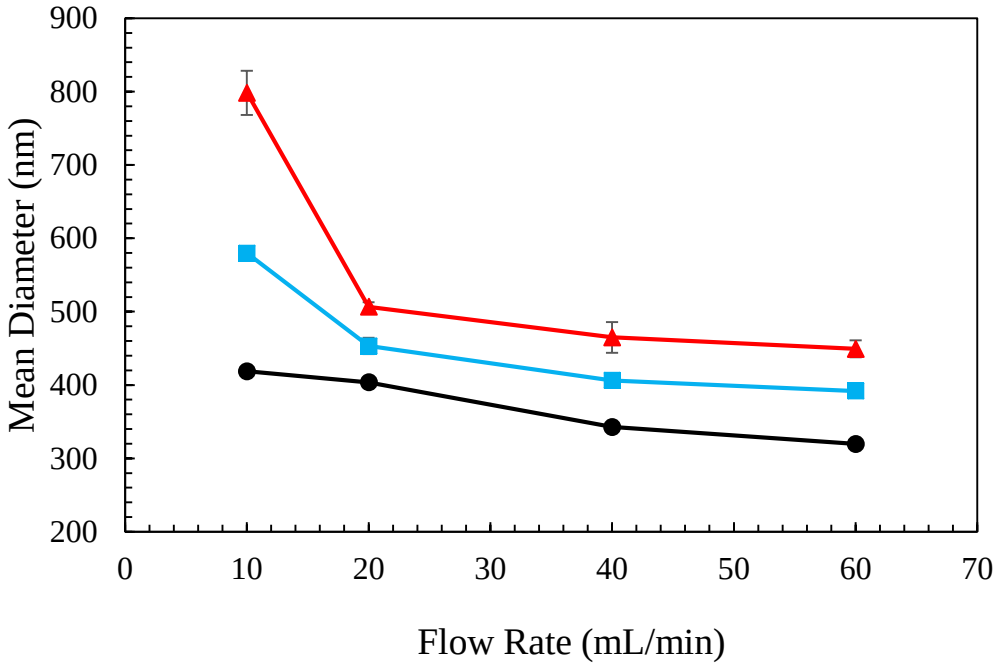

Figure 5.3. Effect of inlet flow rate on the particles size for particles produced with C_{PCL} = 6 mg/ml in acetonitrile for different quenching ratios: QR= 1 (red triangle), QR=0.5 (blue square) and QR=0.12 (black circle).

It was observed acetonitrile (instead of acetone) does not significantly alter the already observed inverse proportionality between particle size and flow rate. Moreover, it was also observed that the particle size decreased as QR was decreased. The effect of QR was more marked for the lower flow rate. Both the effects of FR and QR on the particle size are due to the fact that the nucleation phenomenon occurs when the solvent is effectively displaced and the polymer molecules come in contact with water. The increase in FR makes the mixing more efficient and leads to the fast formation of PCL water interphases and a higher extent of nucleation. For lower flow rates the lower mixing efficiency hinders the fast formation of nuclei, in this condition increasing the amount of quenching water plays a critical role in promoting effective solvent displacement due to dilution, leading to finer particle production. For higher flow rates instead, a good mixing efficiency already promotes the solvent displacement and nuclei formation and therefore increasing the quenching water causes less significant size decrease. The production of finer particles at lower QR occurs because the addition of water in the collection vial freezes the particle growth; furtherly, increasing the amount of dilution water, causes the polymer concentration to sharply drop below the range in which the growth is thermodynamically favored (recall Figure 2.11). Regarding the particle size, it was possible to achieve sufficiently fine particles upon having properly adjusted the operational parameters.

These results are indeed similar to those published by Zelenkova et al for the formation of PCL nanoparticles produced using acetone (Zelenková et al., 2014). In conclusion, it was demonstrated that acetonitrile is a suitable solvent for NP production. This finding displays significant interest also because it allows expanding the spectrum of the drugs which can be incorporated in PCL nanoparticles by the FNP method to the one soluble in acetonitrile.

5.2.3 Production of particles in tetrahydrofuran

The production of PCL nanoparticles in THF was performed similarly to acetonitrile, the particle size was measured for different formulations having initial PCL concentration of 6 mg/ml while changing the inlet flow rate and the quenching ratio. The results of these trials are represented in Figure 5.4. It can be observed that using THF as a polymer solvent, the obtained nanoparticles do not display a clear trend of D_p as a function of FR. Moreover, the effect of QR is not univocally identified as well, indeed while for QR=1 the particles produced are bigger than the ones produced with a QR of 0.5 and 0.12, between these last two conditions no significant difference was observed for FR of 20 and 60 mL/min. As the flow rate is increased, the particles sizes for QR = 0.5 becomes either proximate to the one with QR = 0.12.

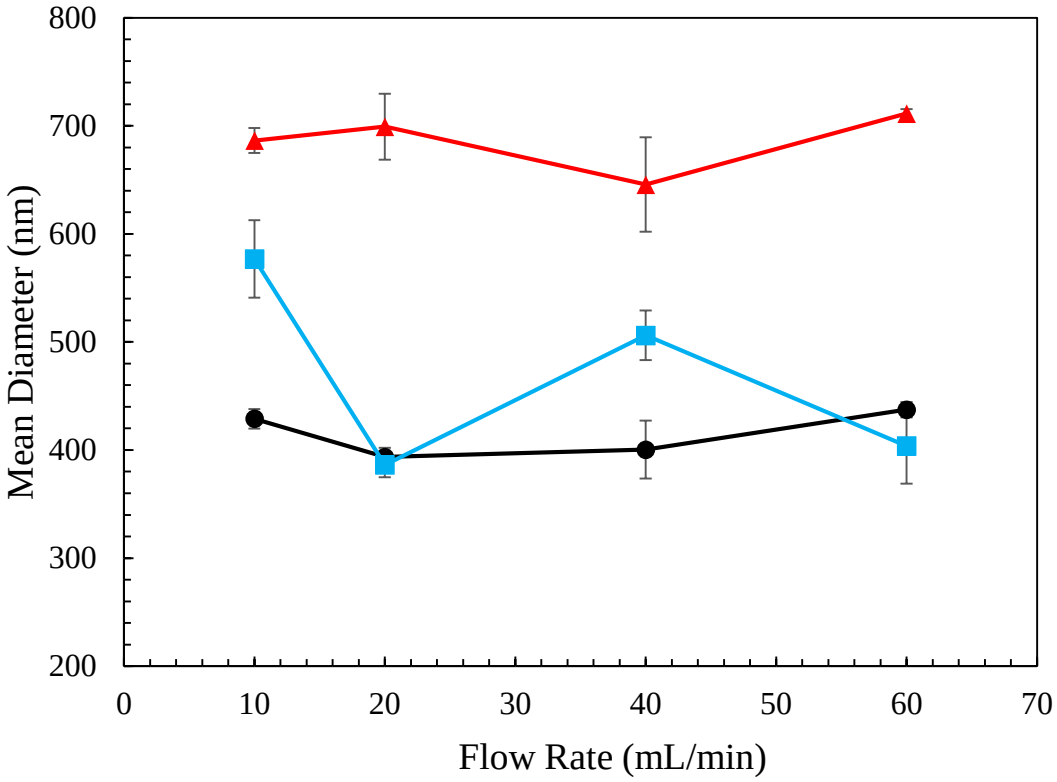

Figure 5.4. Effect of inlet flow rate on the particle size for particles produced with CPCL = 6 mg/ml in THF for different quenching ratios: QR= 1 (red triangle), QR=0.5 (blue square) and QR=0.12 (black circle).

Such results can be discussed by taking into account the peculiarities of the different solvents, Comparing the characteristics of the solvent-antisolvent it was evidenced that the diffusivity of THF in water is 10 times lower if compared to acetone (Donaldson et al., 2016; Hellwege, 1969). Moreover, the PCL was estimated to have a higher solubility in THF compared to acetone (Ferri et al., 2017). This makes the process of nanoprecipitation of PCL in THF more complex and difficult to control. In fact, the lower diffusivities hinder a fast displacement of the solvent. This combined with the good solubility of PCL in THF makes more complex to achieve the supersaturation conditions and the nuclei formation. Based on these considerations it can be stated that using THF the process stability is reduced. In these less stable conditions, the improvement of the mixing efficiency does not significantly affect the particle size. The decrease in diameter upon QR increase, observed in some cases can instead be ascribed to the inhibition of the growth mechanism previously described. The mechanism of PCL particle formation using THF as a solvent is complex and yet to be fully understood. Indeed, as reported by Ferri et al. (2017) the consideration of the thermodynamic and chemical properties of the solvent and antisolvent couple may not fully describe the phenomena occurring in the PCL-THF-Water ternary system. Moreover, no studies about the formation of PCL nanoprecipitation in THF by computational tools such as molecular dynamics were reported in the

literature as instead it was done for the PCL-acetone-water system (Di Pasquale et al., 2014). This makes the knowledge of the phenomena occurring in the THF based system to be much fuzzier respect to the acetone based one.

5.2.4 Choice of the solvent

Based on the analyzed literature reports and the preliminary experiments some comparison among the different solvents can be made to decide which one is more suitable in the drug loading experiments. In Figure 5.5 the particle size of the samples produced with the same initial concentration, i.e. 6 mg/ml and same operative conditions, i.e. QR=1 are shown.

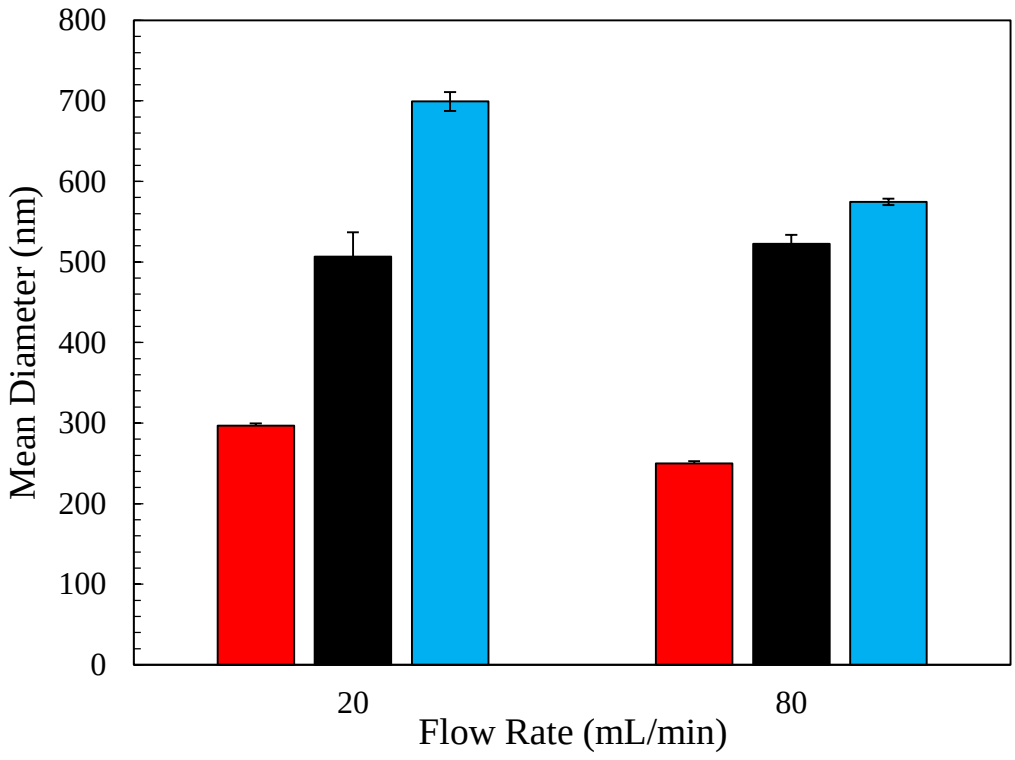

Figure 5.5. Particle size obtained by using different solvents: acetone (red bar), acetonitrile (black bar) and THF blue bar. CPCL = 6 mg/ml and QR=1

It is noticeable that the solvent displays a remarkable effect on the particle size. Particles produced in acetone are finer while the ones produced in acetonitrile and THF are bigger. The effect of the solvent on particle size is complex and has to take into account the thermodynamic of mixing of the binary mixtures formed between each solvent with water. Recalling the previously conducted discussion and the results reported by Ferri et al. (2017), the different sizes obtained with different solvents were explained taking into account the diffusivity of water in the three different solvents.

The diffusivity of water in acetone is greater than the one in acetonitrile and THF respectively. It is noticeable that the higher the diffusivity of water in the solvent, the lower the particle size. Such observation can be explained by considering that both mixing and nucleation are promoted if water diffuses easily inside the solvent and this leads to smaller particles. To select the proper solvent for our applications several factors were taken into account. THF is indeed the worst performing solvent among the investigated ones. This consideration is supported not only by observing that the coarsest particles are produced in THF but also that no clear correlation between particle size and the operating the parameters was identified. Therefore, it is difficult to control particle size by adjusting the flow rate, thus frustrating the main purpose for which the FNP was selected as the encapsulation technique. In the case of acetonitrile, clear D_p versus FR trends was observed proving that it is a potential candidate for the desired application. However, acetone is considered to be the most suitable choice. In fact, the finest particle size was achieved by using acetone, furtherly the process of PCL particle formation using acetone is very well-known and this provides a solid starting base that is necessary to understand the phenomena occurring when different kind of drugs are added to the mixtures. Furthermore, acetone has a lower boiling point than acetonitrile, this simplifies the separation procedure and permits the solvent removal by evaporation without risking to damage the particle structure or the drug activity. Finally, acetonitrile displays higher acute toxicity than acetone and it is more expensive. Considering these aspects acetone was chosen as PCL solvent in the drug loaded nanoparticles production.

5.3 PCL Nanoparticles characterization

For the PCL nanoparticles produced in acetone, some additional analyses were conducted to better understand the chemical and structural properties of the polymer before and after the nanoprecipitation process. All the analysis was conducted on dried samples of a formulation produced with initial PCL concentration of 6 mg/mL processed at FR=20 mL/min with QR=1. In such conditions, it was proved that particle size is sufficiently low, however, extremely low sizes were also avoided to not complicate the particle separation process by centrifugation. Such conditions were proved to allow effective particle separation using reasonable centrifugation times and intensities and thus avoiding particles to be damaged in the centrifuge. SEM images of the dried PCL nanoparticles are displayed in Figure 5.6.

From the low magnification images (top pictures) it can be observed that the particles tend to agglomerate during drying, forming a film. In the image at 5000 X dark shades are observable, (red circles), in this zones the boiling of water bubbles was observed during the analysis. This was due to

residual liquid entrapped in the nanoparticles, that suddenly evaporated upon being heated by the SEM electron beam. The presence of residual liquid in the nanoparticles was considered to be due to the non completed evaporation of water present in the formulation, which was not fully removed during the drying procedure. Moreover, considering that PCL is a hygroscopic polymer, it is reasonable to assume that the nanoparticle system tends to easily entrap water in its network.

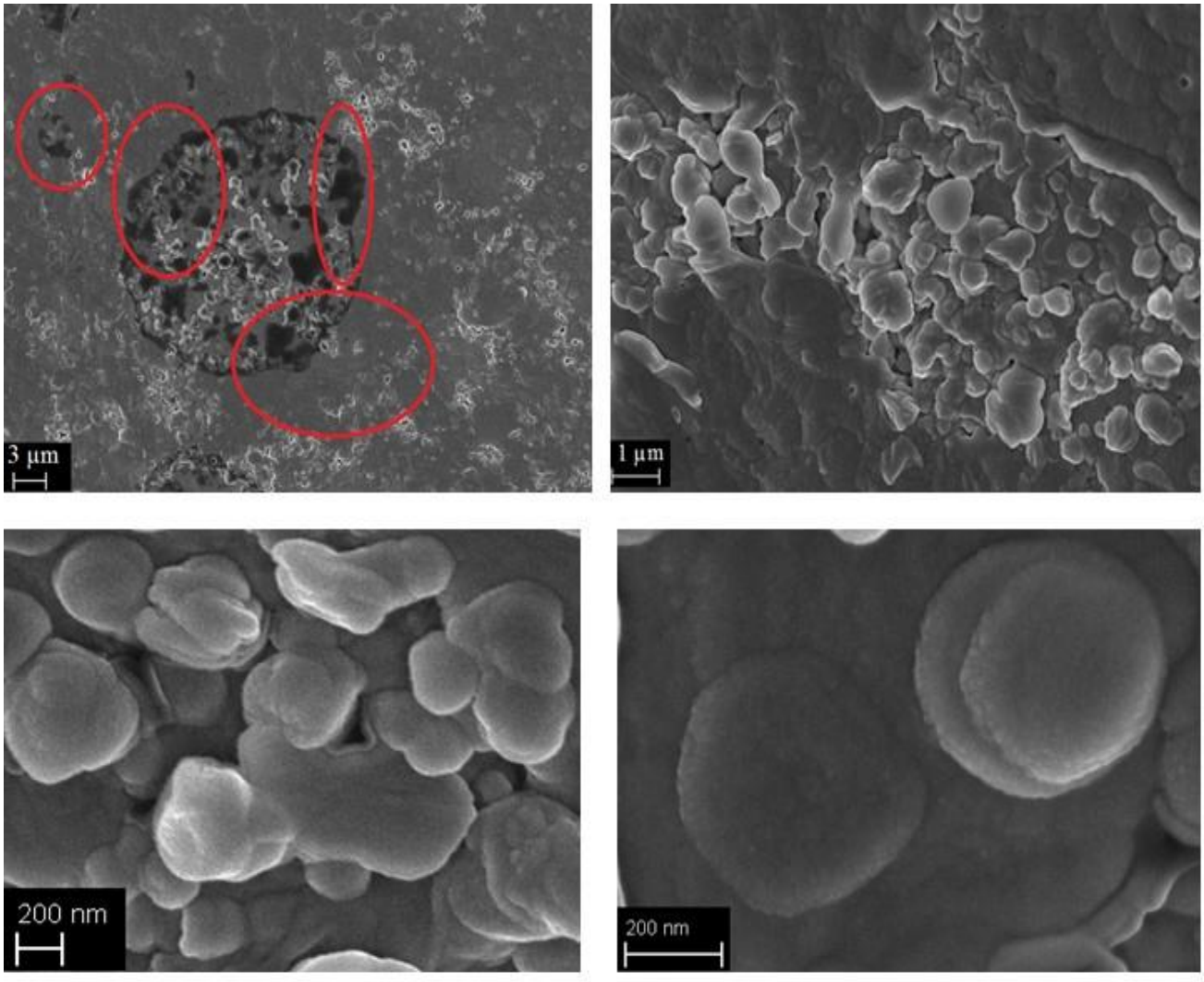

Figure 5.6. SEM images of PCL nanoparticles at different magnifications: 5000 X (top left) 25000 X (top right) 50000 X (bottom left) 150000 X (bottom right).

Increasing magnification (bottom pictures), a cluster of particles with spherical shape was observed. Although it is difficult to univocally assess the morphology of the obtained products due to the high extent of aggregation, SEM images provide clear proof that spherical nanoparticles were obtained. Lastly, by observing the highest magnification images, it can be seen that the nanoparticles have similar diameters to the one measured by DLS, thus corroborating the results obtained by the latter analysis.

From the SEM analysis of the pure PCL analysis, it was, therefore, possible to conclude that, from the nanoprecipitation process, spherical shaped particles were obtained; these particles had size consistent with the one measure by DLS. Highlights on the drying mechanism were obtained, it was confirmed that the particles tend to significantly aggregate during the drying and that water is entrapped in the dried product.

The chemical structure of the obtained PCL nanoparticles was analyzed by ATR-FTIR to investigate the possible chemical changes occurring on the polymer structure upon the nanoprecipitation process. The ATR-FTIR spectrum of the PCL NP and raw PCL are reported in Figure 5.7 while the characteristic absorption bands are reported in Table 5.1.

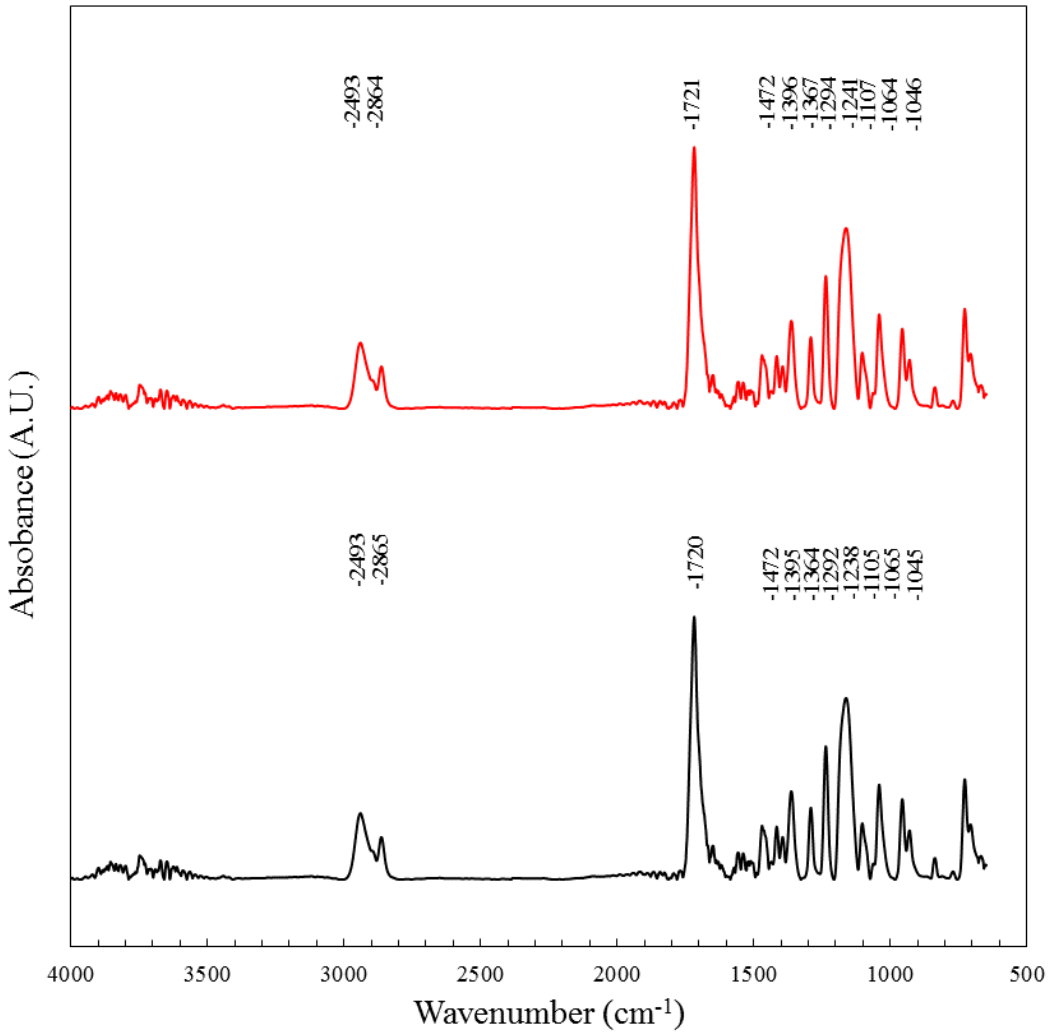

Figure 5.7. Infrared spectrum of the raw PCL (black curve) and PCL NPs (red curve).

The PCL nanoparticles display an infrared spectrum similar to the one of the pristine PCL. The NPs spectrum shows two medium intensity peaks are present at 2943 and 2864 cm^{-1} which correspond to

the asymmetric and the symmetric stretching vibration of the C-H bonds in the macromolecule skeleton. A strong absorbance peak is observed at 1721 cm^{-1} where the stretching vibration of the C=O bond in the ester group is commonly observed. Peaks connected to the bending vibration of the C-H bonds were observed at 1472, 1396, 1367 cm^{-1}. Further absorption bands peculiar of the stretching of C-O were observed at 1292, 1238, 1105, 1065, 1045 cm^{-1}.

Table 5.1. Characteristic absorption bands of the raw PCL and PCL NPs.

Wavenumber (cm^{-1})		**Attribution**
Raw PCL	**PCL NP**	
2943	2943	Asymmetric C-H stretching vibration
2865	2864	Symmetric C-H stretching vibration
1720	1721	Stretching vibrations of C=O bond in esters groups
1472, 1395, 1364	1472, 1396, 1367	Bending vibrations of C-H
1292, 1238, 1105, 1065, 1045	1294, 1241, 1107, 1064,1046	Stretching vibrations of C-O

Comparing the characteristic absorption peaks of the PCL nanoparticles with one of the raw PCL, it is possible to notice that no significant changes in the characteristic absorption wavenumber have occurred. In fact, only small peak shifts were reported (about 2-3 cm^{-1}). These minor peak shifts observed were interpreted taking into account the presence of water in the NPs already observed during SEM analysis. The interaction of water with the functional groups in the polymer chains by hydrogen bond was considered responsible for the minimal differences among the two spectra. The infrared analysis proved that during FNP the PCL does not undergo significant chemical modification

as it is expected from the fact that throughout the nanoparticle formation process the PCL is only dissolved and precipitated without reacting with the other species involved.

The thermal properties of the PCL nanoparticles were investigated by and TGA analyses. The DSC thermogram of the raw polymer and the polymeric nanoparticles are plotted in Figure 5.8 while the main thermal events observed are listed in Table 5.2.

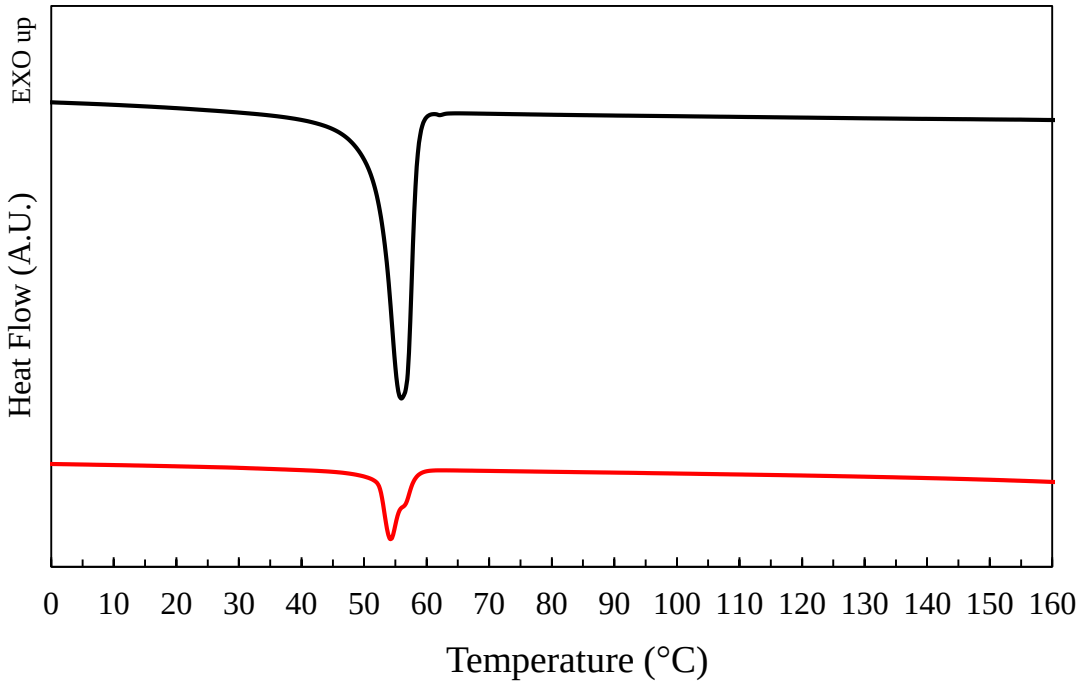

Figure 5.8. DSC thermogram of raw PCL (black curve) and PCL NPs (red curve) for the second heating ramp.

The DSC curves of the raw PCL and the PCL nanoparticles own similar shapes. The main thermal event observed is the endothermic peak attributed to the PCL melting between 50 and 60 °C. Overall no significant peaks in the melting temperature were observed. It was observed a marked decrease in the enthalpy of fusion as well as the crystallinity degree of the nanoparticles sample. Such a phenomenon is explained considering that during the nanoprecipitation process, the polymer molecules are precipitated in a very short time, which does not allow the macromolecules to reassemble in a crystalline state. The crystalline fraction observed in the nanoparticles is attributed to the primary nuclei which crystallize at the beginning of the FNP process as a consequence of the supersaturation.

Table 5.2. List of the thermal events observed during the DSC analysis of PCL NPs.

Sample	PCL	PCL NP
ΔH_{fus} (J/g)	-60.8	-10.8
$T_{fus,\ onset}$ (°C)	51.8	52.1
$T_{fus,\ peak}$ (°C)	55.9	54.3
X_c (%)	43.7	7.8

In Figure 5.9 the results of the TGA analysis of PCL NPs are reported, the main data obtained from the analysis are listed in Table 5.3.

The TGA curves of the PCL nanoparticles display a shape similar to one of the pristine polymer. The main difference observed among the two samples is the onset temperature of the thermal degradation process, which, in the case of PCL NPs occurred at a lower temperature. The decrease in the degradation onset was attributed to a decrease in the polymer molecular weight, in accordance with the results reported by Persenaire et al. (2001). Considering that, the FNP process was not reported to cause depolymerization, the reason for the MW decrease in the NPs sample was attributed to the storage conditions. It was taken into account that between the particle production and the thermal analysis 2-3 days passed to assure the complete drying of the particles. During this time the PCL NP sample was likely to be subject to the attack of the microorganisms normally present in the laboratory environment. Indeed PCL can be de easily degraded by these microorganisms, moreover being nanostructured, higher surface area was available for the bacterial attack (Woodruff and Hutmacher, 2010). Thereafter, the MW loss was attributed to a partial PCL biodegradation occurring during the time between the nanoparticle synthesis and thermal analysis. This MW decrease due to partial biodegradation was also considered to be in part responsible for the lower crystallinity degree of the NP sample observed by the DSC analysis.

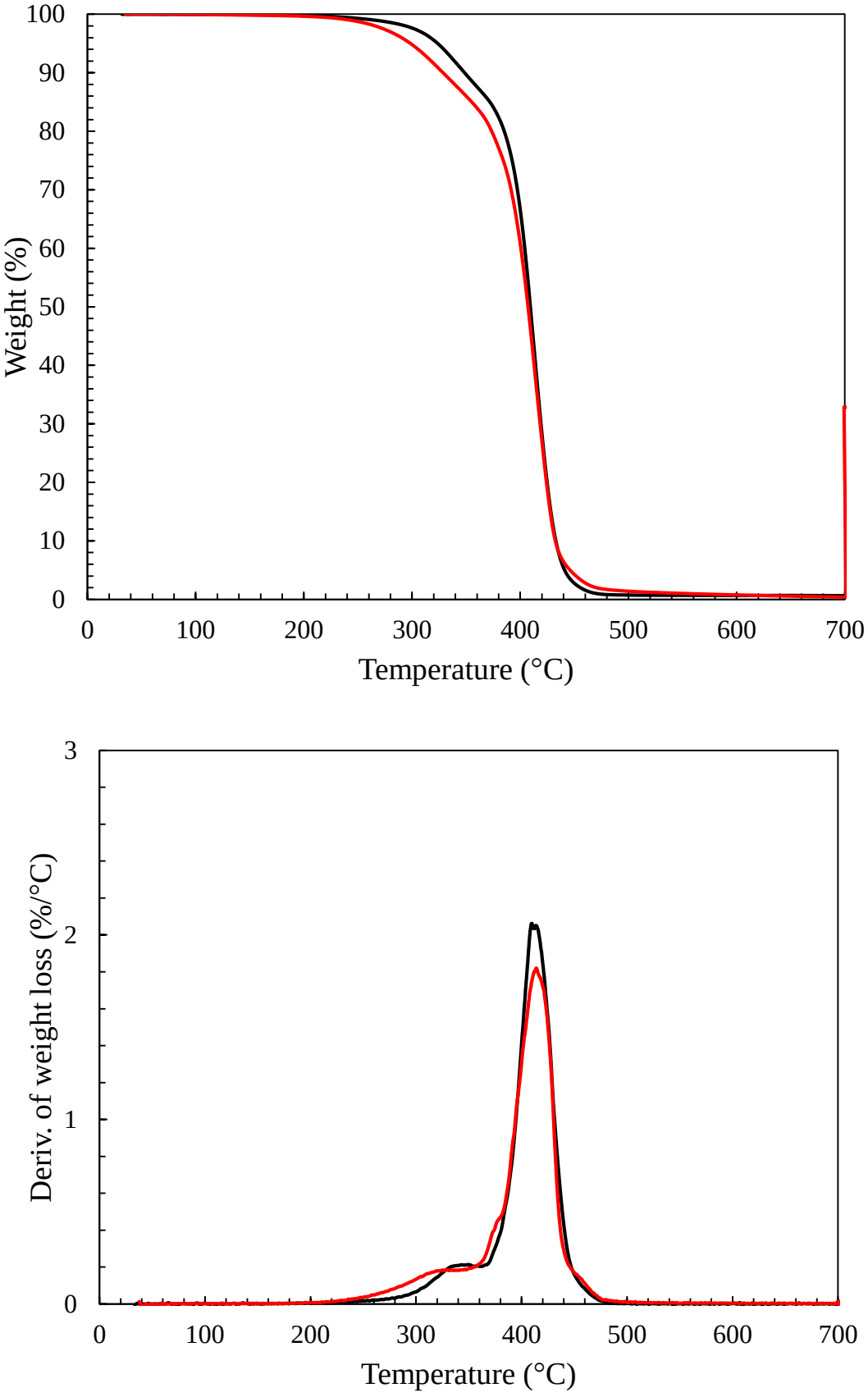

Figure 5.9. TGA analysis of PCL (black curve) and PCL NPs (red curve). TG curve (top) and the first derivative of the TG curve (bottom).

Table 5.3. List of the thermal data obtained from the TGA analysis of PCL NPs.

Sample	$T_{5\%}$ (°C)	T_{max} (°C)	MMLR (%/°C)	Residue at 700 °C (%)
PCL	324	409	2.1	1
PCL NP	298	414	1.8	0

Overall, in the present chapter the results regarding the formation of PCL nanospheres by the FNP methods were reported. The effects of the solvent and of the operating paramenters on the particle size were assessed. Moreover, the different characterization conducted provided insights on the particles physical, chemical and morphological properties.

Chapter 6. Preliminary study on drug encapsulation and release: melatonin as a case study

6.1. Scope of the study

The flash nanoprecipitation method was verified to be effective in producing PCL nanospheres with a suitable size for transdermal application. The FNP technique was then inquired for its applicability in the context of biofunctional textile production. Therefore, some preliminary investigations were conducted to test the drug encapsulation, the textile finishing and the transdermal release properties of the obtained materials. Overall, this research line aimed to verify whether the proposed approaches are suitable for the production of biofunctional textiles by means of a proof of concept study.

For this preliminary set of experiments, melatonin was chosen as the model drug to be tested. Melatonin is known to have partially hydrophobic behavior, it is however also slightly soluble in water. These characteristics make melatonin ideally suitable both for encapsulation by a solvent displacement method and for transdermal release. Indeed, as previously discussed, poorly water soluble substances are known to be easily encapsulated by solvent displacement methods since they cannot diffuse in the antisolvent and so tend to partition inside the core of the polymeric particle. Concerning transdermal release, it is known that, to effectively cross the epidermis, a substance should have a hydrophobic character. However, the drug should have a partial hydrophilic character to diffuse through the dermis and reach the systemic circulation. So the substances with a partially hydrophilic and partially hydrophobic behavior are the ones that can more easily overcome the skin barrier.

Since melatonin has the ideal hydrophilicity characteristics it was selected for these preliminary proof of concept experiments. Indeed the fact that the proposed system works with melatonin was identified as a necessary condition for it to work also with markedly hydrophilic and hydrophobic drugs. Furtherly, the preliminary results obtained for melatonin were considered of significant importance to develop improved methodologies for synthesis and analysis of caffeine and curcumin based biofunctional materials.

To summarize, the scope of the present preliminary study consisted of developing synthesis methods for melatonin loaded nanoparticle suspensions. The produced NPs were employed for the functionalization of cotton fabric whose transdermal release ability was evaluated by the Franz cell test. The specific methodologies used are here described in major detail.

6.1.1 Nanoparticles preparation

For the production of melatonin loaded nanoparticles, the drug was dissolved in the acetone solution together with PCL. Water was used as the antisolvent. PCL was dissolved at a concentration from 6 to 25 mg/mL while melatonin concentrations ranged between 4.56 and 36 mg/mL. The nomenclature of the formulation indicates the initial concentration of PCL and melatonin used in the preparation, and this codification was adopted throughout the manuscript for all preparations. As an example, the name PCL_6MEL_{36} indicates a formulation obtained using 6 mg/mL of PCL and 36 mg/mL of melatonin. Furtherly, the formulation were also described in terms of drug to polymer mass ratio (MR), the latter parameter is defined in equation 6.1.

$$\mathbf{MR} = \frac{m_{drug,in}}{m_{pol,in}}; \tag{6.1}$$

Where $m_{drug,in}$ and $m_{pol,in}$ are the initial mass of drug and polymer fed to mixer respectively. The nanoparticles were collected in the glass vial where 4 mL of water was placed to achieve a QR=1.

6.1.2 Characterization of the nanoparticles suspension

The particle size and Zeta potential of the formulations were measured by DLS technique. The zeta potential analysis was conducted on particle formulations having an initial polymer concentration of 6 mg/mL and melatonin concentration varying from 4.56 to 36 mg/mL.

The LC and EE were evaluated by an indirect protocol, as described in Chapter 3. The suspensions were placed in a rotary evaporator at 45 °C, under vacuum for 15 minutes, to remove acetone; then, it was centrifuged for 10 minutes at 19700 g and the liquid phase was finally separated from the solid NPs. 0.1 ml supernatant sample was diluted in 50 ml of water, filtered through a 0.2 µm cellulose syringe filter and analyzed via UV-Vis spectroscopy. EE and LC were calculated by quantification of free melatonin in the supernatant by mean of the UV/Vis spectrophotometer. The formulations on which it was run the LC and EE test are listed in Table 6.1.

Table 6.1. List of the formulations produced.

Sample name	Melatonin concentration (mg/mL)	PCL concentration (mg/mL)	MR
$PCL_6MEL_{4.56}$	4.56	6.00	0.76
PCL_6MEL_{36}	36.00	6.00	6.00
$PCL_{25}MEL_{4.56}$	4.56	25.00	0.18
$PCL_{25}MEL_{36}$	36.00	25.00	1.44

6.1.3. Fabric functionalization and testing

Knitted cotton fabrics (100% cotton, Nm 30/1, single jersey) were scoured at 95 °C for 30 min in a 4 mg/ml Na_2CO_3 water solution and rinsed under tap water for 10 min to remove impurities and waxes. Thereafter, the fabrics were functionalized by imbibition. A volume of 0.5 mL of freshly prepared nanoparticles suspension was distributed on a 2.5-cm diameter fabric disk. The suspension was added dropwise, taking care that each drop was completely absorbed by the fabric and that any leakage of the suspension from the textile was not occurring, thus assuring a controlled amount of the active substance to be deposited onto the fabric. After the desired suspension volume was delivered to the fabric, the samples were dried in standard textile laboratory conditions (20°C and 65% RH) for 8 hours. The textile sample produced was named based on the NP formulation employed. As an example, COT-PCL_6MEL_{36} indicates cotton fabrics functionalized with the PCL_6MEL_{36} nanoparticle formulation.

To assess the effectiveness of the finishing treatments the fabric surface morphology was examined by a Leica Electron Optics 435 VP scanning electron microscope (Cambridge, UK) with an acceleration voltage of 15 kV, a current probe of 400 pA and a working distance of 20 mm. The samples were mounted on aluminum specimen stubs and sputter-coated with gold in a rarefied argon atmosphere using an Emitech K550 Sputter Coater with a 20 mA current for 240 s.

The capability of functionalized fabrics to release the active principle was tested in vitro using single port Franz diffusion cells. The system was characterized by a 12-ml acceptor compartment and a contact surface of 1.8 cm^2 was used. The acceptor compartment was filled with pH 7.4 phosphate buffer solution kept at a temperature of 33°C by a heating jacket. The skin mimicking membrane was

boiled for 60 minutes to remove glycerol or any other additives and enhance wettability; finally, the fabric patches were placed over the membranes in the donor compartment and sealed over the membrane by a clamp. A drop of acceptor solution was drawn on the fabric sample to ensure contact with the membrane and mimick sweat. Samples of the acceptor fluid were withdrawn at a fixed time interval and analyzed by spectrophotometry; after withdrawal, an equal volume of fresh PBS solution was replaced into the cell. Melatonin's release data were fitted by Zero-Order, First-Order, Higuchi, Hixon-Crowell and Baker-Lonsdale models. The regression was performed by interpolating the data of the curve until the plateau in the cumulative release was reached. The coefficient of determination (R^2) was used to discriminate the best fitting model.

6.2 Production of Melatonin loaded PCL nanoparticles

The nanoparticles were characterized in terms of size, zeta potential, loading capacity and encapsulation efficiency. It was tested whether the proposed methodology displayed effective incorporation of the active principle. Moreover, it was elucidated how the addition of drugs to formulation affected the properties of the PCL nanoparticles.

6.2.1 Particles size and zeta potential

Particle size was measured for different batches produced at different flow rates. The results obtained for the formulation PCL_6MEL_{12} are reported in Figure 6.1. It can be observed that the particle diameter decreased dramatically as the inlet flow rate was increased. A sharp decrease in the particle diameter was observed up to a value of 40 mL/min, above which the NP size tended to reach an asymptotic value of about 280 nm. This trend is analogous to the one observed and discussed in Chapter 5 dealing with the formation of PCL nanospheres. Moreover, these observed trends are consistent with the ones found in the literature for the preparation of nanoparticles by the FNP technique both by experimental and numerical approaches (Chow et al., 2014; Gavi et al., 2007).

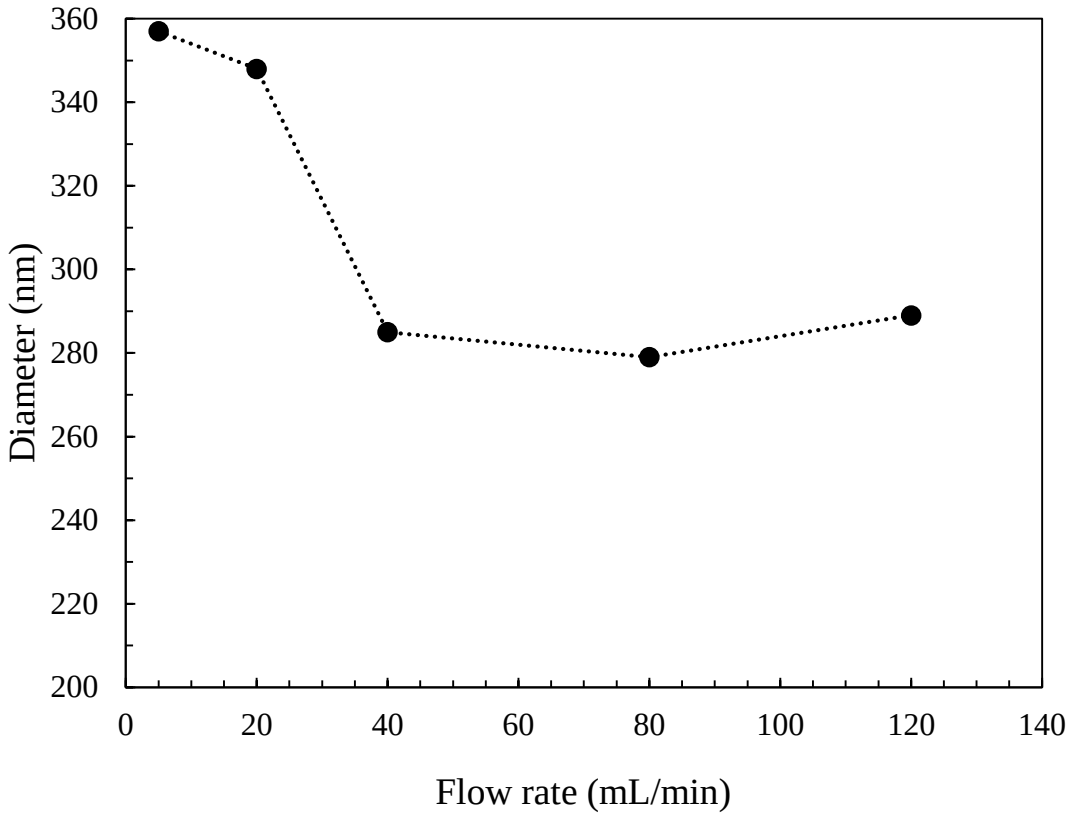

Figure 6.1. Mean particle diameter for different flow rates for the PCL6MEL12 formulation.

Therefore, it was verified that the addition of the drug in the formulation does not compromise the possibility of reducing particle size in accordance with the previously found results (Ferri et al., 2017). To minimize the diameter as required for transdermal applications, further experiments were conducted at 80 mL/min, namely, the value above which NP size was leveled off.

Given that the amount of drug dissolved in the solvent may affect particle formation mechanism, the effect of formulation parameters, i.e. the PCL and the Melatonin initial concentration were studied. In Figure 6.2 the particle size for the different formulations was shown. The increase of either polymer or melatonin concentration causes an increase in the particle size. Such an increase was found to be dependent on the melatonin concentration if PCL concentration was kept constant. Moreover, the increase in particle size versus melatonin concentration was steeper for the higher polymer concentrations. Thus the two factors were observed to act synergistically in displaying a diameter increase.

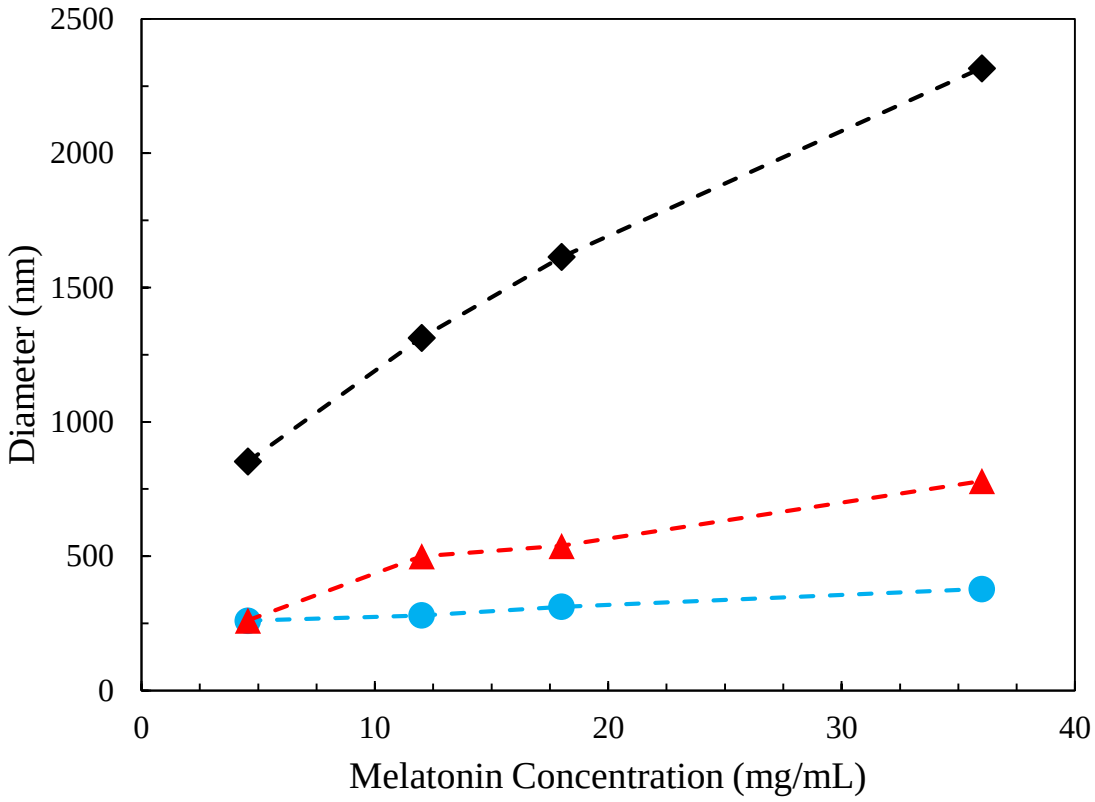

Figure 6.2. Particle size versus inlet PCL and melatonin concentration for samples produced at FR= 80 mL/min at different PCL concentrations: CPCL=6 mg/mL (blue circles), CPCL=10 mg/mL (red triangles) and 25 mg/mL (black diamonds).

The impact of polymer concentration on the diameter of the particles is a well known phenomenon. Indeed, high polymer concentration determines the increase of the number of macromolecules that could assemble over the formed nuclei. Concerning the effects of melatonin addition, it is reasonable that the observed increase of particle size could be due to the loading of the active substance into the particles.

From the investigation of particle size, it was evidenced that it was possible to tune particle size both by adjusting the formulation and the operating parameters. In this way, particles with sizes ranging from 300 nm to a few micrometers were obtained.

Observing the values of zeta potential reported in Figure 6.3. it is noticeable that, upon the addition of the drug, the Zp tends to increase (becoming less negative). Although it is not possible to identify a clear trend Zp as a function of C_{mel}, it is clear that the colloidal stability of the particles decreased upon melatonin addition. Therefore, it is also possible to correlate the particle size increase with

aggregation phenomena that may be more significant when melatonin is added to the system. Surface charge increase is explained by taking into account the melatonin chemical structure. Indeed, the molecule has an amino group that can undergo protonation in the aqueous environment, thus the presence of this molecule on the particles surface, or in the liquor (as free drug) would be responsible for the zeta potential increase.

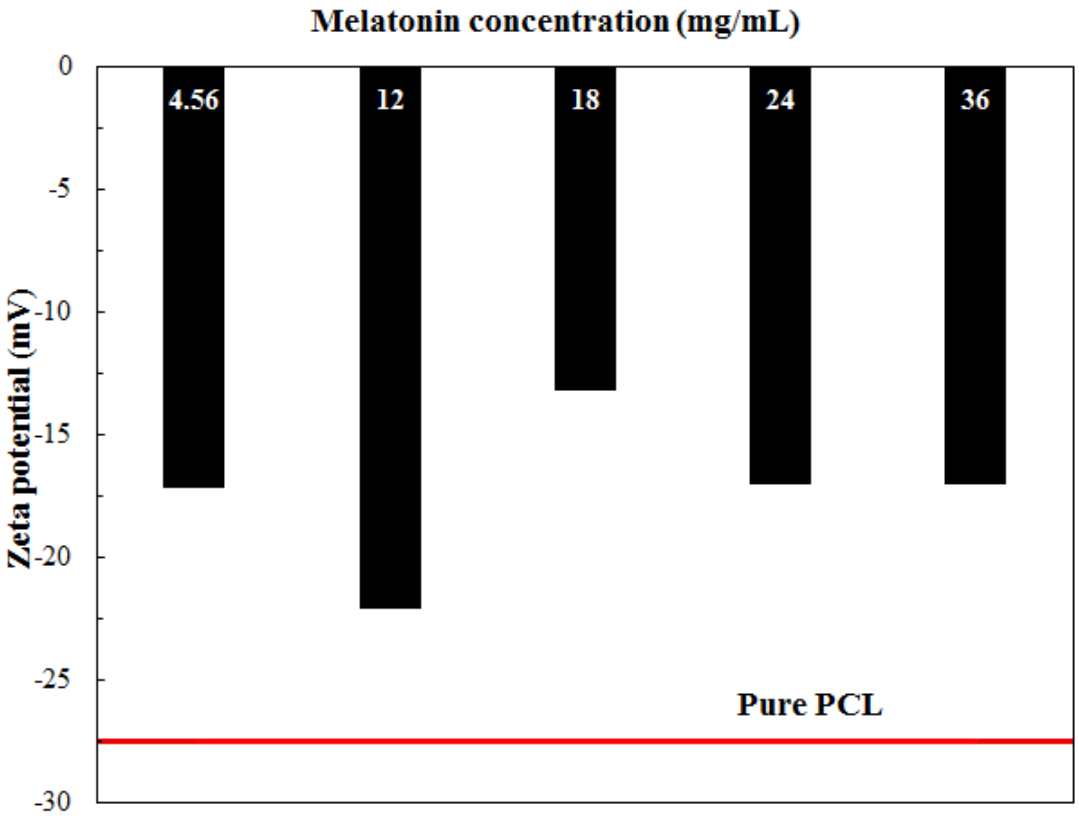

Figure 6.3. Zeta potential of formulations with PCL 6 mg/ml and different melatonin concentrations (Black bars) and for pure PCL (Red line).

6.6.2 Drug incorporation study

The effective drug incorporation was evaluated by calculating the loading capacity and encapsulation efficiency of different formulations with different mean diameters, the results are plotted in Figure 6.4. High process yields were always achieved, leading to the minimum depletion of the active substance during nanoparticle production. This result is because aqueous solubility of melatonin is not particularly high (~2.5 mg/mL) (Kandimalla et al., 1999). Samples produced with low initial

melatonin concentration presented the lowest EE. Also, this result should be interpreted taking into account the drug solubility in water that, even though it is low, is not negligible. Therefore, some melatonin is transferred and dissolved in water during the flash precipitation process and this amount is in percentage more relevant for low initial melatonin concentration. It can then be concluded that in the case of slightly hydrophobic drugs, due to low water solubility, the FNP methods display high but not full incorporation of the active substance. Similar results and encapsulation mechanisms were reported for doxorubicin, a drug with a LogP value of 1.3, thus close to the one melatonin 1.15 (Tam et al., 2016).

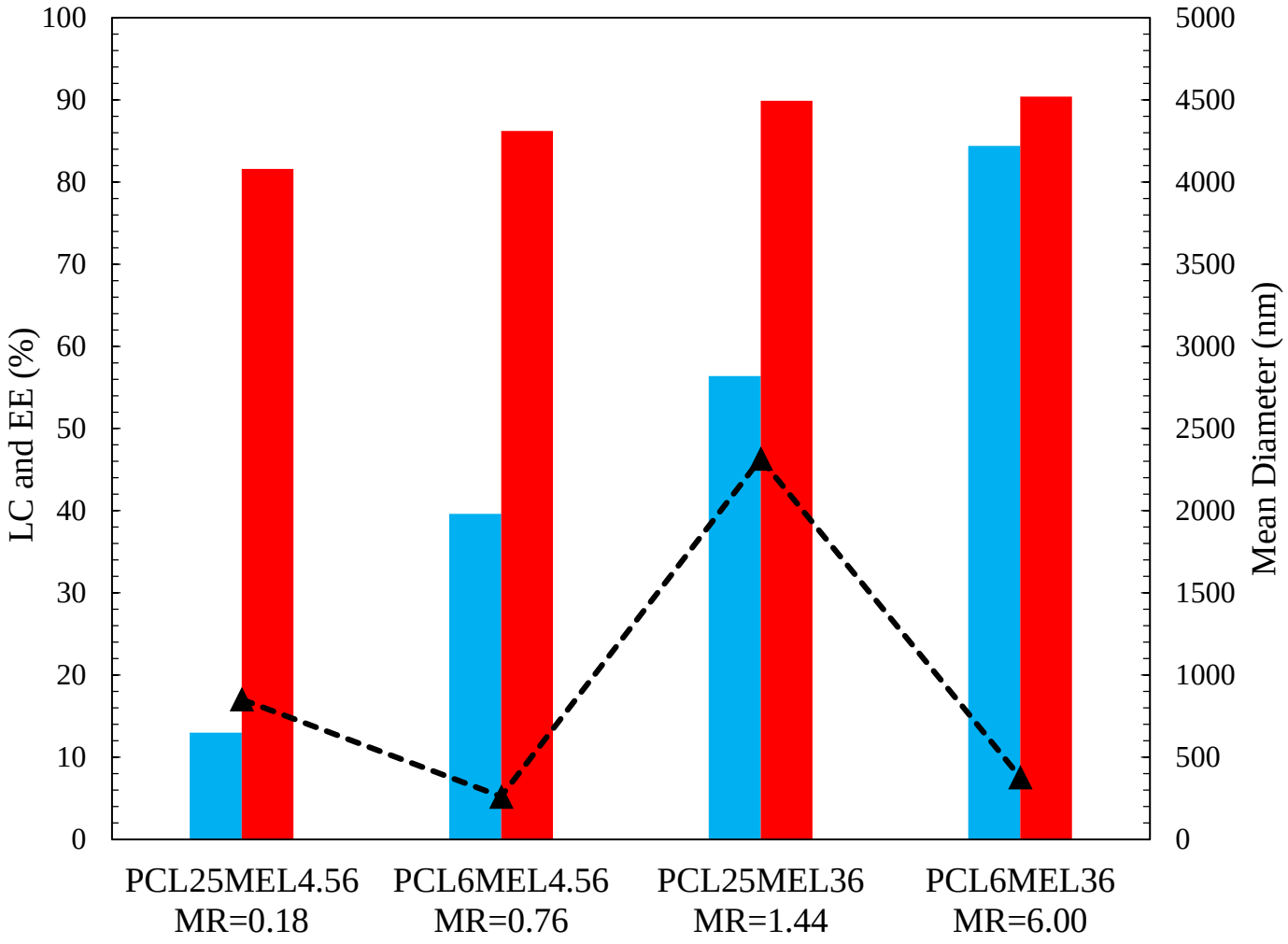

Figure 6.4. Values of EE (red bar) and LC (blue bar) on the primary y-axis and of mean diameter (black triangles) on the secondary y-axis for the different formulations.

It is also observed that a slight increase in EE occurs upon increasing the MR. Especially higher values of EE are displaced when the formulation contained a melatonin concentration approaching

the saturation level (Li et al., 2017). The high values of EE of such formulation are then explained taking into account two possible phenomena. Firstly, being the initial melatonin in acetone solution quite close to the saturation point, a fast mixing with the antisolvent causes a higher level of supersaturation, thus the nucleation of melatonin molecules together with the polymer one and improving the extent of encapsulation. Secondly, it is considered that being partially hydrophilic, melatonin partition between the polymer and liquor. Therefore, with high initial melatonin concentration, a small percentage of the initial melatonin concentration can easily saturate the liquor solution, while the rest remains inside the polymeric matrix. These proposed incorporation mechanisms were found to be consistent with the one previously reported (Chow et al., 2014).

The loading capacity was instead found to be more strongly dependent on the drug-to-polymer mass ratio. This correlation is explained considering the previously described encapsulation mechanisms and recalling the definition of EE and LC. Assuming that the polymer undergoes complete precipitation, which is a reasonable assumption because of the scarce solubility of PCL in water acetone mixtures (Bordes et al., 2010; Ferri et al., 2017), Equation 3.2 and 3.3 can be re-written as:

$$LC = \frac{m_{drug,en}}{m_{pol,in} + m_{drug,en}} \quad \text{and} \quad EE = \frac{m_{drug,en}}{m_{drug,in}};$$

By solving Equation 3.3 for $m_{drug,en}$ and substituting in Equation 3.2 it is obtained:

$$LC = \frac{m_{drug,in} \times EE}{m_{pol,in} + m_{drug,in} \times EE};$$

And by dividing all the terms for $m_{pol,in}$:

$$LC = \frac{MR \times EE}{1 + MR \times EE}; \tag{6.2}$$

From Equation 6.1 it can be observed that, for a given value of EE, LC is a function of the MR. This property is of particular interest since it allowed to achieve the desired drug content in the nanoparticle formulations by adjusting the initial formulation. Finally, it was observed that EE and LC are independent of the diameter of the particles.

To conclude, the investigation of LC and EE proved the effective incorporation of melatonin in PCL nanoparticles, which is indeed a necessary requisite to proceed to the textile finishing. Proving effective incorporation of the drug in the particles also provided a better understanding of the increase of particle size upon melatonin addition.

6.3 Fabric finishing and in drug release studies

Cotton fabrics were impregnated with the nanoparticles formulation. For the imbibition experiments, four formulations were selected. The first two, namely $PCL_{25}MEL_{4.56}$ and $PCL_{25}MEL_{36}$ characterized by high polymer concentration and micrometric size (853 and 2316 nm respectively). The other two formulations, i.e. $PCL_6MEL_{4.56}$ and PCL_6MEL_{36} were prepared using lower concentration and were characterized by lower diameter (260 and 378 respectively). The choice of these specific formulations aimed to investigate the quality of functionalization using particles of different sizes, particularly above and below the 450 nm limit of skin mimicking membrane pore size.

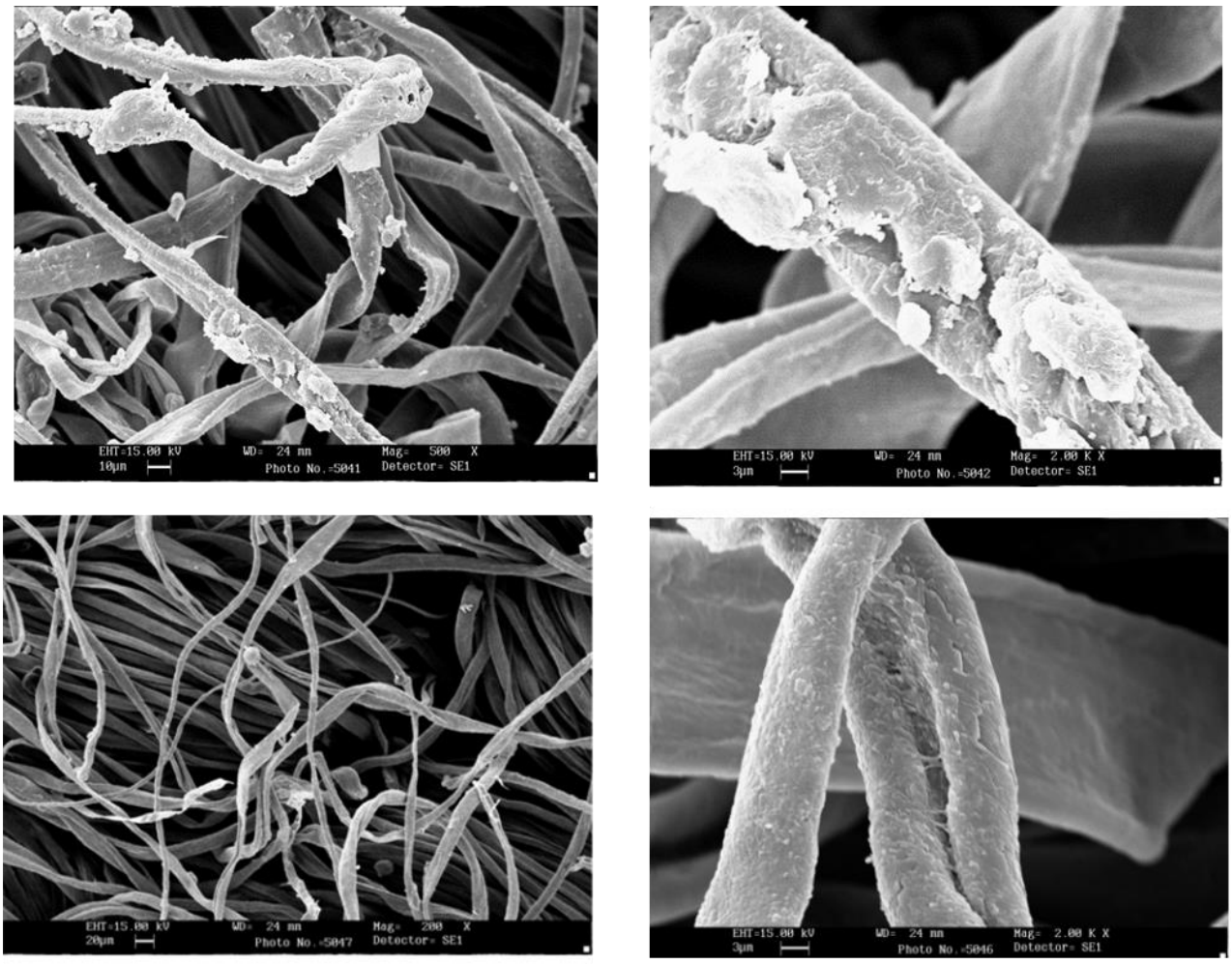

Figure 6.5. SEM image of treated cotton. On top sample COT-PCL25MEL4.56 at 500 X (top left picture, scale bare of 10 µm) and 2000X (top left picture, scale bare of 10 µm). On the bottom sample COT-PCL25MEL36 at 200 X (top left picture, scale bare of 20 µm) and 200.

The fabrics obtained upon NP applications were observed by SEM to investigate NPs adhesion on the fibers and understand the interaction of the particles with the structure of cotton fibers. In Figure

6.5 the SEM images of the samples obtained upon functionalization with bigger size particles, i.e. COT-$PCL_{25}MEL_{4.56}$ and COT-$PCL_{25}MEL_{36}$ are shown.

Observing sample COT-$PCL_{25}MEL_{4.56}$ (Figure 6.5 Top) the surface of the fibers appears to be mostly covered with polymer aggregates which tend to form a film. In the lower magnification image (Figure 6.5 top left) some particles are observed in the background. These latter are attached to the outer surface of the cotton fibers. Similarly, sample COT-$PCL_{25}MEL_{36}$ showed a few particles to be present on the fibers in low magnification image (Figure 6.5 bottom left); while observing the sample at higher magnification (Figure 6.5 bottom left) a polymer film appears to be covering the fiber.

The SEM images of the samples $PCL_6MEL_{4.56}$ and PCL_6MEL_{36} are reported in Figure 6.6.

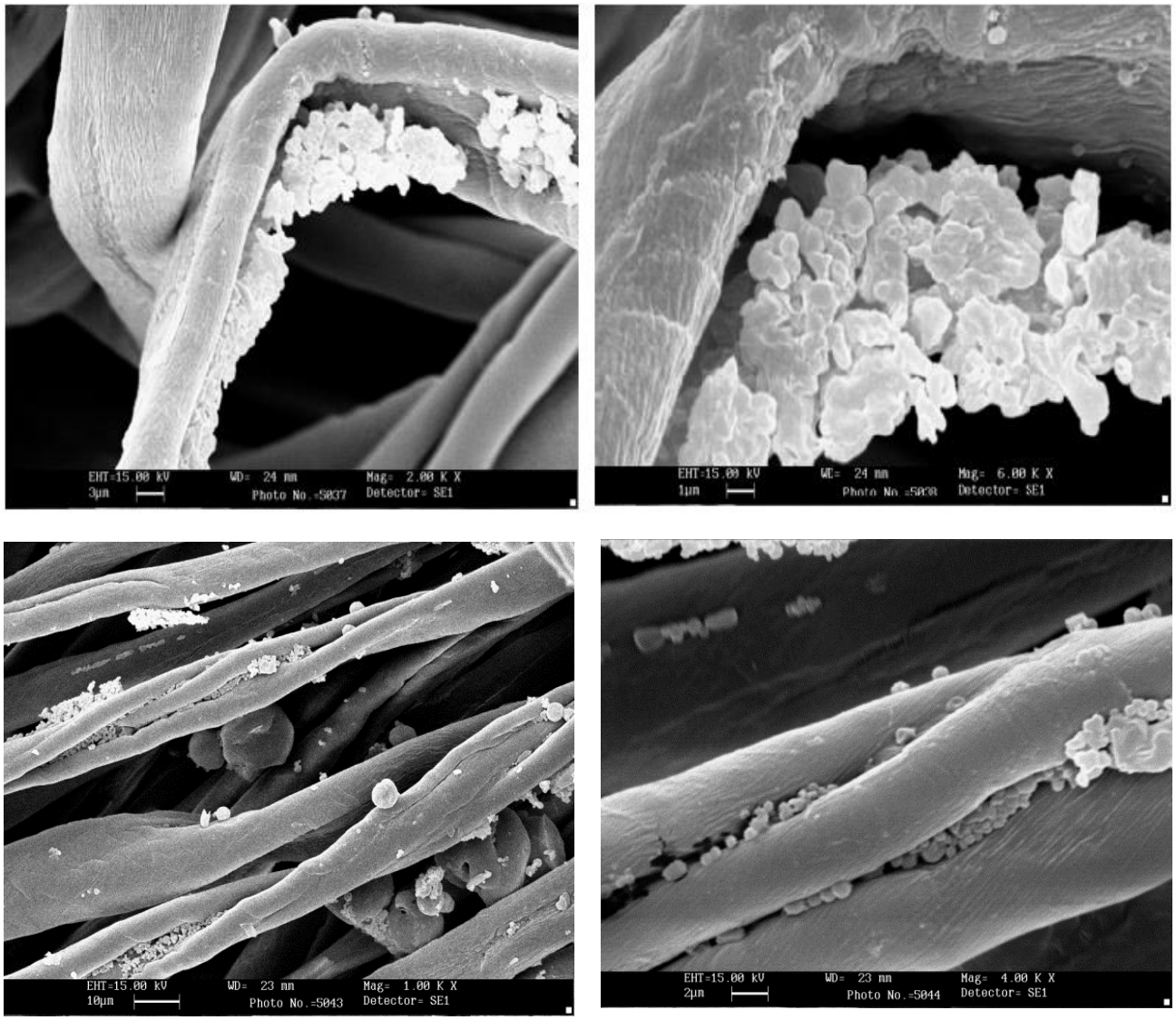

Figure 6. 6. SEM image of treated cotton. On top sample COT-PCL6MEL4.56 at 2000 X (top left picture, scale bare of 3 µm) and 6000X (top left picture, scale bare of 1 µm). On the bottom sample COT-PCL6MEL36 at 1000 X (top left picture, scale bare of 10 µm) and 4000X

Overall, the fabric samples functionalized with small particles display different morphology with respect to big ones. In both cases, the nanosized particles are hosted inside the cavities of the bean-shaped structure of the cotton fiber. Inside the structure of the fibers, the particles have maintained their characteristic spherical shape, even if significant aggregation had occurred. This latter phenomenon is known to occur to the particles during the drying as it was observed in the preliminary investigation about the PCL nanospheres morphology (Figure 5.5).

Overall the SEM analysis highlighted the interaction of the finishing with the fabrics. First of all, it was proved that the proposed finishing treatment leads to the effective functionalization of the textiles. Secondly, two mainly different morphologies were observed, upon functionalization with particle formulations of different sizes. When particles with a diameter in microscale were used the fibers appeared to be covered with a polymeric film and spherical species were rarely observed. Oppositely, employing nanosized particles, these were hosted inside the fiber structure and kept their spherical shape. These morphologies are due to the fact the finer particles can more easily access the interior part of the fiber; once in the core of the fiber they are more protected from the external environment and they keep their spherical shape. Oppositely, coarser particles cannot easily diffuse inside the fabric core and thus tend to interact more with the outer part of the fiber surface. In this part of the fiber, they are more sensitive to the external environment and have a higher tendency to collapse in a polymer film.

Even if aggregation among the particles was observed to occur, it is worth noticing that the nanoparticles supported on the fabrics surface (Figure 6.6) show less significant aggregation if compared with the raw PCL particles, which were observed to drastically collapse and almost lose their spherical structure during drying (Figure 5.5). The fact that these formulations can better hold their structure upon being dropped and dried on the fabrics hints that the fabrics can effectively support and protect these carriers from collapsing during drying.

6.3.1. In vitro Franz cell test

The cumulative drug released for the different formulations is plotted in Figure 6.7. For each formulation, the cumulative drug released was normalized over the total amount of active substance collected in the acceptor compartment during the test.

Observing the cumulative release curves of the four samples it emerges that two samples, namely COT-$PCL_{25}MEL_{4.56}$ and COT-$PCL_{6}MEL_{4.56}$ exhibited fast release kinetics reaching a plateau within

150 minutes. Oppositely, samples COT-PCL$_{25}$MEL$_{36}$ and COT-PCL$_{6}$MEL$_{36}$ were able to release the drug for a prolonged time, indeed the total amount of drug was released over 500 minutes. Such a difference in the characteristic release times between the two couples of samples is due to the significantly different melatonin concentrations in the formulation, and so to the higher melatonin quantities onto the fabrics. Considering that differences in drug concentration is the driving force that makes the mass transfer to occur, higher initial drug concentrations make this driving force higher. The release phenomenon goes on until the driving force lowers to the point at which an equilibrium of concentration between donor and acceptor compartment is reached. Therefore, longer times are required for the system to reach equilibrium with high drug concentration.

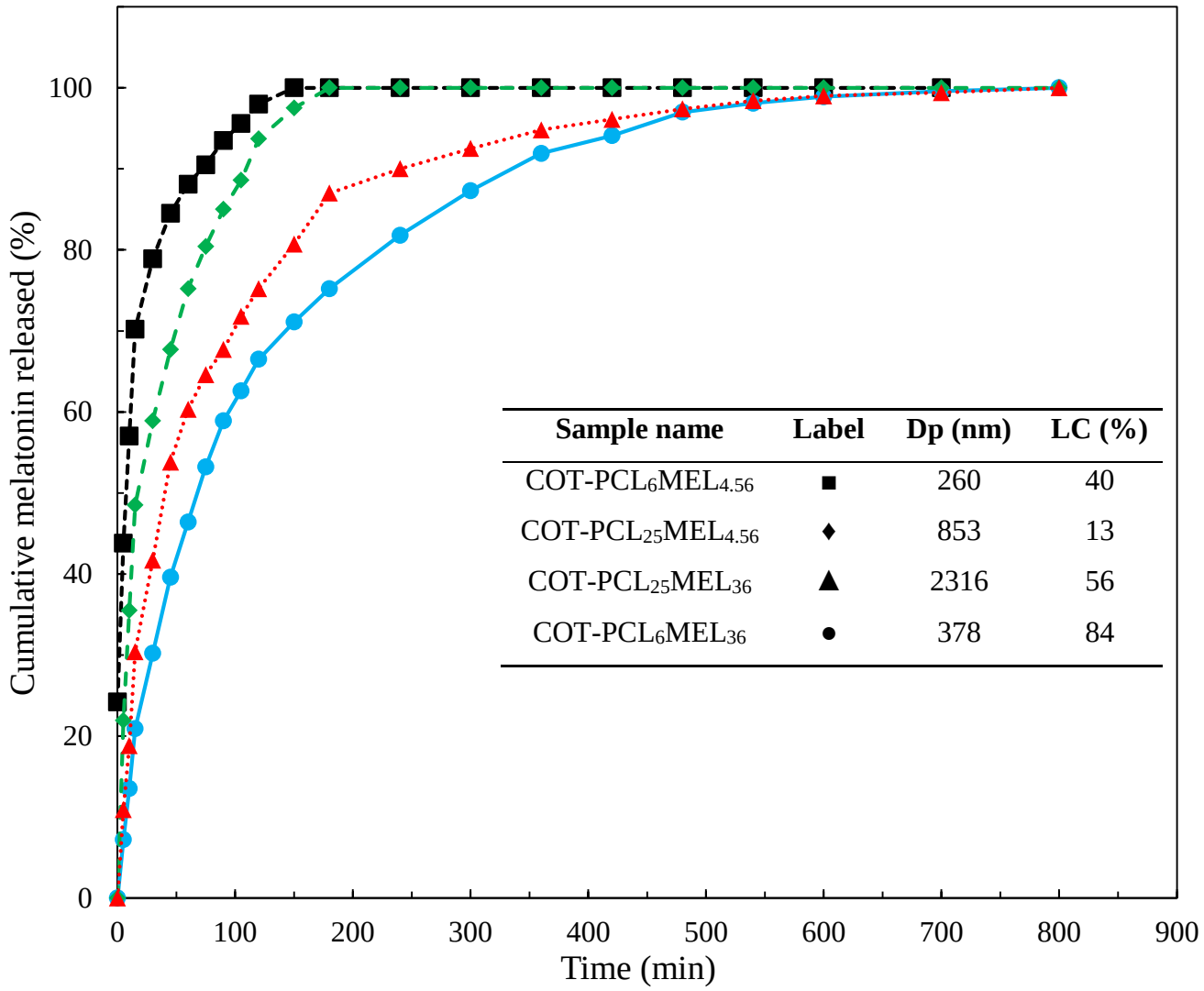

Sample name	Label	Dp (nm)	LC (%)
COT-PCL$_{6}$MEL$_{4.56}$	■	260	40
COT-PCL$_{25}$MEL$_{4.56}$	♦	853	13
COT-PCL$_{25}$MEL$_{36}$	▲	2316	56
COT-PCL$_{6}$MEL$_{36}$	●	378	84

Figure 6. 7. Cumulative release curves for the functionalized patches.

Comparing the release curves of the two samples produced with lower melatonin concentration it is observed that COT-$PCL_6MEL_{4.56}$ displays a faster drug release respect to COT-$PCL_{25}MEL_{4.56}$. These results are ascribed to the different characteristics of the particles used for the fabric imbibition. Indeed, the formulation $PCL_6MEL_{4.56}$ was characterized by a lower size. Being the particles smaller than the pores of the membrane used in the Franz cell experiment, the NPs were capable of crossing the membrane and release the drug. Oppositely, having $PCL_6MEL_{4.56}$ size above the membrane pores, the particles cannot cross the membrane. The release of melatonin then must occur through the diffusion of the drug from the textile substrate and then by the crossing of the skin mimicking membrane by the drug molecules. Taking into consideration the LC of these two formulations, it is noticeable that the one with higher drug content displays faster release kinetics. This is attributed to a combination of the higher LC and small Dp, in facts, being the particles small they can easily cross the membrane and having higher LC they can deliver the melatonin dosage very fast reaching soon the equilibrium concentration.

Focusing on the comparison between the samples with a higher amount of melatonin, i.e. COT-$PCL_{25}MEL_{36}$ and COT-PCL_6MEL_{36}, it is noted that the latter samples display the slowest release kinetics. This result is interpreted taking into account the particular properties of the formulation PCL_6MEL_{36}. Indeed, these NPs had a characteristic size comparable to one of the skin mimicking membrane. This led the particles to partly cross the membrane and partly get stuck inside its pores. Moreover, taking into consideration the high loading content of this formulation, the particles stuck inside the membrane pores can act as a reservoir system with high drug delivery capability. Then the release mechanism hypothesized for this specific sample consists of a first step in which the nanosized particles migrate to the membrane and a second one in which the particles stuck inside the membrane keep releasing the drug. Being the LC high, the same is the time required to release the drug contained inside the structure of the particles leading to slow and controlled release kinetics.

Overall from the analysis of the release curves, it can be concluded that the factor that mostly affected the kinetics of drug release was the initial concentration of melatonin which is known to determine the driving force of mass transfer phenomena. Thereafter, the properties of the nanoparticles, mainly the particle size and the LC, impact drug release kinetics allowing to observe different effects for a given level of initial drug concentration.

The release curves were fitted using the semi-empirical models presented in Chapter 3; the correlation coefficients of every model are listed in Table 6.2. It can be observed that the best fittings are achieved

for the diffusion based models, such as first-order, Higuchi and Baker-Lonsdale. The poor fitting of the Hixon Crowell model is consistent with PCL long degradation kinetics, which makes polymer erosion negligible in the time of the release test.

Among the three diffusion based models, the best fitting model is the Baker and Lonsdale one. The latter was derived for drug diffusing from a spherical matrix, it is then not surprising it most accurately describes the release from the nanospherical system. It of interest to notice that regardless of the different properties of the formulations (such as particle size and loading capacity) the best fitting model was always found to be the Baker and Lonsdale one. This shows that the incorporated drug in a spherical matrix affects mostly the release kinetics. Such an observation is indeed consistent with the characteristics of the samples analyzed and the properties of the models selected for data fitting (Peppas and Narasimhan, 2014).

Table 6.2. Coefficients of determination (R^2) values for release data fitting.

	Zero order	**First order**	**Higuchi**	**Hixon-Crowell**	**Baker-Lonsdale**
COT-PCL$_6$MEL$_{4.56}$	0.33	0.94	0.88	0.79	**0.97**
COT-PCL$_6$MEL$_{36}$	0.63	0.90	0.97	0.82	**0.99**
COT-PCL$_{25}$MEL$_{4.56}$	-0.46	0.71	0.65	0.45	**0.94**
COT-PCL$_{25}$MEL$_{36}$	0.84	0.95	0.98	0.92	**0.99**

By knowing the initial amount of melatonin deposited onto the fabric, the percentage of drug released from the fabric was calculated at the end of the Franz Cell test, these results are reported in Figure 6.8.

Above all, it is observed that for all the fabric samples less than half of the loaded drug was effectively released. The percentage of drug release was found to be similar for all the investigated samples with values between 34 and 39%. Slightly higher values of the released drug were observed for samples COT-PCL$_6$MEL$_{4.56}$ and COT-PCL$_6$MEL$_{36}$, these samples were characterized by small particle size. This shows that incorporating the drug in nanometric size particles leads to an effective enhancement of the transdermal penetration.

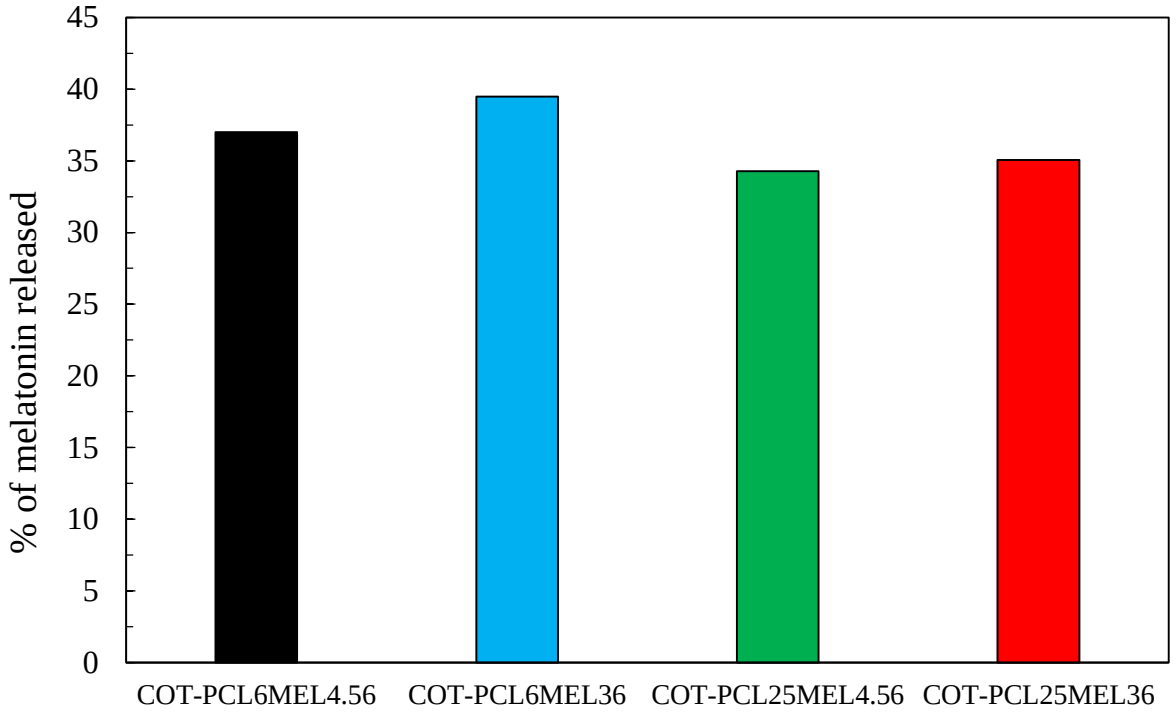

Figure 6.8. Amount of melatonin released respect to the theoretical amount on the fabric.

For all tested samples, the highest percentage of the drug was not released from the textile. This finding evidenced that the release of the active species from the biofunctional textile structure is a critical step that significantly affects the overall release phenomena. As evidenced by in the literature a good contact between the fabric is a necessary condition for the nanocarrier to be released toward the membrane (Martí et al., 2011). Furtherly it is also important to have a transfer medium that allows the drug diffusion, this is generally done by wetting the fabrics at the beginning of the release test (Rubio et al., 2010). This commonly adopted strategy ensure that diffusion phenomena occur in the liquid state and so in relatively short times. However, as the Franz cell test goes on, the liquid at the interface between the fabric and the skin mimicking membrane tends to evaporate. Upon drying, the mass transfer phenomena occurring are limited to the diffusion in the solid state, which is known to occur over a very long time (Bird et al., 1979). This causes the drug elution from the textile to be stopped. The amount of drug released will then be limited to a small part of the total amount deposited onto the fabric.

To conclude, the Franz cell experiments provided insights on the drug release performances of the proposed biofunctional textiles. All the treated samples exhibited a controlled drug release kinetics fitted at best by the Baker and Lonsdale model, as expected from a drug delivery device that exploits spherical carriers. The peculiar properties of the particle formulations showed an impact on both the

time for which the active delivery went on and on the controlled dosage. The nanometric size carriers allowed higher delivery of the active principle thanks to their ability to overcome the skin mimicking membrane.

Part III final remarks

Preliminary studies were conducted to test the validity of the proposed approaches in the context of biofunctional textile preparation. This was done by firstly validating an FNP protocol for the production of PCL nanoparticles. Thereafter the drug loading and the textile finishing were investigated.

Concerning the production protocol of PCL nanospheres three different solvents i.e. acetone, acetonitrile and THF were tested. By conducting experiments with acetone, experiments reported in the literature were replicated, obtaining particles with a suitable size for the dermatological application. Moreover, it was confirmed that the increase in the inlet flow rate leads to a decrease in the particle size. Similar trends were observed when acetonitrile was used as the solvent for PCL. Oppositely such trends were not verified when THF was employed. Finally, among the three solvents acetone was selected for particle production. It was indeed confirmed to produce particles with the lowest diameter. Moreover, acetone has lower toxicity respect to acetonitrile and THF.

Further characterization on the PCL nanoparticles evidenced that the chemical structure of the polymer does not undergo significant changes during the particle formation process. The morphological analysis confirmed that the produced carriers own a spherical shape. A significant tendency to aggregate during the drying was observed, moreover, it was observed that the NP network tends to incorporate water in its structure during drying.

The intermediately hydrophilic substance melatonin was employed for the preliminary loading experiments. The addition of the drug to the formulation was not observed to change the mechanisms of decreasing particle size while increasing the flow rate. Moreover, it was observed that adjusting the initial polymer and drug concentration allowed to produce particles with size ranging from a few hundreds of nanometers to a pair of micrometers. Melatonin was incorporated in the PCL nanostructures with encapsulation efficiency between 80% and 90%. The high but not total incorporation of the active was ascribed to the partition of active molecules between the particles and the liquor as expected from a partially hydrophilic drug. The LC was observed to strongly depend on the drug to polymer mass ratio.

The NPs formulations were used for the cotton fabrics functionalization. The SEM analysis was employed to assess the effectiveness of the finishing treatment. It was evidenced that carriers were successfully attached to the fiber surface. In particular, it was observed that the formulation with small particle diameter displayed a tendency to be incorporated into the interior part of cotton fiber bean like structure while coarser particles did not.

The Franz cell release experiments proved that the biofunctional textile can effectively act as a transdermal delivery system. For all the analyzed samples controlled release kinetics, the Baker-Lonsdale model was fitted at best among semiempirical kinetics models. For all the samples, less than half of the initial dosage was release. Particularly, it was evidenced that particles with a size lower than the pores of the skin mimicking membrane lead to an enhancement of the transdermal delivery.

Part IV Encapsulation of hydrophilic and hydrophobic active principles

Chapter 7. Caffeine, the incorporation of a hydrophilic substance by the FNP method.

7.1 Scope of the study

In this chapter the results concerning the preparation of caffeine loaded PCL nanoparticles are presented and discussed. The present research aims to test the feasibility of incorporating a hydrophilic substance such as caffeine through the FNP technique. Furtherly, the scope of this study is to develop a caffeine nanoformulations with suitable properties for dermatological applications. As more deeply reported in Chapter 4, caffeine aroused significant interest in the field of dermatology; therefore, the successful nanoencapsulation of this drug was considered as a potential advancement in the context of dermatological posologies.

The encapsulation of hydrophilic substances by FNP is a scarcely tackled issue in the literature and the present study delivered novel insights. In a recent review by Martinez Rivas et al. (2017), it was clearly stated that one of the actual limitations of the nanoprecipitation method is its scarce suitability for the encapsulation of hydrophilic molecules. In fact, the use of water as the antisolvent greatly promotes the drug to dissolve in the liquor rather than being incorporated in the polymer spheres. In the last few years, a limited number of studies proposed the use of FNP for the incorporation of partially hydrophilic drugs such as doxorubicin (Tam et al., 2016). However, the incorporation of a strongly hydrophilic substance such as caffeine (logP=-0.55) was not deeply inquired.

Besides the primary aim of testing FNP application to the encapsulation of a hydrophilic substance, the present research proposed a novel method for caffeine carriers production. Indeed, caffeine encapsulation was proposed in the literature to better control the burst release typical of such a hydrophilic drug (Puglia et al., 2016; Rodrigues et al., 2016) through the use of liposomes (Budai, 2013; Chorilli et al., 2013), and polymeric nanoparticles (Yew and Misran, 2016). However, the scientific literature also highlighted that caffeine encapsulation efficiency higher than 30% was rarely achieved using the above-mentioned carriers, whichever the encapsulation method adopted. Thus, caffeine encapsulation is a challenging issue to be tackled.

In the here proposed approach, two FNP protocols were proposed, i.e. using either acetone or water as drug solvent. The effects of caffeine addition on particle size were evaluated, thereafter, the EE and LC were measured both by the direct and indirect method. The effect of the caffeine solvent on the structure of the particles was evaluated as well as the drug release kinetics. Upon having identified

the formulation with the most suitable properties for dermal applications, it was characterized in terms of antioxidant activity.

Taking into account the results obtained and the drawn consideration from the preliminary experiments, the experimental protocols for the nanoparticle synthesis and analyses were adjusted as described in the following paragraphs.

7.1.1 Nanoparticles preparation

The nanoparticle preparation was performed with the FNP protocol described in Chapter 3 with slight modifications. Since caffeine is a very hydrophilic molecule and is soluble both in acetone and in water, two process configurations, as described in Figure 7.1, were used.

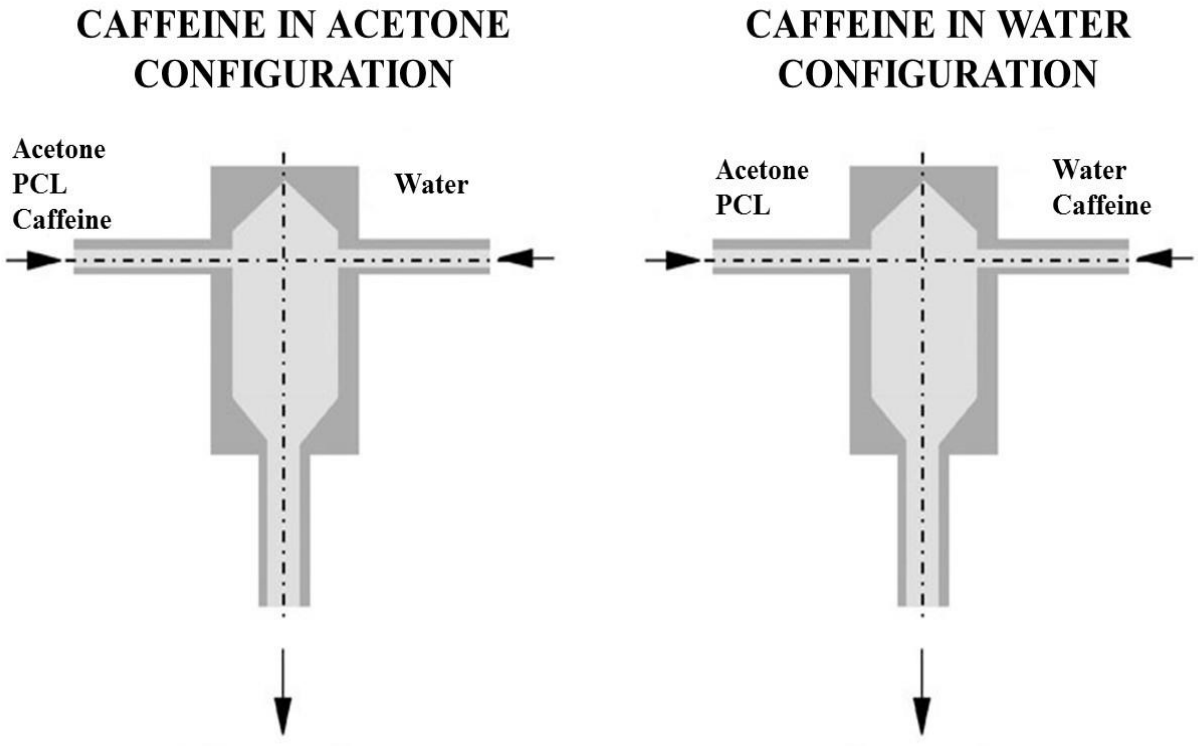

Figure 7.1. Production of caffeine loaded nanoparticles by FNP: on the left caffeine in water configuration, on the right caffeine in acetone configuration.

The first one, hereby defined as caffeine-in-acetone configuration (CIA) consisted of a classic FNP protocol where the drug and the polymer where both dissolved in the solvent stream (Figure 6.1 left). For these experiments, formulations were prepared by dissolving PCL at concentrations between 4.5

and 10 mg/mL and caffeine at concentrations between 0 and 9 mg/mL. The second protocol hereby defined as caffeine-in-water configuration (CIW) consisted of dissolving the drug in the antisolvent stream while the polymer was dissolved in the organic solvent (Figure 6.1 right). Such an approach followed the rationality of dissolving the hydrophilic drug in the solvent in which it was more soluble and thereafter mixing it in the solvent in which it displays lower solubility. For these experiments, formulations were prepared by dissolving PCL at concentrations between 6 and 15 mg/mL and caffeine at concentrations between 0 and 22 mg/mL.

To assess the effect of the flow rate on the particle size, the flow rate was varied between 20 and 80 mL/min. Each particle batch was produced by pumping to the microreactor a 3-ml volume of the solution, the 3 ml volume of antisolvent and the suspensions were collected in a vial containing 3 mL of quenching water achieving a QR = 1. The quenched samples were kept under magnetic stirring for two minutes before being analyzed. The particle size measurement was performed by the DLS technique.

7.1.2 Caffeine encapsulation assessment

The correct assessment of caffeine encapsulation was among the most critical issues tackled in the present research line. Being the incorporation of a hydrophilic substance an uncommon common topic in the literature, it was considered necessary to develop rigorous protocols to prove caffeine incorporation and furtherly calculate the LC and EE values, while eliminating at best the possible bias. Firstly, ATR-FTIR analysis was conducted on the dried nanoparticle to qualitatively assess the presence of caffeine in its structure.

To calculate EE and LC both direct and indirect protocols were developed. In this way, it was possible to analyze both the solid nanoparticles and the liquid supernatant and check the consistency with the initial caffeine quantity by closing the mass balance. Furtherly, particular care was taken to eliminate possible biases in the EE indirect quantification method.

For the EE and LC measurement particles were produced at a FR of 20 mL/min. Right after being synthesized, the polymeric nanoparticles were carefully separated from the liquid phase by an experimental procedure consisting of several steps. Firstly, the NPs suspension was placed in a rotary evaporator at 45 °C, under vacuum for 15 min, to remove acetone. Then, the particles were transferred in a 12 mL falcon tube. An amount of water equal in volume to the one of evaporated acetone was

used to rinse the rotovapor glass and added to the NP suspension to both restore the initial volume of suspension and recover caffeine adhering to the rotovapor glass surface. The NP and the nanoparticles were centrifuged for 1 hour at 15777 g (12000 rpm). The excess supernatant was removed from the particles by a pipette. A 0.1 mL supernatant sample was diluted in 25 ml of water and filtered with a 0.2 µm cellulose syringe filter to furtherly eliminate residual particles. The obtained solution was analyzed by UV-Vis spectroscopy. The centrifuged solid nanoparticles were dried overnight at 40°C. Throughout the described procedures, DLS measurements were taken to check whether PSD significantly changed.

The calculation of LC and EE was performed both by the direct and the indirect method to double-check the reliability of the analysis. In the indirect method, EE and LC were calculated by the determination of free caffeine in the filtered supernatant. The filtered supernatant was analyzed by UV-visible spectrophotometry and the absorbance peak at the wavelength of 273 nm was considered for caffeine quantification. The supernatant of an unloaded PCL suspension was used as blank in the spectrophotometric measurement, to eliminate the interference of unfiltered suspended nanoparticles (smaller than 0.2 µm) in the supernatant due to Tyndall effect. Such a precaution was found to be necessary since the particle size was found to be close to 270 nm thus to caffeine absorption wavelength. The light absorption from the particles due Tyndall effect was found to cause a false increase in the measured concentration of caffeine. Such an issue was considered to be negligible in the quantification of melatonin due to the larger size of the produced particles which were not considered to cause a disturbance in the UV spectroscopy measurement.

In the direct method, LC and EE were calculated by dissolving a weighed amount of dry nanoparticles in acetonitrile and analyzing caffeine absorbance in the resulting solution. This method allowed to estimate gravimetrically the amount of polymer in which caffeine was contained, without relying on the assumption that all PCL was precipitated in the nanoparticle form (as assumed in the indirect method). To verify the quantification procedure, the caffeine mass balance was checked by summing up the amount in the supernatant and the one in the dry nanoparticles. In the case recovered caffeine was lower than 97%, the batch was considered unreliable and discarded.

A complete outline of the formulations investigated for the LC and EE tests is reported in Table 7.1. The formulations were labeled similarly to the melatonin one, the last letter indicates the solvent used for caffeine.

Table 7. 1. List of PCL-caffeine formulations used in the EE and LC test.

Sample label	C_{PCL} (mg/mL)	C_{CAF} (mg/ml)	CAF solvent	MR
$PCL_{4.5}CAF_9A$	4.5	9.0	Acetone	2.00
PCL_6CAF_9A	6.0	9.0	Acetone	1.50
$PCL_{10}CAF_{7.6}A$	10.0	7.6	Acetone	0.76
PCL_6CAF_9W	6.0	9.0	Water	1.50
$PCL_{10}CAF_9W$	10.0	9.0	Water	0.90
$PCL_{15}CAF_9W$	15.0	9.0	Water	0.60

7.1.3. Structural characterization of the nanoparticles

The investigation of the effects of the two process configuration onto the structure of the particles was conducted. For this scope, the particles were characterized by Zeta potential, SEM and XPS. The zeta potential was measured by DLS. For the Zp analysis, particle formulations were appositely produced using a fixed initial PCL concentration of 6 mg/mL and FR of 20 mL/min, the caffeine concentration was varied from 0 to 9 mg/mL. The electron microscopy was used to gain insights about the nanoparticle morphology. The analysis was conducted using FESEM Zeiss Merlin (Oberkochen, Germany) with an acceleration voltage of 5 kV and a current probe of 200 pA. Samples were prepared by dropping the just produced formulation on the aluminum stub. The XPS analysis was used to inquire about the nanoparticle superficial composition. The analysis was performed in etching mode to obtain information about the caffeine content in the outer 20 nm of the surface of the particles.

7.1.4. In vitro release test

In vitro release tests were performed by the dialysis method, using pH=7.4 phosphate buffer solution (PBS) as a receptor medium. Each release sample was prepared as follows: three batches of NP suspensions were produced and centrifuged, then 7 ml of the supernatant volume was removed from each batch and analyzed in terms of LC and EE. 2 ml suspensions from each batch were mixed inside the dialysis tube (MW cut-off 12000 Da, Sigma Aldrich) and sank inside the receptor fluid to make a single release test. The volume of the acceptor fluid was 800 mL, and it was kept under gentle stirring and covered to prevent solvent evaporation. At given time, 5-ml liquid samples were

withdrawn and the withdrawn volume was replaced by fresh PBS solution. Caffeine concentration was determined by UV spectrophotometry. Caffeine cumulative release data were collected and fitted by 5 models, i.e. (i) Zero-Order, (ii) First-Order, (iii) Higuchi, (iv) Hixon-Crowell, (v) Baker-Lonsdale model. The regressions were carried out by interpolating the data until the asymptote in the cumulative release curve was reached. The contribution of free caffeine to the released curves was calculated by subtracting the free caffeine curve from NP curves before regression.

7.1.5. Characterization of the optimal formulation

The results of the different analyses were taken into account to select an optimal PCL-CAF formulation to be employed in the textile finishing. The selected formulation was furtherly characterized in terms of thermal properties and antioxidant activity.
The thermal properties of the caffeine loaded PCL nanoparticles were inquired employing TGA and DSC analyses.

The antioxidant activity of the nanoparticles was investigated by EPR spectroscopy coupled with the spin trapping technique. For the analysis hydroxyls, radicals were generated by mean of the Fenton reaction reported in Equation 7.1.

$$Fe^{2+} + H_2O_2 \rightarrow Fe^{3+} + OH\bullet + HO^- \qquad (7.1)$$

The oxidation of the DMPO spin trap by the generated OH• radical was studied by EPR. For the experiments, the selected nanoparticle suspension was used upon undergoing successive dilutions and acetone removal. 78 μL of the investigated substance were mixed 20 μL H_2O_2 (0.34 mg/mL), 100 μL of DMPO (5.66 mg/mL) and 2μL of $FeSO_4$ (1.52 mg/mL) in an Eppendorf tube. The resulting solution was briefly homogenized, transferred to a quartz microcapillary tube, and placed in the EPR cavity. The spectra were recorded after 5 minutes since the addition of FeSO4.

7.2. Nanoparticle size

The effects of the formulation parameters and process conditions on the particle size were studied. In Figure 7.2 the average diameters of the particles produced with fixed caffeine concentration and varying PCL concentration are reported. It was observed that for both process configurations, the particle size increased as the polymer concentration was increased. Such results are consistent with

the findings of the preliminary experiments and with the ones reported in the literature (Zelenková et al., 2014).

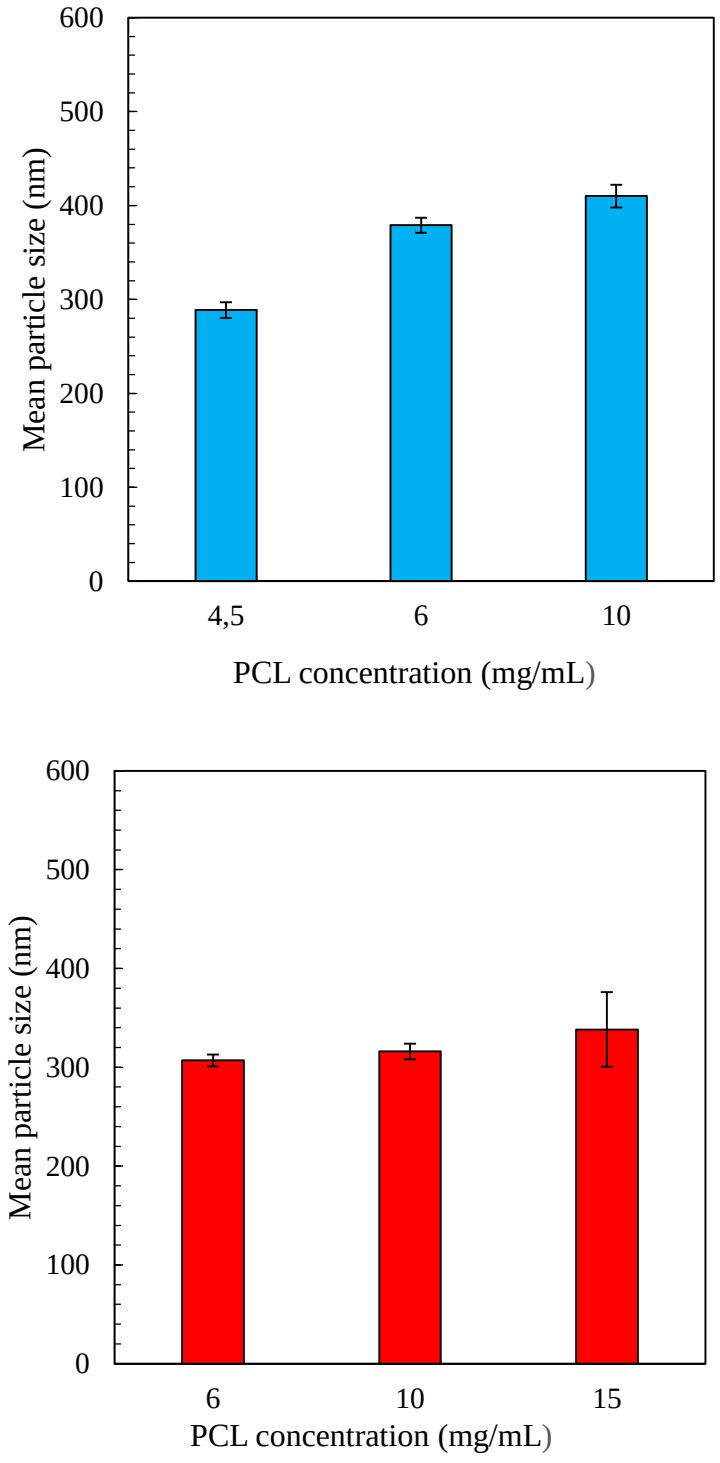

Figure 7.2. Effect of PCL concentration onto particle size for CIA (top) and CIW (bottom). Caffeine concentration was kept at 9 mg/mL. Particles were produced with FR=20 mL/min.

The particle size increase was observed to be more marked when caffeine was dissolved in acetone. Particles produced with the CIW configuration were found to be smaller with respect to the one produced with the CIA, even though the same initial polymer and drug concentration were used.
In Figure 7.3 the size of particles produced with constant PCL concentration and varying caffeine concentration is presented.

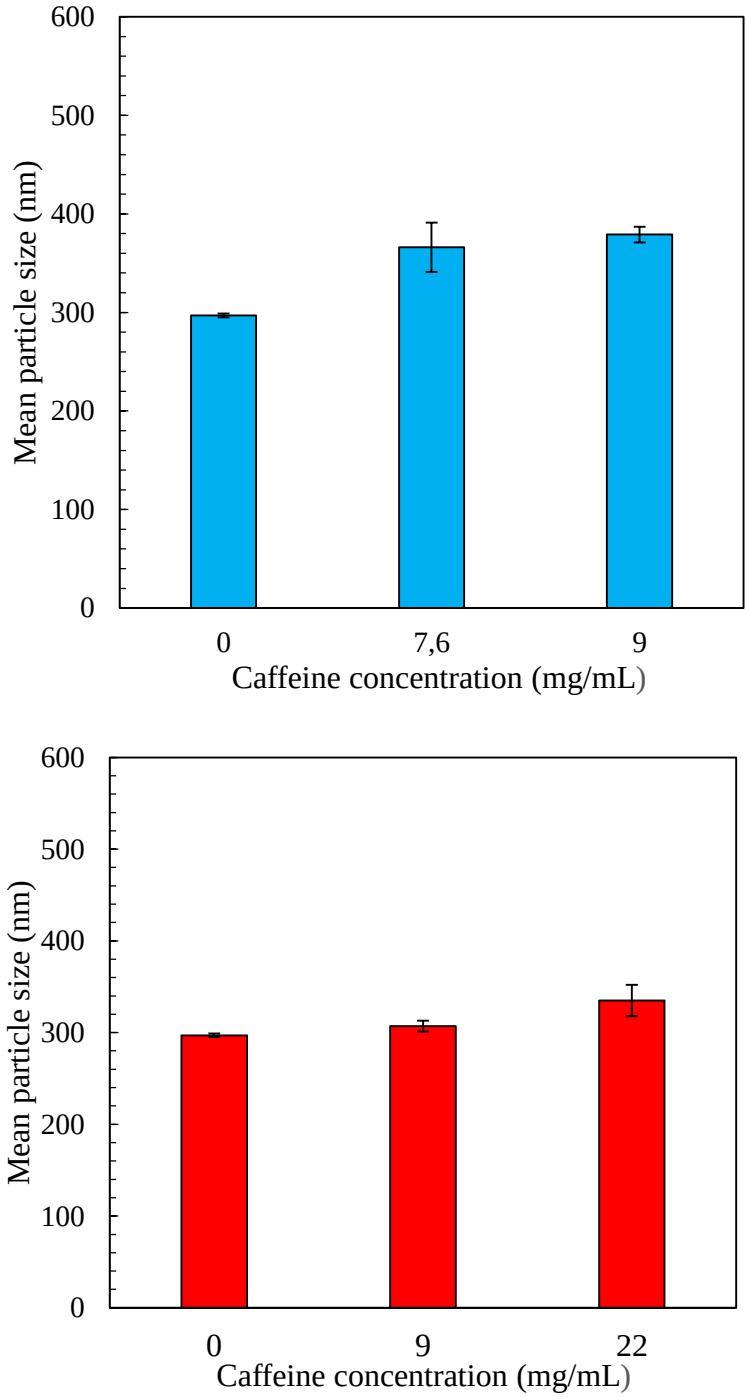

Figure 7.3. Effect of caffine concentration onto particle size for CIA (top) and CIW (bottom). Caffeine concentration was kept at 9 mg/mL. Particles were produced with FR=20 mL/min.

The increase of the initial drug concentration was observed again to cause the formation of coarser particles for both process configurations. Also, this result is consistent with what observed in the preliminary results and with the one observed in literature for other kinds of drugs (Mossotti et al., 2015).

Considering the different formulations, it was evidenced that both the polymer and drug concentrations displayed an effect over the particle size. The ANOVA analysis proved that such effects were statistically significant for both the process configurations. Furthermore, the statistical analysis provided insights on which factor displayed a more significant effect over the particle size. The main effect analysis evidenced that for the CIA configuration the PCL concentration is the factor that mainly influences the particle diameter. On the contrary, if water is used as the caffeine solvent, it was evidenced that the drug concentration is the main factor affecting the particle size.

To inquire the effect of the inlet FR on the particle size upon adding a hydrophilic drug to the formulations, PCL_6CAF_9A and PCL_6CAF_9W were processed between 20 and 80 mL/min and compared with plain PCL nanoparticles with an initial concentration of 6 mg/ mL. The particle diameters collected at different flowrates are reported in Figure 7.4.

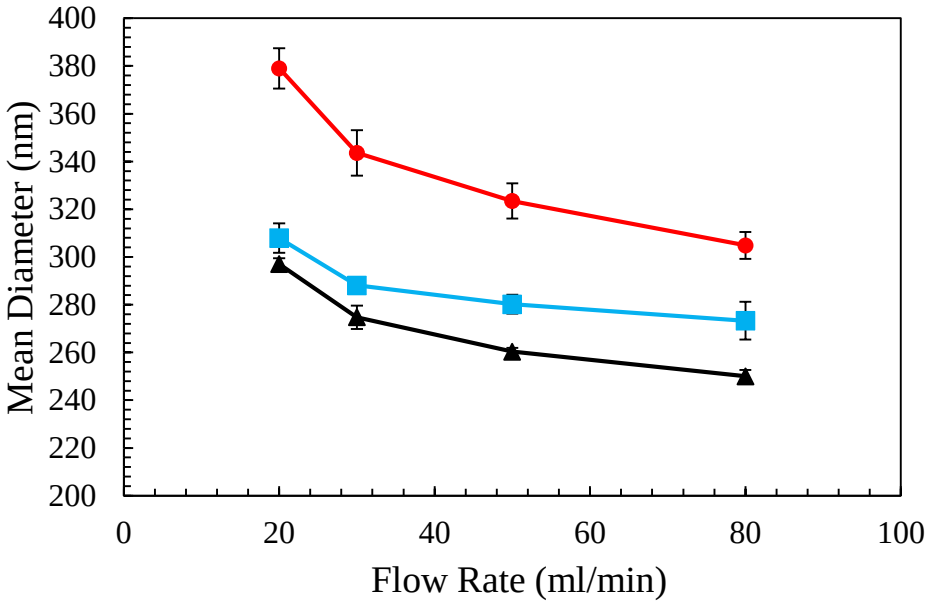

Figure 7.4. Size of PCL-caffeine nanoparticles obtained at different flow rates with different formulations: black triangle: PCL 6 mg/ml; blue square: PCL_6CAF_9W; red circle: PCL_6CAF_9A.

It is observed that, in the selected range of operating conditions, nanoparticles with the required size (from 250 to 400 nm) can be obtained. The average diameter decreases as the inlet flow rate increases, confirming that the flow rate has the already discussed influence. Therefore, it was confirmed that the addition of the hydrophilic drug did not compromise the possibility of controlling the particle diameter by modulating the flow rate.
Overall from the particle size analysis, it was evidenced that, by adjusting formulations and process conditions, particles with a characteristic size between 300 and 400 nm were obtained, thus fulfilling the size requirements for the dermatological applications.

7.3. Drug incorporation

The drug incorporation is a critical issue to be assessed. A first qualitative analysis of the drug incorporation was performed by collecting the infrared spectra of a separated and dried nanoparticle powders; the infrared spectra of the nanoparticles were compared with those of the raw materials, i.e. PCL and caffeine. The FTIR spectra of PCL_6CAF_9W as well as the ones of raw caffeine and pure PCL NPs are reported in Figure 7.5. The characteristic absorption bands are reported in Table 7.2.

The polymer spectrum showed two medium intensity peaks at 2943 and 2864 cm^{-1} which correspond to the stretching vibration of the C-H bonds in the macromolecule skeleton. The peaks at 1721 cm^{-1} were ascribed to the stretching vibration of the C=O bond in the ester groups. The peaks connected to the bending vibration of the C-H bonds were found at 1472, 1396, 1367 cm^{-1}. Further absorption bands peculiar of the stretching of C-O were observed at 1292, 1238, 1105, 1065, 1045 cm^{-1}.

The caffeine spectrum exhibited some weak absorption at 3112, 2920, 2851 cm^{-1} due to the stretching vibrations of the C-H bonds. The peak at 1700 cm^{-1} was correlated to the C=O stretching. The two sharp peaks at 1652 and 1545 cm^{-1} were attributed to the C=N double stretching. The signals typical of the C=C stretching were observed at 1480, 1454, 1428 cm^{-1}. The C-N bond stretching vibrations were observed at 1354, 1284, 1235, 1023 cm^{-1}. Lastly, the peaks at 970, 858 cm^{-1} were attributed to the C=C bond bending.

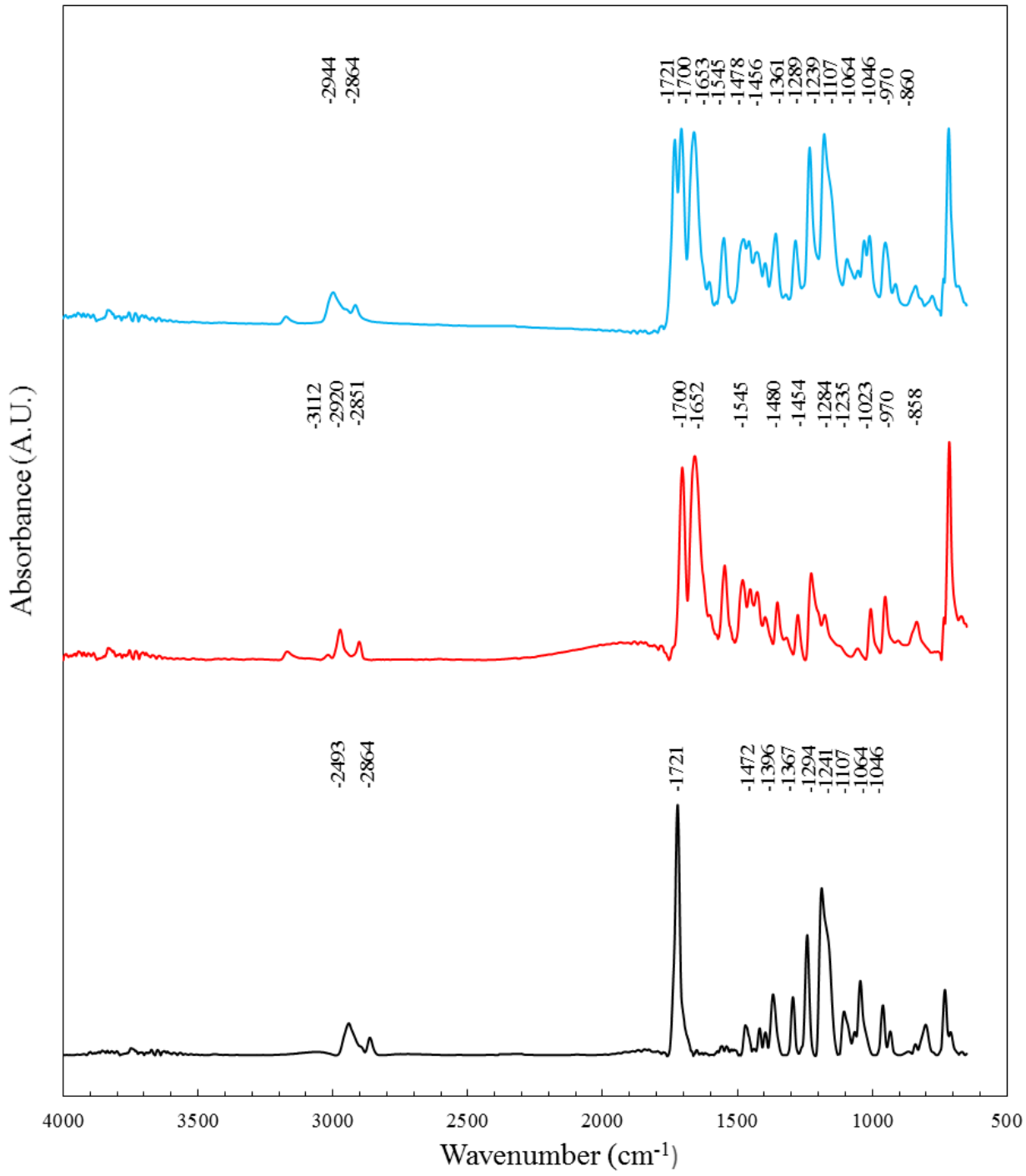

Figure 7.5. ATR-FTIR spectra of PCL (black) caffeine (red) and nanoparticles with PCL_6CAF_9W (blue) formulation.

Table 7.2. Characteristics IR absorption bands for of PCL NP, curcumin and $PCL_{10}CUR_4$ formulation.

Wavenumber (cm^{-1})			Attribution
PCL NP	**Caffeine**	**PCL_6CAF_9**	
2943, 2864	3112, 2920, 2851	2944, 2864	C-H stretching vibration
1721	1700	1721, 1700	C=O stretching vibrations
-	1652, 1545	1653, 1545	C=N stretching vibration
-	1480, 1454, 1428	1478, 1456, 1429	C=C stretching vibration
1472, 1396, 1367		1397, 1361	C-H bending vibrations
	1354, 1284, 1235, 1023	1361, 1289, 1239	C-N stretching vibration
1294, 1241, 1107, 1064,1046		1289, 1239, 1107, 1064, 1046	Stretching vibrations of C-O
	970, 858	970, 860	C=C bending vibrations

The caffeine loaded nanoparticles spectrum exhibited two medium peaks at 2944, 2864 cm^{-1} typical of the stretching vibrations of the C-H bonds in the PCL macromolecular chain. The signal of the C=O stretching was observed at 1721 and 1700 cm^{-1},the first peak was attributed to the C=O vibration in the ester group of PCL while the second one to free carbonyl in the caffeine molecule. The peaks typical of the C=N bond stretching of the caffeine molecule were observed at 1653, 1545 cm^{-1}. The signals due to the C=C stretching vibrations in the caffeine molecule were observed at 1478, 1456, 1429 cm^{-1}. The peaks connected to the C-H bending were found at 1397, 1361 cm^{-1}. Three sharp peaks were observed at 1361, 1289, 1239 cm^{-1} and attributed to the stretching of the C-N bond in the caffeine structure. Several peaks connected to the stretching of the C-O bonds in the polymer chain were observed at 1289, 1239, 1107, 1064, 1046 cm^{-1}. Lastly, the peaks typical of the C=C bending in the caffeine molecule were observed at 970, 858 cm^{-1}.

The infrared analysis of the caffeine loaded nanoparticles showed that the particle powders display the characteristic absorption bands of both the polymer and the drug chemical structures. Therefore, it was concluded that caffeine was successfully incorporated in the polymeric particles. It is interesting to notice that no significant changes in the peak positions have been observed. This confirms that the incorporation of caffeine in the PCL nanoparticles does not cause the chemical modification of the drug and the polymer structure. The slight shifts in some peak positions (of about 2-4 wavenumbers) suggested that caffeine and PCL undergo some weak interaction such as Van der Walls forces and Hydrogen bonding. This suggests an encapsulation mechanism based on weak chemical interaction similar to the ones reported in the literature (Ke et al., 2019; Pinkerton et al., 2017).

Upon having qualitatively proved the presence of caffeine in the nanoparticles system, a quantitave analysis was run by measuring the LC and the EE. The the latter properties were calculated both by the direct and indirect methods. The LC and EE measured for different formulations as a function of MR are shown in Figure 7.6.

It is possible to observe the consistency of the direct and indirect methods; this proves the effective encapsulation of the drug by the NPs system; moreover, it also means an almost complete recovery of caffeine, which proves that no significant degradation of the molecule occurs.

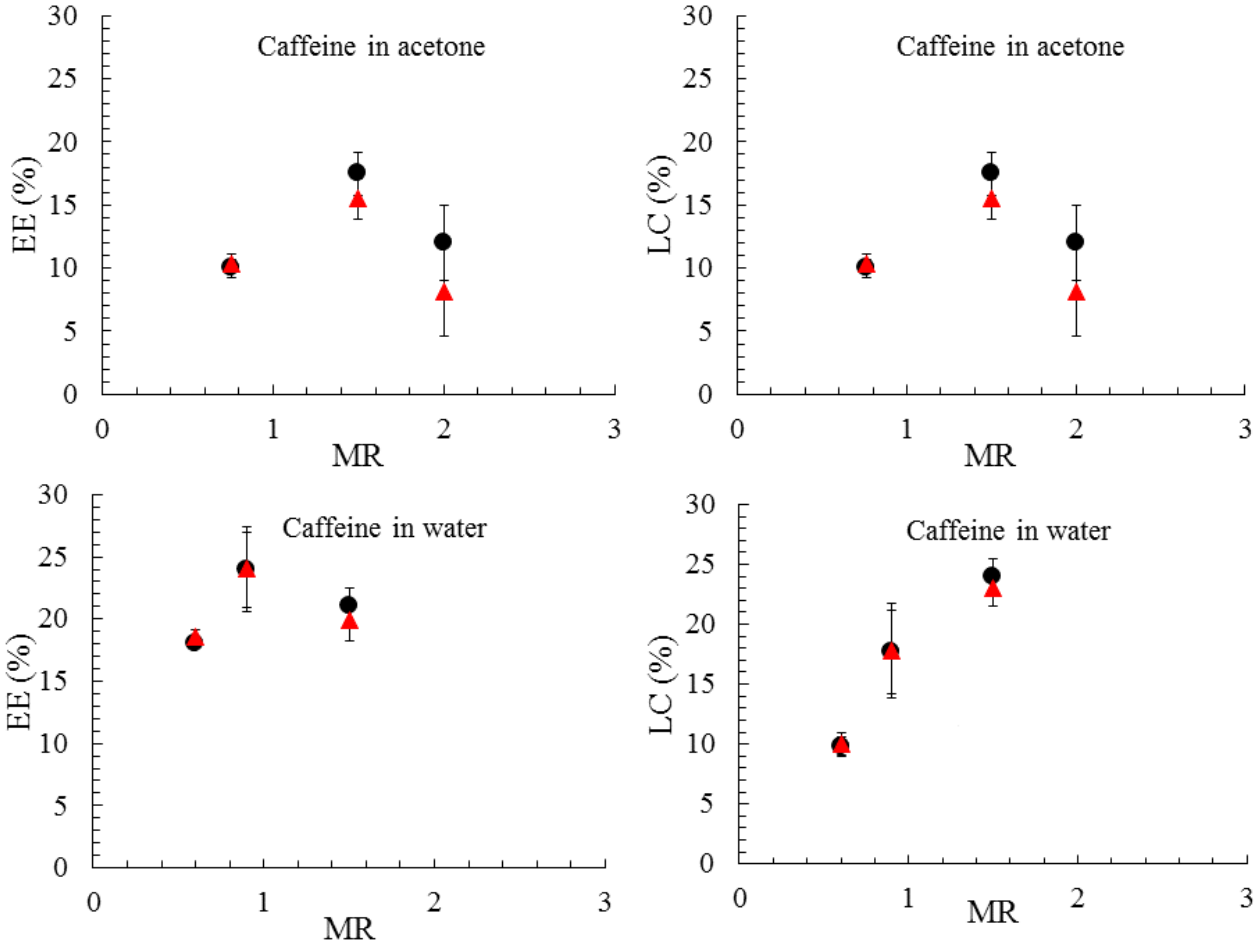

Figure 7.6. LC and EE as a function of MR for samples produced with caffeine in acetone (top) and caffeine in water (bottom). Results obtained with direct (▲) and indirect (●) protocols.

EE values did not show a proportionality with the MR in both cases. Such a bell shaped trend is consistent with what reported by some authors, indeed increasing the MR caused a higher amount of drug leak out of the polymer structure and to partition in the aqueous liquor where caffeine is highly soluble (Dong and Feng, 2004; Martínez Rivas et al., 2017). The process configuration played an effect on the EE, indeed, for CIW configuration the encapsulation efficiency values were found to be 5-10% higher respect to CIA. This result is consistent with the literature, which showed that for FNP processes the EE is mostly affected by the solvent employed and by the drug solubility in the solvent and the antisolvent (Chow et al., 2015; Tam et al., 2016). Overall the EE values are comparable with the ones achieved with those obtained for caffeine by other drug encapsulation procedures (Budai, 2013; Rodrigues et al., 2016; Yew and Misran, 2016) thus confirming the suitability of the FNP method for the encapsulation of a hydrophilic substance.

From the loading capacity analysis, it was observed that the LC is proportional to the MR when caffeine was dissolved in water. Such a trend suggests that LC can be controlled by adjusting the relative content of caffeine and PCL. On the contrary, the CIA formulations did not exhibit a similar proportionality. Particularly, for an MR=2, i.e. for formulation P4.5C9A a lower LC was achieved. such behavior was ascribed to the low initial PCL amount in the formulation, leading to insufficient polymer available for drug encapsulation. LC values were again larger if caffeine is dissolved in water similarly to what observed for the EE.

7.4. Particles structures

Particle size and drug loading analyses confirmed the production of caffeine loaded nanoparticles with characteristics suitable for transdermal release applications, moreover, they evidenced that the process configuration has some impacts on the Dp and drug loading. Such data suggest that different encapsulation mechanisms may occur in the two process configurations, therefore the structure of the particles was investigated by analyzing samples with the same polymer and drug concentrations but produced using different solvents for caffeine. For this inquiry, the formulations PCL_6CAF_9W and PCL_6CAF_9A were selected such a comparison since they both presented relatively high LC and fine size. The chosen samples were analyzed by SEM, Zp measurement, and XPS to obtain insights on their surface properties.

In Figure 7.7 the particles obtained from formulation PCL_6CAF_9W and PCL_6CAF_9A are observed. The microscopical analysis evidenced that the particles have a spherical shape and size consistent with the one measured by DLS. Regarding the surface morphology, it was observed that the nanoparticles produced by dissolving caffeine in acetone own a rough surface; on the contrary, one of the particles produced in CIW appeared smoother.

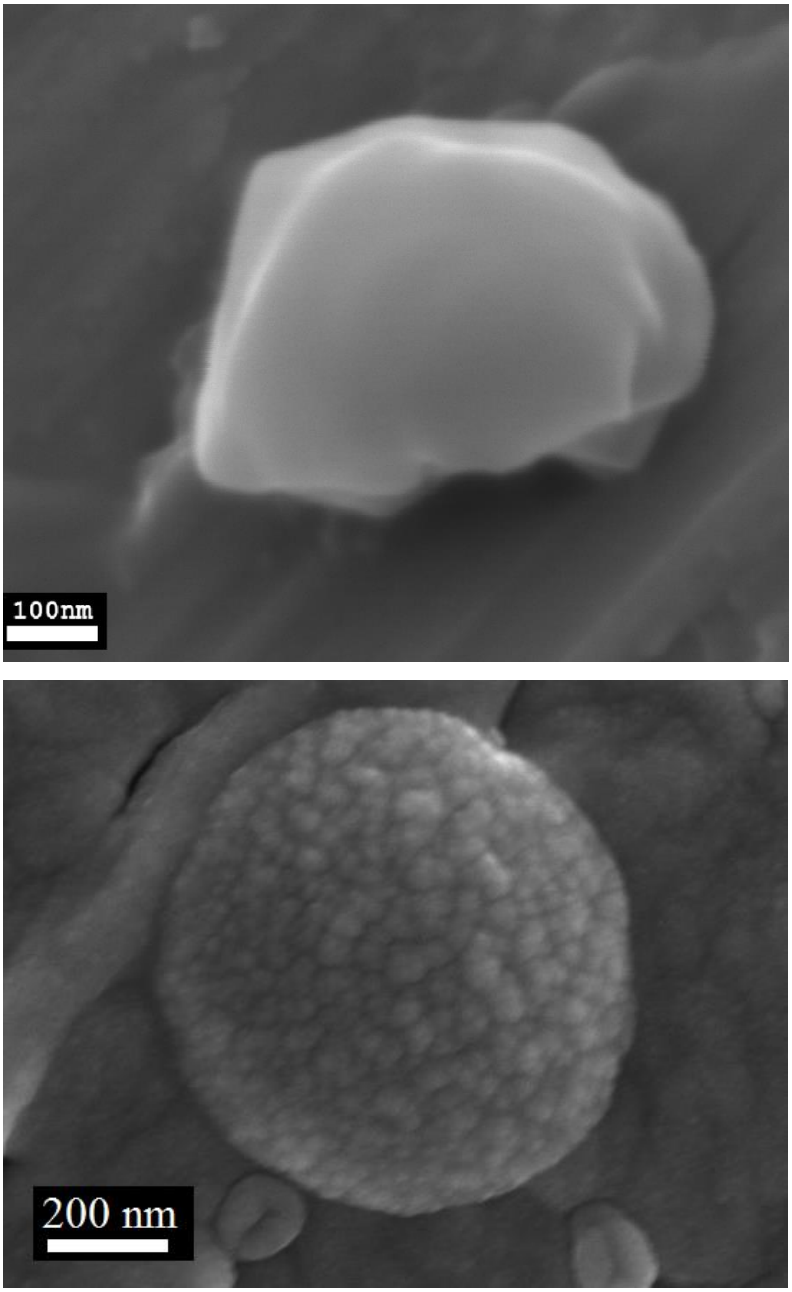

Figure 7.7. FESEM image of NPs produced at 20 ml/min for magnification for PCL_6CAF_9W (top, 90000X magnification) and PCL_6CAF_9A (bottom 150000X magnification).

The zeta potential of the nanoparticles was measured to gain further information about the particle surface properties. The Zp values for formulation produced with the same initial caffeine and PCL concentration but opposite process configuration are reported in Figure 7.8.

Above all it is observed that all the analyzed samples displayed a negative Zp; this was due to the negative charges induced by the carbonyl groups of PCL, which oriented its polar groups toward the aqueous environment during the precipitation process.

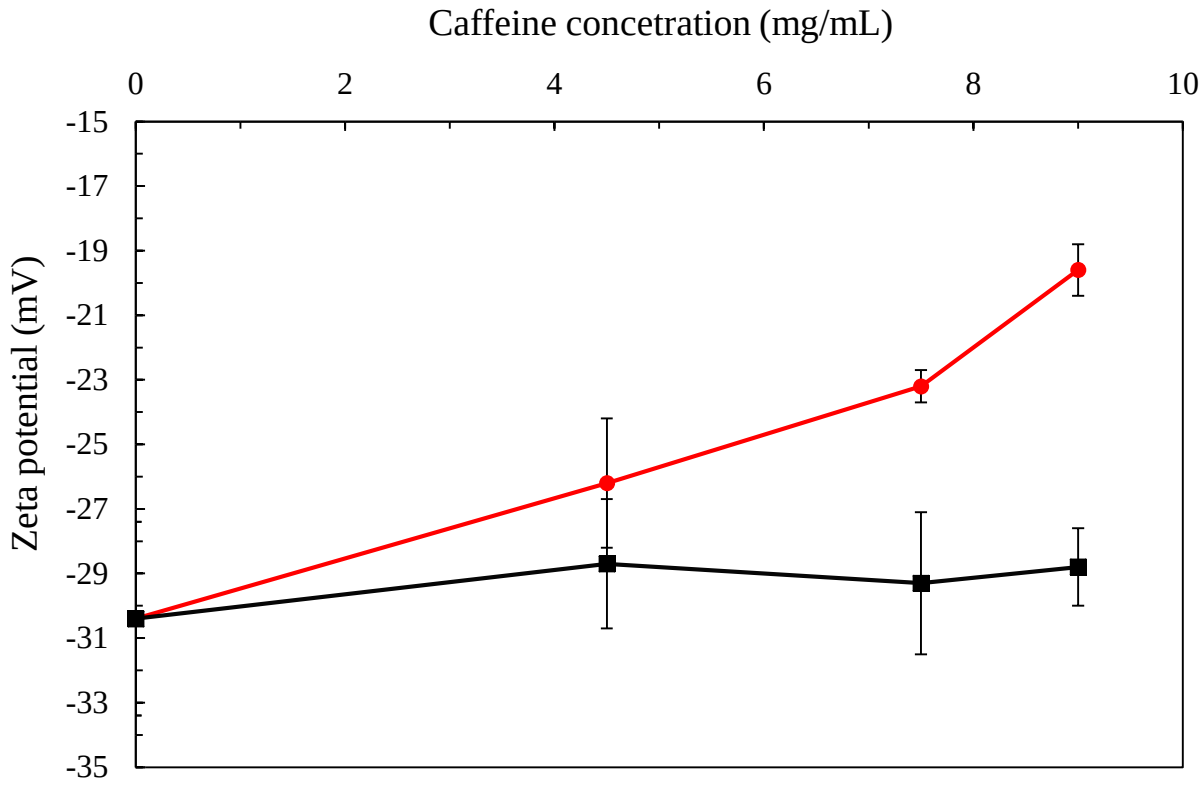

Figure 7.8. The trend of Zp with caffeine concentration for loaded nanoparticles obtained with caffeine dissolved in water (black square) and caffeine dissolved in acetone (red circle).

Regarding the effects of caffeine concentration on the Zp, two different trends were observed for the two process configurations. For the CIW configuration, the changes in caffeine initial concentration were not observed to display any significant changes in particles Zp. On the contrary, when caffeine was dissolved in acetone, it was observed an increase in the zeta potential as the caffeine concentration was increased. This result was explained by considering that the caffeine molecule has nitrogen containing groups in its structure, which can be easily protonated in the aqueous environment.

The increase in zeta potential as a consequence of caffeine addition can, therefore, be correlated to the presence of caffeine on the particle surface which induced a positive charge. Interestingly, a marked increase of Zp was observed only for the CIA configuration. This fact suggests that caffeine is present on the particle surface when it is dissolved in acetone. On the contrary, if the drug was

dissolved in water, it was not present on the particle surface in a sufficient quantity to cause significant changes in the Zp.

The XPS analysis was conducted to obtain further information about the presence of caffeine onto the surface and to verify if the process configuration affects the drug distribution in the thickness of the nanoparticle . Indeed, this technique allows obtaining clear and univocal information of the single elements present on the external surface layers of our system. Considering that caffeine is the only species containing nitrogen atoms, XPS analysis aimed to quantify this atomic species and correlate it to superficial caffeine concentration. An example of a survey scan of the caffeine nanoparticles system is reported in Figure 7.9.

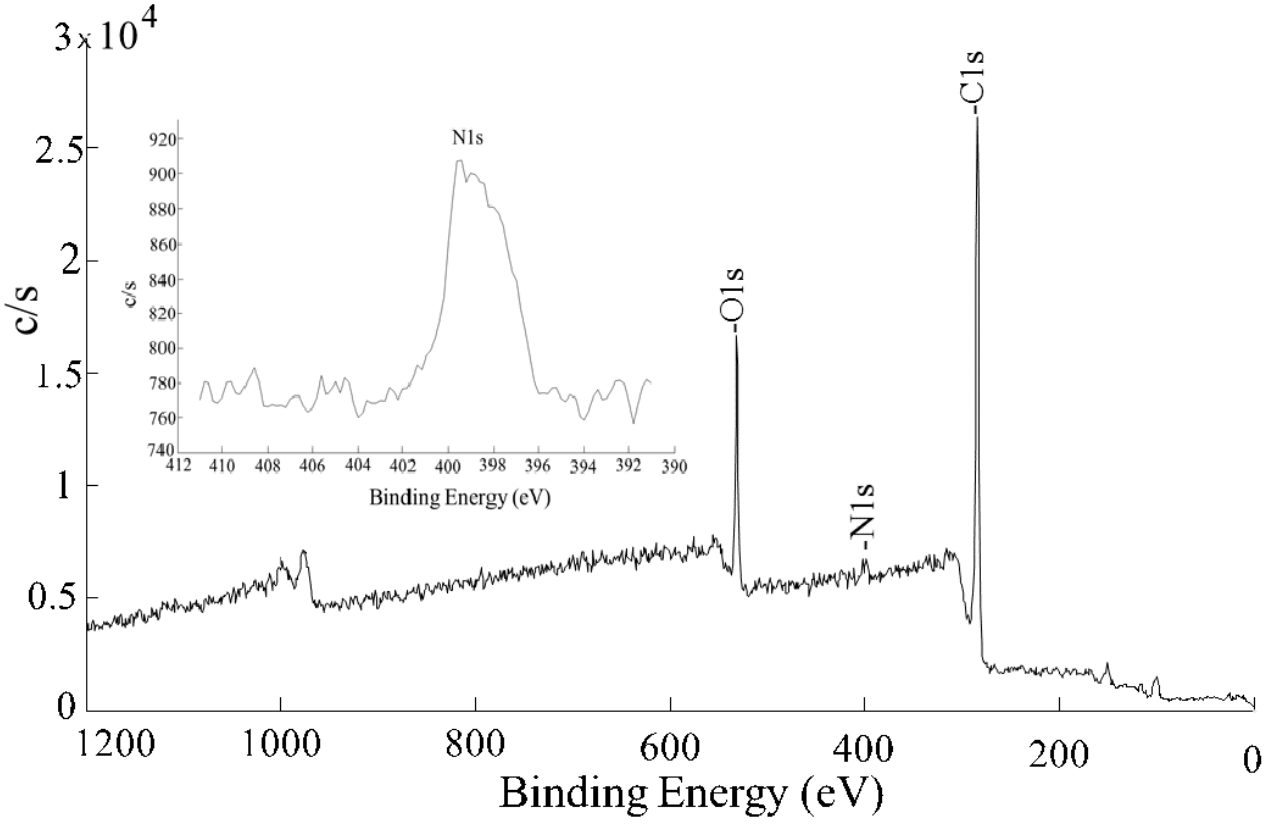

Figure 7.9. XPS survey scan spectrum of the PCL_6CAF_9A formulation. On the top high resolution of the spectral region in which the N1s signal was observed.

The spectrum is characterized by two strong peaks at 285 and 530 eV which were correlated C1s and O1s respectively. Such a result was well expected considering that the carbon and the oxygen are the main atomic species present in PCL and caffeine structure. Moreover, a signal correlated to the presence of N1s was also observed at 400 eV (top of Figure 7.9).

By integrating the area of the peaks the percentage of nitrogen atoms in the samples, thus the caffeine content was calculated. Furthermore, by conducting the XPS analysis in etching mode, it was possible to determine the percentage of caffeine in the first 20 nm of the surface of the particles. These values were compared with the ones of loading obtained by the direct protocol which were considered as the index of the caffeine concentration in the total particle volumes. In Figure 7.10 the superficial and the total caffeine content for the PCL_6CAF_9W and PCL_6CAF_9A are reported.

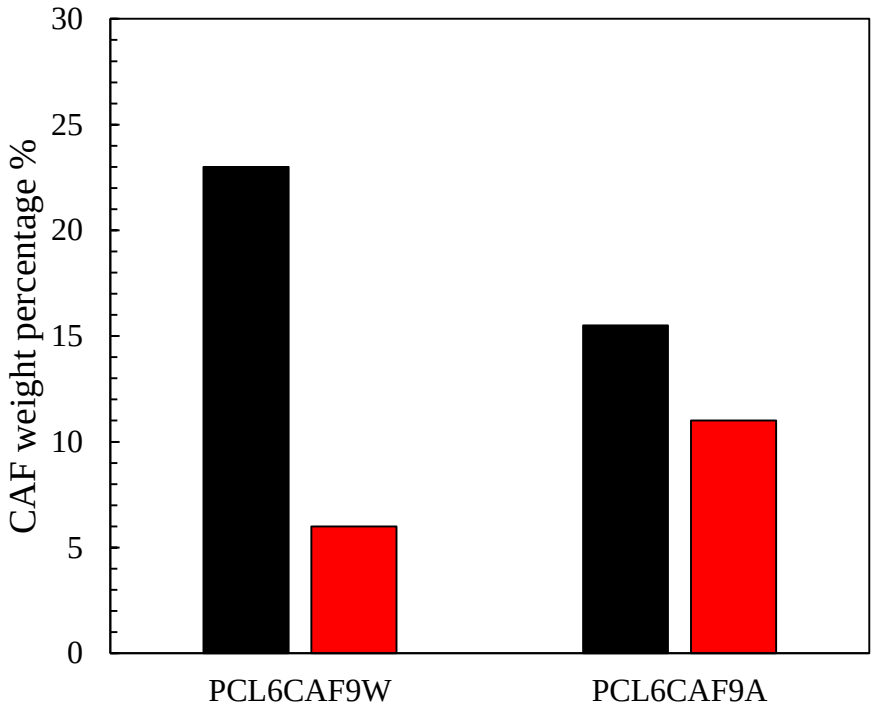

Figure 7. 10. Comparison of surface weight percentage measured by XPS (red bar), with overall LC measured by UV-Vis (black bar) for samples PCL_6CAF_9W and PCL_6CAF_9A.

For the PCL_6CAF_9A it was observed that a significant part of the globally encapsulated drug was present in the surface layers. On the contrary, for the PCL_6CAF_9W a much smaller percentage of caffeine was found in the outer 20 nm of the particle shell. These results evidenced that when caffeine was dissolved in the acetone stream it tended to be mostly adsorbed or incorporated in the outer surface layers of the particles. On the contrary, when water was used as the caffeine solvent it was more incorporated in the particle core. Such a finding was found to be consistent with the results of the Zeta potential measurement.

Based on the data coming from the different analyses, it was concluded that the two different process configurations produced particles with different structures. These were explained by proposing two

different encapsulation mechanisms that are sketched in Figure 7.11. These mechanisms are based on the caffeine chemical structure, taking into account its possible interactions with the solvents and the polymer.

When caffeine is dissolved in water it tends to be protonated (Bahrami et al., 2013) and can, therefore, interact with the negatively charged carbonyl group of PCL by hydrogen bonding and Van der Walls interactions. The interactions between the oppositely charged species contribute to drug encapsulation in the polymer matrix with a mechanism similar to the one explained by Pinkerton et al (2017).

Oppositely, when caffeine is dissolved in acetone, it does not undergo protonation before the FNP process occurs. It can be assumed that it diffuses toward water upon jet collision since it is the solvent to which the drug has the greatest affinity. Oppositely, PCL tends to nanocluster in an acetone environment during the solvent displacement process (Di Pasquale et al., 2014; Lavino et al., 2017). Once caffeine-water interaction occurs, the drug can undergo protonation and thereafter interact electrostatically with PCL, but such interactions would occur only during the growth and aggregation stages on the FNP process.

These two different proposed particle formation mechanisms not only provide a qualitative explanation to the two observed morphologies but also provide some insights on the observed loading and particle size. In fact, the electrostatic interaction favors the encapsulation of caffeine, and this justifies the higher drug loading observed with caffeine fed in the water stream.

On the other hand, notwithstanding the loading is lower, a more marked increase in the NP diameter is observed when caffeine is fed in acetone. The PCL-caffeine electrostatic interactions reduce the stability of the colloidal system and, as evidenced by Zp measurement, may enhance growth and aggregation phenomena causing the final particle size to be higher.

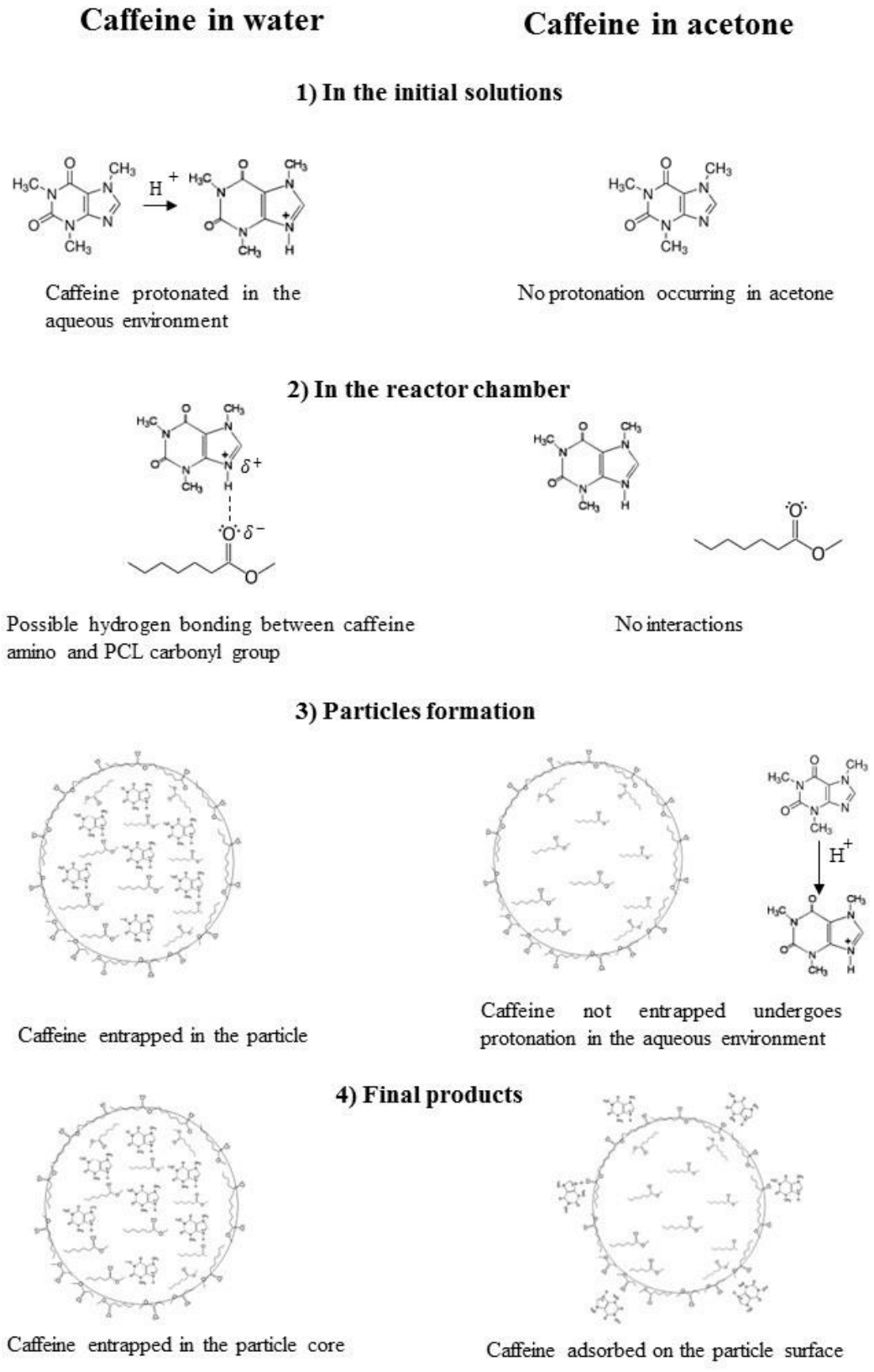

Figure 7.11. Different encapsulation mechanisms for the CIW and CIA configurations.

7.5. In vitro drug release

The release kinetics was studied by dialysis test and the cumulative release curves, shown in Figure 7.12, were obtained by normalizing the release data over the maximum mass of drug recovered in the receptor fluid; in the histogram of the same Figure, it is plotted the percentage amount of drug released respect to the initial amount encapsulated in the nanoparticles.

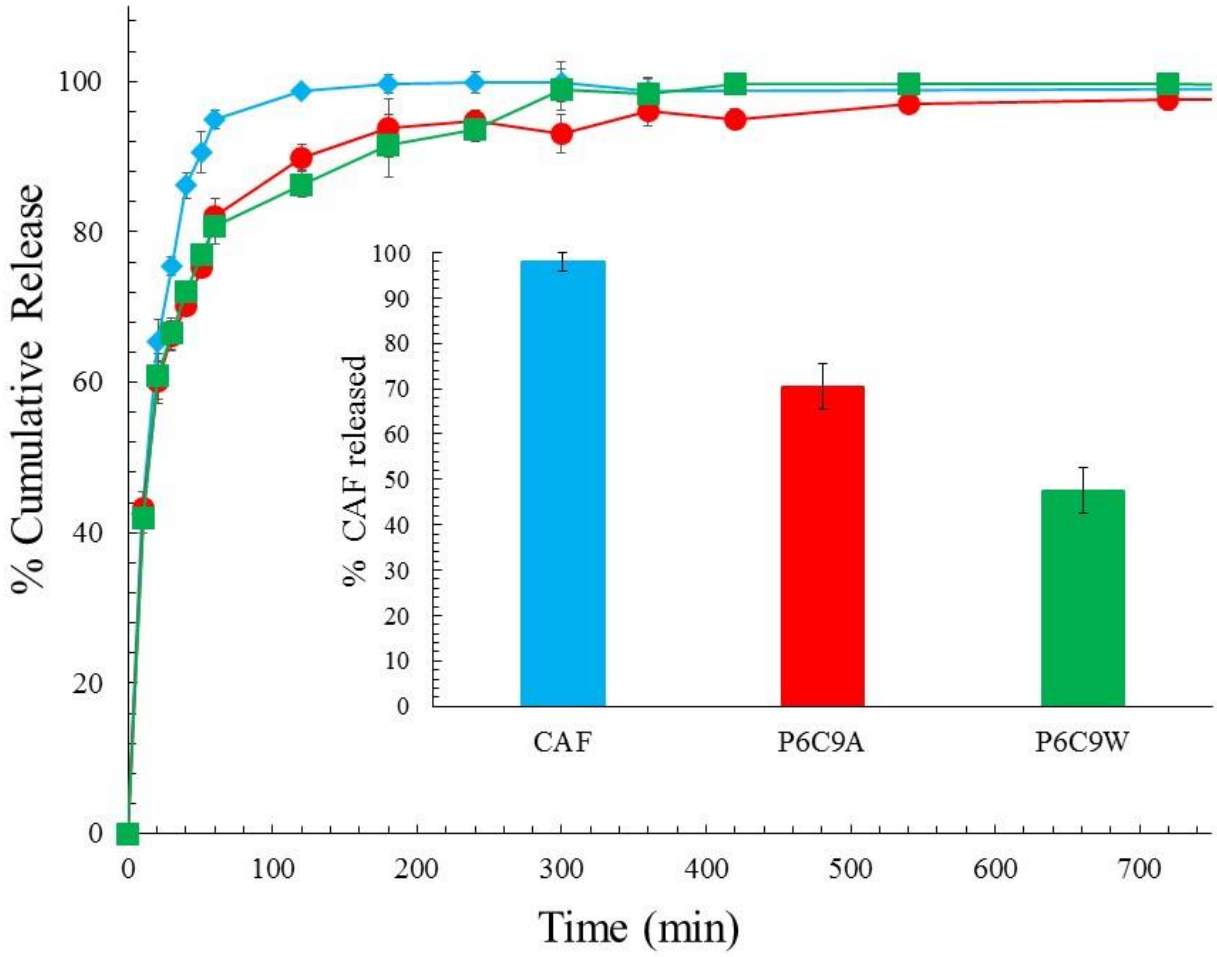

Figure 7.12. Cumulative normalized release curves and total drug released histograms for caffeine (blue), PCL_6CAF_9A (red) and PCL_6CAF_9W (green).

The caffeine solution, used as control, displayed a very fast release and the concentration peak in PBS was reached in one hour, as it occurs in the human body. The NPs systems curves instead are characterized by a smoother rise in drug release with the plateau reached in approximately 6 hours, demonstrating the capability of NPs to delay and control caffeine release.

An initial burst release was noticed and was ascribed to free caffeine in the supernatant, such amount was quickly released in less than 30 minutes after which a change in the slope of the curves occurs, suggesting that the release from the nanoparticles was taking place. Concerning the total amount of caffeine released at the plateau, the control caffeine solution released the whole drug amount while the NPs formulations only a fraction of it. These results can be explained considering the slow degradation of PCL, occurring over a long time (e.g. weeks).

The observed release was therefore only due to caffeine diffusion from the core to the NP surface without any effect of polymer erosion; being the kinetics dominated by diffusion, the shapes of the release curves are similar for both the nanoparticle systems.

The two different formulations showed, instead, different fractions of caffeine released respect to the loaded amount. As a matter of fact, it can be easily forecasted that caffeine is released more easily if located in the outer surface layers. Therefore, the PCL_6CAF_9A which contains about 70% of the incorporated drug in the outer 20 nm (as evidenced by XPS analysis) displayed a higher amount of drug released if compared to sample PCL_6CAF_9W.

To better elucidate the drug release mechanism, the release test data were fitted by different kinetic models. The regression coefficients for each model (R^2) were reported in Table 7.3.

Table 7.3. The correlation coefficient for fitting of the release curves with different kinetic models.

Sample	Zero order	First order	Higuchi	Hixon Crowell	Baker Lonsdale
Caffeine	0.14	0.90	0.60	0.48	0.70
PCL_6CAF_9A	0.19	0.85	0.84	0.69	0.89
PCL_6CAF_9W	0.07	0.94	0.84	0.84	0.99

Free caffeine solutions fit the first order model, as expected when release is controlled by only by diffusion through the dialysis membrane and without any other resistance to mass transfer. Concerning the NPs samples, they were better fitted by diffusion-based models rather than erosion based ones, thus corroborating the hypothesis that the polymer degradation did not occur. For the sample PCL_6CAF_9W, the best fitting was by Baker and Lonsdale equation, as it was expected given the spherical structure of the particles and the distribution of the drug inside the polymer matrix.

The PCL_6CAF_9A sample displayed a higher correlation coefficient when fitted with the first order or Baker and Lonsdale equation, therefore exhibiting a release behavior between the one of free caffeine and PCL_6CAF_9W. Such a release pattern was considered consistent with the particle structure; indeed, caffeine adsorbed onto particles surface, was promptly released according to the first order model while that incorporated was released according to Baker–Lonsdale kinetics, which describes the release from a spherical matrix.

The evaluation of drug release showed that the two different NPs structures obtained by dissolving caffeine either in acetone or in water lead to different functional properties, as sketched in Figure 7.13. If acetone is used as the solvent, the particle displayed a fast and total release, while if water is used as the solvent, the particle displayed a more controlled and partial release of the active principle, acting indeed as reservoir systems.

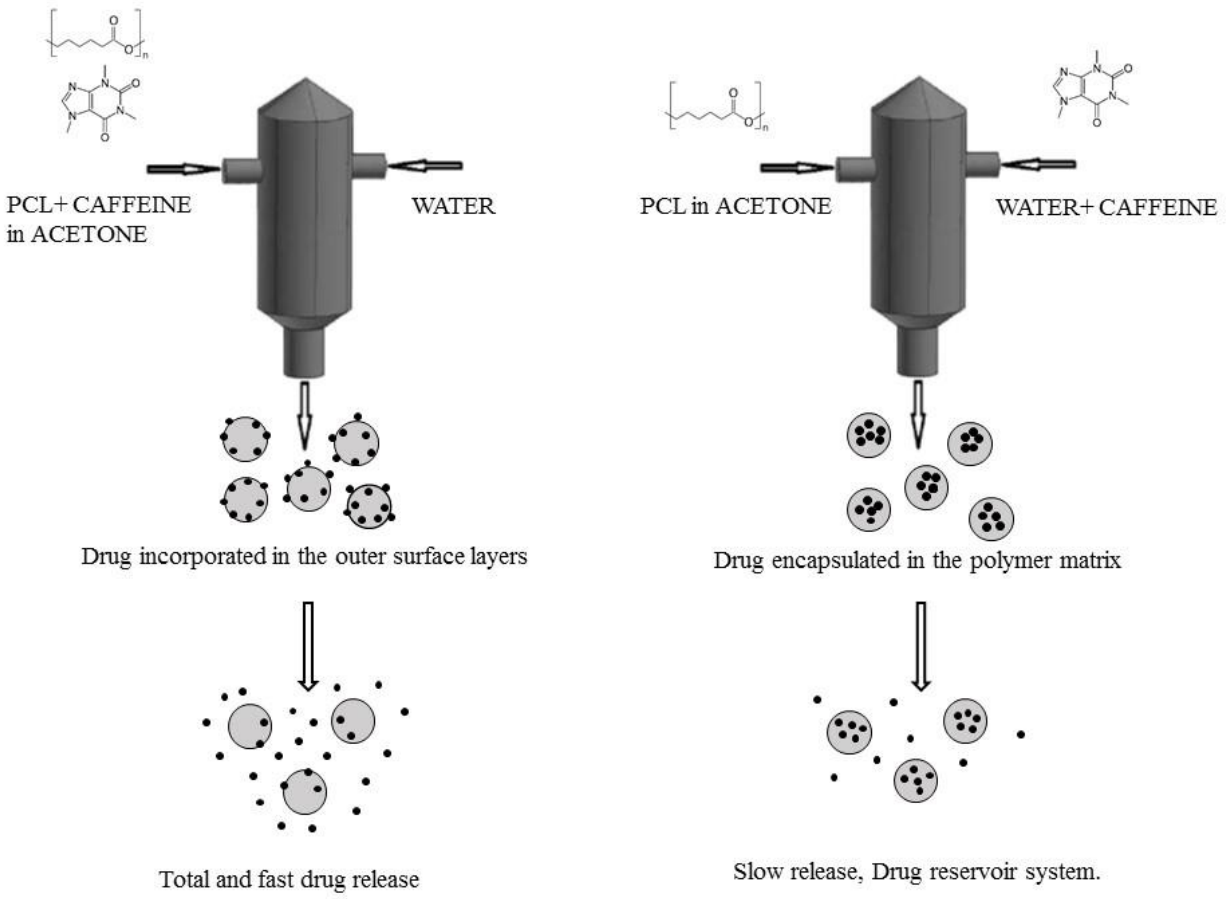

Figure 7.13. Particle structure and release properties obtained with different process configurations.

The particles produced with CIW configuration were smaller in size and higher loading capacities. Furthermore, they displayed higher surface polarity, as evidenced by Zp measurement and were able to act as a drug reservoir upon in vitro testing. Considering these particle properties, the formulation PCL_6CAF_9W was identified as the optimal one to be employed in the textile finishing.

7.6. Thermal properties

The thermal properties of the caffeine loaded nanoparticles were investigated by DSC and TGA techniques. The analysis was run on the PCL_6CAF_9W formulation and compared with one of the raw materials. The DSC thermogram of the for caffeine loaded nanoparticles is depicted in Figure 7.14 while the main thermal events observed are listed in Table 7.4.

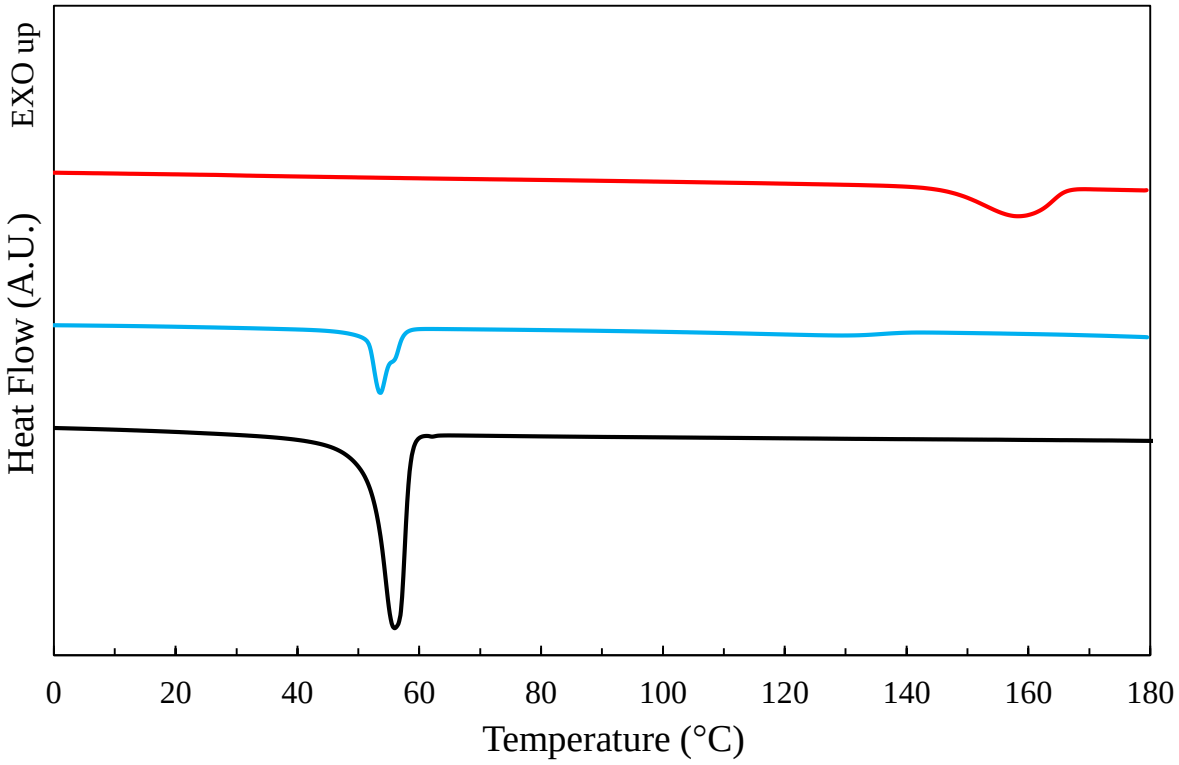

Figure 7.14. DSC thermogram of PCL (black curve), caffeine powder (red curve) and caffeine loaded nanoparticles (blue curve).

As already discussed, the PCL thermogram was mainly characterized by a single fusion peak between 50 and 60 °C while the caffeine powder exhibited an endothermic phase transition around 145 °C.

Concerning the caffeine nanoparticles sample, it was observed a single melting peak around 50 °C. The peak was attributed to the fusion of the PCL shell of the nanoparticles. Instead, no endothermic

peak for the caffeine crystalline phase transition was observed. The absence of this endothermic transformation was ascribed to the fact that upon being encapsulated caffeine was not anymore in a crystalline phase. Such an observation is consistent with some results reported in the literature where the absence of phase transition endothermic peak in the DSC analysis was correlated to the drug to be molecularly dispersed inside the nanocarrier (Mihailiasa et al., 2016; Puglia et al., 2016).

Table 7.4. List of the thermal events observed during the DSC analysis of curcumin loaded nanoparticles.

Sample	PCL	Caffeine	PCL-CAF NP
ΔH_{endo} (J/g)	-60.8	-20.3	-13.8
$T_{endo,\ onset}$ (°C)	51.8	146.3	51.5
$T_{endo,\ peak}$ (°C)	55.9	158.2	53.7
X_c (%)	43.7		24.8

In Figure 7.15 the results of the TGA analysis of caffeine loaded PCL nanoparticles are reported, the main data obtained from the analysis are listed in Table 7.5.

Caffeine thermal degradation was initiated around 220 °C and proceeded sharply until the total degradation of the sample. PCL displayed the degradation onset at a higher temperature, the sample was completely degraded and no residue was left.

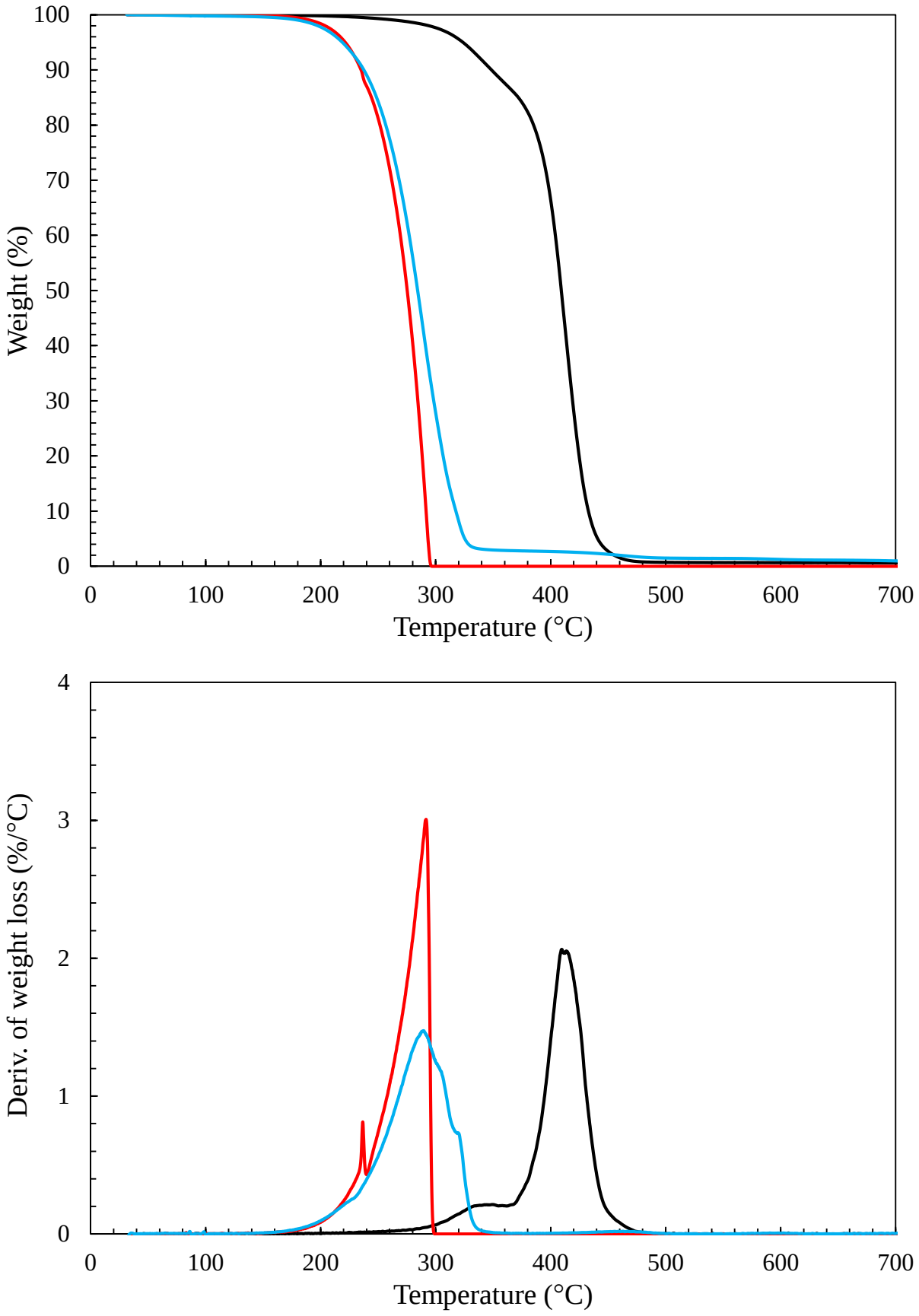

Figure 7.15. TGA analysis of PCL (black curve), caffeine (red curve) and PCL_6CAF_9W (blue curve). TG curve (top graph) and first derivative of the TG curve (bottom graph).

The caffeine loaded nanoparticle TG curve showed a degradation onset similar to the one of the pure drug. The degradation proceeded with lower rate respect to the caffeine one until 340°C where only 5% of the sample was left. Thereafter, the rest of the sample was fastly degraded being the temperature above the one where PCL degradation occurs. Comparing the DTG curve of pure caffeine and caffeine loaded nanoparticles it was observed that the nanoparticles sample does not present the small peak at 230 °C. Such a peak observed on the caffeine sample was ascribed to the release of volatile compounds during the fusion. Therefore, the absence of this fusion related peak furtherly confirms that the caffeine contained in the NPs is not in crystalline form, consistently with what observed by DSC analysis. Overall, observing the degradation pathway of the PCL_6CAF_9W sample it was observed a unique degradation step. It was observed that the PCL degradation was initiated earlier respect to the pure PCL sample. This fact led to the hypothesis that some interactions between the two materials occurred. The caffeine degradation products were supposed to interact with PCL decreasing its thermal stability, thus making the overall sample degradation to occur in a unique step. Overall it was observed that the material is fully stable at the usage temperature for the biomedical and textile applications.

Table 7.5. List of the thermal data obtained from TGA analysis of PCL-caffeine nanoparticles.

Sample	$T_{5\%}$ (°C)	T_{max} (°C)	MMLR (%/°C)	Residue at 700 °C (%)
PCL	324	409	2.1	1
Caffeine	221	291	3.0	0
PCL-CAF NP	219	289	1.5	1

7.7. Antioxidant activity

In Figure 7.16 the EPR spectra collected in the presence of the different samples are reported. It is possible to observe that the control spectrum, obtained by letting the oxidation of DMPO freely occur, is characterized by the presence of four antiphase signals (namely at an applied magnetic field of 3407 G, 3408 G, 3422 G, 3423 G, 3437 G, 3438 G, 3452 G, 3453 G). These signals are due to the presence of OH groups attached to the spin trap DMPO upon its oxidation by OH· radical.

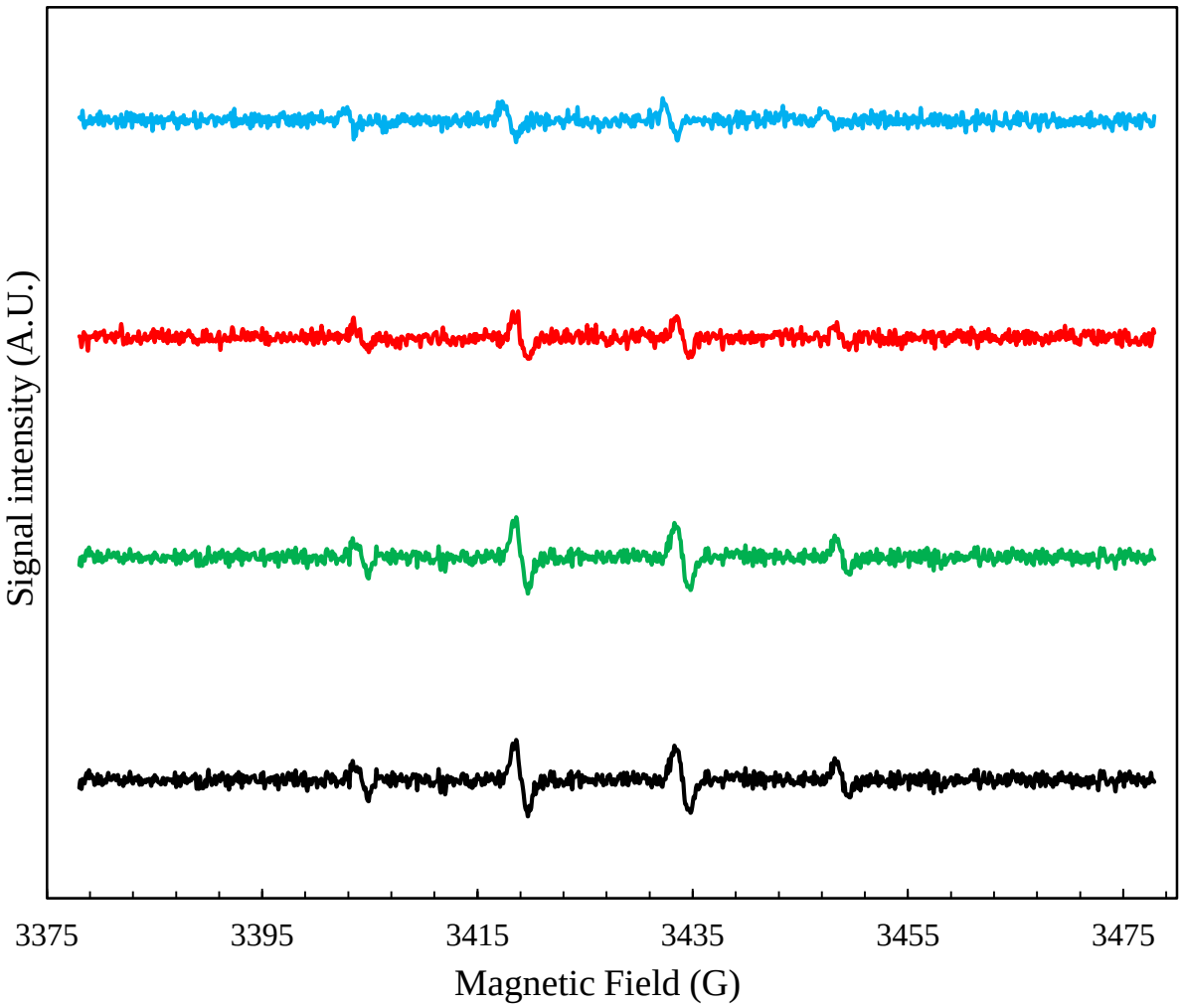

Figure 7.16. EPR spectra for the analyzed samples: Control (black curve), PCL NP (green curve), caffeine (red curve) and caffeine loaded nanoparticles (blue curve).

The intensity of the antiphase signals is known to be proportional to the quantity of the oxidized species DMPO-OH. Observing the spectrum of the unloaded PCL nanoparticles no significant

differences can be observed with the control one. This fact shows that the PCL interacts neither with the radical generation by Fenton reaction nor with the oxidation of the spin trap.

On the contrary, in the presence of caffeine, either free or encapsulated, it is possible to observe that the intensity of the antiphase signals of the DMPO-OH is significantly reduced. This phenomenon is due to the fact that caffeine molecules can interact with OH· radical preferentially respect to DMPO and therefore prevent it from getting oxidized to DMPO-OH.

By correlating the intensity of the EPR antiphase signals with the DMPO-OH concentration the antioxidant activity was calculated. In Figure 7.14 the antioxidant efficiency of the nanoparticles formulation upon different dilutions and of the equivalent free caffeine solution is reported.

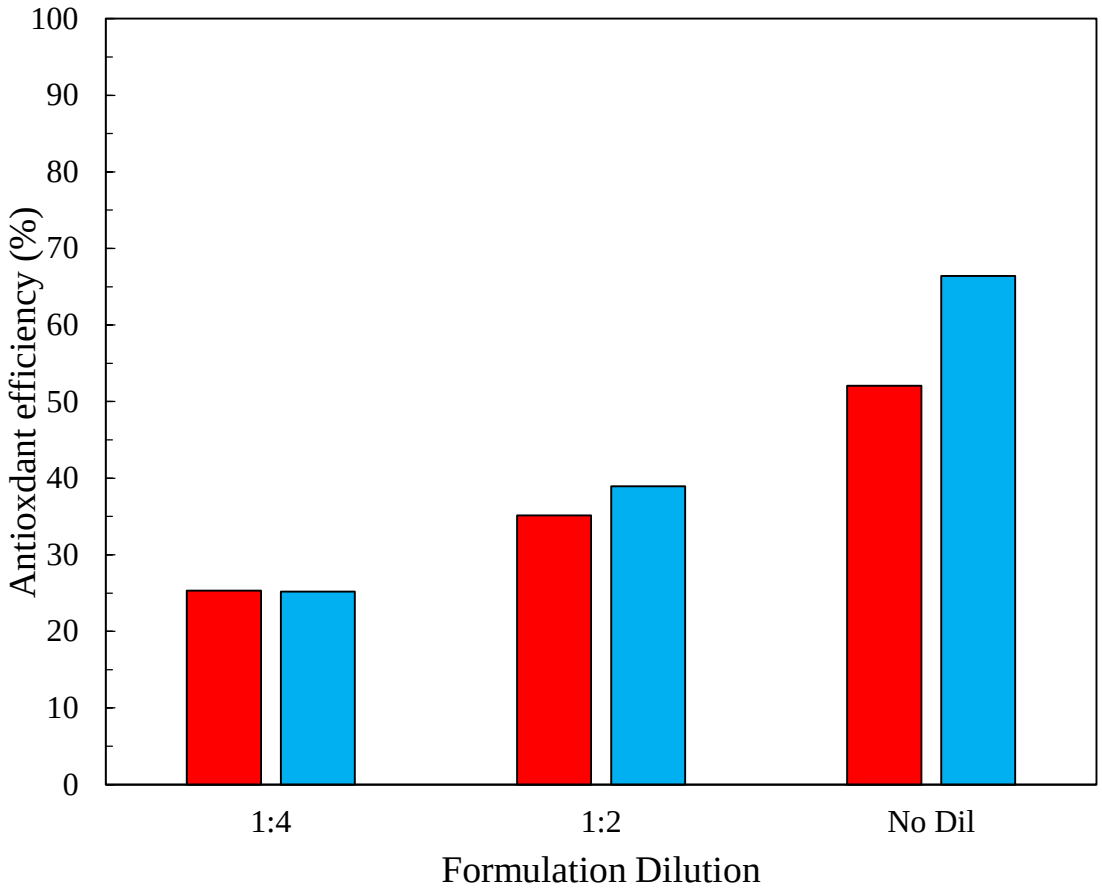

Figure 7. 17. Antioxidant efficiency of the caffeine loaded nanoparticles (blue bar) and free caffeine (red bar).

It can be observed that the less diluted samples displayed higher antioxidant efficiencies. For more concentrated samples, it can be observed that free caffeine solutions displayed higher antioxidant properties respect to the encapsulated ones. Such a result was due to the fact that upon being encapsulated caffeine was less available to interact with OH· radical if compared to free caffeine, due to the shielding effect exerted by the polymer. Interestingly, the gap between the antioxidant activity

of the NP formulation and the solution becomes narrower for more diluted samples. This phenomenon is due to the fact that being caffeine a hydrophilic molecule, was partially extracted from the nanoparticle system upon dilution; therefore, the quantity of caffeine available for reaction and consequently the antioxidant activity was increased. Overall, it was proved that the nanoparticle formulation displays a strong antioxidant activity being able to halve the $OH^{\cdot}$ radical attacking the DMPO molecule and therefore proving its potential effectiveness in protecting the skin from radical oxygen species.

Overall the analysis conducted in the present chapter proved the feasibility of producing caffeine loaded PCL nanoparticles with suitable size for dermatological applications and controlled structure. The nanocarriers displayed a control over the release kinetics and an effective antioxidant activity.

Chapter 8. Incorporation of hydrophobic drugs: curcumin

8.1 Scope of the study

The flash nanoprecipitation technique was proven to effectively incorporate drugs of marked hydrophilic and mild hydrophobic character. To gain insights about the performances of the proposed FNP system in the incorporation of hydrophobic drugs, curcumin was selected as a model substance.

Besides being a valid model as hydrophobic active principles, curcumin owns peculiar characteristics which make it of particular interest for the present application. Firstly, it is a chromophore, this makes it particularly interesting in textile finishing applications. Indeed, the colorimetric techniques can be exploited to test the quality of the finishing treatment. Secondly, being a fluorescent molecule, it can be easily traced and this is a significant advantage for biological applications. More specifically curcumin was proved to be a powerful antioxidant that attracted significant attention in the treatment of skin diseases.

The production of curcumin loaded nanoparticles by FNP was reported by some authors (Chow et al., 2015; Ke et al., 2019). These works were considered in designing the synthesis and the analyses of the present work. Furtherly, the presented research proposed different concepts respect to the ones already reported in the literature. Indeed the present work aims to produce NPs for textile finishing application. Therefore the synthesis method was significantly simplified avoiding the use of chemical auxiliaries such as stabilizers or crosslinking agents. Moreover, a homopolymer was employed instead of block-co-polymers.

Overall the present research aims to produce curcumin loaded PCL nanoparticles with optimal properties for dermatological treatment while keeping the process conditions simple and cost effective. Another important scope of the present research line is to inquire whether the proposed encapsulation technique has the potential of improving curcumin interactions with living tissues.

To tackle these issues, several curcumin-PCL formulations were synthesized. The properties of such nanoparticle formulations were investigated to individuate the one with the ideal properties for dermatological and textile applications. Thereafter the selected formulation was furtherly characterized with different techniques, thus a more complete picture of its physical-chemical properties was obtained. Finally, an investigation of the potential biological application was run with a particular focus on the antioxidant activity and the drug release profile.

Taking into account the results obtained and the consideration from the previous research lines, the experimental protocols for the nanoparticle synthesis and analyses were adjusted as described in this chapter.

8.1.1 Preparation of curcumin-PCL formulation

The curcumin loaded PCL nanoparticles were prepared by direct FNP protocol. The polymer and the drug were both dissolved in the acetone stream. PCL was dissolved at the concentration of 6 and 10 mg/mL while curcumin concentration was set to 1, 4 and 6.5 mg/mL. The complete list of the studied formulations is reported in Table 8.1.

Table 8.1. List of the tested formulations for PCL-Curcumin nanoparticles.

Formulation	Curcumin concentration (mg/ml)	PCL concentration (mg/ml)	MR
PCL_6CUR_1	1.0	6.0	0.2
PCL_6CUR_4	4.0	6.0	0.7
$PCL_6CUR_{6.5}$	6.5	6.0	1.1
$PCL_{10}CUR_1$	1.0	10.0	0.1
$PCL_{10}CUR_4$	4.0	10.0	0.4
$PCL_{10}CUR_{6.5}$	6.5	10.0	0.7

The flow rate and the quenching ratio were kept at 50 mL/min and 0.5 respectively. The pumped volume was 3 mL for each stream and the collection vial was filled with 6 mL of water, the collected suspensions were stirred for about 2 minutes before being analyzed.

8.1.2 Particles analysis and formulation optimization

Several analyses were conducted on the curcumin loaded nanoparticles to investigate the properties of the different formulations and identifies the more suitable for the textile finishing. Particle size and zeta potential were measured trough the DLS technique. Statistical analysis was conducted on the DLS data to evaluate the effects of curcumin and PCL concentration on the particle size and zeta potential.

The EE and LC were evaluated by the indirect method. The separation of the nanoparticles from the supernatant was performed by filtration using a syringe filter in cellulose with a porosity of 0.2 µm. The filtered liquid was diluted with acetone and analyzed either by spectrophotometry or by fluorescence spectroscopy. The separation and analysis method was validated by running preliminary centrifugation: however, since centrifugation did not display any changes in the results, this step was aborted to simplify the overall procedures. The spectrophotometric intensity of the absorption peak at 420 nm was considered. For fluorescence spectroscopy analysis the samples were excited at a fixed wavelength of 422 nm to collect the fluorescent emission spectra, the emission peak at 560 nm was used for curcumin quantification.

8.1.3 Characterization of the optimal formulation

The properties of the selected formulation were furtherly investigated. The chemical structure of the curcumin loaded NP studied using ATR-FTIR. The particle morphology was inquired by SEM. To avoid the excessive aggregation observed in the previous set of SEM images, the NP suspension was diluted 1:10 before being applied to the SEM aluminum stubs. Particular care was paid to allow the suspensions to be spread uniformly on the stub. The prepared samples where metalized by sputter coating with chromium and observed with an SEM JEOL JSM-7800F LV equipped with a Field Emission Gun (Tokyo Japan).

A colloidal stability test was conducted to investigate the shelf life of nanoparticle products. The samples were collected in vials, covered with aluminum paper to protect curcumin from photodegradation. The vials were stored in the fridge at a temperature of 4°C. At given times, the samples were recovered and shaken to assure homogenization, thereafter an aliquot of the suspension was analyzed by DLS to monitor the changes in particle size and zeta potential over a time of 2 months.

The traceability of the nanoparticles was investigated by fluorescence microscopy. The particles were marked by adding the Nile red dye together with curcumin and PCL in the acetone solution fed to the CIJM. The Nile red quantity in the formulation was fixed to 5% by weight respect to curcumin. The excitation wavelength of 480 nm was used for curcumin imaging while Nile red observation was set at 540 nm. The two images were then merged to inquire about the co-localization of the two fluorescent species. DSC and TGA were conducted to gain insights on the thermal properties of the optimal formulation.

8.1.4 Biofunctional properties assessment

The biofunctional properties of the selected formulation were investigated through antioxidant activity and Franz cell test. For the antioxidant assay, the EPR spin trapping method was used. Since curcumin displays a chelating effect toward metal ions such as Fe^{3+}, a non-Fenton reaction based protocol was developed for the radical generation. The selected reactions involved the auto degradation of hydrogen peroxide which generates hydroxyl radicals (Equation 8.1).

$$H_2O_2 \Rightarrow 2OH^{\cdot} \quad (8.1)$$

The generated hydroxyl radicals react with the dimethyl sulfoxide medium to generate methyl radicals as described in Equations 8.2 and 8.3:

$$(CH_3)_2SO + OH^{\cdot} \Rightarrow CH_3^{\cdot} + CH_3SOOH \quad (8.2)$$

$$DMPO + OH^{\cdot} \Rightarrow DMPOOH^{\cdot} \quad (8.3)$$

The produced methyl radical reacts with the DMPO spin trap to form the $DMPOCH_3^{\cdot}$ radical adduct (Equation 8.4).

$$DMPO + CH_3^{\cdot} \Rightarrow DMPOCH_3^{\cdot} \quad (8.4)$$

The formation of the $DMPOOH^{\cdot}$ and $DMPOCH_3^{\cdot}$ was monitored by EPR spectroscopy to investigate the radical scavenging activity of the NPs toward the $OH^{\cdot}$ and $CH_3^{\cdot}$ radical respectively.
The experiments were performed by mixing 25 μL of the investigated formulation, 25 μL of DMSO, 25 μL of DMPO (5.66 mg/mL) and 25 μL of H_2O_2 (0.34 mg/mL) in an Eppendorf tube. Distilled water was used as control while nanoparticle suspensions were tested after dilution. Spectra of unloaded nanoparticles suspensions and free curcumin solution were collected for comparison.

The release test was conducted on a double ported vertical Franz diffusion cell with 2.6 cm^2 of the exchange area and 6 mL of acceptor compartment. The drug loaded nanoparticle formulation was placed in the donor compartment; an equivalent amount of curcumin solution was used as control. The skin mimicking membrane consisted of a dialysis membrane similar to the one used for caffeine loaded nanoparticle release test (MW cut-off 12000 Da, Sigma Aldrich). The acceptor fluid was a PBS solution, to which 10% by volume of ethanol was added to avoid curcumin saturation in the acceptor solution. Regular withdrawals were performed during the first 5 hours and thereafter the

experiment was left to run overnight. After 24 h, the last withdrawing was done and the total amount of drug released was obtained. Data from the first 5 hours of release test were used to fit the kinetic models of zero order, first order, Higuchi, Baker and Lonsdale and Hixon Crowell.

8.2 Nanoparticles properties and evaluation of the optimal formulation

In the first part of the study, six curcumin PCL formulations were produced. To identify the optimal formulation, the particles were characterized in terms of size, zeta potential, loading capacity and encapsulation efficiency.

8.2.1 Particle size analysis

The particle size for the different formulations was measured by the DLS technique. In Figure 8.1 the average diameters of the different NPs formulations are plotted against the initial polymer concentration for the different curcumin concentrations.

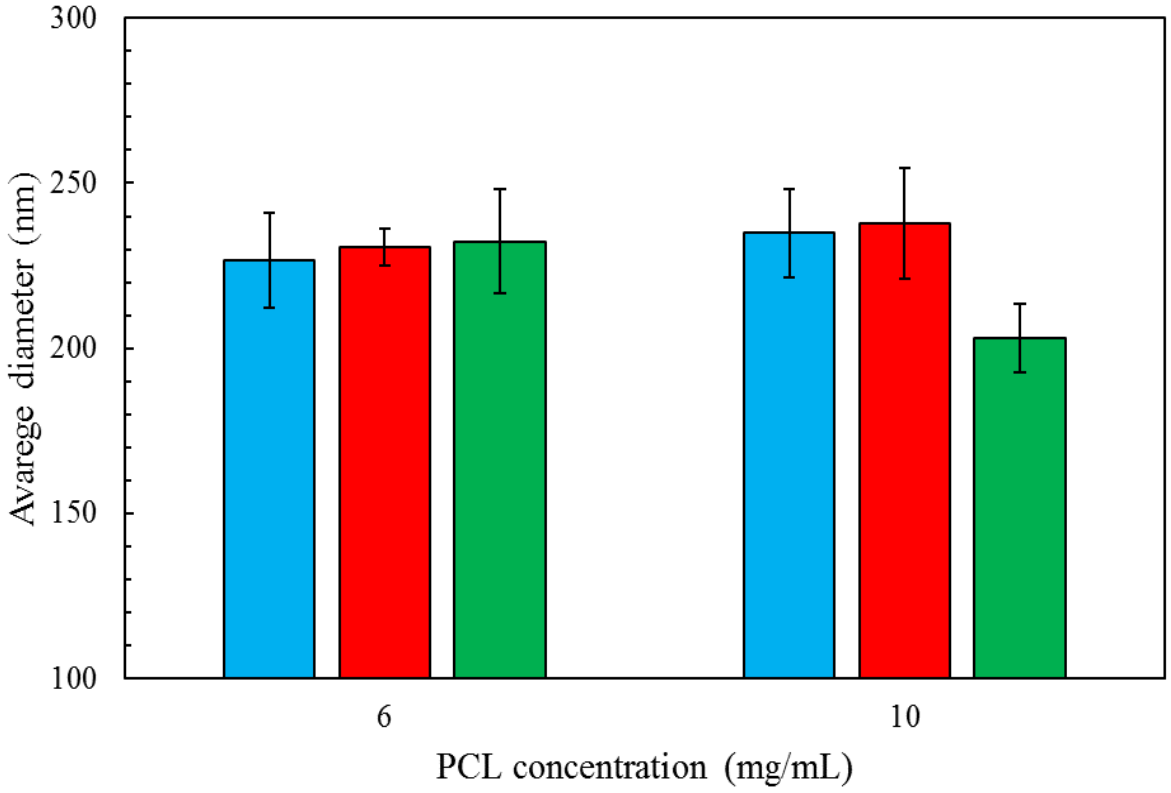

Figure 8.1. The particle size of the different formulation as function of the polymer concentration for different curcumin concentrations i.e. 1 mg/mL (blue bar) 4 mg/mL (red bar) and 6.5 mg/mL (green bar).

For all the produced formulations, particle diameters between 200 and 230 nm were found. These values of particle sizes are below the skin pores, therefore all the proposed formulations display suitable size for transdermal release.

It is worth noticing that, in the case of curcumin, lower average sizes were observed respect to the other drugs. Such an outcome can be explained by taking into account the hydrophobic nature of curcumin and its almost null water solubility. Given the fact that the solvent solution contained two water insoluble species, the supersaturation level upon jet collision was much higher respect to the already discussed cases in which the drug was at least partially water soluble. The higher level of supersaturation is known to significantly increase the nucleation rate leading to the formation of finer particles.

The effects of the drug and polymer concentration on the particle size were not immediately evident. Indeed, from Figure 8.1, it is observed that the differences in average diameter appear to be lower than standard deviations. By performing statistical analysis, it was evidenced that the change in the polymer concentration does not display statistically significant effects over the particle size (p-value > 0.05); on the contrary, the curcumin concentration does (p-value < 0.05). The main effect analysis furtherly proved that it is the curcumin concentration that mostly affects the Dp. The interaction analysis revealed that the two factors display a synergistic effect on the diameter of the particles.

8.2.2 Zeta potential

The zeta potentials of the different formulations were measured and plotted in Figure 8.2 as a function of curcumin concentration for the two different initial PCL concentrations. For all the formulations the zeta potential has negative values between -30 and -20 mV similarly to the other drugs.

The average zeta potential tended to be affected by the changes in concentration of either the curcumin and the PCL. The ANOVA analysis revealed that both curcumin and PCL concentrations display a statistically significant effect on PCL the zeta potential (p-value < 0.05). In particular, the main effects analysis revealed that PCL concentration is the main factor affecting Zp.

The zeta potential is conventionally used as an index of the particle's colloidal stability. Indeed, such property is an important requirement for particle application since particle aggregation leads to undesired side effects. Higher absolute values of zeta potential are taken as an index of greater

colloidal stability. For all the PCL curcumin formulation, the average Zp values allow classifying the particle population as stable according to the literature (Bhattacharjee, 2016). Formulation $PCL_{10}CUR_4$ displays indeed the highest absolute value of average values of zeta potential making it potentially more stable than the others.

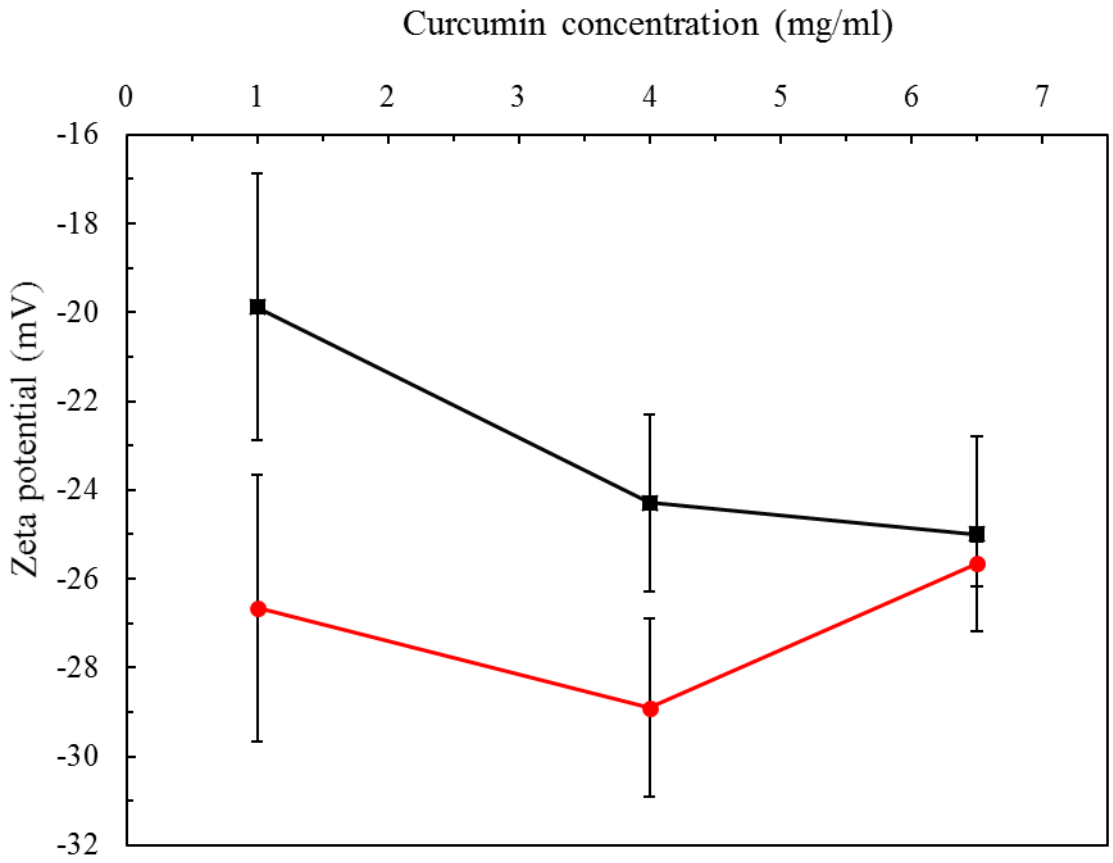

Figure 8.2. Particle zeta potential as function of curcumin concentration for different initial PCL concentrations: CPCL= 10 mg/mL (red circle) and CPCL= 6 mg/mL (black square)

8.2.3. Drug loading evaluation

In Figure 8.3 the values of LC and EE are reported as a function of the drug initial concentration. It is clear that, regardless of the polymer or curcumin concentration, high values of encapsulation efficiency were achieved. Indeed, for the investigated formulations, the EE was found to be between 97% and 99%.

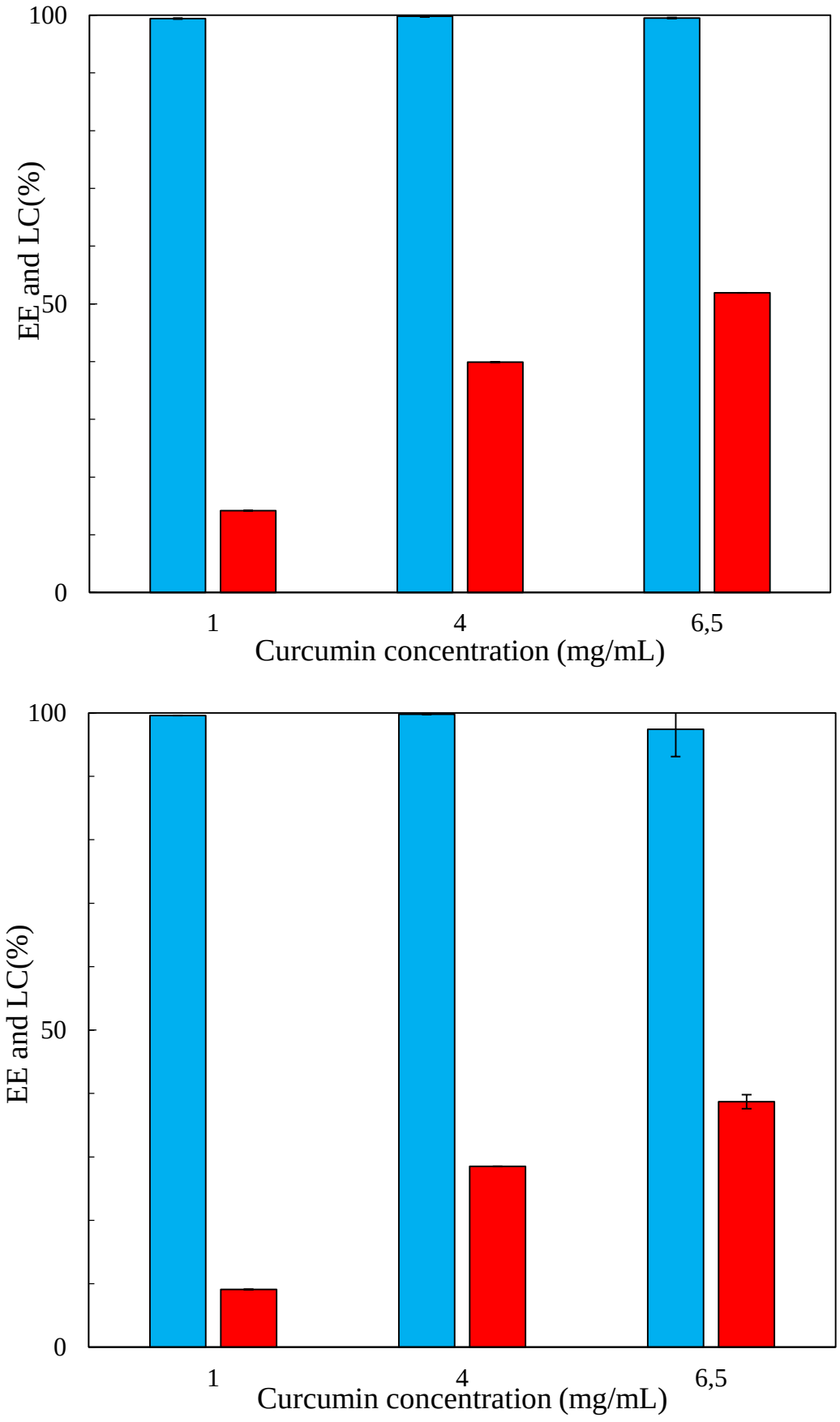

Figure 8.3. EE (blue bar) and LC (red bar) values for a function of curcumin concentrations for C_{PCL}= 6 mg/mL (top) and C_{PCL}= 10 mg/mL (bottom).

These high values of EE are explained by the hydrophobicity of curcumin. Being not soluble in water, this drug does did not partition between the polymer and the aqueous liquor, as it occurred with melatonin and caffeine. Therefore, curcumin was incorporated in the core of the particles; this result was found to be consistent with the ones reported in the literature for poorly water soluble substances (Tao et al., 2019).

Moreover, the high EE values corroborated the hypothesis that, being a hydrophobic molecule, curcumin nucleated together with the polymer upon mixing with water. Such an incorporation mechanism explains also the small particle sizes and is consistent with the ones reported for these kinds of substances (D'Addio and Prud'homme, 2011).

The loading capacity was found to increase as the curcumin concentration was increased, this trend was valid for both the tested PCL concentrations. It can also be observed that the increase in loading capacity was more marked for an initial PCL concentration of 6 mg/mL. Recalling Equation 6.1 and assuming the EE to be unitary (which is a reasonable assumption given the values obtained for curcumin) the following expression can be obtained:

$$LC = \frac{C_{drug,in}}{C_{pol,in} + C_{drug,in}}; \quad (8.1)$$

From Equation 8.1 it is clear that for very high values of encapsulation efficiency the loading capacity can be expressed as an increasing function of the initial drug concentration. The polymer concentration is a parameter that determines the extent of the LC increase. Having established such a correlation between the loading capacity and initial drug and polymer concentrations, it is straightforward to design the formulation to obtain the desired loading capacity. Furtherly, it can be concluded that among the investigated properties, the LC is the one that is more significantly dependent on the formulation parameters.

The formulation $PCL_{10}CUR_{6.5}$ showed peculiar characteristics, displaying the lowest size and encapsulation efficiency as well. Since, the supersaturation level and the nucleation rate are high, it can be assumed that curcumin molecules form nuclei independently from the polymer ones. This caused a fraction of these curcumin molecules to not be incorporated in the polymeric particles, leading to lower EE. Furtherly, due to the high nucleation rate, also the particle size was lowered (Saad and Prud'homme, 2016). However, it is important to point out that the measured differences

with the other formulations are quite low (25 nm in size and 3% in EE) and so they were not considered to be extremely meaningful.

Based on the data collected by the analysis of particle size, zeta potential, loading capacity and encapsulation efficiency, a proper choice of the optimal formulation for the textile finishing was made. Among the tested formulations, $PCL_{10}CUR_4$ was selected as the optimal one. First of all, it displayed fine particle size and almost total encapsulation efficiency. Secondly, it was evidenced to have the highest absolute values of zeta potential. Furtherly it displayed a loading capacity value of 28.5% which was reported to be optimal for dermatological formulations (Argenziano et al., 2017). Moreover, it displayed properties similar to the ones of the optimal PCL caffeine formulation (PCL_6CAF_9W). This last point makes formulation $PCL_{10}CUR_4$ to be the ideal candidate for textile finishing to compare the effects of the different drugs on the properties of the biofunctional textile.

8.3 Characterization of the optimal formulation

Upon testing the different particle formulations and identification of the optimal one, further characterizations were performed to better inquire about the properties and performances of such formulation. Therefore, the $PCL_{10}CUR_4$ nanoparticles were investigated by FTIR and SEM, the colloidal stability of the particles was monitored over time and their traceability was observed by fluorescence microscopy. The thermal properties of the optimal formulation were investigated by TGA and DSC.

8.3.1 SEM observations

The morphology of the particles was observed by SEM. The analysis was conducted on the optimal curcumin loaded formulation as well as on unloaded PCL nanoparticles processed under the same PCL concentrations and process conditions. The SEM images of the unloaded PCL nanoparticles and $PCL_{10}CUR_4$ formulation are shown in Figure 8.4.

Regarding the unloaded PCL NPs samples, a particle assembly in the low magnification image is shown (Figure 8.4 top left). Again this is due to the tendency of the particles to agglomerate during drying.

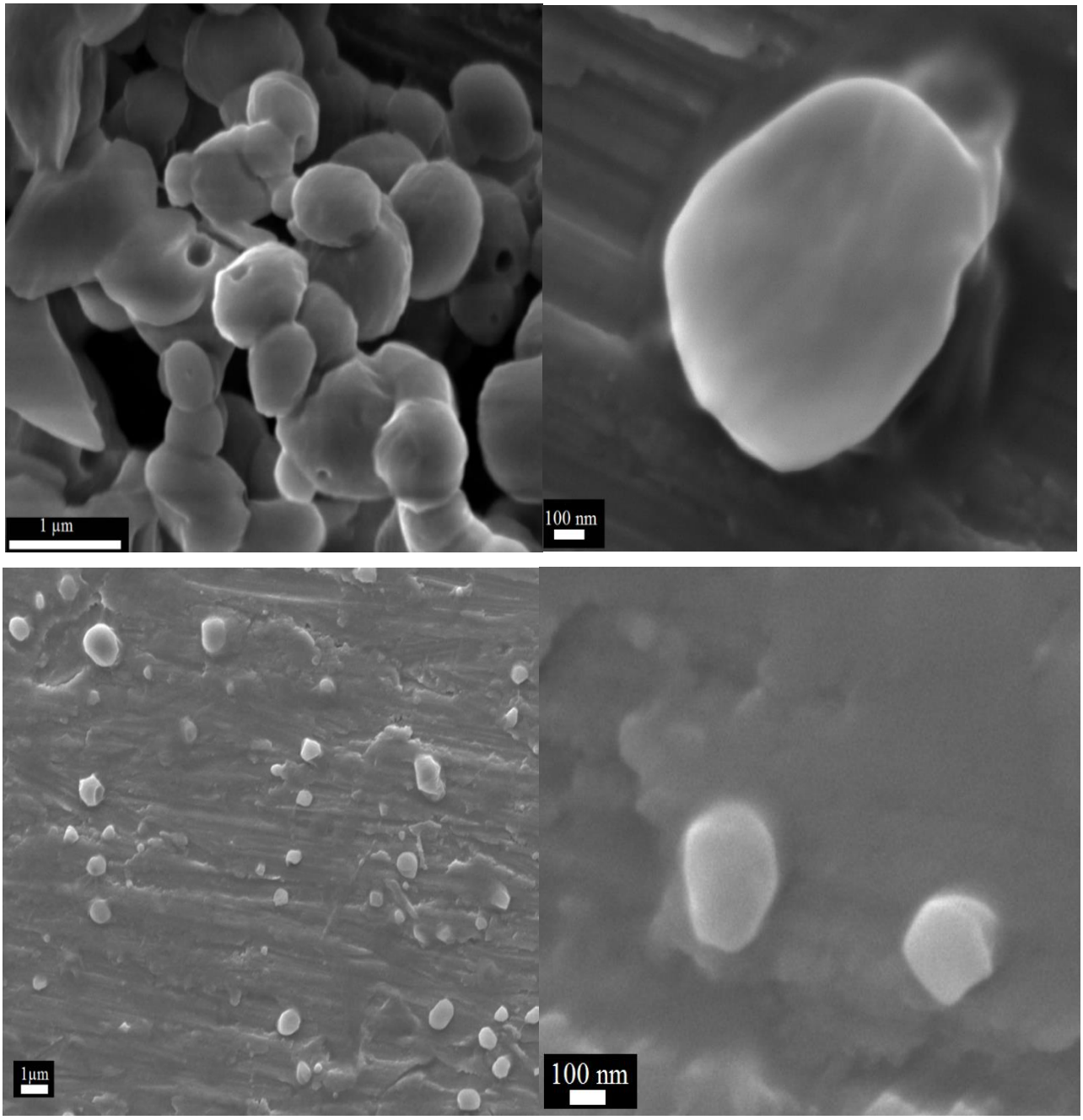

Figure 8. 4. SEM image of un loaded PCL nanoparticles (top images) with magnification of 2000X (top left) and 50000X (top right) and of $PCL_{10}CUR_4$ formulation (bottom images) with magnification of 5000X (bottom left) and 40000X (bottom right).

It is noticeable that some particles present some holes in their structure. The presence of these holes is explained taking into account the particle formation mechanism proposed by Di Pasquale et al. (2014). In that study, molecular dynamics simulations highlighted that upon jet collision nanoclusters of PCL and acetone were formed. Therefore, it is reasonable that the formed particles entrap some of

the solvents in their structure. This solvent leaked out during particle drying causing the formation of the holes observed in the image. By observing the PCL NPs at higher magnification (Figure 8.4 top right) it was furtherly confirmed that the particles own round shape and smooth surface.

From the images of the curcumin loaded samples, it was observed no curcumin crystals are present. Such crystals generally show a flower like morphology (Thorat and Dalvi, 2014); the absence of free curcumin species is consistent with the results of EE analysis and furtherly proves the optimal incorporation of the drug in the polymeric nanospheres.

8.3.2 Colloidal stability test

The colloidal stability was performed by monitoring the size and zeta potential of the $PCL_{10}CUR_4$ formulation. The particles were stored in the fridge at 4°C for over two months. The test was run for three independent samples and the results are plotted in Figure 8.5**.** It can be observed that both the particle size and zeta potential of every single sample, do not undergo significant changes over the investigation time.

Taking the average of the three tested samples the diameter is found to stay stable between 230 and 240 nm. Similarly, the zeta potential values are found to be mostly in between -30 and -25 mV. A slight decrease in the average diameter over the three samples after the 60 days. However, the ANOVA analysis highlighted that time does not display a statistically significant effect on the particle size (p-value > 0.05). This allows concluding that in the considered storage conditions the particle aggregation and size variation are negligible.

The fact that both the particle size and the zeta potential were not undergoing significant changes over time proved the high colloidal stability of the nanoparticle suspensions. This finding can be explained, according to the DLVO theory, by the balance between the electrostatic repulsive forces and the attractive Van der Walls interactions (Missana and Adell, 2000)

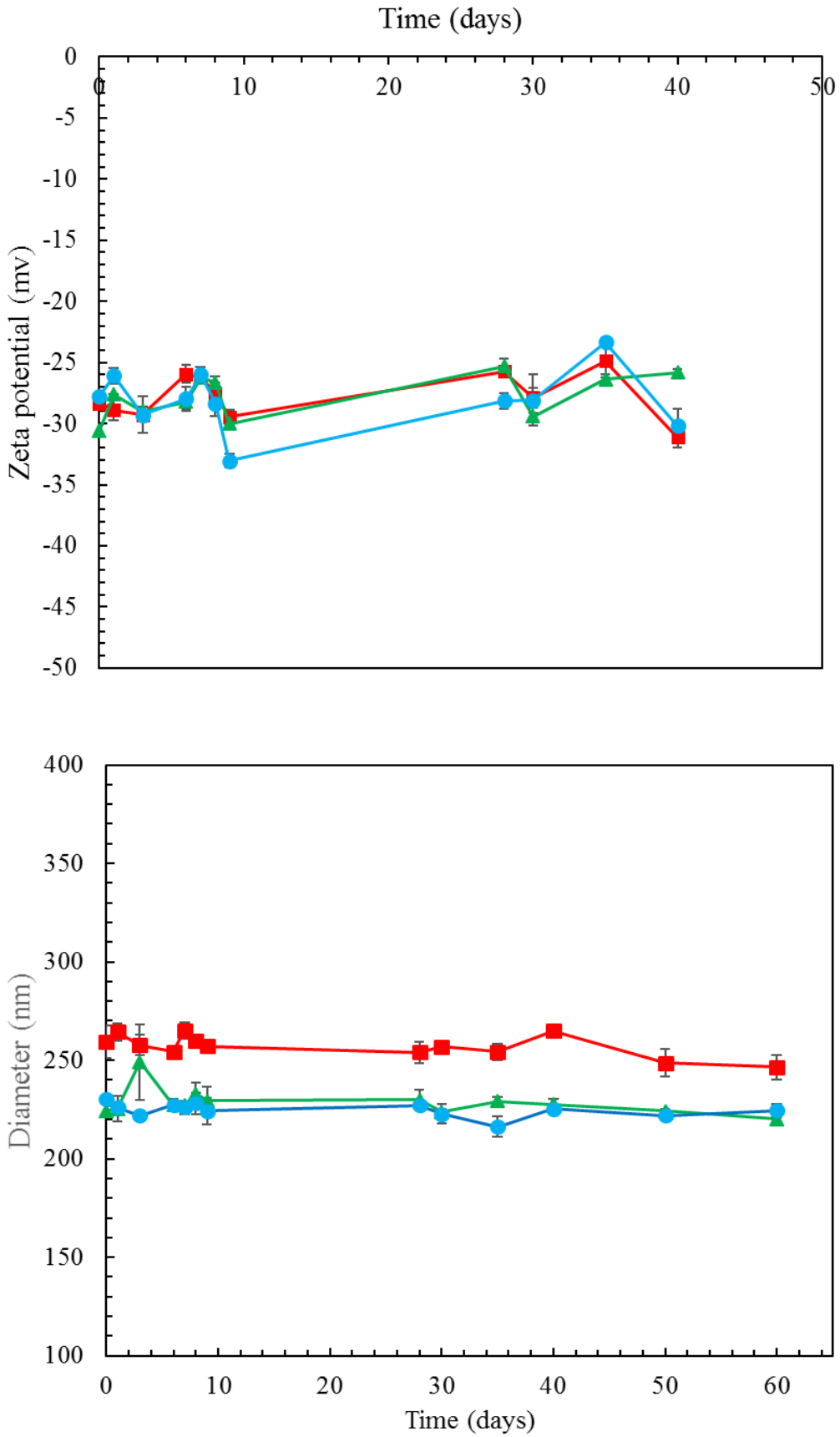

Figure 8.5. Trends of zeta potential (top graph) and (bottom graph) particle size for $PCL_{10}CUR_4$ NPs formulations. The three curves represent three independent replicates.

In the present system, the electrostatic repulsive forces due to the electric double layer can be considered high as observed by the high absolute values of zeta potential. Concerning the Van der Waals attractive forces, it can be roughly estimated that in a PCL based system they are quite low. In fact, such forces can be correlated to the difference of the refractive indexes of the colloid material and the dispersant (Bhattacharjee, 2016). In the present case, the differences between the refractive indexes of PCL (1.476) and water (1.511) is quite small. Therefore, the good stability of the presented system can be attributed to the combination of low attractive forces and high repulsive forces which overall prevents particle aggregation. Such good colloidal stability was considered a reason why the SEM images of sample $PCL_{10}CUR_4$ showed well dispersed particles and scarce NPs agglomeration.

8.3.3 Infrared spectroscopy analysis

The chemical structure of the selected curcumin loaded nanoparticle formulation was inquired by infrared spectroscopy. The FTIR spectra of $PCL_{10}CUR_4$ as well as the ones of the raw curcumin and pure PCL NPs are reported in Figure 8.6. The characteristic absorption bands are reported in Table 8.2.

The PCL NPs spectrum was characterized by two medium intensity peaks at 2943 and 2864 cm^{-1} which correspond to the asymmetric and the symmetric stretching vibration of the C-H bonds in the macromolecule skeleton. The strong absorbance peak at 1721 cm^{-1} was attributed to the stretching the C=O bond in the ester group. Peaks connected to the bending vibration of the C-H bonds in the polymer chain were observed at 1472, 1396, 1367 cm^{-1}. Further absorption bands peculiar of the stretching of C-O were observed at 1292, 1238, 1105, 1065, 1045 cm^{-1}.

The Curcumin spectrum exhibited a weak absorption peak at 3501 cm^{-1} correlated with the stretching vibrations of the O-H bond in the phenol group. The strong absorption signal at 1626 cm^{-1} due was attributed to the C=O bond in the keto-enol group. The presence of sharp peaks at 1602, 1507, and 1456 cm^{-1} was associated to the C=C double bonds in the curcumin aromatic rings. The peak at 1427 cm^{-1} was ascribed to the bending of the olefinic C-H. The absorption band between 1300 and 1000 cm^{-1} was mainly characterized by the peaks of the C-O stretching at 1274, 1232, 1152, 1114 and 1026.

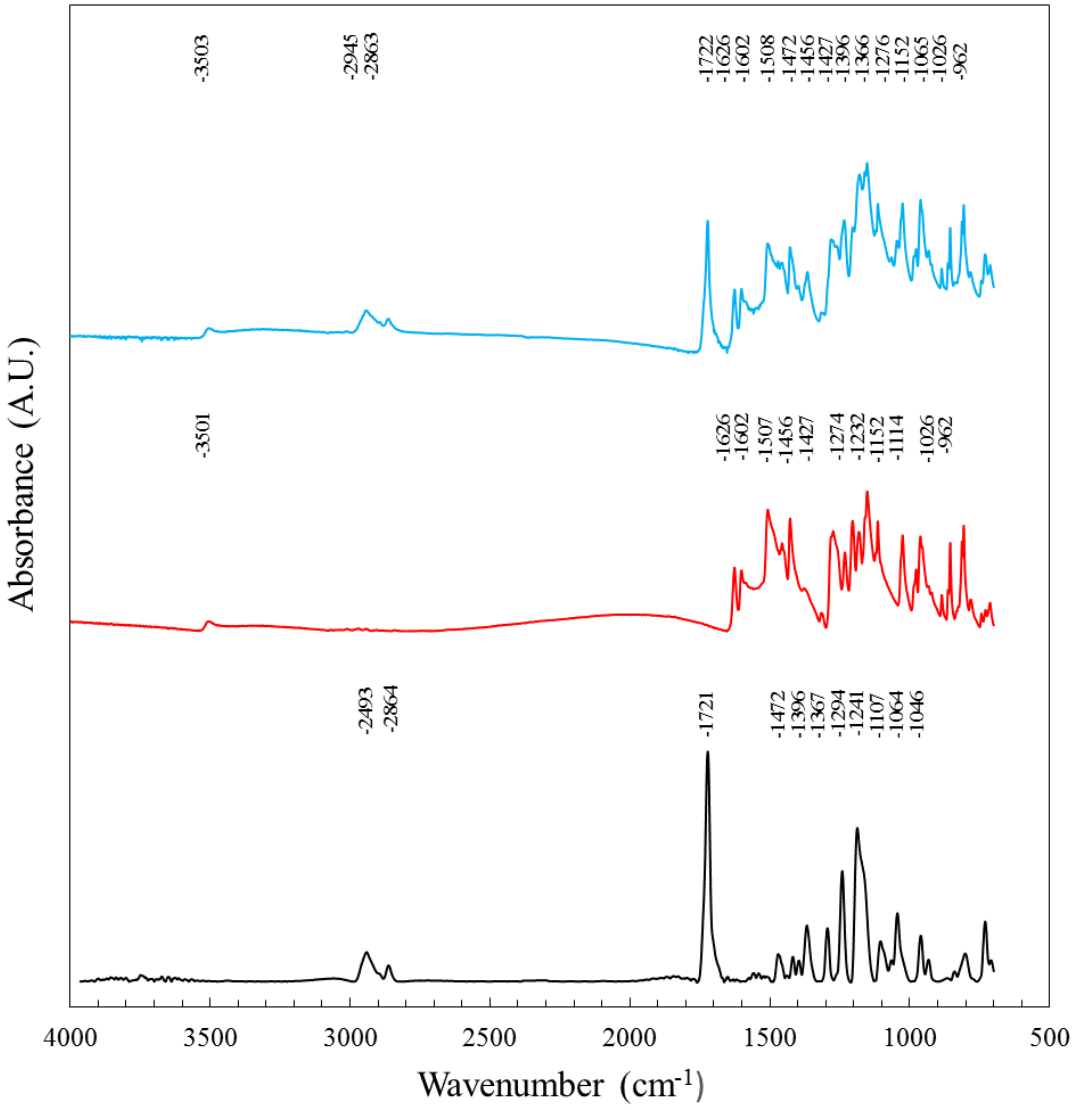

Figure 8.6. ATR-FTIR spectra of: PCL (bottom), curcumin (middle) and nanoparticles with $PCL_{10}CUR_4$ formulation (top).

The infrared spectrum of the $PCL_{10}CUR_4$ formulation displays absorption bands similar to one of the two constituent materials. A weak absorption peak at 3503 cm^{-1} was ascribed to the stretching vibrations of the O-H bond in the curcumin phenol group. Two medium intensity peaks were found at 2945 and 2863 cm^{-1} and correlated to the asymmetric and the symmetric stretching vibration of the C-H bonds in the PCL polymer chain. Two strong absorbance peaks of C=O stretching were observed at 1722 and 1626 cm^{-1} and correlated to the ester group of PCL and to the keto-enol group of curcumin respectively. The peaks at 1602, 1508, and 1456 cm^{-1} were associated to the C=C double bonds in the curcumin aromatic rings. The peaks connected to the bending vibration of the C-H bonds in PCL skeleton and curcumin were observed at 1472, 1427, 1396, 1366 cm^{-1}. Several signals connected to the stretching vibration of the C-O were found in the region between 1300 and 1000 cm^{-1}; more

precisely at 1276, 1232, 1152, 1065, 1113 1026, 1045, 1026 cm^{-1}. Lastly, the peak C-H aromatic stretching was found at 962 cm^{-1}.

Table 8.2. Characteristics IR absorption bands for PCL NP, curcumin and $PCL_{10}CUR_4$ formulation.

Wavenumber (cm^{-1})			Attribution
PCL NP	**Curcumin**	**$PCL_{10}CUR_4$**	
-	3501	3503	Streching O-H in phenol group
2943	-	2945	Asymmetric C-H stretching vibrations
2864	-	2863	Symmetric C-H stretching vibration
1721	-	1722	Stretching vibrations of C=O bond in esters groups
-	1626	1626	Stretching C=O in the keto-enol group
-	1602, 1507, 1456	1602, 1508, 1456	Stretching vibration C=C aromatic
1472, 1396, 1367	1427	1472, 1427, 1396, 1366	Bending vibrations of C-H
1294, 1241, 1107, 1064,1046	1274, 1232, 1152, 1114, 1026	1276, 1232, 1152, 1113, 1065, 1045, 1026	Stretching vibrations of C-O
-	962	962	Stretching of C-H aromatic

Overall no significant changes in the peak positions nor the formations of new peaks were observed. This confirms that the incorporation of curcumin in the PCL nanoparticles does neither imply the chemical modification of the drug and the polymer structure nor the chemical interaction among the two species. The slight shift in some peak positions (of about 2-4 wavenumbers) suggests that curcumin and PCL undergo some weak interaction such as Van der Walls forces and Hydrogen bonding. Indeed similar kinds of interaction between the drug and the polymer, upon encapsulation by an FNP method, were reported in the literature (Ke et al., 2019).

8.3.4 Fluorescence microscope observations

The nanoparticles were marked by the addition of the Nile Red dye to the formulation and observed by fluorescence microscopy. The images of the nanoparticles under different excitation wavelengths and their colocalization is reported in Figure 8.7.

In the picture a), it can be observed that, upon excitation at a 480 nm wavelength, green fluorescence is emitted. This green fluorescence is known to be due to the curcumin molecules (Akbari et al., 2018). It is important to notice that the fluorescent light comes from circular spots that can be identified as the nanoparticles.

In image b), the sample is observed under an excitation wavelength of 540 nm, in this case, the particles are characterized by red fluorescence emission which is due to the Nile red dye added in the formulation. It was observed the total incorporation of the red dye in the structure of the particles, which is well expected since it is more hydrophobic than curcumin (LogP = 5) (Bader et al., 2016). The incorporation of the dye was furtherly verified with an EE indirect test similar to the one conducted for curcumin and no residual Nile red was found in the supernatant. Therefore, being entrapped in the core, the dye can act as a tracking system for the particles.

Image c) is obtained by the superposition of images a) and b). Very precise colocalization of the fluorescent marker and the drug is observed. The possibility of easily observing both the red marked polymer particle and the green fluorescent drug allows tracking of the interaction of the NP system with living tissues.

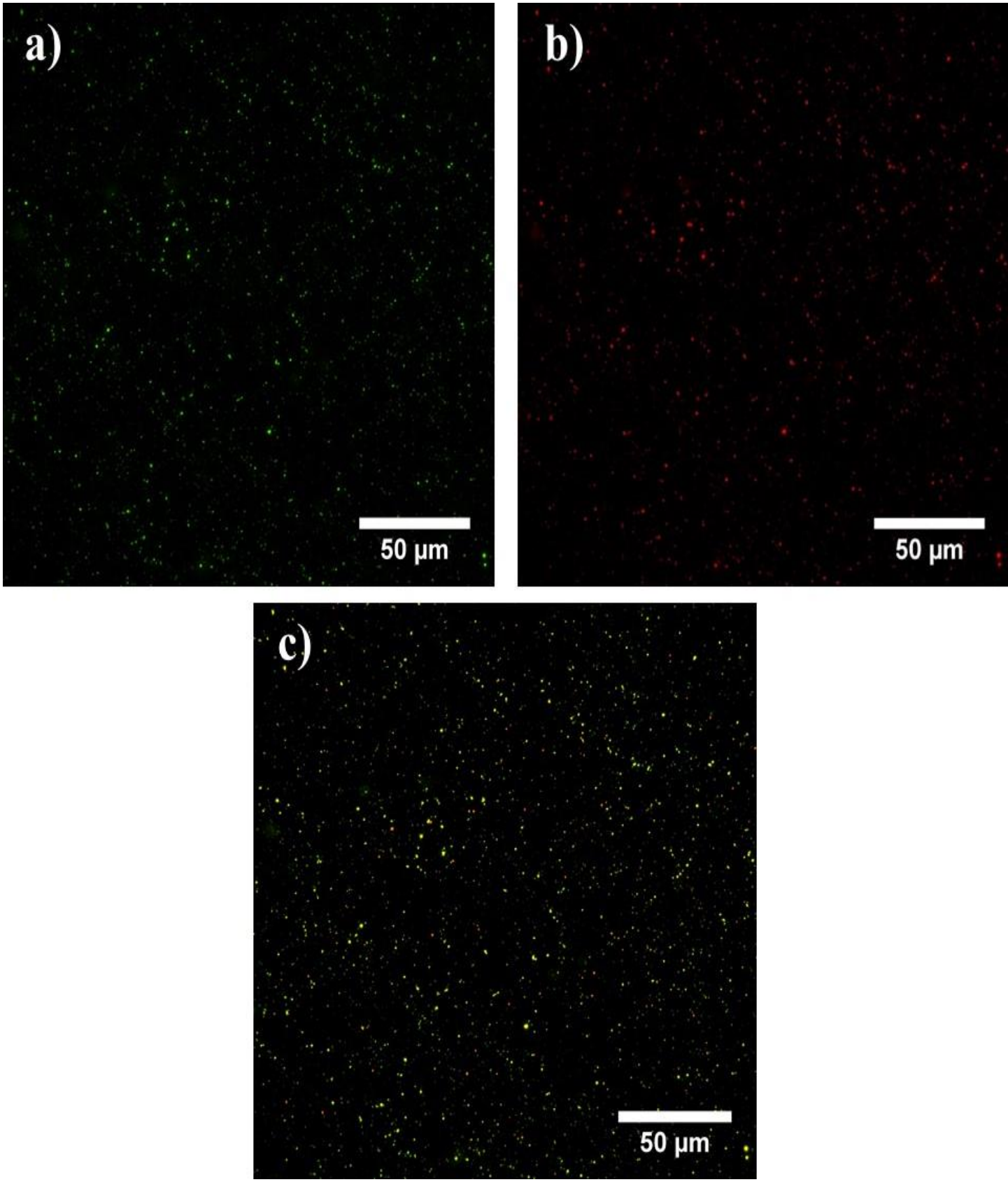

Figure 8.7. Fluorescence microscopy observations of the $PCL_{10}CUR_4$ nanoparticles upon marking with the Nile red fluorescent dye: a) excitation wavelength of 480 nm, b) excitation wavelength of 540 nm and c) colocalization of pictures a) and b).

8.3.5 Thermal analyses

The thermal properties of the curcumin loaded nanoparticles were investigated by DSC and TGA techniques. The analysis was run on the $PCL_{10}CUR_4$ formulation and compared with one of the raw materials. The DSC thermogram of the for curcumin loaded nanoparticles is depicted in Figure 8.8 while the main thermal events observed are listed in Table 8.3.

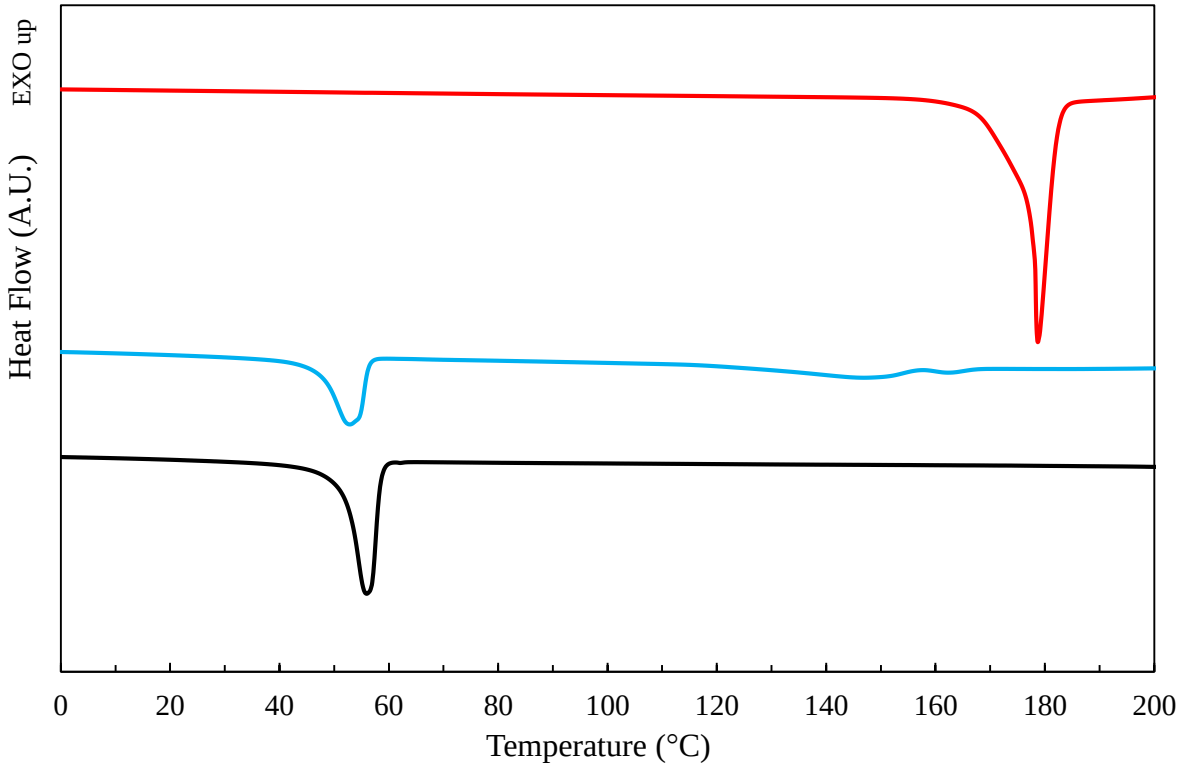

Figure 8.8. DSC thermogram of PCL (black curve), curcumin loaded nanoparticles (blue curve) curcumin powder (red curve).

As already discussed the PCL thermogram was mainly characterized by a single fusion peak between 50 and 60 °C while the curcumin powder exhibited a melting peak around 180 °C. Concerning the curcumin nanoparticles sample, it was observed a single melting peak around 50 °C. The peak was attributed to the fusion of the PCL shell of the nanoparticles. Instead, no trace of the curcumin fusion peak was observed in the nanoparticle sample. The absence of the curcumin fusion peak was connected to the fact that the drug was incorporated in polymeric nanoparticles. Indeed, while the curcumin powder owned a crystalline structure, the encapsulated one was dispersed at the molecular level inside the polymer matrix; having lost its crystalline structure it did not undergo fusion. Such a result was consistent with the ones reported in the literature regarding drugs incorporated inside nanocarriers (Mihailiasa et al., 2016; Puglia et al., 2016).

Interestingly, it was observed that in the case of curcumin loaded nanoparticles the polymer did not undergo a significant reduction of the crystallinity degree. As explained in Chapter 5 the reduction of X_c was partially due to the fast nanoprecipitation process and partially ascribed to the sample biodegradation during storage. The addition of curcumin was supposed to play a role in both phenomena. Firstly, it was observed to increase the nucleation rate leading to a higher formation of crystalline nuclei. Secondly, being an antimicrobial active principle it was likely to hinder the biodegradation of the PCL molecule during the storage conditions.

Table 8.3. List of the thermal events observed during the DSC analysis of curcumin loaded nanoparticles.

Sample	**PCL**	**Curcumin**	**PCL-CUR NP**
ΔH_{fus} (J/g)	-60.8	-129.0	-39.7
$T_{fus,\ onset}$ (°C)	51.8	177.3	47.1
$T_{fus,\ peak}$ (°C)	55.9	178.7	53.0
X_c (%)	43.7		39.9

In Figure 8.9 the results of the TGA analysis of for the curcumin loaded nanoparticle are reported, the main data obtained from the analysis are listed in Table 8.3.

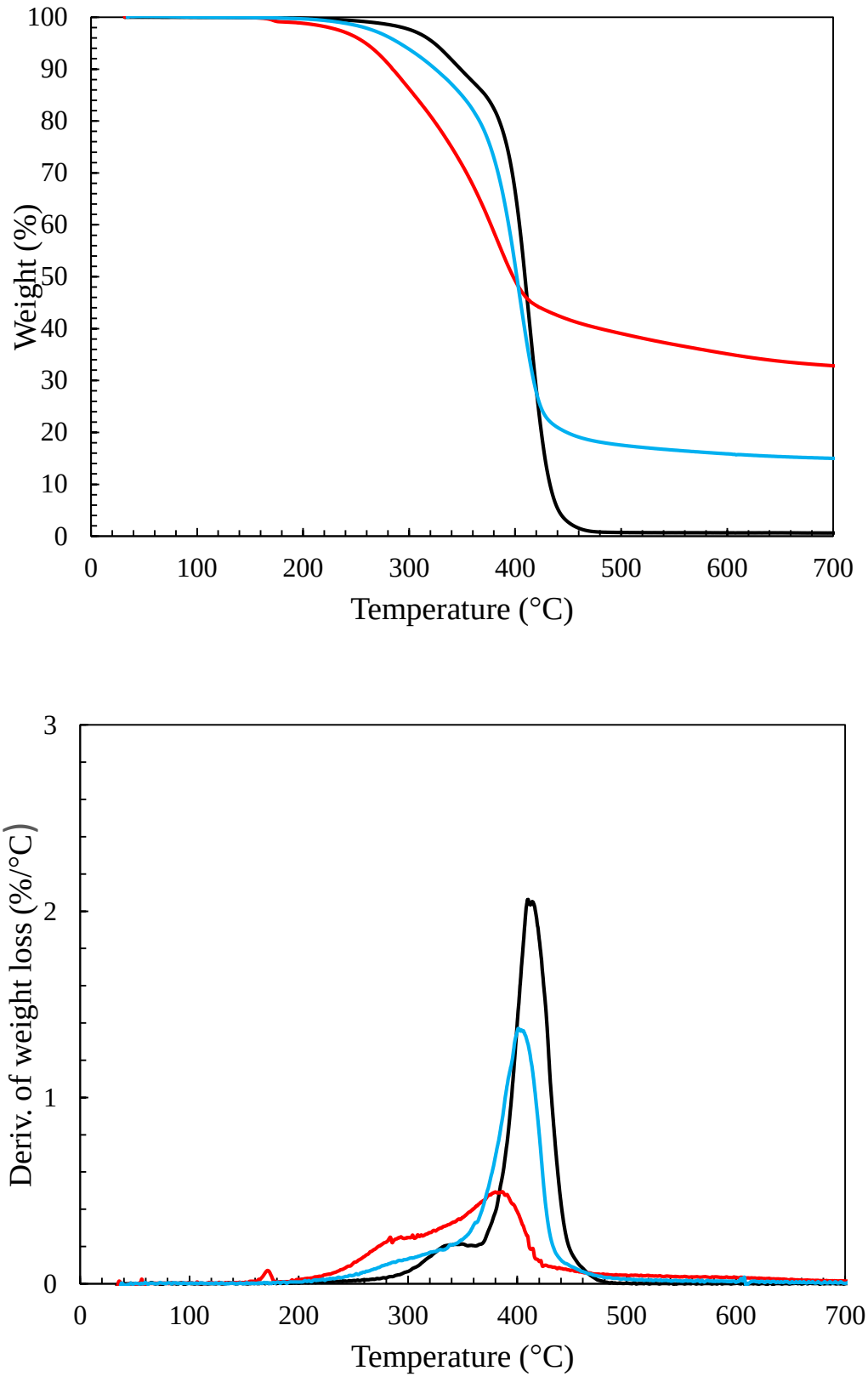

Figure 8.9. TGA analysis of PCL (black curve) and curcumin (red curve) and $PCL_{10}CUR_4$ (blue curve). TG curve (top graph) and first derivative of the TG curve (bottom graph).

As previously reported curcumin thermal degradation started around 260°C, thereafter it went on leaving a char residue of about 33% of the initial sample weight. PCL instead displayed the degradation onset at a higher temperature, the sample was completely degraded and no char residue was left. The curcumin loaded nanoparticle TG curve display characteristics between the ones of the two raw materials. The onset of degradation was observed to be around 290°C. The degradation proceeded in a unique step reaching the maximum degradation rate at 400°C. A residue of 15% of the initial sample weight was observed. This char residue was ascribed to residual curcumin since PCL was completely degraded at 700°C. Considering that the fraction of curcumin in the sample was 28.5% and that for pure curcumin one the observed residue was one third of the initial weight, in the $PCL_{10}CUR_4$ a higher residue than the theoretical one (about 9.5%) was found. This result hinted that some interaction occurred between curcumin and PCL during the degradation process. Such positive interaction led to a lower percentage of the active molecule to be degraded, therefore, it was concluded that the incorporation in polymer shell protects curcumin from thermal degradation phenomena.

Table 8.4. List of the thermal data obtained from TGA analysis of PCL-curcumin nanoparticles.

Sample	$T_{5\%}$ (°C)	T_{max} (°C)	MMLR (%/°C)	Residue at 700 °C (%)
PCL	324	409	2.1	1
Curcumin	259	386	0.5	33
PCL-CUR NP	291	400	1.4	15

8.4 Biofunctional properties of the PCL-curcumin nanoparticles

The increasing interest in using curcumin in dermatological formulations is connected to its antioxidant properties, which are known to be effective in the prevention and treatment of skin diseases. Therefore, the biofunctional properties of the nanoparticles were assessed by testing their antioxidant activity and by evaluating the drug release kinetics by the Franz cell experiment.

8.4.1 Antioxidant properties of the nanoparticles

The antioxidant properties of the curcumin loaded NPs were investigated by EPR/spin trapping method. The spectra of the spin trap DMPO were recorded upon the addition of the different species and reported in Figure 8.8. It is possible to observe that the control spectrum was characterized by ten positive antiphase signals due to the binding of the radical species to the spin trap. The signals at an applied magnetic field 3407 G, 3421 G and 3438 G are attributed to the binding of the OH · radical while the ones at 3398 G, 3404 G, 3415 G, 3418 G, 3431G, 3433 G and 3448 G due to the binding of the CH_3· radical. In the presence of the unloaded PCL nanoparticles, no significant change in the peak intensity was observed meaning that the polymeric system did not exert any antioxidant effect.

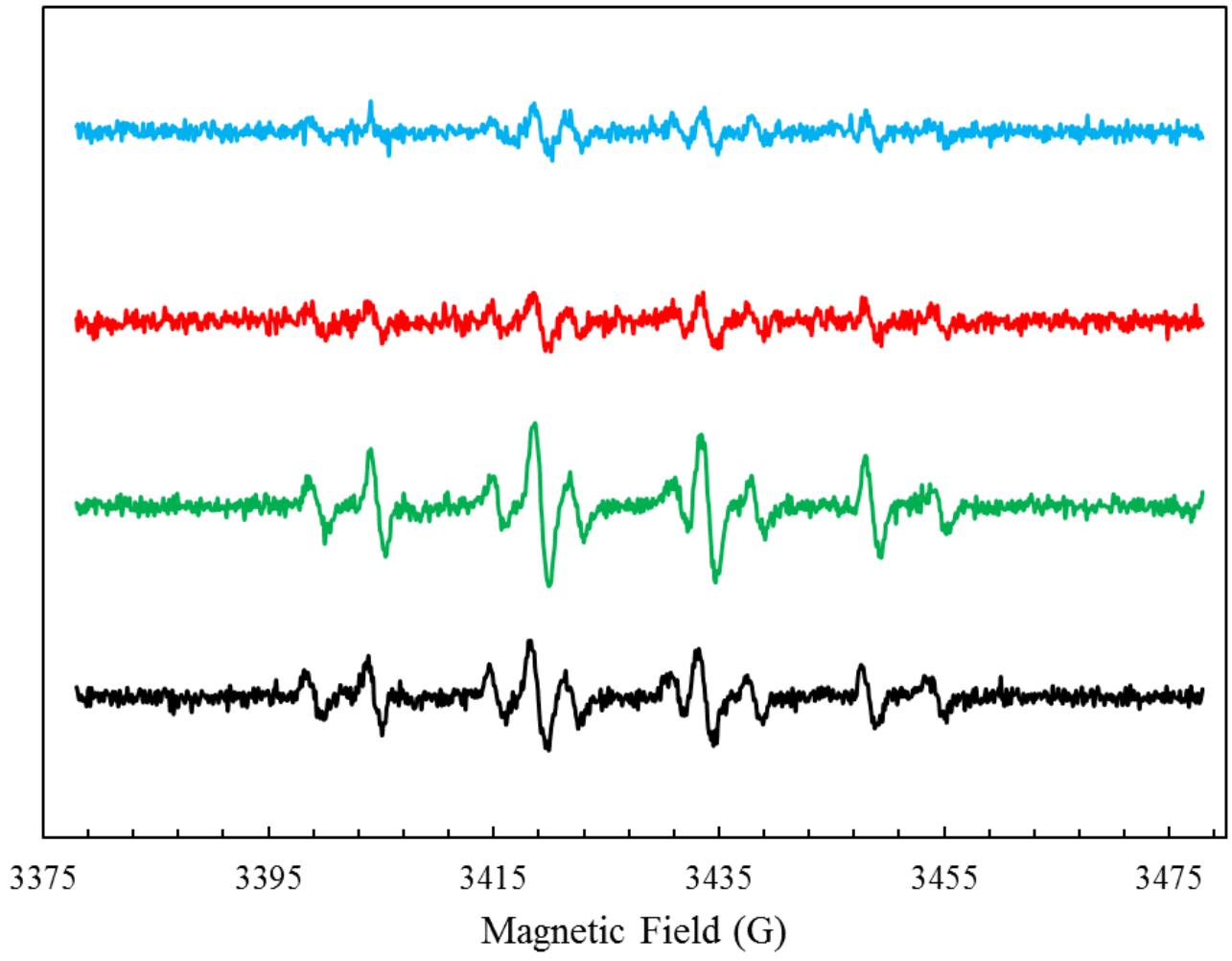

Figure 8.10. EPR spectra for the analyzed samples: Control (black curve), PCL NP (green curve), curcumin (red curve) and curcumin loaded nanoparticles (blue curve).

Such finding is indeed consistent with the polymer chemical structure which does not contain any functional group that can be reactive against the generated free radicals. Concerning the spectra of curcumin and curcumin loaded nanoparticles, it is, instead, evident that the intensity of the antiphase signals was lowered. This phenomenon is due to the fact that curcumin molecule preferentially reacts with the OH · and CH_3· radicals causing the measured concentration of DMPO-OH and DMPO-CH_3 to be lowered.The scavenging activity of the curcumin formulation against these two radical species was calculated and reported in Figure 8.9**.**

Concerning the scavenging effects of the curcumin formulations against the hydroxyl radicals, it can be observed that, for all the tested concentrations, about half of the generated radicals were absorbed by the curcumin formulations. The free curcumin tends to have better OH· scavenging efficiency for lower concentrations. Such a result can be associated with the fact that the analysis was conducted in an aqueous environment. Therefore, curcumin molecules tend to form precipitates for higher concentrations and have poor dispersion that limits the extent of reactions with the hydroxyl radical.

For the nanoparticles formulation instead, the highest scavenging activity was observed for the not diluted sample. It is interesting to notice that for all the tested concentrations the curcumin loaded nanoparticles displayed higher hydroxyl radical scavenging effects respect to the free drug; particularly, for the not diluted formulation, the scavenging efficiency raises by 20% upon encapsulation. This indeed shows that the incorporation in the PCL matrix improves the activity of curcumin allowing more effective reactions with the OH· radical.

Regarding the scavenging activity against the methyl radical, it was found to slightly increase with concentration both for free and encapsulated curcumin. This highlights that the reactivity of free curcumin with CH_3· radical was not hindered by the scarce solubility of the drug as, on the contrary, it occurs for the OH· radical. The encapsulation in the PCL matrix leads to an improvement of the scavenging activity also against the methyl radical.

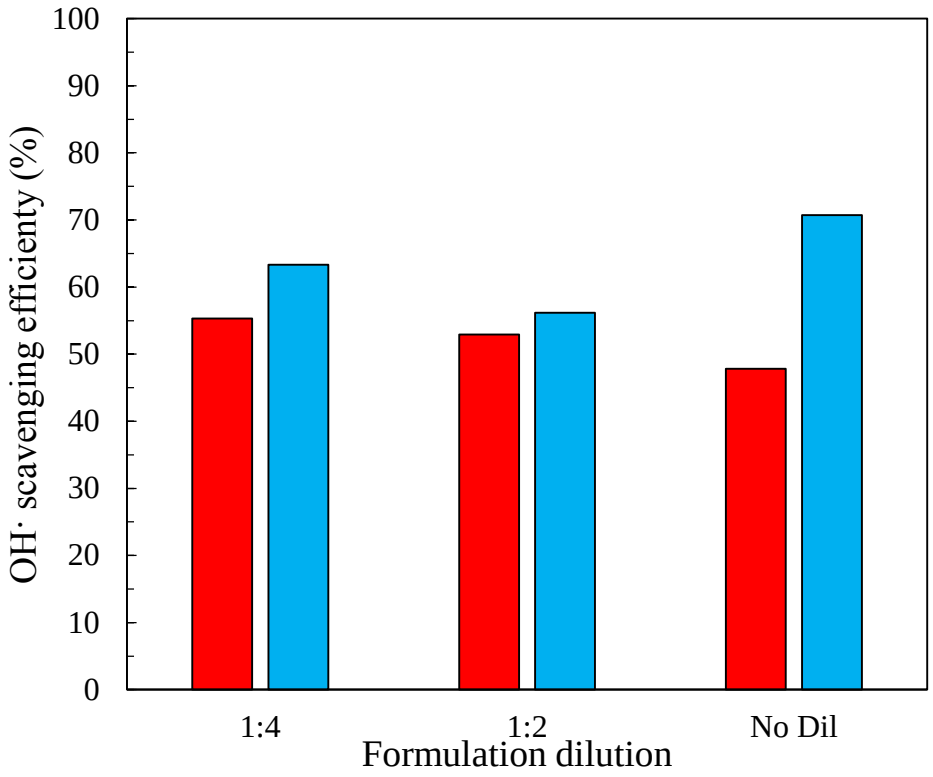

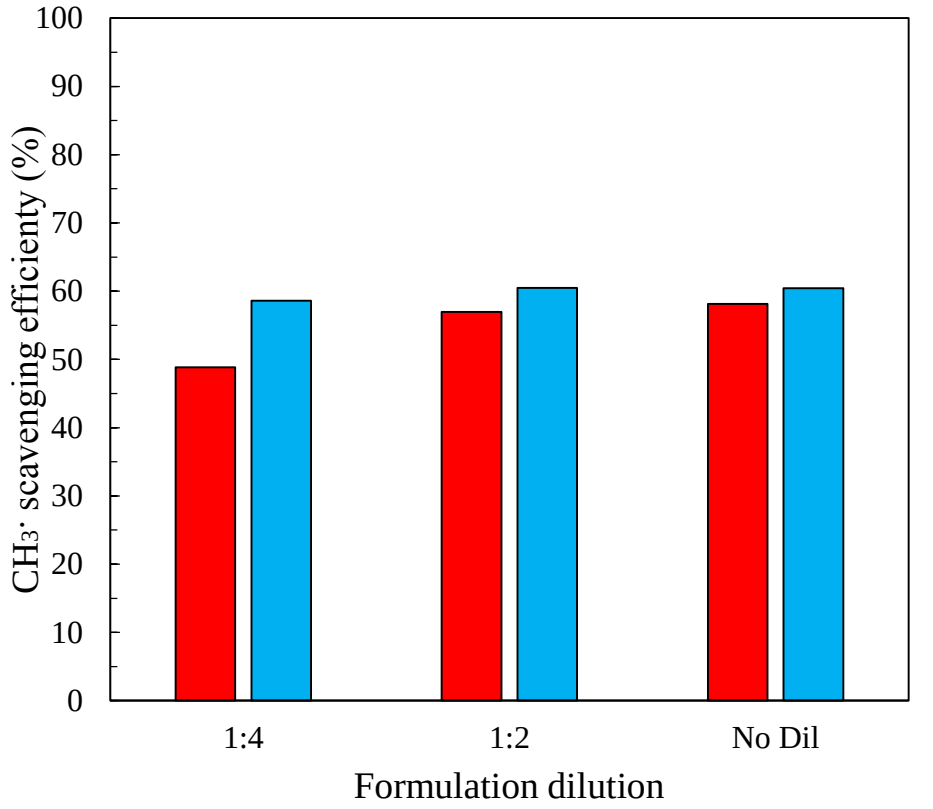

Figure 8.11. Scavenging efficiency of the curcumin (red bar) and curcumin loaded nanoparticles (blue bar) against OH· radical (top graph) and CH3· radical (bottom graph).

By summing and normalizing the individual scavenging properties toward the two studied radical species, the total antioxidant activity was obtained. The antioxidant activity values, represented in Figure 8.10, show that, for all dilution ratios, the nanoparticles display antioxidant activity above 50% thus halving the number of harmful radicals potentially interacting with the living tissues. In particular, the direct application of the $PCL_{10}CUR_4$ formulation led to the depletion of 66% of the radical species proving to be a powerful antioxidant.

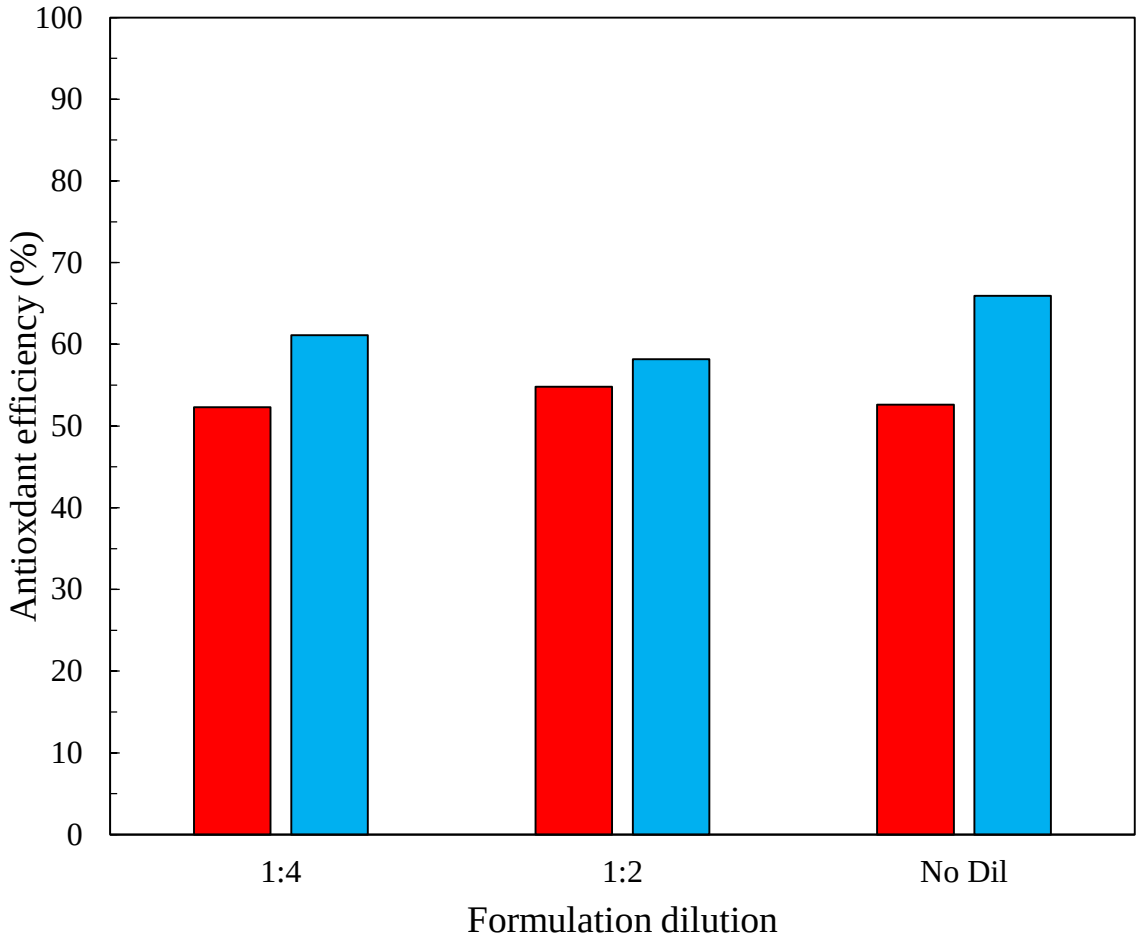

Figure 8.12. Antioxidant efficiency of the curcumin (red bar) and curcumin loaded nanoparticles (blue bar).

Overall it can be concluded that the incorporation in the PCL system boosted the antioxidant properties of curcumin. This finding is consistent with the literature regarding the nanoencapsulation of curcumin or other hydrophobic molecules (Coradini et al., 2014). Indeed, the antioxidant activity of these species tends to be hindered by their scarce chemical activity in biological (aqueous environment). The nanoencapsulation was therefore identified as a strategy to structure and improve the activity of this species leading to an improvement of their biofunctional properties (Yen et al., 2010)

8.4.2 In vitro Franz cell test

The drug release kinetics of the $PCL_{10}CUR_4$ formulation was assessed via the in vitro Franz diffusion cell test. In Figure 8.11 the release profiles of the nanoparticle formulations are shown, an equivalent curcumin solution was used as control.

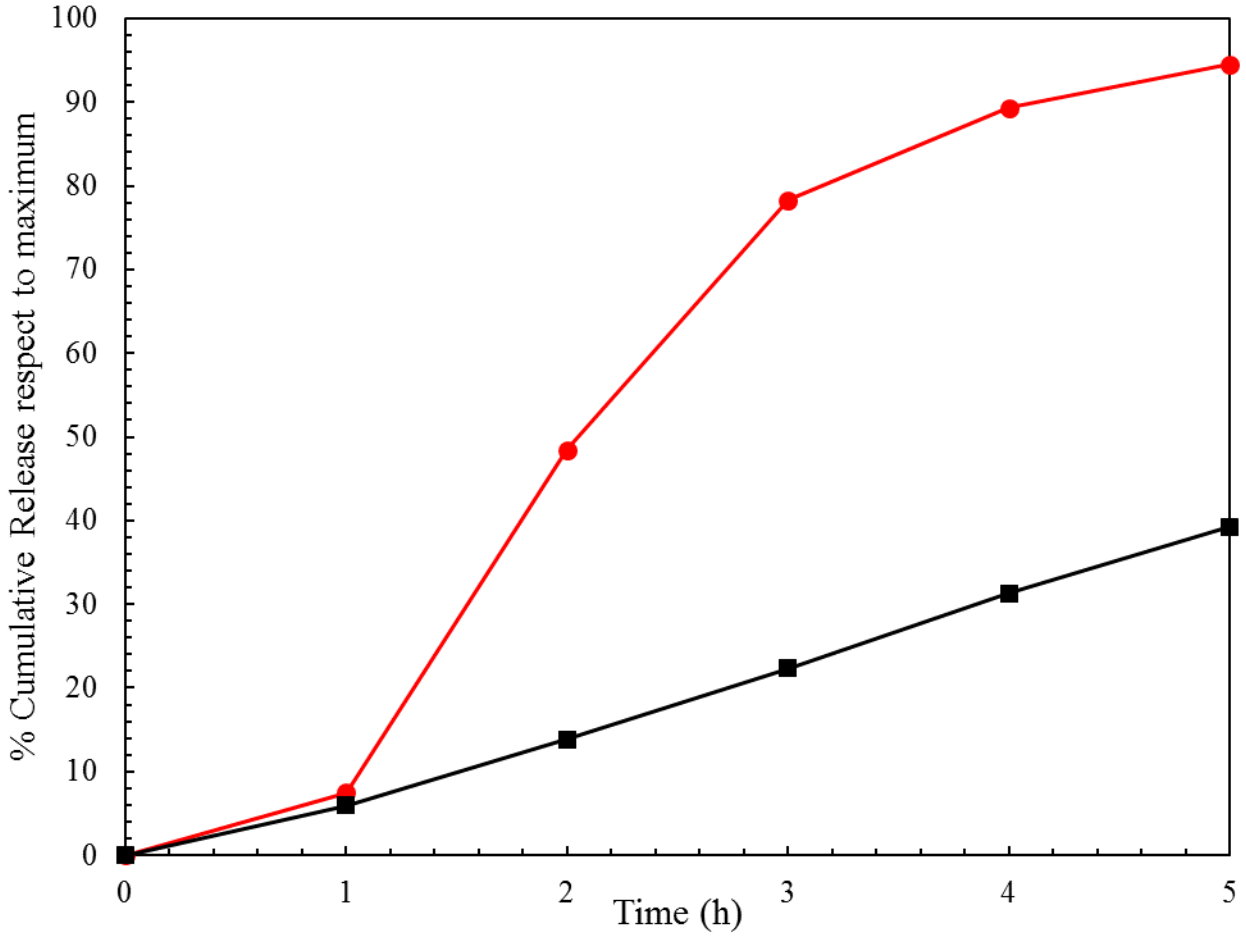

Figure 8.13. Curcumin permeation kinetics from free curcumin (red curve) and curcumin loaded nanoparticles (black curve). Results are plotted in terms of percentage respect to the total amount of curcumin released in each test.

The experiment was monitored regularly for the first 5 hours, then left overnight and, after 24 hours, the acceptor solutions were withdrawn. The cumulative amount of curcumin released after 24 was used to normalize the amount of drug released and to calculate the cumulative release curve. It is possible to observe that the curcumin control starts to fast release the drug after 2 hours and reaches an amount of 95% after 5 hours.

The curcumin loaded nanoparticles, instead, gradually elute the drug, releasing about the same amount of substance for each time unit. The nanoparticles system is also observed to act as a drug

reservoir since the amount of curcumin released after 5 hours is 40% respect to the total amount released after 24 h; such values are less than half the one observed for the free curcumin solution. To better investigate the drug release kinetics, the data were fitted with semi-empirical kinetic models, the correlation coefficient of the data fitting are reported in Table 8.3.

Table 8. 5. The correlation coefficient for the fitting of the release curves with different kinetic models.

Sample	Zero order	First order	Higuchi	Hixon Crowell	Baker Lonsdale	Drug released after 24 h
Free Curcumin	R^2=0.93	R^2=0.94	R^2=0.85	R^2=0.96	R^2=0.90	18.8 µg
Curcumin NP	R^2=0.99	R^2=0.98	R^2=0.84	R^2=0.98	R^2=0.82	78.5 µg

It can be observed that, in the case of free curcumin, it is not easy to identify predominant kinetics since the R^2 are very close to each other. Slightly higher correlation values were observed for the Hixon Crowell model. Such correlation is connected to the fact that curcumin has very low aqueous solubility and therefore may also form precipitates in the donor compartment. Then such aggregates must undergo dissolution causing the data to be well fitted by the Hixon model based on matrix erosion. For the nanoparticle formulation, it is evident that the zero order kinetics displays the best fitting. This fact is due to the good capability of the nanoparticles systems to slowly and continuously release the drug; this allows to not reach the saturation concentration in the time interval among each withdrawing. Therefore, the curcumin concentration in the acceptor compartment is kept low and does not affect the release of the drug. By comparing the total amount of drug released after 24 hours, reported in Table 8.3 it can be observed that the nanoparticle formulation delivered a drug amount 4 times higher respect to the curcumin solution. This result is strictly related to the continuous and controlled release of the nanoparticles respect to the free drug. Indeed being curcumin a poorly water soluble molecule, the burst release typical of the free drug causes an immediate saturation of the acceptor compartment. On the contrary, the encapsulated drug was slowly eluting the active principle without saturating the solution in the time elapsing between two withdrawings. Therefore it is concluded that the incorporation in the nanoparticles both controls and enhances the transdermal delivery of curcumin.

Part IV final remarks

In the present part of the thesis, the results regarding the encapsulation of the active principles were presented. Particularly, the focus was paid on highlighting the performances of the proposed FNP method on two drugs with marked differences in terms of hydrophilicity, i.e. caffeine and curcumin. For both the substances, the properties of the different formulations were inquired to select the most suitable one to be used in biofunctional textiles preparation.

The research conducted on the caffeine encapsulation proved the feasibility of incorporating a hydrophilic active principle in the nanoparticles matrix by employing the flash nanoprecipitation technique. Such results allowed to overcome one of the limitations of the FNP method. Interestingly it was observed that the choice of caffeine solvent affected the particle structure. Indeed, the classical FNP configuration, in which the drug is dissolved in the organic solvent lea to nanospheres where the drug was mainly adsorbed onto the surface of the particles in the outer surface layers of the particles. Oppositely, when the hydrophilic drug was dissolved in the antisolvent, the drug was found to be more incorporated in the core polymeric structure. The differences in particle structures were ascribed to different encapsulation mechanisms. Furtherly the process configuration influenced the particle critical particle properties. Indeed, the particles produced in CIW mode displayed finer size, higher EE and slower release kinetics if compared with the ones produced in CIA configuration. Therefore, considering the different analyses performed, the formulation PCL_6CAF_9W was selected as the optimal one to be employed in the textile finishing. This chosen formulation was proven to have a marked scavenging effect against the $OH^{\cdot}$ radical species achieving an antioxidant efficiency above 50%.

The research about curcumin incorporation investigated six PCL-CUR formulations designed based on the results obtained in the previous research lines. The formulations were screened by mean of size, zeta potential, LC, EE analyses. All the formulations displayed fine particle size and high EE. Taking into account all the performed analyses the $PCL_{10}CUR_4$ was chosen as the optimal formulation. This NP formulation was proven to own exceptional colloidal stability since it did not exhibit aggregation phenomena for at least two months. The EPR spectroscopy analysis showed how the proposed formulation displays strong scavenging properties against different radical species. The incorporation of curcumin in the PCL system was proven to enhance the radical scavenging activity of curcumin displaying an antioxidant efficiency of 66%. The in vitro Franz cell test evidenced that the curcumin loaded nanoparticles can deliver the active principle in a controlled way according to a zero order kinetics furthermore the amount of curcumin release was increased upon encapsulation

cluing the nanoparticles formulation act as an enhancer of transdermal release. The proposed nanoparticle system was therefore considered found to be meeting the requirements for dermatological formulations.

Overall, in the present part, it was proved that the FNP is a suitable method to produce PCL nanoparticles loaded with either hydrophilic and hydrophobic active principles. The hydrophilicity of the core substance was observed to impact the particle formation mechanism and, consequently to display different particle properties. For caffeine, the encapsulation was mainly ascribed to the Van der Walls interaction occurring between the amino groups in the caffeine molecule and the carbonyl groups in the polymer chain. Instead, curcumin encapsulation was connected to the hydrophobic drug precipitation together with the polymer upon the jet collision. The latter mechanism leads to finer particles and higher EE. Both the nanoparticle formulations displayed low particle size, effective antioxidant activity a controlled drug release kinetics. Therefore, nanoparticles with suitable properties for dermatological applications were obtained for both the investigated active principles. It was then considered of interest to employ such particles for the production of biofunctional textiles.

Part V The textile applications

Chapter 9. Textile applications of the caffeine and curcumin formulations

9.1 Scope of the study and experiments conducted

In the previous chapters, it was proved that the flash nanoprecipitation is a suitable technique for the preparation of PCL nanoparticles loaded with both hydrophilic and hydrophobic substances. After studying the production of caffeine and curcumin loaded PCL nanoparticles, the application of the carriers to the cotton fabrics was investigated.

The scope of the present research is to test the effectiveness of a finishing treatment for the proposed NPs systems and to evaluate the biofunctional properties that such a finish imparts to the cotton fabrics.

As far as the methodology to apply the carrier to the textile was concerned, several options have been considered on the base of the literature and the preliminary results obtained with the melatonin functionalized fabrics. Conventionally, resin finishing or chemical grafting of the carrier onto the fibers have been proposed for the preparation of biofunctional textiles. The rationality of such an approach is to achieve high fastness and durability of the capsule treatment. However, achieving high fastness is neither a priority nor a very desirable condition for the present application, indeed, a strong bonding between the particles and the textile hinders carrier detachment and therefore drug release.

On the contrary, the scope is to have weak interaction between the textiles and the particles so that the latter could be released to the skin. Considering also that resin treatments or chemical grafting are more complex and potentially harmful, they were excluded. Recalling the results discussed in Chapter 6 it was evidenced that the imbibition method was effective in achieving the functionalization of the textile and drug release in the in vitro Franz cell test. However, some improvements to this approach were investigated.

Indeed, it was observed that, upon spreading on the fabric, the particles tended in some cases to aggregate forming a polymer film. For this reason, the proposed finishing treatment consists of a cold impregnation followed by rinsing. Such a method takes inspiration from the layer by layer deposition with the variation of applying a single layer of nanoparticles. Indeed, the LbL deposition presents the advantage of depositing monolayers of the finishing agent of textiles, the interaction among the two species are electrostatic forces and the amount of finish deposited is self-limiting. Therefore, the proposed method was proposed to deposit a uniform single layer while keeping the interactions

between NPs and textile substrates weak so that the particles can be released. Furthermore, the impregnation is easier than the imbibition process to implement in the production line.

If effective, the proposed functionalization may open the possibility of developing easily rechargeable biofunctional textiles, thus making this technology more easily available to consumers. Therefore, such a finishing approach was tested with the carriers loaded with the two different active principles assessing the performances of the system for both hydrophilic and hydrophobic substances.

To achieve this goal, it was firstly verified if the proposed finishing permits an effective functionalization of the fabrics. Thereafter the variations in the physical-chemical properties of the functionalized fabrics respect to the pristine ones were assessed. Finally, the biofunctional properties of the functionalized fabrics were investigated with particular focus on the protection from UV rays and the antioxidant activity. Regarding the Franz cell release test, it was conducted using excised porcine skin with the scope of obtaining more realistic information about the performances of the proposed material in a biological environment. The details regarding the specific experiments conducted are reported in the next paragraphs.

9.1.1 Biofunctional textile preparation

Pure cotton, plain woven (110 g/m^2) was used. Freshly produced drug loaded PCL nanoparticles suspensions were used. Caffeine and curcumin NPs were prepared according to the protocol described in Chapters 7 and Chapter 8 respectively; formulations PCL_6CAF_9W and $PCL_{10}CUR_4$ were used. The properties of the nanoparticles formulation used for the textiles finishing are recalled in Table 9.1.

Table 9.1. Properties of the NPs formulation used for textile finishing.

Sample	Size (nm)	MR	LC (%)	EE (%)	Zp (mV)
PCL_6CAF_9W	307.8	1.5	24.0	21.6	-28.8
$PCL_{10}CUR_4$	237.9	0.4	28.5	99.9	-28.9

Several NPs batches were produced and mixed in a single beaker to obtain 50 mL of nanosuspension. The fabric samples were dipped in the suspension for 10 seconds so that the cotton fabric was

completely soaked. Thereafter, the fabric samples were removed from the beaker and briefly rinsed with deionized water. The samples were dried overnight in a laboratory oven under ventilation at 35°C.

9.1.2 Characterization of textile materials

The functionalized fabrics were characterized by several techniques to verify if the proposed treatment allows effectively to attach the particles on the fabric surfaces. ATR-FTIR analysis was run on the fabric to observe the presence of NPs on the cotton fibers and to investigate the chemical interactions between the fabric and the carriers.

The amount of drugs incorporated in the functionalized fabrics was assessed by the following extraction protocols. Briefly, the fabric pieces with 2.6 cm^2 we kept under magnetic stirring for 24 hours in a proper solvent (water for caffeine and ethanol for curcumin). Thereafter the amount of drug in the solvent was analyzed by spectrophotometry for caffeine and by spectrofluorometry for curcumin, thus providing information on the quantity of drugs that was incorporated in the fabrics. Colorimetric analysis was performed to inquire about the effectiveness of the nanoparticle treatment, its evenness and repeatability.

The fabric morphology was analyzed by SEM to investigate the distribution of the particles of the NPs onto the cotton fibers. The samples were prepared by mounting the fabric pieces on aluminum stubs using carbon tape. The prepared samples where metalized by sputter coating with chromium before analysis with a cold field emission SEM Hitachi S4800 (USA) with an acceleration voltage of 3 kV.

To inquire about the modification of cotton surface properties Zeta potential and contact angle analyses were conducted. The surface zeta potential of the fabric samples was measured to inquire about changes in the textile surface charge due to electrostatic interactions between cotton and the nanoparticle surfaces. The streaming potential method was used for Zp analysis. Water contact angle analysis was run to test potential modification in cotton hydrophilicity. The sessile drop method was used.

9.1.3 Assessment of textile biofunctional properties

The biofunctional properties of the functionalized fabrics were studied in terms of antioxidant activity, UV protection factor and skin permeation test. The UV protection properties were

investigated by collecting the UV transmittance spectra of the fabric, the UPF was then calculated according to Equation 3.7.

For the antioxidant activity test, the EPR/spin trapping method proposed for the nanoparticles was adapted for the study of the textile samples. For the analysis, the free radicals were generated using the reactions previously described for the investigation of caffeine and curcumin antioxidant properties. The pieces of functionalized fabric, with an area between 1.5 and 2 cm^2 were added in the Eppendorf tube and homogenized with the reactive mixture. The solution was then placed into the EPR capillary tube for analysis.

The skin permeation tests were performed on a double ported Franz diffusion cell to understand the interaction of the biofunctional textiles with skin. In the donor compartment, a disk of functionalized cotton was placed over the skin membrane. The disk has the same diameter of the membrane (2.6 cm^2), a drop of PBS solution was poured on the donor compartment to assure the contact between the textile and the membrane. The skin mimicking membrane consisted of excised pig ear skin. The skin slices were isolated with a dermatome from the outer side of pig ears, obtained from a local butcher, and were then frozen at -18 °C. Before starting the permeation experiment, the skin membrane was immersed for 30 minutes in NaCl 0.9% w/w saline solution, in the presence of 0.01% sodium azide to preserve skin integrity throughout the test. After equilibration, the skin layers were washed in a saline solution and placed between the two Franz cell compartments with the stratum corneum facing the donor compartment.

The acceptor fluid composition changed depending on the tested drug: PBS was used for caffeine while, for curcumin analysis, 10% v/v of ethanol was added to the phosphate buffer solution to prevent drug saturation in the acceptor fluid. The release kinetics was monitored until the equilibrium was observed to be reached. The receiving phase was withdrawn at regular times and replaced with the same amount of fresh receiving medium. The collected liquid receptor samples were then analyzed by spectrophotometry in the case of caffeine and by spectrofluorometry in the case of curcumin.

9.2 Effectiveness of the finishing treatment

To assess whether the drug loaded nanoparticles had been successfully applied onto the fabrics the ATR-FTIR spectra were collected. The spectra of cotton fabric functionalized with caffeine loaded NPs, pristine cotton and caffeine loaded NPs are shown in Figure 9.1 while the characteristic absorption bands are reported in Table 9.2.

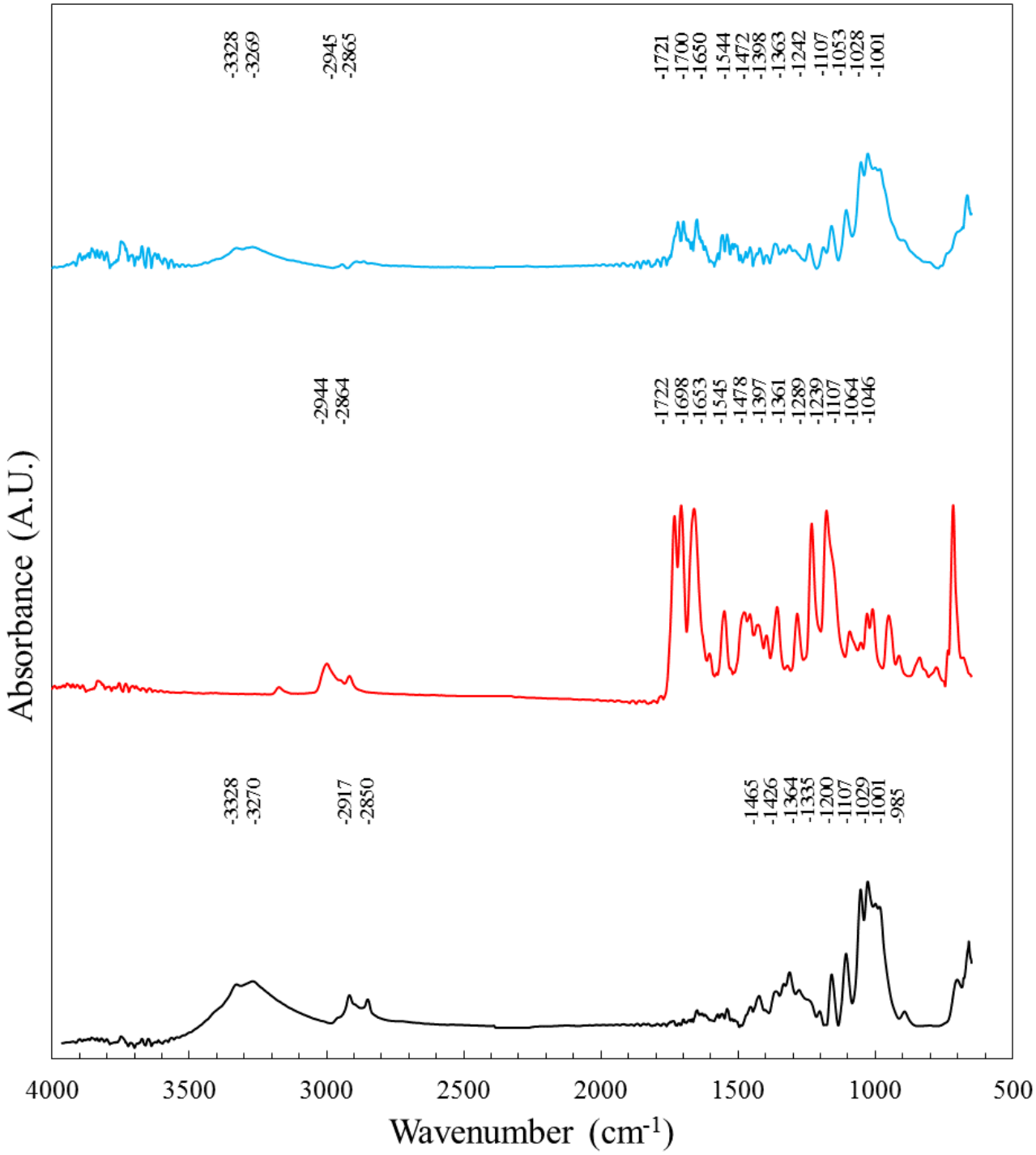

Figure 9. 1. ATR-FTIR spectra of cotton (black) PCL_6CAF_9W (red) and COT- PCL_6CAF_9W (blue).

Table 9.2. Characteristic IR absorption bands for cotton PCL_6CAF_9W and COT- PCL_6CAF_9W.

Wavenumber (cm^{-1})			Attribution
Cotton	**PCL_6CAF_9W**	**COT- PCL_6CAF_9W**	
3328, 3270	-	3328, 3269	Streching O-H group
2917,2850	2944, 2864	2945, 2865	C-H stretching vibrations
-	1722, 1698	1721, 1700	C=O stretching vibration
	1653, 1545	1650, 1544	C=N stretching vibrations
	1478, 1456, 1429	1472, 1455, 1431	C=C stretching vibrations
1465, 1426, 1364, 1335, 1314, 1280, 1200, 1158	-	1472, 1423, 1363, 1335, 1315, 1160	Bending of O-H group
	1397, 1361	1398, 1363	Bending vibrations of C-H
	1361, 1289, 1239	1363, 1242	C-N stretching vibrations
1107, 1054, 1029, 1001, 985	1289, 1239, 1107, 1064, 1046	1107, 1053, 1028, 1001	Stretching vibrations of C-O

The cotton IR spectrum is characterized by a broad absorption band with peaks at 3270, 3328 cm^{-1} due to the stretching vibration of the hydroxyl groups. Two low intensity peaks were observed at 2917, 2850 cm^{-1} and attributed to stretching vibrations of the C-H bond. A series of low intensity peaks were observed between 1500 and 1150 cm^{-1}. This zone is characterized by the signals connected to the bending vibrations of the O-H bond which were found precisely at 1465, 1426, 1364, 1335, 1314, 1280, 1200, 1158 cm^{-1}. Several sharp peaks were observed in the lower spectral region at 1107, 1054, 1029, 1001, 985 cm^{-1}. These signals were attributed to the stretching vibration of the C-O bond.

The caffeine loaded nanoparticles spectrum exhibited two medium peaks at 2944, 2864 cm^{-1} attributed to the stretching vibrations of the C-H bonds. Four strong peaks were observed at 1722, 1698, 1653, 1545 cm^{-1}; the first two were ascribed to the stretching of the C=O bond while the other to the stretching of the C=N bond. The signals due to the C=C stretching vibrations were observed at 1478, 1456, 1429 cm^{-1}; while the peaks connected to the C-H bending were found at 1397, 1361 cm^{-1}. Three sharp peaks were observed at 1361, 1289, 1239 cm^{-1} and attributed to the stretching of the C-N bond. Finally, several peaks connected to the stretching of the C-O bonds were found at 1289, 1239, 1107, 1064, 1046 cm^{-1}.

The functionalized fabrics displayed a spectrum similar to the one of the pristine cotton. Indeed, it showed the peaks connected to i) the stretching vibrations of the O-H bond between 3300 and 3000 cm^{-1}, ii) the C-H stretching between 3000 and 2800 cm^{-1}, iii) the O-H bending between 1500 and 1100 cm^{-1} and iv) the C-O stretching between 1100 and 900 cm^{-1}. Moreover, it is possible to observe the presence of some of the characteristic peaks of the nanoparticle formulations. Indeed, the absorption bands of the C=O stretching were found at 1721 and 1700, as well as the ones of the C=N stretching, observed at 1650 and 1544 cm^{-1}. Furthermore, the peaks ascribed to the C=C stretching were present at 1472, 1455 and 1431 cm^{-1}; similarly, a series of peaks connected to stretching of C-N bond was observed at 1363 and 1242 cm^{-1}.

The observation of the characteristic peaks of the PCL_6CAF_9W formulation proves the presence of the caffeine loaded nanoparticles onto the textile surface. Overall the nanoparticles peaks were not shifted or underwent only minor shifts. Thus, it is concluded that the particles were not chemically bonded to the textiles and that the two materials interacted by weak interactions such as Van der Waals force and Hydrogen bonding.

The infrared spectra of cotton fabric functionalized with curcumin loaded NPs, pristine cotton and curcumin loaded NPs are shown in Figure 9.2 while the characteristic absorption bands are reported in Table 9.3. The pristine cotton spectrum displays the previously described absorption bands.

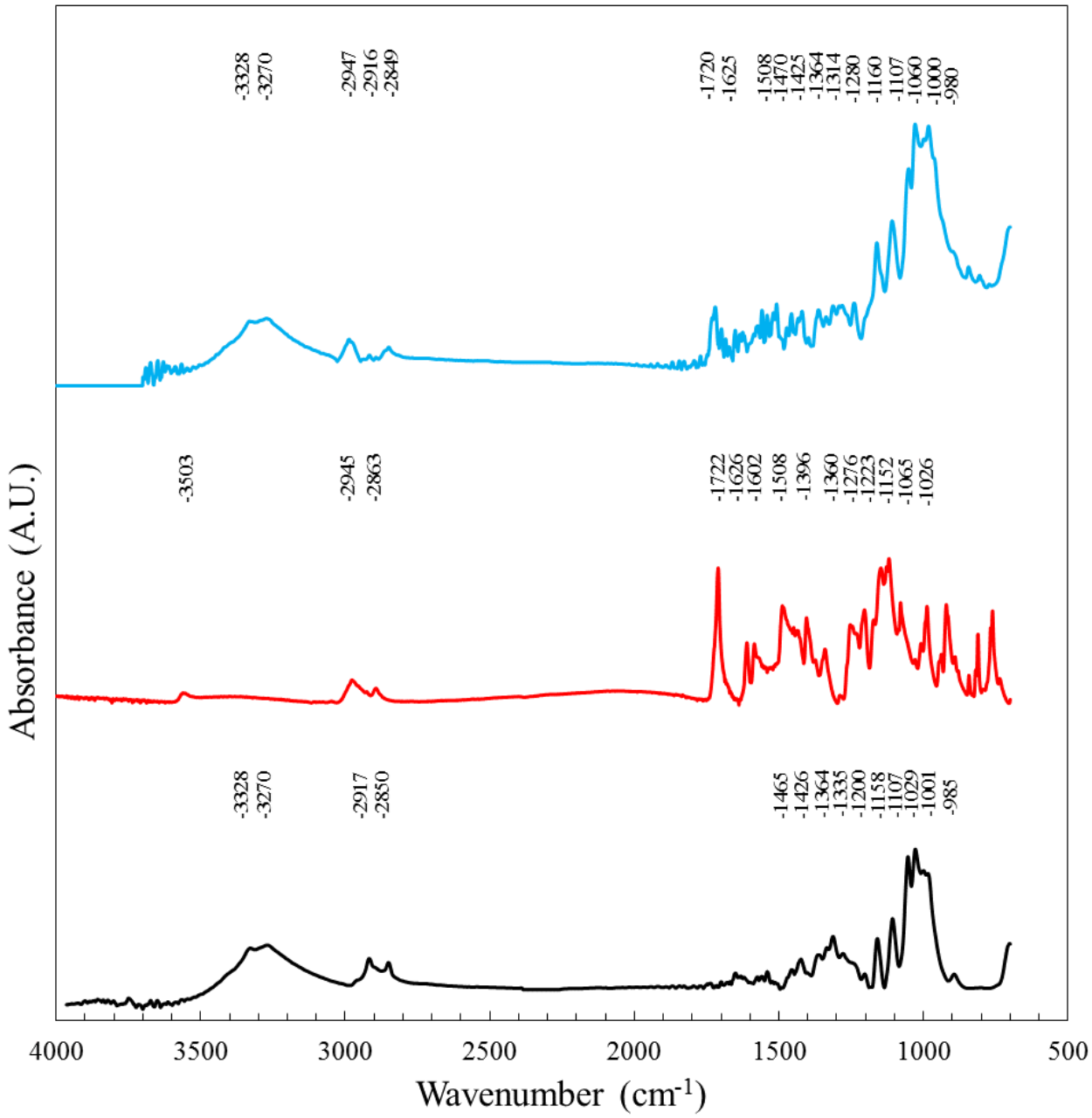

Figure 9. 2. ATR-FTIR spectra of Cotton (black) $PCL_{10}CUR_4$ (red) COT- $PCL_{10}CUR_4$ (blue).

Table 9. 3. Characteristic IR absorption bands of cotton, $PCL_{10}CUR_4$, COT- $PCL_{10}CUR_4$.

Wavenumber (cm^{-1})			Attribution
Cotton	**$PCL_{10}CUR_4$**	**COT- $PCL_{10}CUR_4$**	
3328, 3270	3503	3330, 3270	O-H stretching vibrations
2917,2850	2945, 2863	2947, 2916, 2849	C-H stretching vibrations
	1722, 1626	1720, 1625	Stretching vibrations of C=O
	1602, 1508, 1456	1508, 1457	Stretching vibration C=C aromatic
1465, 1426, 1364, 1335, 1314, 1280, 1200, 1158	-	1470, 1425, 1364, 1336, 1314, 1280, 1160	Bending of O-H group
	1472, 1427, 1396, 1366	1470, 1425, 1396, 1364	Bending vibrations of C-H
1107, 1054, 1029, 1001, 985	1276, 1232, 1152, 1113, 1065, 1045, 1026	1280, 1239, 1160, 1060, 1051, 1030, 1000, 980	Stretching vibrations of C-O

The infrared spectrum of the $PCL_{10}CUR_4$ formulation displays a weak absorption peak at 3503 cm^{-1} ascribed to the stretching vibrations of the O-H bond. Two medium intensity peaks were observed at 2945 and 2863 cm^{-1} and correlated to the stretching vibrations of the C-H bonds in the PCL polymer chain. Two strong absorbance peaks of C=O stretching were observed at 1722 and 1626 cm^{-1}. The peaks at 1602, 1508, and 1456 cm^{-1} were associated to the C=C double bonds in aromatic rings. The peaks connected to the bending vibration of the C-H were observed at 1472, 1427, 1396, 1366 cm^{-1}.

Several signals connected to the stretching vibration of the C-O were found in the region between 1300 and 1000 cm^{-1}; more precisely at 1276, 1232, 1152, 1065, 1113 1026, 1045, 1026 cm^{-1}.

Analogously to caffeine treated textiles, the COT- $PCL_{10}CUR_4$ sample shows a similar spectrum to the one of the pristine cotton. It was possible to identify the well-known absorptions bands of cotton fabrics. Furthermore, some of the characteristic peaks of the $PCL_{10}CUR_4$ nanoparticle formulation were observed. Two absorption peaks were found at stretching were found at 1720 and 1625 cm^{-1}; the first one was connected to the stretching of C=O in the polyester chain of PCL, while the second one was attributed to the C=O stretching in the curcumin keto-enol groups. Furtherly, two peaks due to the C=C stretching in the curcumin aromatic rings were found at 1508 and 1457 cm^{-1}.

The presence of these signals connected to the NPs chemical structure shows that the proposed finishing treatment allows to effectively apply the curcumin loaded nanoparticles onto the cotton surface. Moreover, the absence of significant shifts in the particle peaks position indicates a weak interaction between the particles and textiles. This is the desired situation to effectively deliver the drug.

Infrared analysis qualitatively proved the presence of NPs on to the cotton fabrics. To obtain quantitative information about the amount of drug loaded onto the fabrics, the samples underwent extraction of the active principle and spectroscopic quantification. Such analysis revealed that in the sample COT-PCL_6CAF_9W the amount of loaded drug was 0.29 mg/cm^2; while on sample COT-$PCL_{10}CUR_4$, the quantity of curcumin was of 0.52 mg/cm^2. The fact that for curcumin higher drug amounts were loaded on the fabrics is consistent with the formulation properties. Indeed, the curcumin nanoparticles formulations had a lower diameter than the caffeine one. This characteristic eased the interaction of the particles with the fabric surface. Indeed, as reported in Chapter 6 particles with smaller sizes tend to be more easily incorporated in the cotton fibrous system. Furtherly the curcumin nanoparticles display higher drug loading with respect to the caffeine. This furtherly explains why more drug was found in the COT-$PCL_{10}CUR_4$ sample respect to the COT-PCL_6CAF_9W one.

The functionalized textiles were also investigated by colorimetric analysis to investigate modifications in the fabric color intensity and the evenness of the treatment. The color intensity values are plotted for different wavelengths in Figure 9.3. Only samples treated with curcumin or curcumin loaded NP are presented since other samples exhibited null K/S values for the inquired wavelengths. Indeed, it was well expected since both caffeine and PCL do not absorb light in the visible range.

The cotton fabrics show a K/S peak at 440 nm and the spectrum shape is not changed upon drug encapsulation. The maximum color intensity value is higher for the samples functionalized with a free curcumin solution (K/S = 6.8) rather than for curcumin loaded nanoparticles (K/S=2.3). The fact that the COT-$PCL_{10}CUR_4$ sample displayed lower color intensity was an expected result considering that the colored substance was incorporated inside the polymeric NPs structure. It is worth to notice that the color intensity upon encapsulation is about 30% with respect to the one of the free drug. Such a value is similar to the LC of the particles (28.5%). Therefore, it was concluded that the incorporation leads to a reduction of color intensity; the extent of this color reduction is consistent with the amount of dye loaded in particles.

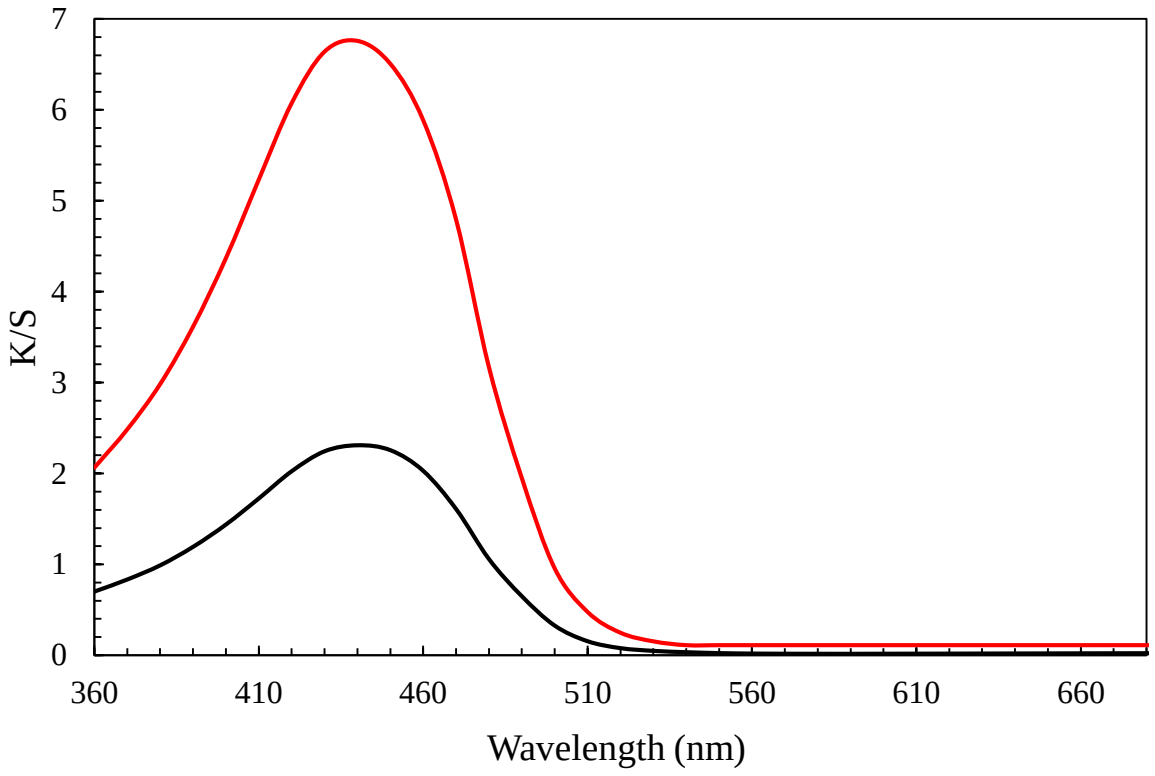

Figure 9.3. Color strength values for different wavelengths for cotton fabrics treated with free curcumin (red curve) and curcumin loaded nanoparticles (black curve).

The colorimetric analysis was also employed to assess whether the proposed finishing treatment guarantees replicable results by investigating the color uniformity over different samples. For this investigation, 18 fabric samples were treated. The collected spectra are reported in Figure 9.4.

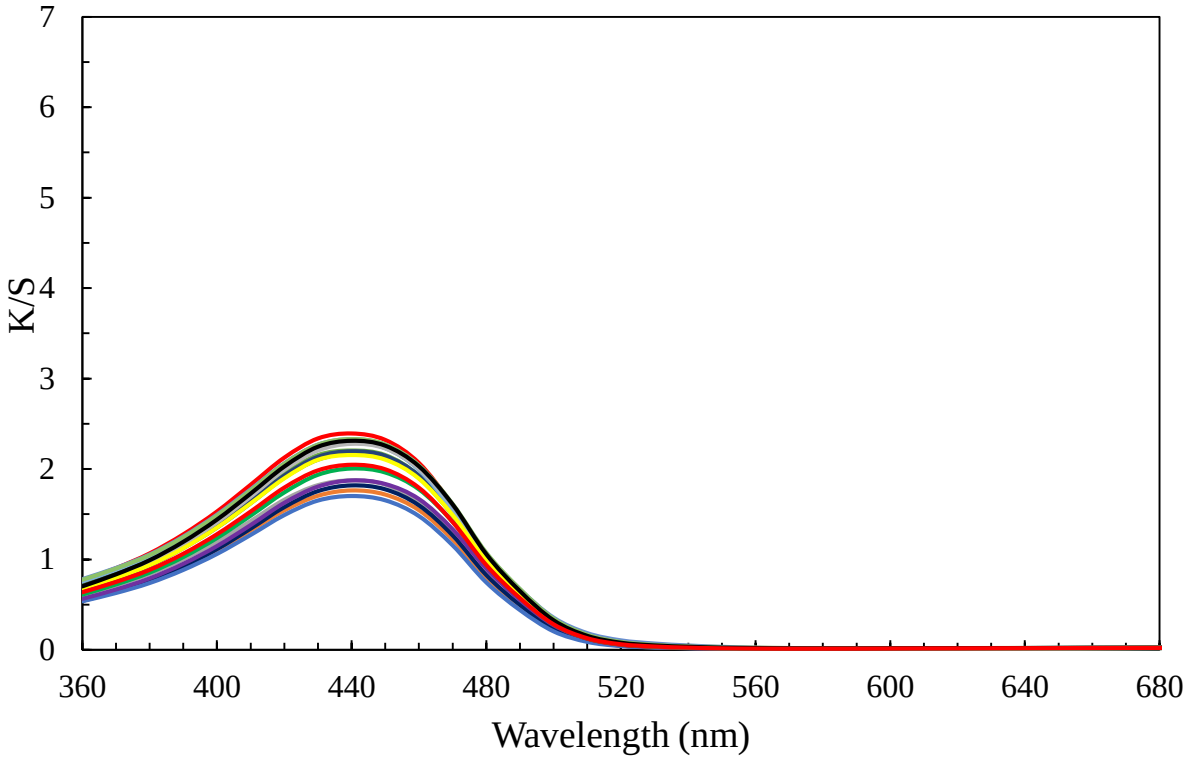

Figure 9.4. K/S values for 18 cotton fabrics functionalized with curcumin loaded nanoparticles.

It can be observed that all the collected spectra display the same shape. Furthermore, the maximum color intensity values were found to be very narrow; indeed, the average K/S values at 440 nm was found to be of 2.15 with a standard deviation of 0.24. From these observations, it can be concluded that similar amounts of curcumin loaded NP were deposited on each textile sample. Therefore, the proposed finishing method displays good replicability in terms of the amount of NPs deposited.

To investigate how the nanoparticles are distributed on the fabric surface at the microscopic scale, the samples were observed by scanning electron microscope. The SEM images of cotton fabrics treated with the PCL nanoparticles suspensions are shown in Figure 9.5. By observing the samples at low magnification, the NPs seem to form a uniform film on the cotton fabrics and the particle shape is barely observable. Oppositely, observing fibers at higher magnification (Figure 9.5 bottom), uniformly distributed particles are visible on the cotton surface. It is noticed that on the outer surface of the fabrics the particles collapsed and aggregated into a polymer film. Oppositely, in the inner part of the fibers, particles are less aggregated and more uniformly distributed over the textile surface. These morphologies show that upon penetrating inside the cotton fiber core, the particles are more effectively supported and protected by the textile material and thus, they can effectively maintain their spherical structure.

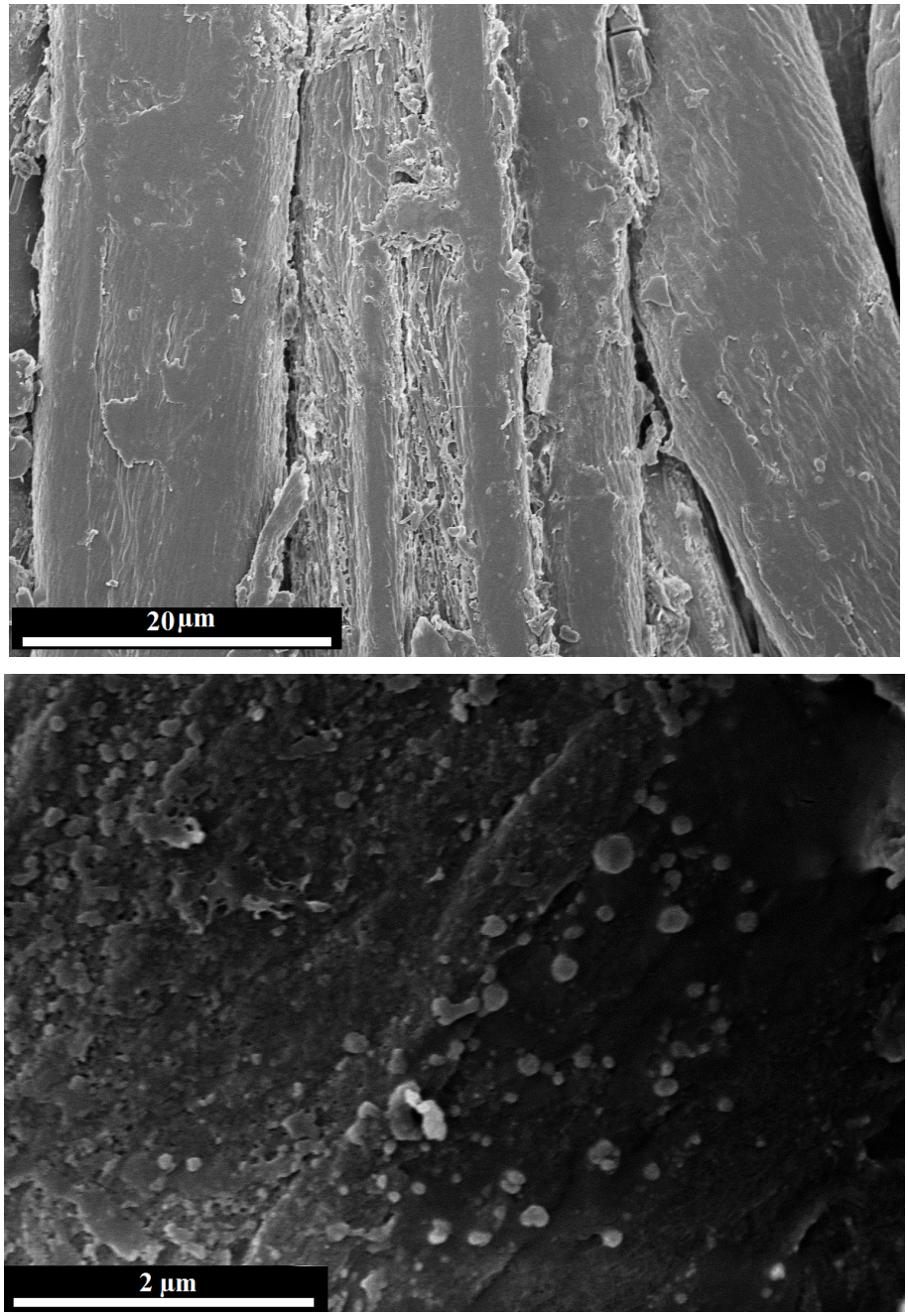

Figure 9.5. SEM images of cotton fabrics treated with unloaded PCL nanoparticles at 2000 X magnification (top picture) and 20000X magnification (bottom picture).

The SEM images of the fabrics functionalized with caffeine loaded nanoparticles are reported in Figure 9.6. Observing the fabric morphology at 300 X magnification the presence of the nanoparticles on the textiles is noticeable. The particles tend to be agglomerated in big clusters, however, also some not aggregated particles are observable. By observing the same sample at 5000 X magnification insights about the distribution of the nanoparticles on the fiber can be obtained.

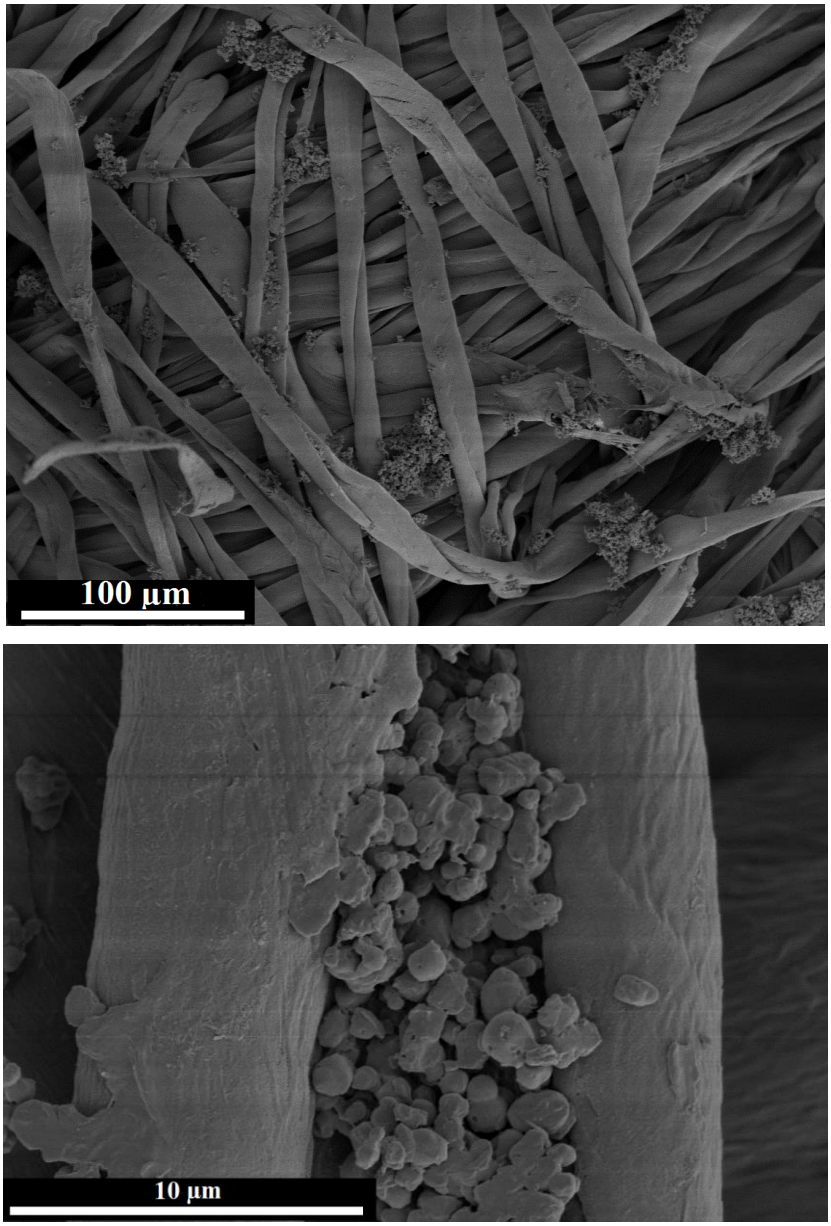

Figure 9.6. SEM images of cotton fabrics treated with caffeine loaded PCL nanoparticles at a magnification of 300 X (top image) and 5000 X (bottom image).

The particles are shown to be mostly incorporated inside the in the interior part of the kidney-bean shaped structure typical of the cotton fabric. The observed morphology was ascribed to the nanometric particle size which leads to easy diffusion of the particles inside the inner part of the cotton fiber structure.

The morphology of the fabrics functionalized with curcumin loaded nanoparticles is displayed in Figure 9.7.

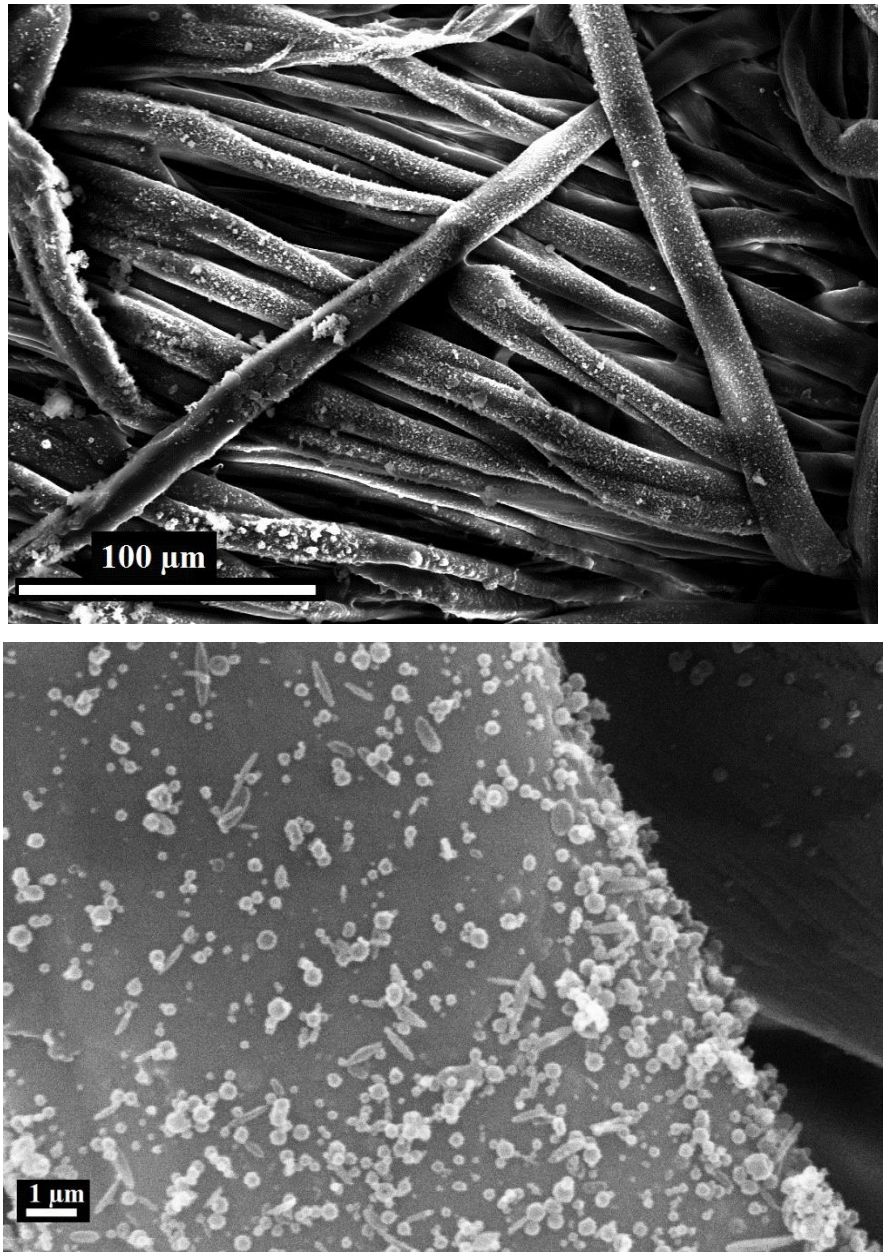

Figure 9.7. SEM images of cotton fabrics treated with curcumin loaded PCL nanoparticles at a magnification of 500 X (top image) and 10000 X (bottom image).

A broad overlook of the sample morphology is observable in the 500 X picture (top image). It can be observed that the sample appears to be fully covered with nanoparticles. The latter are uniformly distributed over the fabric surface and have maintained their original shape, although some particle aggregates are still noticeable in some areas of the samples. Observing a single fiber at higher magnification (bottom picture 10000 X) the nanoparticles are evenly distributed on the fabric surface without significant aggregation. The observed particles exhibit diameters consistent with the ones measured by dynamic light scattering (i.e. 230 nm), it can be therefore concluded that aggregation phenomena occurring during NPs drying were significantly limited in this case. The cotton fibers

acted as very effective support for the nanoparticles which prevented excessive aggregation. The reason why less aggregated morphologies were observed in the curcumin based textiles can be ascribed to the exceptional colloidal stability observed for the curcumin loaded samples.

The SEM analysis highlighted that, upon functionalization with the drug loaded nanoparticles, the fabric samples display different morphologies depending on the employed active principle. The COT-$PCL_{10}CUR_4$ sample exhibited a uniform coverage of a single layer of well-dispersed particles on the fiber surfaces. On the contrary, the sample COT-PCL_6CAF_9W showed the particles to be majorly aggregated in clusters and to be preferentially hosted inside the bean shaped core of the cotton fabrics.

The two different morphologies of the textiles functionalized with the nanoparticles were connected to the physical chemical properties of the NPs formulation and to the nature of the encapsulated drug. The SEM images of the two nanoparticle formulation and of the textile samples functionalized with them are reported for comparison in Figure 9.8.

For the formulation containing the hydrophilic substance, it has to be considered that that some drug was found to be partially incorporated inside the PCL matrix and partially adsorbed on the outer surface of the particle structure. Thus the surface of the PCL_6CAF_9W formulation is expected to be more hydrophilic than the one of the $PCL_{10}CUR_4$ formulation. The hydrophilic surface favored the interaction of the particles with hydrophilic fabric promoting its accumulation in the fiber core. Oppositely the less affine $PCL_{10}CUR_4$ formulation was found to mainly interact with the outer part of the fibers without accumulating in the core.

The formulation $PCL_{10}CUR_4$ displayed great colloidal stability and as proved by the SEM imaging, it was found to not undergo agglomeration during drying. This good stability was observed to be kept during the finishing process leading to a uniform coverage of the fabrics by the nanoparticles. On the contrary, the PCL_6CAF_9W nanoparticles formulation was observed to form agglomerates, similar nanoparticle assemblies were found on the treated textile leading to less uniform coverage respect to the one observed for the curcumin treated sample.

In both cases, similar morphologies and extent of agglomeration were observed for the particle formulation and the treated textiles. This finding shows that the morphology of the NPs treated textiles is correlated to the properties of the particle formulation used as finishing agents.

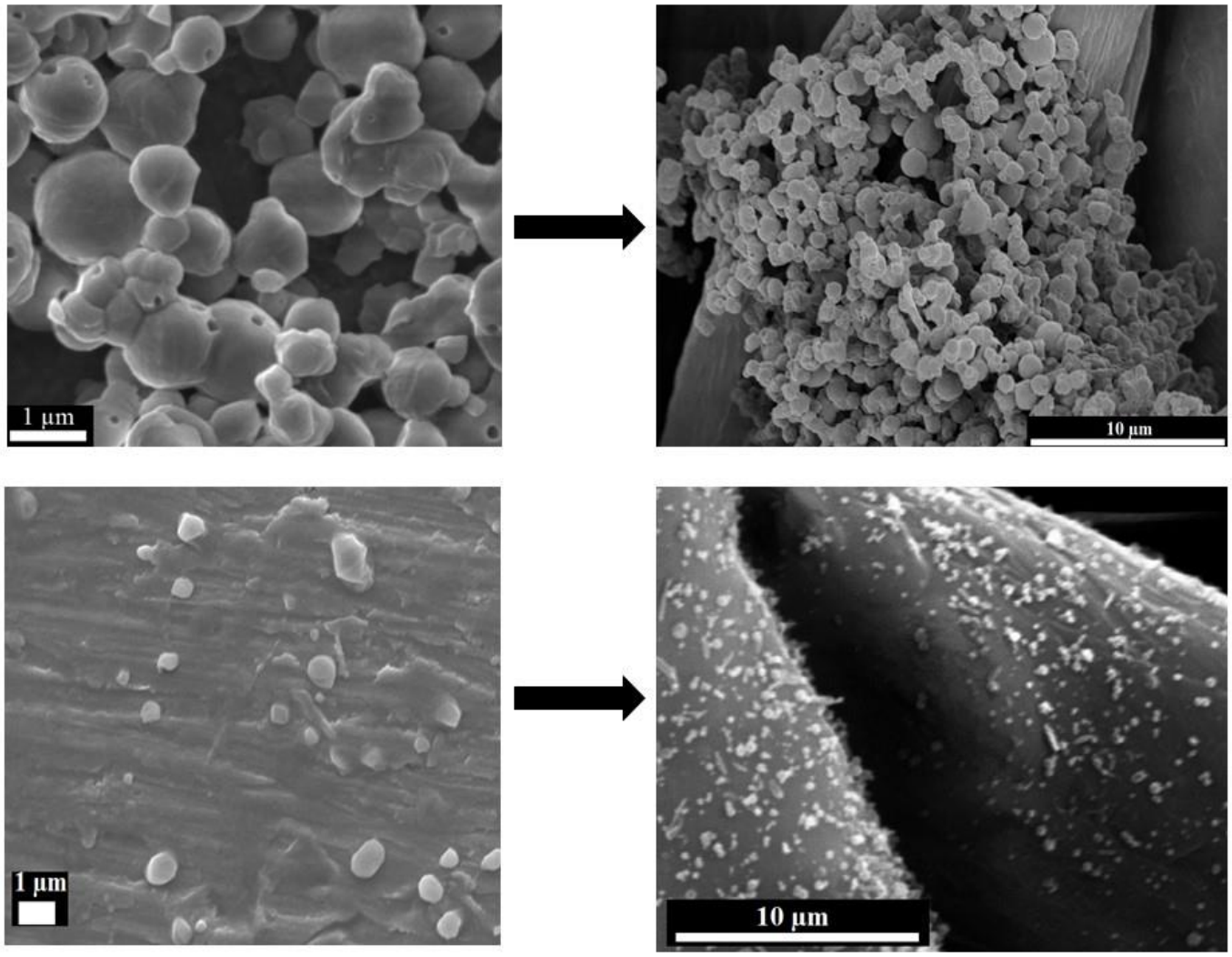

Figure 9.8. Comparison of the morphologies of the nanoparticles samples with the ones of the functionalized textiles. Samples: caffeine loaded NP (top left 10000X), cotton functionalized with caffeine loaded NPs (top right 4000X) curcumin loaded NP (bottom left 50

9.3 Effects of the finishing on the properties of the fabrics

Having proved the effectiveness of the finishing treatment, it was investigated whether the application of NPs does affect the textile surface properties. For this purpose, the contact angle and surface zeta potentials were measured. The Zeta potentials of the textile samples were measured with the streaming potential method to gain information about the surface charge of the fabric before and after the finishing treatment, the results of the analysis are plotted in Figure 9.9.

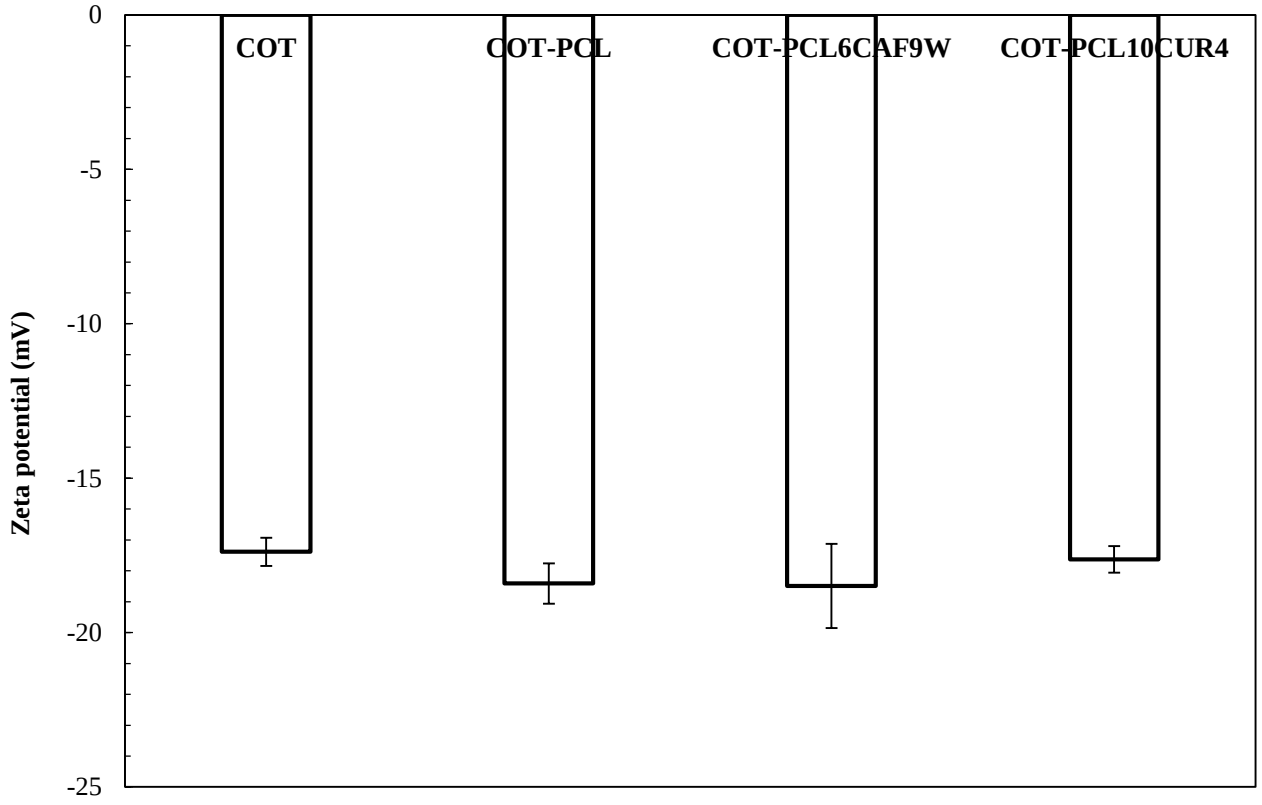

Figure 9.9. Surface Zeta potential of the textiles with the nanoparticles.

It can be observed that the application of the PCL nanoparticles made the surface zeta potential to be slightly more negative respect to the one of pristine cotton. Indeed, this average Zeta potential decrease can be ascribed to the fact that Zeta potential of the particles was measured to be lower than the one of the pristine cotton fabrics. Taking into account the standard deviations it can be observed that the changes in surface zeta potential are quite similar for the different finishing treatments. Furthermore, the ANOVA analysis evidenced that the changes in zeta potential are not statistically significant respect to the cotton control (p-value > 0.05).

The fact that the observed changes in zeta potential are not marked was explained considering that the nanoparticles are present only in small amounts onto the fabric surfaces Therefore, the proposed finishing does not induce significant changes in the surface charge of the textile.

The contact angle analysis was performed to verify if the finishes changed this surface property. Being cellulose a markedly hydrophilic material, plain cotton immediately adsorbed the water droplets, setting therefore a null contact angle. On the contrary, upon treatment with NPs formulation and drug solution, the water drop stuck to the textile surface for a few seconds before being absorbed.

The shape of the droplet onto the textile surface as soon as the two came in contact was used to perform the contact angle measurement, whose results are reported in Figure 9.10. It can be observed that, upon treatment with the free drug, the cotton displayed different contact angles depending on the drug applied.

For caffeine, the contact angle increase was negligible, indeed quite similar behavior to the pristine cotton was observed. Instead, upon the application of curcumin, the contact angle markedly increased. The coating with a hydrophobic substance like curcumin causes the contact angle to increase. Similarly, it can be observed that the sample treated with plain PCL nanoparticles (which is a hydrophobic polymer) undergo a marked increase of the contact angle.

For caffeine treated fabrics, both the effect of the drug and the polymers were observed. Indeed, the sample displayed an increase in the initial contact angle which can be ascribed to the hydrophobic PCL, however, such an increase is less marked with respect to pure PCL. Such behavior was connected to the presence of hydrophilic caffeine on the textile on the particles and the fabric surface. Thus, the presence of both hydrophilic and hydrophobic substances makes the initial contact angle to be lower with respect to the one of the pure PCL nanoparticles.

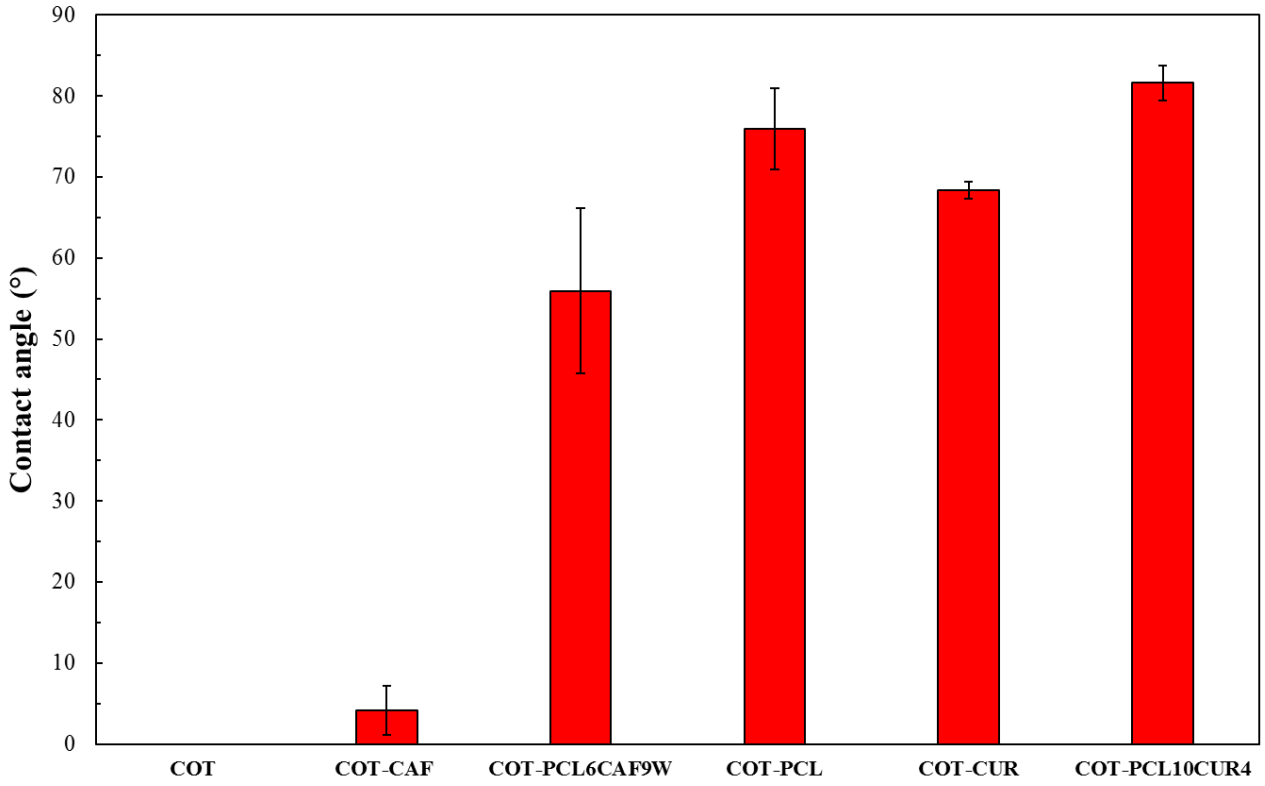

Figure 9.10. Contact angles for the textiles treated with free and encapsulated drugs and PCL nanoparticles.

Upon finishing with the curcumin loaded nanoparticles the highest contact angle was observed. This result was ascribed to the synergistic effects of the two hydrophobic substances used in the finishing. Moreover, the increase of the contact angle was correlated to the surface morphology of the functionalized fabric. Indeed, as shown in Figure 9.7, these sample shows a very uniform layer of nanoparticles on the fiber surface which makes the surface roughness increase. Therefore, the higher contact angle was also ascribed to the higher surface roughness, in accordance with the Cassie and Baxter theory (Seo et al., 2015).

Comparing the fabrics functionalized with the drug loaded nanoparticles formulations, it was observed that data collected for the sample COT-PCL_6CAF_9W are more dispersed respect to the sample COT-$PCL_{10}CUR_4$ ones. This fact may be correlated to the observed fabric morphologies in which curcumin loaded nanoparticles are present on the fabric as uniform coating while the caffeine loaded ones are mostly present as aggregated clusters. It is then reasonable that a more uniform coating has as a consequence more uniform results in the contact angle measurements.

To conclude, the contact angle analysis evidenced that the finishing treatment induces some modification in the textile surface properties but the fabrics remain hydrophilic as the lifetime of the water drops on the fabric is less than 10 seconds. This means that the surface treatment does not modify the hydrophilic nature of cotton but just hindered the water drop diffusion and immediate absorption by the fabric. The present section, therefore, proved that the application of the nanoparticles onto the textile surface does not significantly alter the properties of the pristine fabrics in terms of surface charge and hydrophilicity. These analyses proved that the NPs application does not compromise the appreciated properties of the cotton textiles in terms of handle and comfort.

9.4 Biofunctional characterization of the treated fabrics

The finishing treatment of cotton fabrics with drug loaded NPs lead to a successful application on the textile surface while not significantly altering the properties of the fabric. The biofunctional properties of the treated fabrics were studied to inquire whether and to what extent the proposed fabrics display beneficial effects to the user's skin.

9.4.1 Protection from UV radiations

UV radiation is considered one of the primary causes of damages to human skin, it is connected to an increase of oxidative stress, to skin aging and to arise of several skin diseases. To investigate the

capacity of the proposed fabrics to shield UV radiation, UV spectroscopy was employed in transmission mode. By observing the UV spectra in Figure 9.11, it can be observed that pristine cotton fabrics display low transmission values for wavelengths lower than 300 nm. Such behavior is ascribed to cellulose chemical structure which brings several hydroxyl groups which are known to absorb in the low UVB region. The application of unloaded PCL nanoparticles does not cause significant changes in the transmission values in the low UV region. However, for wavelengths higher than 300 nm the transmittance values are significantly decreased of about 5%. Considering that PCL does not absorb light in this spectral region, this may be connected to the filling of the woven porous structure by the particles which hinder the UV ray transmission or to the absorption of the light by the NP system due to Tyndall effect (Heller et al., 1946).

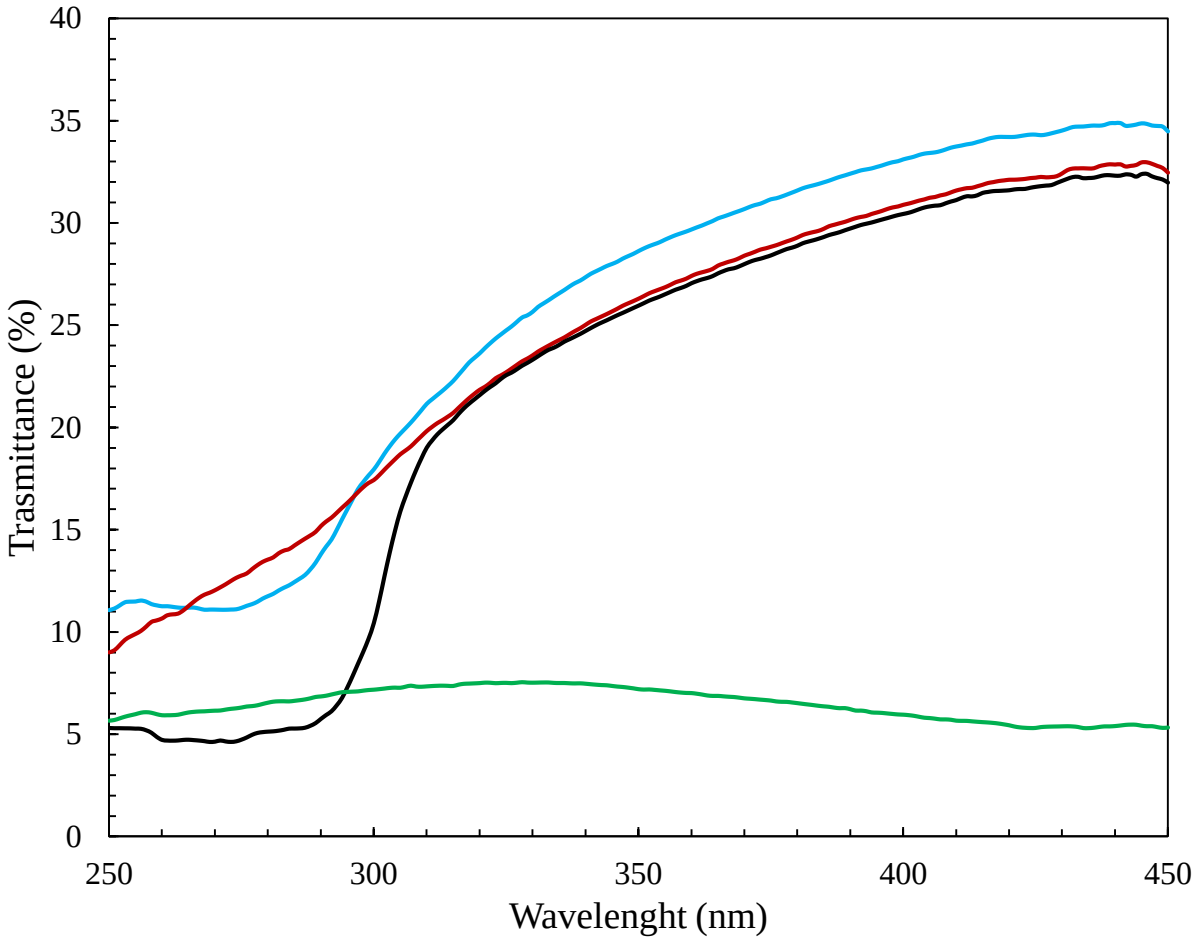

Figure 9.11. UV transmission spectra of cotton fabrics treated with different carriers: pristine cotton (blue curve), unloaded PCL nanoparticles (red curve), caffeine loaded nanoparticles (black curve) and curcumin loaded nanoparticles (green curve).

The spectrum of the COT-PCL_6CAF_9W sample is similar to the one of pure PCL for wavelengths higher than 300 nm. In the UVB regions, instead, the transmittance values are significantly decreased, staying below 5%. Such a result is not surprising as caffeine absorptions peaks are in the UVB region,

specifically around 273 nm: the marked light absorption causes the transmission values to be decreased respect the other samples. The spectra of the COT-$PCL_{10}CUR_4$ sample displayed the lowest transmission values for higher wavelengths (UVA) and similar values to the ones of caffeine in the UVB region. The collected transmission spectrum is consistent with the fact that the curcumin molecule is a chromophore, therefore it absorbs light at wavelengths above 400 nm, as it was also proven by the K/S measurement. The tails of the strong absorption peaks in the visible range cause the material to effectively absorb UV light making the transmittance values to be reduced.

From the transmission spectra, the UV protection factor values were calculated by applying Equation 3.7. The UPF values of the different samples are plotted in Figure 9.12. The cotton fabric used as control displayed a 4.8 UPF value. The functionalization with unloaded PCL nanoparticles had average UPF values of 5.1, however, such an increase was not statistically significant (p-value >0.05). On the contrary, caffeine functionalized samples displayed a statistically significant increase of the UPF (p-value<0.05) which can be attributed to the decreased values of UV transmittance observed both in the UVA and UVB regions respect to pristine cotton. The functionalization with curcumin loaded nanoparticles almost triplicated the UV protection factor respect to control.

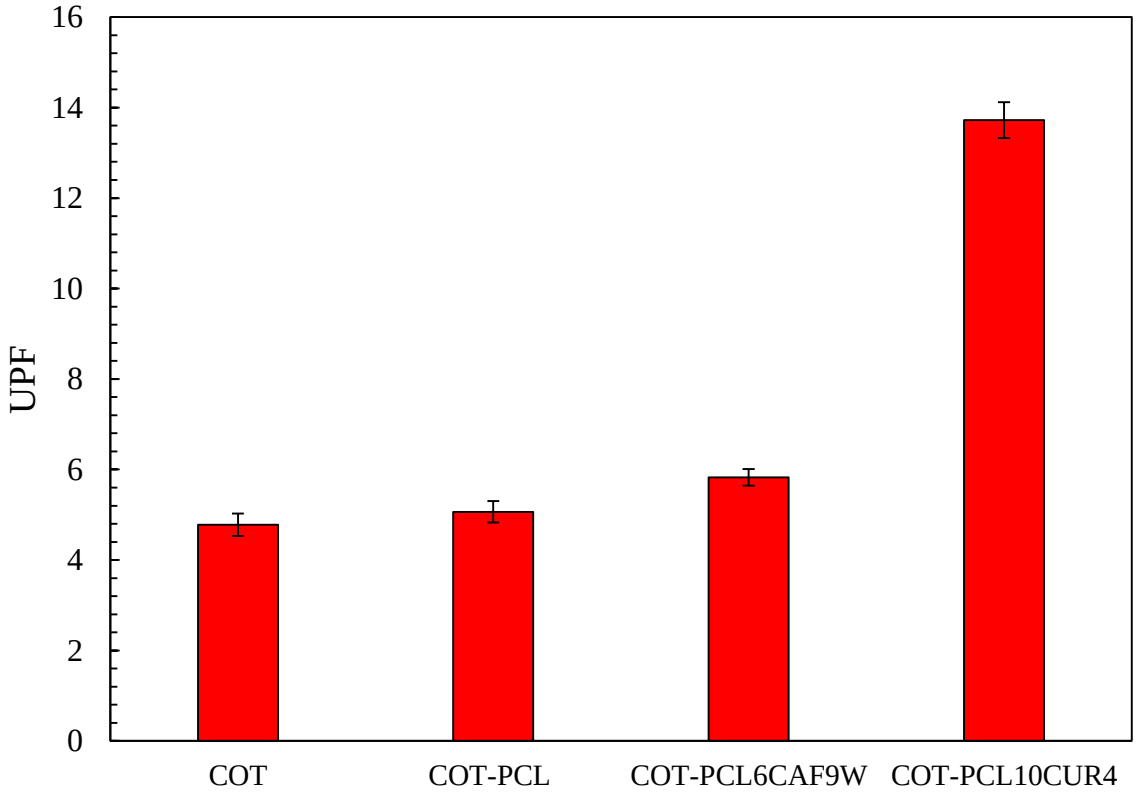

Figure 9.12. UV protection factors of the fabrics functionalized with loaded and unloaded PCL nanoparticles.

Comparing the UPF values of the textiles functionalized with drug loaded nanoparticles it can be observed that curcumin is more effective in blocking UV rays all over the spectral range. However, it should be also taken into account that caffeine treated textiles display better absorption at the lowest wavelengths, which are indeed more energetic and therefore more harmful radiations. In both cases, it was proven that the finishing treatment imparted to the fabrics UV shielding properties.

9.4.2 Antioxidant activity

The biofunctional textiles were characterized in terms of antioxidant activity by employing similar methodologies to the ones presented in Chapters 7 and 8 to evaluate the antioxidant properties of the nanoparticle formulations. The EPR-Spin trapping method, widely employed to characterize colloidal suspensions, was for the first time adapted to the analysis of textile materials. The results of the EPR analyses conducted on the fabrics treated with caffeine loaded nanoparticles are reported in Figure 9.13.

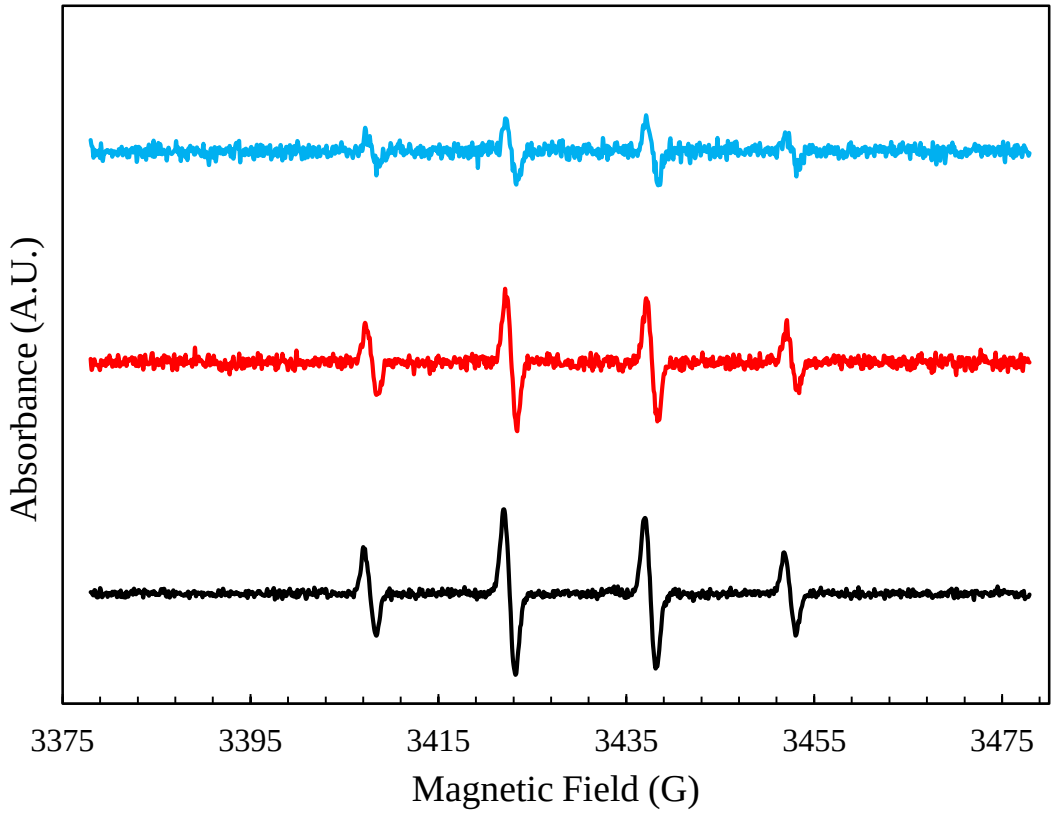

Figure 9.13. EPR spectra of the spin trap DMPO collected in presence of the different samples: control (black curve) cotton (red curve) and cotton functionalized with caffeine loaded nanoparticles (blue curve).

The control spectrum is characterized by four signals in antiphase in the region between 3400 and 3460 G, which are typical of hydroxyl radical attached to the DMPO spin trap. The intensity of these

antiphase signals is proportional to the number of radicals that attached the spin trap and therefore was used to assess the antioxidant activity of the investigated materials.

In both the pristine and functionalized cotton, it was observed an attenuation of the signal intensity which demonstrates that OH· radicals preferentially attack the textile samples rather than DMPO. In the case of pristine cotton, antioxidant efficiency was 22%, which is ascribable to oxidation of the cellulose molecules reacting with the OH. A more significant attenuation of the DMPO-OH peak intensity was observed upon application of caffeine loaded nanoparticles onto cotton, which raises antioxidant efficiency to 56%. Given that the antioxidant activity of caffeine loaded NPs had already been proved in Chapter 7, it can be stated that the antioxidant properties of the formulation are extended to the textile upon the finishing treatment.

The EPR spectra of the curcumin loaded NP treated textiles together with the control spectra are reported in Figure 9.14.

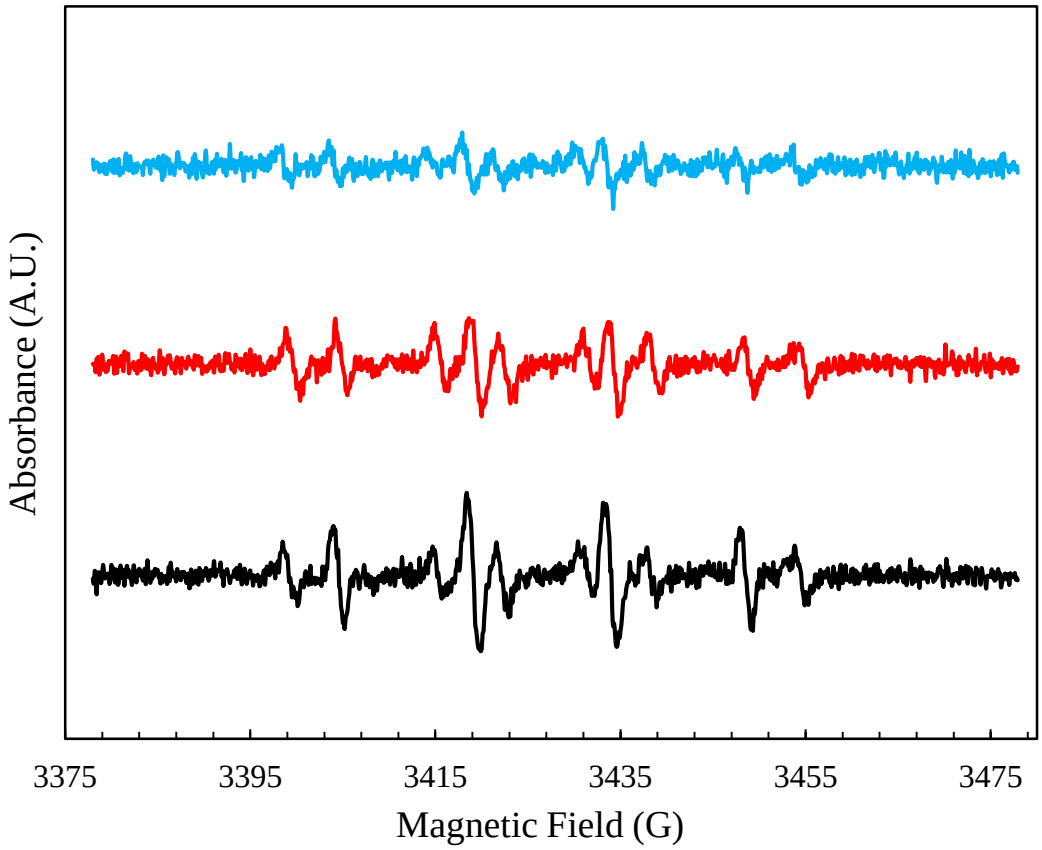

Figure 9.14. EPR spectra of the spin trap DMPO collected in presence of the different samples: control (black curve) cotton (red curve) and cotton functionalized with curcumin loaded nanoparticles (blue curve).

For this analysis hydroxyl and methyl radicals were generated by a non Fenton reaction. Therefore, the control spectrum is characterized by eight antiphase signals associated with the attack of the spin trap by the CH_3· and OH· radicals. Antiphase signal intensity was observed to be attenuated in the presence of the cotton fabric. Similarly, to the previous case, such a result arises from the interaction of the CH_3· and OH· radicals with the cellulose molecules. The application of curcumin loaded nanoparticles furtherly attenuated the antiphase signals.

From the EPR spectra, the scavenging effects toward the single radical species and the total antioxidant activities were obtained, as shown in Figure 9.15. A moderate scavenging activity was observed for the pristine cotton as a consequence of the reaction between the cellulose molecule and the generated radicals. Given the radical scavenging effects observed on the curcumin loaded nanoparticles suspensions, the addition of curcumin loaded NPs significantly increased the fabric antioxidant activity, as expected. Stronger scavenging effect toward the methyl radical compared to hydroxyl one was observed, the overall antioxidant activity was about 45%, proving an effective shielding of the treated fabric against radical species.

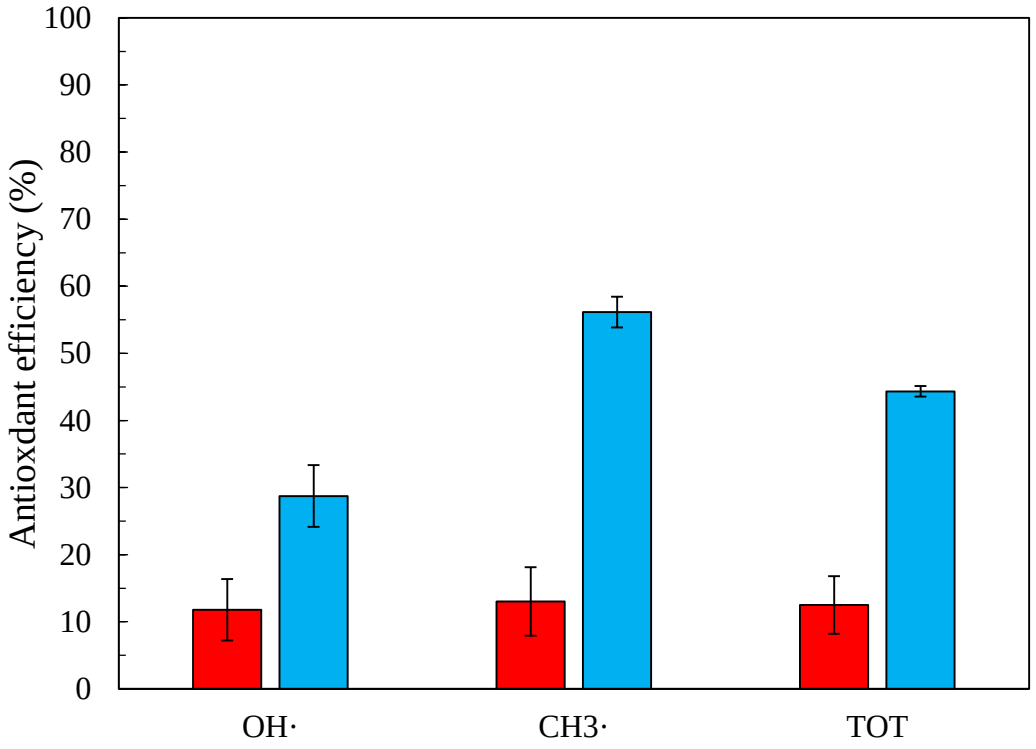

Figure 9.15. Radical scavenging activity of pristine cotton (red bar) and cotton functionalized with curcumin loaded nanoparticles (blue bar).

The reported EPR analysis proves that the functionalized fabrics displayed an antioxidant effect and neutralize different radical species. Such property works synergistically with the previously discussed

UV shielding properties. Indeed, the biofunctional fabrics own the potential to both prevent ROS formation by absorbing the UV radiation and to scavenge the free radicals caused as a consequence of the transmitted UV light.

9.4.2. Skin permeation test

A The interaction of the developed biofunctional textiles with skin was studied by performing Franz cell experiments on skin tissue excised from porcine ears. This release test does not only allow to determine the kinetics of transdermal release but also provides information about accumulation in the dermal layers of the investigated formulation using a skin model very similar to the human one. In the previous chapters, some in vitro released tests were performed on the drug loaded nanoparticles proving their capability in controlling the drug release kinetics respect to the free drugs. Based on these results, the NP formulations were used as the control in the skin permeation experiments to investigate whether the application on a textile substrate modifies the dermal penetration of the encapsulated drugs. In Figure 9.16, the transdermal release kinetics of caffeine loaded nanoparticles and of the corresponding treated fabrics are shown.

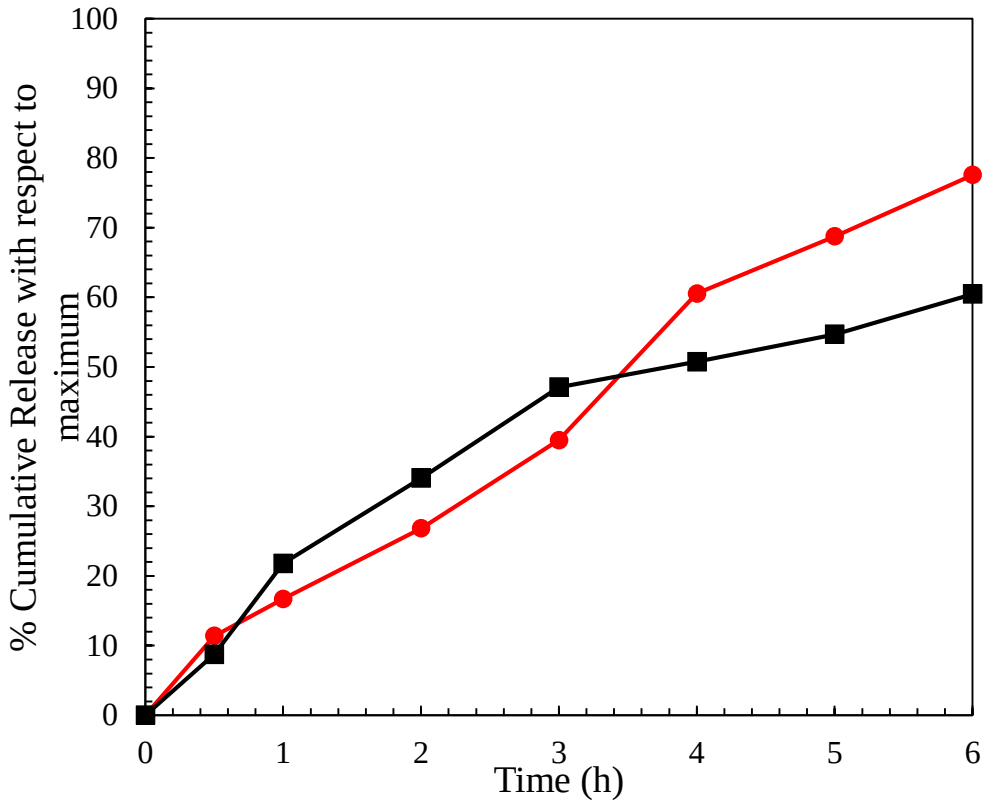

Figure 9.16. Caffeine permeation kinetics from PCL_6CAF_9W formulation (red curve) and the sample COT-PCL_6CAF_9W (black curve). Results are plotted in terms of percentage respect to the total amount of caffeine released in each test.

It can be observed that both the nanoparticles formulation and the textile display a continuous release of the drug during the time. In the case of COT-PCL_6CAF_9W however, the rise shows a small decline between 3 and 4 hours where the two curves intersect.

The two release curves appear to have similar shapes, therefore, the data were fitted with the different kinetic models to elucidate the permeation mechanisms, the correlation coefficients are reported in Table 9.3. In the case of caffeine loaded NPs, it can be observed that the zero order, first order and Hixon Crowell methods display high correlation coefficients. The good fitting with a zero order kinetic indicates the good control of caffeine release by the nanoparticle formulation. The fact that both first order (diffusion based) and Hixon-Crowell (erosion based) indicates that in the present set up the erosion component plays a role in the drug release mechanism. This finding is explained considering that the release test was performed on a biological membrane where partial biodegradation of PCL can occur. Therefore, in this ex vivo set up the release kinetics is a result of both diffusion and erosion mechanism.

Concerning the transdermal permeation from the biofunctional textile, it can be observed that, oppositely, the best fitting was obtained with Higuchi and Baker-Lonsdale models, which describe the diffusive release from porous matrices. The reason why the release from the textile sample is more diffusion controlled could be connected to the morphology of the sample COT-PCL_6CAF_9W (Figure 9.6), indeed the particles were observed to be agglomerated in porous clusters and entrapped in the core of bean shaped structure of the cotton fibers. Then diffusion phenomena must occur for the nanoparticles to be released from the textile network and to the skin membrane.

Table 9. 4. The correlation coefficient of fitting of the release curves with different kinetic models.

Sample	Zero order	First order	Higuchi	Hixon Crowell	Baker Lonsdale
PCL_6CAF_9W	R^2=0.98	R^2=0.97	R^2=0.90	R^2=0.98	R^2=0.87
COT-PCL_6CAF_9W	R^2=0.86	R^2=0.95	R^2=0.97	R^2=0.93	R^2=0.98

Interestingly, neither the nanoparticle formulations nor the biofunctional textile showed a burst release. This observation, together with the high correlations coefficients of the controlled release kinetic models, allow to conclude that the proposed system is effective in controlling the release of the active principle.

The permeation rate of curcumin loaded NPs and the corresponding treated fabrics are reported in Figure 9.17. Similarly to caffeine, both the curcumin NP formulation and curcumin loaded textile displayed a consistent increase in released drug dosage over time.

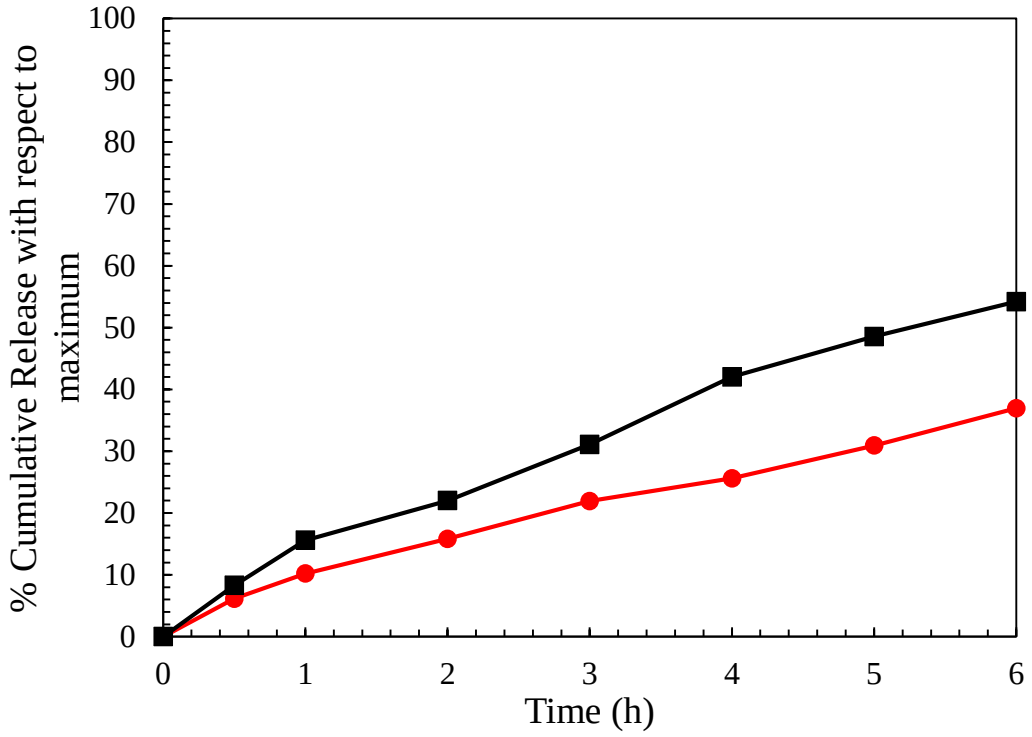

Figure 9.17. Curcumin permeation kinetics from the $PCL_{10}CUR_4$ formulation (red curve) and the COT-$PCL_{10}CUR_4$ sample (black curve). Results are plotted in terms of percentage respect to the total amount of curcumin released in each test.

The NP formulation release curves displayed almost linear kinetics similar to the one observed during the in vitro Franz cell experiment reported in Chapter 8. The biofunctional textile displayed a release pattern analogous to the one of the NP formulation with higher percentages of drug release in the first 6 hours. The results of the fitting of the release data with the semi-empirical models are reported in Table 9.4.

The permeation profile of curcumin loaded NPs can be described both by the diffusion and the erosion based models i.e. first order and Hixon Crowell equations. Analogously to caffeine loaded nanoparticles, this results is explained by the fact that the biodegradation of PCL in the biological membrane makes the mechanisms of diffusion and erosion to be simultaneously present. Similarly, the curcumin based biofunctional textile is well fitted by several models, the higher correlation coefficients were obtained for Hixon Crowell and zero order kinetics. Thus this biofunctional textile

delivers the drug in a controlled mechanism that involves the degradation of the carrier in the porcine skin membrane.

For the curcumin functionalized cotton, the diffusion component of the release was observed to be less significant respect to the caffeine one. Such a phenomenon was correlated to the different morphology the textile samples. In facts, in the case of curcumin, the particles were found to be uniformly covering the outer fiber surface without being incorporated in the bean core of the cotton fibers. Then the release of the particles from the fabrics toward the skin membrane was expected to be eased respect to the case where the particles had to be detached and released from the fiber core.

Table 9.5. The correlation coefficient obtained from the fitting of the release curves with different kinetic models.

Sample	Zero order	First order	Higuchi	Hixon Crowell	Baker Lonsdale
$PCL_{10}CUR_4$	R^2=0.96	R^2=0.99	R^2=0.95	R^2=0.98	R^2=0.93
COT- $PCL_{10}CUR_4$	R^2=0.97	R^2=0.96	R^2=0.94	R^2=0.99	R^2=0.87

The drug release tests were run until it was observed that an equilibrium condition was reached and no more release of the drug occurred. Then, the drug was extracted from the porcine skin and quantified to obtain information about the drug accumulated in the skin membrane. The amount of drug released to the acceptor compartment and accumulated in the skin together with the time of drug release was observed are reported in Table 9.5.

The time for which the effective release of the drug occurred was observed to be prolonged when the NPs were supported on the textile substrate. Such an increase is particularly marked in the case of curcumin which was kept to be delivered over three days. This phenomenon was interpreted taking into account the different phenomena affecting the drug release for the NP formulations and the biofunctional textiles.

The nanoparticles suspensions are dispersed in a liquid medium. Once applied on the skin the particles can permeate the epidermal layers by mass transfer phenomena occurring in a liquid state. As time goes on the formulation liquid drop tends to evaporate causing the drying of the NPs. The drying of the formulation causes the stop of the drug release. Indeed as drying occurs the particles tend to

agglomerate significantly reducing their permeation capability. Moreover, the evaporation of the dispersant depletes the medium through which the mass transfer occurs.

On the contrary, the biofunctional textile the NPs were supported on a porous and hydrophilic substrate. Such a substrate was observed to act as a reservoir for the sweat mimicking liquid applied to promoted the diffusion from the fabrics to the skin. The presence of cotton permits to prevent fast evaporation of the transport medium and to limit the particle agglomeration. This leads to a more prolonged release from the fabrics respect to the directly applied particle formulations.

For both the substances, the amount of drug accumulated in the skin was found to be higher when the release occurred from the textile substrate. Such a result was explained considering that in the case of biofunctional textiles a larger contact area is available between the drug delivery system and the skin since the textile uniformly covers the skin membrane.

Table 9. 6. Amount of drug released and accumulated for the different samples.

Sample	Time of release (h)	Amount of drug released in the receptor fluid ($\mu g/cm^2$)	Amount of drug accumulated in the skin ($\mu g/cm^2$)
PCL_6CAF_9W	24	186.6	101.3
COT-PCL_6CAF_9W	26	43.6	170.4
$PCL_{10}CUR_4$	24	3.8	129.7
COT- $PCL_{10}CUR_4$	74	6.0	198.4

In the case of caffeine, the amount of drug released to the acceptor fluid was found to be higher when the nanoparticles suspensions were directly administered. Considering that caffeine is a water soluble molecule it is not surprising that it was quickly released from the water dispersed nanoparticles to the aqueous acceptor fluid.

Oppositely, in the case of biofunctional cotton, the caffeine loaded particles need to be firstly detached from the fabric to reach the skin and thereafter release the drug. Therefore, the pathway the drug must

undergo to reach the acceptor fluid is more complex leading lowers drug amount to be delivered in the acceptor fluid.

Concerning curcumin, it can be observed that the application of the biofunctional textile enhances both the topical and transdermal release. Such phenomenon was ascribed to the uniform dispersion of the particles onto the textile surface observed in Figure 9.7, this morphology is responsible for a good spreading of NP monolayer over a larger skin surface area and leads to an effective enhancement of the released dosage. For both the suspension and the fabric it can be observed that the quantity of drug released is significantly lower respect to the accumulated one. This fact is due to the curcumin hydrophobicity that eases the permeation in the fatty skin layer but limits the diffusion in the aqueous acceptor medium.

The skin permeation test demonstrated that the application of the NPs on the textile fabrics does not significantly alter the drug release kinetics. Supporting the particles on the fabrics lead to an increase of the released dosage at the topical level and to more prolonged release time. In conclusion, the proposed biofunctional textile represents an effective strategy for dermal delivery to administer effective dosages of drugs in a controlled way over a long time reducing the number of administrations required by the user.

Part V final remarks

The final part of the present work was devoted to the application of the NP formulation to the cotton substrate. The optimized caffeine and curcumin nanoparticle formulations were used as case studies to evaluate the performances of the biofunctional textiles upon functionalization with two very different substances in terms of hydrophilicity.

The proposed finishing treatment consisted of a cold impregnation with the scope of achieving functionalization with a simple scalable method. Thus the research evaluated the suitability of the treatment in applying the particles on the textile substrate and the performances of the obtained materials.

The effective application of the nanoparticles onto the textile substrate was demonstrated both by infrared analysis and by extraction of the active principle from the textile substrate. Furthermore, the datacolor test proved good replicability of the finishing treatment in terms of quantity of curcumin applied.

The SEM observation provided insights on the functionalized fabric morphologies and on the particle interaction with the textile. It was evidenced that the distribution of the particles on the fabric surface depended on the loaded drug and the different particle properties. Indeed, the hydrophobic and highly stable curcumin nanoparticles were well dispersed on the fiber outer surface. For caffeine loaded nanoparticles, instead, the particles were found as aggregated clusters, that were preferentially hosted inside the bean shaped cavity of the cotton surface.

The zeta potential and the contact angle analyses evidenced that the physical properties of the cotton fabrics were not significantly altered by the nanoparticles functionalization. Such a finding was ascribed to the fact that the proposed treatment deposited monolayer of particles and that the number of particles deposited was sufficiently low to not cause alteration of the particle properties, as they do not form a continuous layer on the fabric surface.

Regarding the fabric biofunctional properties, it was instead proved a significant improvement of the fabric performances upon the nanoparticle treatment. The fabrics ability of shielding UV rays was boosted by both the drug loaded nanoparticles formulation. The extent of the UV protection factor increase was found to be mostly related to the photochemical characteristics of the active molecules. Indeed, the curcumin treatment displayed the most significant improvement of the UPF as it was expected from a chromophore. On the contrary. the caffeine nanoparticle treatment displayed a less marked UPF increase but allowed a more significant reduction of the radiations transmitted in the low UV region.

By adapting and employing the EPR/Spin trapping method for investigating the radical scavenging properties of textile materials, it was possible to prove that the nanoparticle functionalization imparted antioxidant properties to the textile fabrics. Thus, the proposed biofunctional textiles are capable of both screening the UV radiation and quenching the radical species. The combination of these properties was considered promising in terms of the prevention and treatment of UV and ROS associated skin diseases.

The Franz cell test was conducted on excised porcine skin to finally obtain informations on the performances of the NP formulations and of the biofunctional textiles on an environment similar to human skin. The permeation test revealed that the kinetics of drug release was affected both by diffusion phenomena and by the biodegradation of the PCL in the biological membrane. The textile material proved to effectively support the nanoparticles without significantly hindering their release kinetics. The proposed method was proven to be effective for achieving the skin permeation of both drugs.

Overall it was proved the possibility of applying drug loaded nanoparticles to cotton fabrics by simple and scalable routes. Such a surface functionalization imparted biofunctional properties to the textile so that the proposed materials display beneficial properties to the user's health.

General conclusion and future perspectives

The work presented in this manuscript was performed in the frame of the Erasmus Mundus Joint Doctorate in Sustainable Management and Design of textiles. In the context of this international program, the research was carried out firstly in Politecnico di Torino, then in ENSAIT and finally at Soochow University. The principal objective of the present thesis was to report the development of novel processes and products in the field of biomedical textiles. Particular focus was paid in the design of fabrics which allow the delivery of active principles to the skin both for topical and systemic treatments. The encapsulation of the active principles in nanometric size carriers was employed as a strategy to improve the interaction among the drug and the textile substrate and to effectively promote the permeation of the actives in the skin layers. Moreover, the immobilization of the drug loaded nanocarriers on the textile substrate was proposed as a way to minimize the number of required applications of the topical medicament, leading to the production of a wearable drug delivery device.

At the beginning of this study particular focus was paid on individuating a suitable approach to for the biofunctional textiles production. By mean of critical literature analysis, the background knowledge of the different fields which come in play in the biofunctional textile production was discussed and presented. Firstly, the basic of skin physiology was resumed to well elucidate the physical and biochemical properties of the target tissue. Thereafter an overlook of skin pathologies and dermatological drug administration routes was provided. From this report the current challenges in skin treatment and transdermal delivery were identified; furtherly the complexity of the skin barrier was identified as the main factor hindering the vast application of transdermal route as a strategy for the administration of systemic drugs. Given the difficulties encountered by several drugs in overcoming the skin layers, the different permeation enhancement strategies were analyzed and critically compared taking into account both the effectiveness in transdermal delivery and the risk of causing side skin damages.

By this investigation, it was evidenced how the incorporation of the active principle in finely designed nanometric size carrier significantly improve transdermal permeation while not causing significant damages to the skin tissue. The different kinds of nanocarriers employed in dermatology were reviewed; the principal properties and performances of hydrogels, cyclodextrins, nanobubbles, liposomes, polymeric and ceramic nanoparticles were discussed. Such analysis took into account both the case of topical administration of the nanocarrier suspension both the immobilization of the carrier on a textile substrate. Among the various carrier proposed in literature polymeric nanoparticles were

estimated to be more suitable for biofunctional textile preparation. Such choice was mainly dictated both by the proven capability of the NPs system to enhance dermatological delivery and by the good compatibility between polymeric shells and textile substrates. Furtherly nanoparticles can be produced by several processes some of them are highly productive and therefore suitable to prepare the amount of carrier suitable to meet the production scale of the textile industry. Upon having considered different technologies for nanoparticle production the Flash nanoprecipitation method was evaluated as the most suitable one. Indeed, FNP is a simple, economic, productive and sustainable technique which, according to literature, leads to the production of a large amount of nanocarriers while meeting the quality characteristics required for dermatological administration.

The experimental work then focused on proving firstly the suitability of the FNP method to produce drug loaded nanoparticles to be employed in the biofunctional textile preparation. The methodology to prove this concept can be summarized in three main experimental procedures. Firstly, it was inquired if the FNP allows producing particles with suitable characteristics to be employed in dermatological delivery. Secondly, it was verified if such nanoparticles can be applied to the fabric substrate by a simple finishing treatment which could allow easy recharging of the biofunctional textiles. Finally, the properties of the produced biofunctional textiles were inquired to verify the possibility of such material to benefit the user's health. Polycaprolactone was chosen as the polymer to produce the nanoparticles given its biocompatibility and biodegradability which have made it of increasing interest in biomedical applications.

To inquire about the performances of the proposed systems on the incorporation and delivery of different active substances three model drugs were studied. These chosen drugs were caffeine, melatonin and curcumin which represent a model for hydrophilic, mildly hydrophobic and strongly hydrophobic substances respectively. Each substance was firstly encapsulated in the PCL NP system. The outcome of the encapsulation processes was evaluated in terms particle size and the drug content. To properly evaluate the LC and EE of the produced nanoparticles, different experimental protocols proposed were proposed and optimized based on the chemical characteristics of each substance. For textile functionalization, the imbibition and the impregnation protocols were proposed. The biofunctional properties were evaluated in terms of antioxidant activity, UPF, and drug release. For the antioxidant activity evaluation methods based on EPR spectroscopy and spin trapping were proposed while the drug delivery properties were evaluated in a Franz cell experiment.

Some preliminary experiments were run to inquire about the characteristics of PCL nanoparticles formation by FNP methods and to verify their consistency with the results reported in the literature. Acetone, acetonitrile and THF were used as solvents. When acetone and acetonitrile were employed as solvents it was observed that the average particle diameter tended to decrease as the flow rate was increased. Moreover, the use of acetone led to a finer particle size. Based on these results and considering the also the cost and environmental compliance, acetone was chosen as the solvent for particle production.

Melatonin was the first drug to be investigated. In fact, owning a middle hydrophilicity level was considered to be more suitable for a preliminary study about the drug encapsulation and release. The study evidenced how the observed D_p vs FR trends are not altered by the addition of the drug in the process. Moreover, it was observed that increasing the polymer and drug concentration leads to an increase in the average diameter. High values of EE were observed (>80%) due to the scarce water solubility of melatonin. The fabrics were effectively functionalized by the imbibition method as proved by the SEM imaging, however, in some cases, significant aggregation of the particles onto the textile surface was observed. The Franz cell test, conducted using artificial membrane highlighted controlled release kinetics which was best fitted by the Baker and Lonsdale model as expected to occur in the case of spherical matrices such as the nanoparticles. The studies conducted on melatonin highlighted that the proposed approach can lead to effective drug encapsulation and biofunctional textile preparation and constituted a solid base to tackle the investigation on the other drugs.

A deep study about the drug encapsulation was conducted using caffeine and curcumin as model drugs. The scope of these investigations was to highlight the performance of the encapsulation system using two extremely different drugs from the hydrophilicity point of view. Furtherly, it was aimed to propose for each drug an optimal nanoformulation to be employed for textile finishing.

The encapsulation of caffeine was identified as a challenging issue since the incorporation of hydrophilic active principles was a scarcely discussed topic in literature. To approach the issue two different process configurations were proposed i.e. the CIA and CIW ones. Firstly, the study evidenced how the addition of caffeine does not affect the D_p vs FR trends. The effective incorporation of the drug was proven both by the direct and indirect measurement protocols. Although the EE was found to be lower than the one observed melatonin, values comparable with the one found in the literature were observed. The characterization conducted on the nanoparticles pointed out that the different configurations lead to different particles structure. The particles produced in CIA configuration owned most of the caffeine adsorbed on the surface while for CIW the drug was more

embedded in the particle core. These two particles structures displayed different release behavior in the dialysis test, the CIA displayed a fast release of most of the drug content while CIW nanoparticles showed to act a reservoir system. Based on these results the formulation PCL_6CAF_9W was found to be optimal one and was proven to possess antioxidant properties by the EPR experiment. For these reasons, such formulation was chosen to be used for the textile finishing.

Curcumin was tested as the model hydrophobic drug. The curcumin loaded nanoparticles displayed fine size (below 250 nm) and EE proximate to 100%, consequently, it was possible to tune the LC by adjusting the formulation parameters. Such results were correlated with the scarce water solubility of the active principle which makes it take part in the nucleation process in the reactor chamber. The characterization of the six tested formulations led to the choice of $PCL_{10}CUR_4$ as the optimal one. The chosen formulation displayed high colloidal stability upon being stored in the fridge. Indeed, no aggregation phenomena were observed over two months. The curcumin loaded NPs were found to be observable by fluorescent microscopy, moreover, upon addition of Nile red to the formulation it was proven to be possible to track both the NP and the active principle. This last property is considered promising to move forward in vivo application. The antioxidant activity assay evidenced that the curcumin loaded nanoparticles display strong scavenging activity against the hydroxyl and the methyl radical. The in vitro Franz cell test evidenced that the curcumin loaded nanoparticles can deliver the active principle in a controlled way according to zero-order kinetics and enhancing the transdermal penetration of the substance.

The last part of the present thesis was devoted to the application of the produced nanoparticles to the cotton substrates. Caffeine and curcumin loaded nanoparticles were used as a case study due to their extremely different hydrophilicity level. The optimal formulations of the two drugs were employed in the impregnation of the textile. The proposed treatment allowed to successfully apply the NP on the textile surface as proven by several analyses. Moreover, in the case of curcumin, a good color uniformity found in the different samples proved that the same quantity of the active principle was deposited on the fabric surface. The SEM observation showed that curcumin NP uniformly covered the fabric surface while caffeine loaded NP tends to aggregate in clusters and to be hosted in the cotton bean shaped fiber core. These two different morphologies were connected to the different hydrophilicity and colloidal stability of the formulations. The finishing was proven to effectively impart biofunctional properties to the textiles. Effective UV shielding was observed for both the treated fabrics, the extent of UPF increase was correlated with the different photochemical properties of the active principles. The EPR-Spin trapping technique was adapted to the analyzed textile surface; the analysis revealed how the treated fabrics own effective antioxidant properties. The Franz cell

experiment was finally conducted on the excised porcine skin membrane to obtain information on the material drug eluting performance on a tissue similar to the human one. In this biological environment, the kinetics of drug release resulted to be also affected by PCL biodegradation. Moreover, the cotton substrate was proven to effectively support the NP system while enhancing drug release performances. The amount of drug accumulated in the skin layers was in facts higher in the case of biofunctional textiles respect to the NP suspensions. The combination of antioxidant and UV protection makes the proposed biofunctional textiles to be a tool to protect the user from the damages connected to UV radiations and to the free radicals generated by it. Furtherly the proven effectiveness in delivering topical antioxidants in the skin layers makes the biofunctional textile a potential tool to limit the free radical induced diseases in the skin tissue.

Overall in the present thesis, the suitability of producing biofunctional textiles by finishing treatment based on PCL nanoparticles was studied. The encapsulation processes were run with different model drugs using the FNP method. It was shown how this process allowed the incorporation of active substances with different degrees of hydrophilicity. For all the investigated substances it was proved that the adjustment of the process parameters and formulations leads to particles of different particle sizes. Upon having optimized such parameters it was possible to obtain particles with an average diameter lower than the size of skin pores and therefore suitable to be used as dermatological formulation. The EE was found to be higher for the more hydrophobic substances like melatonin and curcumin while more modest values of EE were obtained for caffeine. Such results are indeed consistent with the literature which generally employed FNP as a tool to encapsulate poorly water soluble drugs. The study here conducted on hydrophilic substances however proved that by adjusting process configuration the technique can be employed also on hydrophilic drugs. Considering the PCL system drug with logP between -0.55 and 4.12 were incorporated, therefore the present thesis work provides useful insights on how to design an encapsulation system by FNP for substances whose logP is included in that range. It was then proved that using the FNP method is possible to obtain particles whose properties meet the criteria for dermatological application. Such results combined with the intrinsic good productivity and easiness of scale up of the FNP provides a good starting point toward making the industrial production of such biofunctional textile feasible.

Concerning the textile application of the produced nanoparticles, it was highlighted how simple processes that do not require curing or resin applications can successfully permit the fabric functionalization. Using such a strategy, provided the advantages of simplifying the process and easing the detachment of the particles for the drug delivery applications. For the investigated cases it was observed that the biofunctional properties of the textiles depend on the kind of drug used

functionalization. However, the strategy of immobilizing the drug loaded nanoparticles presented some interesting features. In fact, upon reaching equilibrium conditions the formulation would be partially on the fabrics and partially delivered. Such distribution allowed to simultaneously improve the UPF of the fabrics while delivering the drug to the skin and scavenging the radical species; leading to a combined action against the UV induced skin damage. Furthermore, the immobilization on the textile made possible to use the particles as a dry formulation. This could provide advantages in terms of cytocompatibility since once the formulation was dried on the fabrics the organic solvents necessary for the FNP process would be evaporated and thus the risk connected with solvent induced irritation will be reduced.

The present work proposed and tested some novel concepts in biofunctional textiles production. Such a topic combines the interests of several scientific communities, such as the one of chemical and textiles engineers, material scientists, drug technologists and dermatologists. The further development of such technology can be identified in these different scientific fields.

In the field of materials science and drug technology, further investigations could lead to the development of improved nanocarriers. Such carriers would indeed display further functional properties that improve their therapeutic effects. In the present thesis, the carriers were developed by choosing a single polymer and varying drugs over a logP range. Therefore, further studies may focus on either loading another kind of actives, or to test the possibility of using different kinds of polymeric shells and assess their capability of incorporating different drugs. Indeed, PCL displayed the interesting property of acting as a drug reservoir since it biodegrades slowly. The employment of polymers that undergo faster biodegradation may be studied to produce devices that display faster release, thus tackling acute infections.

In the context of pharmaceutical science, it is also of crucial importance to take into account regulatory issues and design the nanocarriers in such a way they could achieve approval by the regulatory agencies. Regarding of biofunctional textile it is necessary to assess the safety of the nanomaterials employed for the fabric functionalization. Therefore, future studies should focus on assessing the cytocompatibility of the here proposed nanoparticle systems. Particularly being the nanoformulations applied topically it necessary to prove it does not display cytotoxicity toward skin cells such as the HaCat line.

In the field of chemical and process engineering, some future studies may inquire about the improvement and optimization of the nanoparticles production processes. As evidenced in the present

manuscript the main issue hindering the commercialization of biofunctional textiles is the different production scale of pharmaceutical carriers and textile finishes. Thus the carrier production process is of crucial importance to allow a sufficient production of the carriers used for textile functionalization. Moreover, in the present thesis, it was evidenced that fine tuning of the process parameters critically affected the main quality characteristics of the nanoparticles. Particularly, process conditions that allowed to increase both the productivity and particle qualities were identified. Nevertheless, further research may focus on investigating novel process conditions which may lead to a further decrease of the particle size or to an increase of the EE when hydrophilic substances are loaded.

Regarding the textile engineering field, the present thesis proposed an approach for the fabric functionalization which was supposed to imply the fabric to be rechargeable by the user. Further studies in this field should then inquire about the outcomes of such an approach its compliance with the regulations about biomedical devices. The present thesis proved that a cold impregnation allowed to effectively impart biofunctional properties to the fabrics. Future studies may test whether similar properties can be imparted to the textile by running such a finishing treatment in a domestic washing machine, thus making the biofunctional textile to rechargeable by the user itself.

Overall, it can be concluded that the present thesis provided novel insights about the production of biofunctional textiles. The results obtained opened rooms for further development of this field which display the potential to positively impact society and people's life.

Research valorization and publications.

Articles in peer reviewed Journals.

1) D. Massella, F. Leone, R. Peila, A. Barresi, A. Ferri, "Functionalization of Cotton Fabrics with Polycaprolactone Nanoparticles for Transdermal Release of Melatonin". JFB. (2017), 9 1. doi:10.3390/jfb9010001.

2) D. Massella, E. Celasco, F. Salaün, A. Ferri, A. Barresi. "Overcoming the Limits of Flash Nanoprecipitation: Effective Loading of Hydrophilic Drug into Polymeric Nanoparticles with Controlled Structure" Polymers. (2018), 10, 1092. doi:10.3390/polym10101092.

3) D. Massella, M. Argenziano, A. Ferri, J. Guan, S. Giraud, R. Cavalli, A. Barresi, F. Salaün. "Bio-Functional Textiles: Combining Pharmaceutical Nanocarriers with Fibrous Materials for Innovative Dermatological Therapies". Pharmaceutics (2019), 11, 403. doi:10.3390/pharmaceutics11080403.

4) D. Massella, S. Giraud, J. Guan, A. Ferri, F. Salaün. "Textiles for health: a review of textile fabrics treated with chitosan microcapsules" Environ Chem Lett. (2019). doi:10.1007/s10311-019-00913-w.

Conference papers

1) D. Massella, A. Ancona, N. Garino, V. Cauda, J. Guan, F. Salaun, A.A. Barresi, A. Ferri, "Preparation of bio-functional textiles by surface functionalization of cellulose fabrics with caffeine loaded nanoparticles". IOP Conf. Ser.: Mater. Sci. Eng. 460 (2018) 012044. doi:10.1088/1757-899X/460/1/012044.

Book chapter

1) D. Massella, S. Giraud, J. Guan, A. Ferri, F. Salaün. "Manufacture Techniques of Chitosan-Based Microcapsules to Enhance Functional Properties of Textiles" in: G. Crini, E. Lichtfouse (Eds.), Sustainable Agriculture Reviews 35 (2019), Springer International Publishing, Cham: pp. 303–336. doi:10.1007/978-3-030-16538-3_8.

Participation in Conferences and Workshops

Oral presentations

1) “Production of PCL nanoparticles by flash nanoprecipitation for controlled release of caffeine”. Present at the Merck Young Chemists Symposium (MYCS 2017); held in Rimini November 2017.

2) "Preparation of bio-functional textiles by surface functionalization of cellulose fabrics with caffeine loaded nanoparticles". Presented at the Autex conference held in Istanbul 20-23 June 2018.

3) “Encapsulation processes for the production of biofunctional textiles”. Presented during the 4ème Journée des Jeunes Polymeristes du Nord, organized by French Polymer Studies Group, held in Lille on the 27th of June 2019.

Poster presentations

1) “Assessment of antioxidant and drug releasing properties of cellulose fabrics functionalized with polymeric nanoparticles as potential bio-functional garments”. Presented during MILAN POLYMER DAYS congress in February 2018.

2) "Flash Nanoprecipitation as a simple route to produce smart polymeric drug delivery devices". Presented during the conference "Polymers function design and applications" held in Barcelona 21-23 March 2018

3) “Preparation of an antioxidant and drug releasing textile by functionalization of cellulose fabric with curcumin loaded nanoparticles” presented during the workshop “Journée Stratégique de la SFR Technologie de la Santé et Médicaments” organized by Lille university consortium on 10th Dec 2018. Winner of the best poster award.

4) "Biofunctional textiles: a link between conventional garments and nanomedicine to prevent and heal skin diseases". Presented during the 6th Nanotoday conference held in Lisbon on the 16-20th June 2019.

Research Honors and Awards

1) Second Place in the “Innovation for change 2017” competition organized by CERN, Politecnico di Torino and College des Ingegneurs.

2) Awarded with the “EZ founder scholarship” by the Ermenegildo Zegna Group.

3) Second Place in the national contest “Chimicapisce” organized by the Italian Chemical Society for the thesis dissemination in a three minutes pitch.

4) Second Place in the “Reaxis Early career award” organized by Elsevier and Italian chemical society.

5) Best Poster award in the Journée Stratégique de la SFR Technologie de la Santé et Médicaments.

6) Reviewer activity for scientific journals in the field of pharmacology and material science.

Bibliography

AbdElhady, M.M., 2012. Preparation and Characterization of Chitosan/Zinc Oxide Nanoparticles for Imparting Antimicrobial and UV Protection to Cotton Fabric. Int. J. Carbohydr. Chem. 2012, 1–6. https://doi.org/10.1155/2012/840591

Abdel-Mottaleb, M.M.A., Moulari, B., Beduneau, A., Pellequer, Y., Lamprecht, A., 2012. Surface-Charge-Dependent Nanoparticles Accumulation in Inflamed Skin. J. Pharm. Sci. 101, 4231–4239. https://doi.org/10.1002/jps.23282

Abdul-Karim, R., Cowey, L., 2017. Challenging the standard of care in advanced melanoma: focus on pembrolizumab. Cancer Manag. Res. Volume 9, 433–442. https://doi.org/10.2147/CMAR.S92546

Abraham, J., Mathew, S., 2019. Merkel Cells: A Collective Review of Current Concepts. Int. J. Appl. Basic Med. Res. 9, 9–13. https://doi.org/10.4103/ijabmr.IJABMR_34_18

Abtew, M.A., Bruniaux, P., Boussu, F., Loghin, C., Cristian, I., Chen, Y., Wang, L., 2018. A systematic pattern generation system for manufacturing customized seamless multi-layer female soft body armour through dome-formation (moulding) techniques using 3D warp interlock fabrics. J. Manuf. Syst. 49, 61–74. https://doi.org/10.1016/j.jmsy.2018.09.001

Aggarwal, B.B., Sundaram, C., Malani, N., Ichikawa, H., 2007. CURCUMIN: THE INDIAN SOLID GOLD, in: Aggarwal, B.B., Surh, Y.-J., Shishodia, S. (Eds.), The Molecular Targets and Therapeutic Uses of Curcumin in Health and Disease. Springer US, Boston, MA, pp. 1–75. https://doi.org/10.1007/978-0-387-46401-5_1

Agnhage, T., Zhou, Y., Guan, J., Chen, G., Perwuelz, A., Behary, N., Nierstrasz, V., 2017. Bioactive and multifunctional textile using plant-based madder dye: Characterization of UV protection ability and antibacterial activity. Fibers Polym. 18, 2170–2175. https://doi.org/10.1007/s12221-017-7115-x

Agnihotri, S.A., Mallikarjuna, N.N., Aminabhavi, T.M., 2004. Recent advances on chitosan-based micro- and nanoparticles in drug delivery. J. Controlled Release 100, 5–28. https://doi.org/10.1016/j.jconrel.2004.08.010

Akbari, E., Akhavan, O., Hatamie, S., Rahighi, R., 2018. Curcumin as a green fluorescent label to revive the fluorescence property of functionalized graphene oxide nanosheets. J. Drug Deliv. Sci. Technol. 45, 422–427. https://doi.org/10.1016/j.jddst.2018.04.010

Al Hanbali, O.A., Khan, H.M.S., Sarfraz, M., Arafat, M., Ijaz, S., Hameed, A., 2019. Transdermal patches: Design and current approaches to painless drug delivery. Acta Pharm. 69, 197–215. https://doi.org/10.2478/acph-2019-0016

Al-Hashimi, N., Begg, N., Alany, R., Hassanin, H., Elshaer, A., 2018. Oral Modified Release Multiple-Unit Particulate Systems: Compressed Pellets, Microparticles and Nanoparticles. Pharmaceutics 10, 176. https://doi.org/10.3390/pharmaceutics10040176

Ali, S.W., Rajendran, S., Joshi, M., 2011. Synthesis and characterization of chitosan and silver loaded chitosan nanoparticles for bioactive polyester. Carbohydr. Polym. 83, 438–446. https://doi.org/10.1016/j.carbpol.2010.08.004

Alonso, C., Carrer, V., Barba, C., Coderch, L., 2018. Caffeine delivery in porcine skin: a confocal Raman study. Arch. Dermatol. Res. 310, 657–664. https://doi.org/10.1007/s00403-018-1854-4

Alonso, C., Martí, M., Martínez, V., Rubio, L., Parra, J.L., Coderch, L., 2013. Antioxidant cosmeto-textiles: Skin assessment. Eur. J. Pharm. Biopharm. 84, 192–199. https://doi.org/10.1016/j.ejpb.2012.12.004

Alonso, D., Gimeno, M., Sepúlveda-Sánchez, J.D., Shirai, K., 2010. Chitosan-based microcapsules containing grapefruit seed extract grafted onto cellulose fibers by a non-toxic procedure. Carbohydr. Res. 345, 854–859. https://doi.org/10.1016/j.carres.2010.01.018

Amjadi, M., Mostaghaci, B., Sitti, M., 2017. Recent Advances in Skin Penetration Enhancers for Transdermal Gene and Drug Delivery. Curr. Gene Ther. 17. https://doi.org/10.2174/1566523217666170510151540

Amjadi, M., Sheykhansari, S., Nelson, B.J., Sitti, M., 2018. Recent Advances in Wearable Transdermal Delivery Systems. Adv. Mater. 30, 1704530. https://doi.org/10.1002/adma.201704530

Anand, P., Kunnumakkara, A.B., Newman, R.A., Aggarwal, B.B., 2007. Bioavailability of Curcumin: Problems and Promises. Mol. Pharm. 4, 807–818. https://doi.org/10.1021/mp700113r

Ancona, A., Dumontel, B., Garino, N., Demarco, B., Chatzitheodoridou, D., Fazzini, W., Engelke, H., Cauda, V., 2018. Lipid-Coated Zinc Oxide Nanoparticles as Innovative ROS-Generators for Photodynamic Therapy in Cancer Cells. Nanomaterials 8, 143. https://doi.org/10.3390/nano8030143

Anirudhan, T.S., Nair, A.S., 2018. Temperature and ultrasound sensitive gatekeepers for the controlled release of chemotherapeutic drugs from mesoporous silica nanoparticles. J. Mater. Chem. B 6, 428–439. https://doi.org/10.1039/C7TB02292A

Ansari, K.A., Vavia, P.R., Trotta, F., Cavalli, R., 2011. Cyclodextrin-Based Nanosponges for Delivery of Resveratrol: In Vitro Characterisation, Stability, Cytotoxicity and Permeation Study. AAPS PharmSciTech 12, 279–286. https://doi.org/10.1208/s12249-011-9584-3

Anu Bhushani, J., Anandharamakrishnan, C., 2014. Electrospinning and electrospraying techniques: Potential food based applications. Trends Food Sci. Technol. 38, 21–33. https://doi.org/10.1016/j.tifs.2014.03.004

Arda, O., Göksügür, N., Tüzün, Y., 2014. Basic histological structure and functions of facial skin. Clin. Dermatol. 32, 3–13. https://doi.org/10.1016/j.clindermatol.2013.05.021

Ardila, N., Ajji, Z., Heuzey, M.-C., Ajji, A., 2018. Chitosan electrospraying: Mapping of process stability and micro and nanoparticle formation. J. Aerosol Sci. 126, 85–98. https://doi.org/10.1016/j.jaerosci.2018.08.010

Argenziano, M., Banche, G., Luganini, A., Finesso, N., Allizond, V., Gulino, G.R., Khadjavi, A., Spagnolo, R., Tullio, V., Giribaldi, G., Guiot, C., Cuffini, A.M., Prato, M., Cavalli, R., 2017. Vancomycin-loaded nanobubbles: A new platform for controlled antibiotic delivery against methicillin-resistant Staphylococcus aureus infections. Int. J. Pharm. 523, 176–188. https://doi.org/10.1016/j.ijpharm.2017.03.033

Argenziano, M., Haimhoffer, A., Bastiancich, C., Jicsinszky, L., Caldera, F., Trotta, F., Scutera, S., Alotto, D., Fumagalli, M., Musso, T., Castagnoli, C., Cavalli, R., 2019. In Vitro Enhanced Skin Permeation and Retention of Imiquimod Loaded in β-Cyclodextrin Nanosponge Hydrogel. Pharmaceutics 11, 138. https://doi.org/10.3390/pharmaceutics11030138

Arpagaus, C., Collenberg, A., Rütti, D., Assadpour, E., Jafari, S.M., 2018. Nano spray drying for encapsulation of pharmaceuticals. Int. J. Pharm. 546, 194–214. https://doi.org/10.1016/j.ijpharm.2018.05.037

Arpagaus, C., John, P., Collenberg, A., Rütti, D., 2017. Nanocapsules formation by nano spray drying, in: Nanoencapsulation Technologies for the Food and Nutraceutical Industries. Elsevier, pp. 346–401. https://doi.org/10.1016/B978-0-12-809436-5.00010-0

Arpicco, S., Battaglia, L., Brusa, P., Cavalli, R., Chirio, D., Dosio, F., Gallarate, M., Milla, P., Peira, E., Rocco, F., Sapino, S., Stella, B., Ugazio, E., Ceruti, M., 2016. Recent studies on the delivery of hydrophilic drugs in nanoparticulate systems. J. Drug Deliv. Sci. Technol. 32, 298–312. https://doi.org/10.1016/j.jddst.2015.09.004

Artusio, F., Bazzano, M., Pisano, R., Coulon, P.-E., Rizza, G., Schiller, T., Sangermano, M., 2018. Polymeric nanocapsules via interfacial cationic photopolymerization in miniemulsion. Polymer 139, 155–162. https://doi.org/10.1016/j.polymer.2018.02.019

Asadi, H., Rostamizadeh, K., Salari, D., Hamidi, M., 2011. Preparation of biodegradable nanoparticles of tri-block PLA–PEG–PLA copolymer and determination of factors controlling the particle size using artificial neural network. J. Microencapsul. 28, 406–416. https://doi.org/10.3109/02652048.2011.576784

AS/NZS, 2017. Standards Association of Australia, and Standards New Zealand. Sun Protective Clothing: Evaluation and Classification. Jointly published by SAI Global Limited under licence from Standards Australia Limited, 2017, 4399:1996.

Assadpour, E., Jafari, S.-M., 2017. Spray drying of folic acid within nano-emulsions: Optimization by Taguchi approach. Dry. Technol. 35, 1152–1160. https://doi.org/10.1080/07373937.2016.1242016

Averina, E., Allémann, E., 2013. Encapsulation of alimentary bioactive oils of the Baikal Lake area into pH-sensitive micro- and nanoparticles. LWT - Food Sci. Technol. 53, 271–277. https://doi.org/10.1016/j.lwt.2013.01.020

Awasthi, S., Pandya, U., Singhal, S.S., Lin, J.T., Thiviyanathan, V., Seifert, W.E., Awasthi, Y.C., Ansari, G.A., 2000. Curcumin-glutathione interactions and the role of human glutathione S-transferase P1-1. Chem. Biol. Interact. 128, 19–38. https://doi.org/10.1016/s0009-2797(00)00185-x

Bader, C.A., Shandala, T., Carter, E.A., Ivask, A., Guinan, T., Hickey, S.M., Werrett, M.V., Wright, P.J., Simpson, P.V., Stagni, S., Voelcker, N.H., Lay, P.A., Massi, M., Plush, S.E., Brooks, D.A., 2016. A Molecular Probe for the Detection of Polar Lipids in Live Cells. PLOS ONE 11, e0161557. https://doi.org/10.1371/journal.pone.0161557

Badri, W., Miladi, K., Nazari, Q.A., Fessi, H., Elaissari, A., 2017. Effect of process and formulation parameters on polycaprolactone nanoparticles prepared by solvent displacement. Colloids Surf. Physicochem. Eng. Asp. 516, 238–244. https://doi.org/10.1016/j.colsurfa.2016.12.029

Bahrami, H., Tabrizchi, M., Farrokhpour, H., 2013. Protonation of caffeine: A theoretical and experimental study. Chem. Phys. 415, 222–227. https://doi.org/10.1016/j.chemphys.2013.01.022

Baino, F., Hamzehlou, S., Kargozar, S., 2018. Bioactive Glasses: Where Are We and Where Are We Going? J. Funct. Biomater. 9, 25. https://doi.org/10.3390/jfb9010025

Banche, G., Prato, M., Magnetto, C., Allizond, V., Giribaldi, G., Argenziano, M., Khadjavi, A., Gulino, G.R., Finesso, N., Mandras, N., Tullio, V., Cavalli, R., Guiot, C., Cuffini, A.M., 2015. Antimicrobial chitosan nanodroplets: new insights for ultrasound-mediated adjuvant treatment of skin infection. Future Microbiol. 10, 929–939. https://doi.org/10.2217/fmb.15.27

Bansal, M., Jamil, S., 2018. MICELLAR MICROPARTICLES: A NOVEL APPROACH TO TOPICAL DRUG DELIVERY SYSTEM. Int. J. Appl. Pharm. 10, 1. https://doi.org/10.22159/ijap.2018v10i5.27506

Barone, J.J., Roberts, H.R., 1996. Caffeine consumption. Food Chem. Toxicol. 34, 119–129. https://doi.org/10.1016/0278-6915(95)00093-3

Barry, B.W., 1987. Mode of action of penetration enhancers in human skin. J. Controlled Release 6, 85–97. https://doi.org/10.1016/0168-3659(87)90066-6

Bashari, A., Shakeri, M., Shirvan, A.R., Najafabadi, S.A.N., 2018. Functional Finishing of Textiles via Nanomaterials, in: ul-Islam, S., Butola, B.S. (Eds.), Nanomaterials in the Wet Processing of Textiles. John Wiley & Sons, Inc., Hoboken, NJ, USA, pp. 1–70. https://doi.org/10.1002/9781119459804.ch1

Basilico, N., Magnetto, C., D'Alessandro, S., Panariti, A., Rivolta, I., Genova, T., Khadjavi, A., Gulino, G.R., Argenziano, M., Soster, M., Cavalli, R., Giribaldi, G., Guiot, C., Prato, M., 2015. Dextran-shelled oxygen-loaded nanodroplets reestablish a normoxia-like pro-angiogenic phenotype and behavior in hypoxic human dermal microvascular endothelium. Toxicol. Appl. Pharmacol. 288, 330–338. https://doi.org/10.1016/j.taap.2015.08.005

Bassetti, M., Peghin, M., Castaldo, N., Giacobbe, D.R., 2019. The safety of treatment options for acute bacterial skin and skin structure infections. Expert Opin. Drug Saf. 18, 635–650. https://doi.org/10.1080/14740338.2019.1621288

Bastiancich, C., Scutera, S., Alotto, D., Cambieri, I., Fumagalli, M., Casarin, S., Rossi, S., Trotta, F., Stella, M., Cavalli, R., Musso, T., Castagnoli, C., 2014. Cyclodextrin-Based Nanosponges as a Nanotechnology Strategy for Imiquimod Delivery in Pathological Scarring Prevention and Treatment. J. Nanopharmaceutics Drug Deliv. 2, 311–324. https://doi.org/10.1166/jnd.2014.1071

Baum, L., Ng, A., 2004. Curcumin interaction with copper and iron suggests one possible mechanism of action in Alzheimer's disease animal models. J. Alzheimers Dis. JAD 6, 367–377; discussion 443-449.

Bazbouz, M., Tronci, G., 2019. Two-layer Electrospun System Enabling Wound Exudate Management and Visual Infection Response. Sensors 19, 991. https://doi.org/10.3390/s19050991

Bazylińska, U., Lewińska, A., Lamch, Ł., Wilk, K.A., 2014. Polymeric nanocapsules and nanospheres for encapsulation and long sustained release of hydrophobic cyanine-type photosensitizer. Colloids Surf. Physicochem. Eng. Asp. 442, 42–49. https://doi.org/10.1016/j.colsurfa.2013.02.023

Bazzano, M., 2018. Development of UV-based polymerization techniques for the production of drug delivery devices (PhD Thesis). Politecnico di Torino.

Bazzano, M., Pisano, R., Brelstaff, J., Spillantini, M.G., Sidoryk-Wegrzynowicz, M., Rizza, G., Sangermano, M., 2016. Synthesis of polymeric nanocapsules by radical UV-activated interface-emulsion polymerization. J. Polym. Sci. Part Polym. Chem. 54, 3357–3369. https://doi.org/10.1002/pola.28226

Benson, H.A., Sarveiya, V., Risk, S., Roberts, M.S., 2005. Influence of anatomical site and topical formulation on skin penetration of sunscreens. Ther. Clin. Risk Manag. 1, 209–218.

Bessada, S., Rita C. Alves, M. P. P. Oliveira, 2018. Coffee Silverskin: A Review on Potential Cosmetic Applications. Cosmetics 5, 5. https://doi.org/10.3390/cosmetics5010005

Beylot, C., Auffret, N., Poli, F., Claudel, J.-P., Leccia, M.-T., Del Giudice, P., Dreno, B., 2014. *Propionibacterium acnes* : an update on its role in the pathogenesis of acne. J. Eur. Acad. Dermatol. Venereol. 28, 271–278. https://doi.org/10.1111/jdv.12224

Bhattacharjee, S., 2016. DLS and zeta potential – What they are and what they are not? J. Controlled Release 235, 337–351. https://doi.org/10.1016/j.jconrel.2016.06.017

Bird, R.B., Stewart, W.E., Lightfoot, E.N., Sebastiani, E., 1979. Fenomeni di trasporto. CEA, Milano.

Bordes, C., Fréville, V., Ruffin, E., Marote, P., Gauvrit, J.Y., Briançon, S., Lantéri, P., 2010. Determination of poly(ε-caprolactone) solubility parameters: Application to solvent substitution in a microencapsulation process. Int. J. Pharm. 383, 236–243. https://doi.org/10.1016/j.ijpharm.2009.09.023

Bornare, A.S., Saudagar, R.B., 2017. Nanostructured Lipid Carrier (NLC): A Modern Approach for Transdermal Drug Delivery. Res. J. Pharm. Technol. 10, 2784. https://doi.org/10.5958/0974-360X.2017.00493.0

Brainard, G.C., 1978. Pineal research: the decade of transformation. J. Neural Transm. Suppl. 3–10.

Briggaman, R.A., Wheeler, C.E., 1975. The epidermal-dermal junction. J. Invest. Dermatol. 65, 71–84.

Budai, L., 2013. Liposomes for Topical Use: A Physico-Chemical Comparison of Vesicles Prepared from Egg or Soy Lecithin. Sci. Pharm. 81, 1151–1166. https://doi.org/10.3797/scipharm.1305-11

Budhian, A., Siegel, S.J., Winey, K.I., 2007. Haloperidol-loaded PLGA nanoparticles: Systematic study of particle size and drug content. Int. J. Pharm. 336, 367–375. https://doi.org/10.1016/j.ijpharm.2006.11.061

Burgess, D.J., 1994. Complex Coacervation: Microcapsule Formation, in: Dubin, P., Bock, J., Davis, R., Schulz, D.N., Thies, C. (Eds.), Macromolecular Complexes in Chemistry and

Biology. Springer Berlin Heidelberg, Berlin, Heidelberg, pp. 285–300. https://doi.org/10.1007/978-3-642-78469-9_17

Butstraen, C., Salaün, F., Devaux, E., Giraud, S., Vroman, P., 2016. Application of Flame-Retardant Double-Layered Shell Microcapsules to Nonwoven Polyester. Polymers 8, 267. https://doi.org/10.3390/polym8070267

Butt, S., Hasan, S.M.F., Hassan, M.M., Alkharfy, K.M., Neau, S.H., 2019. Directly compressed rosuvastatin calcium Tablets that offer hydrotropic and micellar solubilization for improved dissolution rate and extent of drug release. Saudi Pharm. J. 27, 619–628. https://doi.org/10.1016/j.jsps.2019.03.002

Cal, K., Sollohub, K., 2010. Spray Drying Technique. I: Hardware and Process Parameters. J. Pharm. Sci. 99, 575–586. https://doi.org/10.1002/jps.21886

Camerlo, A., Vebert-Nardin, C., Rossi, R.M., Popa, Ana.-M., 2013. Fragrance encapsulation in polymeric matrices by emulsion electrospinning. Eur. Polym. J. 49, 3806–3813. https://doi.org/10.1016/j.eurpolymj.2013.08.028

Carneiro, S., Costa Duarte, F., Heimfarth, L., Siqueira Quintans, J., Quintans-Júnior, L., Veiga Júnior, V., Neves de Lima, Á., 2019. Cyclodextrin–Drug Inclusion Complexes: In Vivo and In Vitro Approaches. Int. J. Mol. Sci. 20, 642. https://doi.org/10.3390/ijms20030642

Carrer, V., Guzmán, B., Martí, M., Alonso, C., Coderch, L., 2018. Lanolin-Based Synthetic Membranes as Percutaneous Absorption Models for Transdermal Drug Delivery. Pharmaceutics 10, 73. https://doi.org/10.3390/pharmaceutics10030073

Carreras, N., Alonso, C., Martí, M., Lis, M.J., 2015. Mass transport model through the skin by microencapsulation system. J. Microencapsul. 32, 358–363. https://doi.org/10.3109/02652048.2015.1028495

Cavalli, R., Soster, M., Argenziano, M., 2016. Nanobubbles: a promising efficienft tool for therapeutic delivery. Ther. Deliv. 7, 117–138. https://doi.org/10.4155/tde.15.92

Chatterjee, S., Hui, P., Kan, C., 2018. Thermoresponsive Hydrogels and Their Biomedical Applications: Special Insight into Their Applications in Textile Based Transdermal Therapy. Polymers 10, 480. https://doi.org/10.3390/polym10050480

Chen, T., Li, C., Li, Y., Yi, X., Wang, R., Lee, S.M.-Y., Zheng, Y., 2017. Small-Sized mPEG–PLGA Nanoparticles of Schisantherin A with Sustained Release for Enhanced Brain Uptake and Anti-Parkinsonian Activity. ACS Appl. Mater. Interfaces 9, 9516–9527. https://doi.org/10.1021/acsami.7b01171

Chen, Y.-Y., Lu, Y.-H., Ma, C.-H., Tao, W.-W., Zhu, J.-J., Zhang, X., 2017. A novel elastic liposome for skin delivery of papain and its application on hypertrophic scar. Biomed. Pharmacother. 87, 82–91. https://doi.org/10.1016/j.biopha.2016.12.076

Chien, Y.W., Valia, K.H., 1984. Development of a Dynamic Skin Permeation System for Long-Term Permeation Studies. Drug Dev. Ind. Pharm. 10, 575–599. https://doi.org/10.3109/03639048409041408

Chilajwar, S.V., Pednekar, P.P., Jadhav, K.R., Gupta, G.J., Kadam, V.J., 2014. Cyclodextrin-based nanosponges: a propitious platform for enhancing drug delivery. Expert Opin. Drug Deliv. 11, 111–120. https://doi.org/10.1517/17425247.2014.865013

Chiou, H., Chan, H.-K., Heng, D., Prud'homme, R.K., Raper, J.A., 2008. A novel production method for inhalable cyclosporine A powders by confined liquid impinging jet precipitation. J. Aerosol Sci. 39, 500–509. https://doi.org/10.1016/j.jaerosci.2008.02.002

Choi, Y.-J., Chung, S.-T., Oh, M., Kim, H.-S., 2005. Investigation of Crystallization in a Jet Y-Mixer by a Hybrid Computational Fluid Dynamics and Process Simulation Approach. Cryst. Growth Des. 5, 959–968. https://doi.org/10.1021/cg049670x

Chorilli, M., Calixto, G., Rimério, T.C., Scarpa, M.V., 2013. Caffeine Encapsulated in Small Unilamellar Liposomes: Characerization and In Vitro Release Profile. J. Dispers. Sci. Technol. 34, 1465–1470. https://doi.org/10.1080/01932691.2012.739535

Chow, S.F., Sun, C.C., Chow, A.H.L., 2014. Assessment of the relative performance of a confined impinging jets mixer and a multi-inlet vortex mixer for curcumin nanoparticle production. Eur. J. Pharm. Biopharm. 88, 462–471. https://doi.org/10.1016/j.ejpb.2014.07.004

Chow, S.F., Wan, K.Y., Cheng, K.K., Wong, K.W., Sun, C.C., Baum, L., Chow, A.H.L., 2015. Development of highly stabilized curcumin nanoparticles by flash nanoprecipitation and lyophilization. Eur. J. Pharm. Biopharm. 94, 436–449. https://doi.org/10.1016/j.ejpb.2015.06.022

Chuang, S.-Y., Lin, Y.-K., Lin, C.-F., Wang, P.-W., Chen, E.-L., Fang, J.-Y., 2017. Elucidating the Skin Delivery of Aglycone and Glycoside Flavonoids: How the Structures Affect Cutaneous Absorption. Nutrients 9, 1304. https://doi.org/10.3390/nu9121304

Cintra, G., Pinto, L., Calixto, G., Soares, C., Von Zuben, E., Scarpa, M., Gremião, M., Chorilli, M., 2016. Bioadhesive Surfactant Systems for Methotrexate Skin Delivery. Molecules 21, 231. https://doi.org/10.3390/molecules21020231

Cintrón, M., Hinchliffe, D., 2015. FT-IR Examination of the Development of Secondary Cell Wall in Cotton Fibers. Fibers 3, 30–40. https://doi.org/10.3390/fib3010030

Claustrat, B., Brun, J., Chazot, G., 2005. The basic physiology and pathophysiology of melatonin. Sleep Med. Rev. 9, 11–24. https://doi.org/10.1016/j.smrv.2004.08.001

Contado, C., Vighi, E., Dalpiaz, A., Leo, E., 2013. Influence of secondary preparative parameters and aging effects on PLGA particle size distribution: a sedimentation field flow fractionation investigation. Anal. Bioanal. Chem. 405, 703–711. https://doi.org/10.1007/s00216-012-6113-5

Conte, C., Caldera, F., Catanzano, O., D'Angelo, I., Ungaro, F., Miro, A., Pellosi, D.S., Trotta, F., Quaglia, F., 2014. β-Cyclodextrin Nanosponges as Multifunctional Ingredient in Water-Containing Semisolid Formulations for Skin Delivery. J. Pharm. Sci. 103, 3941–3949. https://doi.org/10.1002/jps.24203

Coradini, K., Lima, F.O., Oliveira, C.M., Chaves, P.S., Athayde, M.L., Carvalho, L.M., Beck, R.C.R., 2014. Co-encapsulation of resveratrol and curcumin in lipid-core nanocapsules improves their in vitro antioxidant effects. Eur. J. Pharm. Biopharm. 88, 178–185. https://doi.org/10.1016/j.ejpb.2014.04.009

Costa, P., Sousa Lobo, J.M., 2001. Modeling and comparison of dissolution profiles. Eur. J. Pharm. Sci. 13, 123–133. https://doi.org/10.1016/S0928-0987(01)00095-1

Coulembier, O., Degée, P., Hedrick, J.L., Dubois, P., 2006. From controlled ring-opening polymerization to biodegradable aliphatic polyester: Especially poly(β-malic acid) derivatives. Prog. Polym. Sci. 31, 723–747. https://doi.org/10.1016/j.progpolymsci.2006.08.004

Cui, H., Jin, Z., Zheng, D., Tang, W., Li, Y., Yun, Y., Lo, T.Y., Xing, F., 2018. Effect of carbon fibers grafted with carbon nanotubes on mechanical properties of cement-based composites. Constr. Build. Mater. 181, 713–720. https://doi.org/10.1016/j.conbuildmat.2018.06.049

Czajkowska-Kośnik, A., Szekalska, M., Winnicka, K., 2019. Nanostructured lipid carriers: A potential use for skin drug delivery systems. Pharmacol. Rep. 71, 156–166. https://doi.org/10.1016/j.pharep.2018.10.008

da Silva, E.Z.M., Jamur, M.C., Oliver, C., 2014. Mast Cell Function: A New Vision of an Old Cell. J. Histochem. Cytochem. 62, 698–738. https://doi.org/10.1369/0022155414545334

D'Addio, S.M., Kafka, C., Akbulut, M., Beattie, P., Saad, W., Herrera, M., Kennedy, M.T., Prud'homme, R.K., 2010. Novel Method for Concentrating and Drying Polymeric Nanoparticles: Hydrogen Bonding Coacervate Precipitation. Mol. Pharm. 7, 557–564. https://doi.org/10.1021/mp900260q

D'Addio, S.M., Prud'homme, R.K., 2011. Controlling drug nanoparticle formation by rapid precipitation. Adv. Drug Deliv. Rev. 63, 417–426. https://doi.org/10.1016/j.addr.2011.04.005

Darlenski, R., Fluhr, J.W., 2012. Influence of skin type, race, sex, and anatomic location on epidermal barrier function. Clin. Dermatol. 30, 269–273. https://doi.org/10.1016/j.clindermatol.2011.08.013

De Falco, F., Guarino, V., Gentile, G., Cocca, M., Ambrogi, V., Ambrosio, L., Avella, M., 2019. Design of functional textile coatings via non-conventional electrofluidodynamic processes. J. Colloid Interface Sci. 541, 367–375. https://doi.org/10.1016/j.jcis.2019.01.086

Devasagayam, T.P.A., Kamat, J.P., Mohan, H., Kesavan, P.C., 1996. Caffeine as an antioxidant: inhibition of lipid peroxidation induced by reactive oxygen species. Biochim. Biophys. Acta BBA - Biomembr. 1282, 63–70. https://doi.org/10.1016/0005-2736(96)00040-5

Dharadhar, S., Majumdar, A., Dhoble, S., Patravale, V., 2019. Microneedles for transdermal drug delivery: a systematic review. Drug Dev. Ind. Pharm. 45, 188–201. https://doi.org/10.1080/03639045.2018.1539497

Di Pasquale, N., Marchisio, D.L., Barresi, A.A., 2012. Model validation for precipitation in solvent-displacement processes. Chem. Eng. Sci. 84, 671–683. https://doi.org/10.1016/j.ces.2012.08.043

Di Pasquale, N., Marchisio, D.L., Barresi, A.A., Carbone, P., 2014. Solvent Structuring and Its Effect on the Polymer Structure and Processability: The Case of Water–Acetone Poly-ε-caprolactone Mixtures. J. Phys. Chem. B 118, 13258–13267. https://doi.org/10.1021/jp505348t

Dias, M., 1999. Topical delivery of caffeine from some commercial formulations. Int. J. Pharm. 182, 41–47. https://doi.org/10.1016/S0378-5173(99)00067-8

Ding, J., Zhang, J., Li, J., Li, D., Xiao, C., Xiao, H., Yang, H., Zhuang, X., Chen, X., 2019. Electrospun polymer biomaterials. Prog. Polym. Sci. 90, 1–34. https://doi.org/10.1016/j.progpolymsci.2019.01.002

Diss, L.B., Robinson, S.D., Wu, Y., Fidalgo, S., Yeoman, M.S., Patel, B.A., 2013. Age-Related Changes in Melatonin Release in the Murine Distal Colon. ACS Chem. Neurosci. 4, 879–887. https://doi.org/10.1021/cn4000617

Dochia, M., Sirghie, C., Kozłowski, R.M., Roskwitalski, Z., 2012. Cotton fibres, in: Handbook of Natural Fibres. Elsevier, pp. 11–23. https://doi.org/10.1533/9780857095503.1.9

Donaldson, S.H., Jahnke, J.P., Messinger, R.J., Östlund, Å., Uhrig, D., Israelachvili, J.N., Chmelka, B.F., 2016. Correlated Diffusivities, Solubilities, and Hydrophobic Interactions in Ternary

Polydimethylsiloxane–Water–Tetrahydrofuran Mixtures. Macromolecules 49, 6910–6917. https://doi.org/10.1021/acs.macromol.6b01514

Dong, Y., Feng, S.-S., 2004. Methoxy poly(ethylene glycol)-poly(lactide) (MPEG-PLA) nanoparticles for controlled delivery of anticancer drugs. Biomaterials 25, 2843–2849. https://doi.org/10.1016/j.biomaterials.2003.09.055

Doshi, J., Reneker, D.H., 1995. Electrospinning process and applications of electrospun fibers. J. Electrost. 35, 151–160. https://doi.org/10.1016/0304-3886(95)00041-8

EC, 2009. Anon (2009) Regulation (EC) No 1223/2009 of the European Parliament and of the Council of 30 November 2009 on cosmetic products. Off. J. EU L. 342, 59–209.

Eckhart, L., Lippens, S., Tschachler, E., Declercq, W., 2013. Cell death by cornification. Biochim. Biophys. Acta BBA - Mol. Cell Res. 1833, 3471–3480. https://doi.org/10.1016/j.bbamcr.2013.06.010

Elzein, T., Nasser-Eddine, M., Delaite, C., Bistac, S., Dumas, P., 2004. FTIR study of polycaprolactone chain organization at interfaces. J. Colloid Interface Sci. 273, 381–387. https://doi.org/10.1016/j.jcis.2004.02.001

EN ISO, 2018. EN ISO 10993. Biological evaluation of medical devices -- Part 1: Evaluation and testing within a risk management process.

Esatbeyoglu, T., Huebbe, P., Ernst, I.M.A., Chin, D., Wagner, A.E., Rimbach, G., 2012. Curcumin-From Molecule to Biological Function. Angew. Chem. Int. Ed. 51, 5308–5332. https://doi.org/10.1002/anie.201107724

Espinosa-Andrews, H., Báez-González, J.G., Cruz-Sosa, F., Vernon-Carter, E.J., 2007. Gum Arabic−Chitosan Complex Coacervation. Biomacromolecules 8, 1313–1318. https://doi.org/10.1021/bm0611634

Eugene Kellogg, G., Abraham, D.J., 2000. Hydrophobicity: is LogPo/w more than the sum of its parts? Eur. J. Med. Chem. 35, 651–661. https://doi.org/10.1016/S0223-5234(00)00167-7

European Pharmacopeia, 2001. Addendum 2001, Dissolution test for transdermal dosage forms. Conseil de l'Europe, Strasbourg, France, Section 2.9.4, pp 110-111.

Fang, J., Lu, J., Holmgren, A., 2005. Thioredoxin reductase is irreversibly modified by curcumin: a novel molecular mechanism for its anticancer activity. J. Biol. Chem. 280, 25284–25290. https://doi.org/10.1074/jbc.M414645200

Fathi-Azarbayjani, A., Qun, L., Chan, Y.W., Chan, S.Y., 2010. Novel Vitamin and Gold-Loaded Nanofiber Facial Mask for Topical Delivery. AAPS PharmSciTech 11, 1164–1170. https://doi.org/10.1208/s12249-010-9475-z

FDA, 2014. Guidance for Industry: Safety of Nanomaterials in Cosmetic Products; Availability, 36532-36533 [2014-15032] :: Food And Drug Administration :: Department Of Health And Human Services :: Regulation Tracker :: Justia [WWW Document]. URL https://regulations.justia.com/regulations/fedreg/2014/06/27/2014-15032.html (accessed 10.7.19).

FDA, 2007. Nanotechnology Task Force Report 2007 [WWW Document]. URL https://www.fda.gov/science-research/nanotechnology-programs-fda/nanotechnology-task-force-report-2007 (accessed 10.7.19).

Fernández-Caramés, T., Fraga-Lamas, P., 2018. Towards The Internet-of-Smart-Clothing: A Review on IoT Wearables and Garments for Creating Intelligent Connected E-Textiles. Electronics 7, 405. https://doi.org/10.3390/electronics7120405

Ferrari, E., Asti, M., Benassi, R., Pignedoli, F., Saladini, M., 2013. Metal binding ability of curcumin derivatives: a theoretical vs. experimental approach. Dalton Trans. 42, 5304. https://doi.org/10.1039/c3dt33072a

Ferri, A., Kumari, N., Peila, R., Barresi, A.A., 2017. Production of menthol-loaded nanoparticles by solvent displacement. Can. J. Chem. Eng. 95, 1690–1706. https://doi.org/10.1002/cjce.22867

Fessi, H., Puisieux, F., Devissaguet, J.Ph., Ammoury, N., Benita, S., 1989. Nanocapsule formation by interfacial polymer deposition following solvent displacement. Int. J. Pharm. 55, R1–R4. https://doi.org/10.1016/0378-5173(89)90281-0

Figueira, D.R., Miguel, S.P., de Sá, K.D., Correia, I.J., 2016. Production and characterization of polycaprolactone- hyaluronic acid/chitosan- zein electrospun bilayer nanofibrous membrane for tissue regeneration. Int. J. Biol. Macromol. 93, 1100–1110. https://doi.org/10.1016/j.ijbiomac.2016.09.080

Fischer, T.W., Hipler, U.C., Elsner, P., 2007. Effect of caffeine and testosterone on the proliferation of human hair follicles *in vitro*: Caffeine and testosterone. Int. J. Dermatol. 46, 27–35. https://doi.org/10.1111/j.1365-4632.2007.03119.x

Fontana, M.C., Durli, T.L., Pohlmann, A.R., Guterres, S.S., Beck, R.C.R., 2014. Polymeric controlled release inhalable powder produced by vibrational spray-drying: One-step preparation and in vitro lung deposition. Powder Technol. 258, 49–59. https://doi.org/10.1016/j.powtec.2014.03.011

Freeman, S.C., Sonthalia, S., 2019. Histology, Keratohyalin Granules, in: StatPearls. StatPearls Publishing, Treasure Island (FL).

Freitas, S., Merkle, H.P., Gander, B., 2005. Microencapsulation by solvent extraction/evaporation: reviewing the state of the art of microsphere preparation process technology. J. Control. Release Off. J. Control. Release Soc. 102, 313–332. https://doi.org/10.1016/j.jconrel.2004.10.015

Furusawa, M., Narita, Y., Iwai, K., Fukunaga, T., Nakagiri, O., 2011. Inhibitory Effect of a Hot Water Extract of Coffee "Silverskin" on Hyaluronidase. Biosci. Biotechnol. Biochem. 75, 1205–1207. https://doi.org/10.1271/bbb.110106

Ganachaud, F., Katz, J.L., 2005. Nanoparticles and Nanocapsules Created Using the Ouzo Effect: Spontaneous Emulsification as an Alternative to Ultrasonic and High-Shear Devices. ChemPhysChem 6, 209–216. https://doi.org/10.1002/cphc.200400527

Garino, N., Limongi, T., Dumontel, B., Canta, M., Racca, L., Laurenti, M., Castellino, M., Casu, A., Falqui, A., Cauda, V., 2019. A Microwave-Assisted Synthesis of Zinc Oxide Nanocrystals Finely Tuned for Biological Applications. Nanomaterials 9, 212. https://doi.org/10.3390/nano9020212

Gavi, E., Rivautella, L., Marchisio, D.L., Vanni, M., Barresi, A.A., Baldi, G., 2007. CFD Modelling of Nano-Particle Precipitation in Confined Impinging Jet Reactors. Chem. Eng. Res. Des. 85, 735–744. https://doi.org/10.1205/cherd06176

Ghayempour, S., Montazer, M., 2017. Tragacanth nanocapsules containing Chamomile extract prepared through sono-assisted W/O/W microemulsion and UV cured on cotton fabric. Carbohydr. Polym. 170, 234–240. https://doi.org/10.1016/j.carbpol.2017.04.088

Gindy, M.E., Prud'homme, R.K., 2009. Multifunctional nanoparticles for imaging, delivery and targeting in cancer therapy. Expert Opin. Drug Deliv. 6, 865–878. https://doi.org/10.1517/17425240902932908

Ginsberg, G., Hattis, D., Russ, A., Sonawane, B., 2004. Physiologically Based Pharmacokinetic (PBPK) Modeling of Caffeine and Theophylline in Neonates and Adults: Implications for Assessing Children's Risks from Environmental Agents. J. Toxicol. Environ. Health A 67, 297–329. https://doi.org/10.1080/15287390490273550

Goldstein, E.R., Ziegenfuss, T., Kalman, D., Kreider, R., Campbell, B., Wilborn, C., Taylor, L., Willoughby, D., Stout, J., Graves, B.S., Wildman, R., Ivy, J.L., Spano, M., Smith, A.E., Antonio, J., 2010. International society of sports nutrition position stand: caffeine and performance. J. Int. Soc. Sports Nutr. 7, 5. https://doi.org/10.1186/1550-2783-7-5

Goletz, S., Zillikens, D., Schmidt, E., 2017. Structural proteins of the dermal-epidermal junction targeted by autoantibodies in pemphigoid diseases. Exp. Dermatol. 26, 1154–1162. https://doi.org/10.1111/exd.13446

Gómez-Mascaraque, L.G., Sanchez, G., López-Rubio, A., 2016. Impact of molecular weight on the formation of electrosprayed chitosan microcapsules as delivery vehicles for bioactive compounds. Carbohydr. Polym. 150, 121–130. https://doi.org/10.1016/j.carbpol.2016.05.012

Goodman, J.T., Mullis, A.S., Dunshee, L., Mitra, A., Narasimhan, B., 2018. Automated High-Throughput Synthesis of Protein-Loaded Polyanhydride Nanoparticle Libraries. ACS Comb. Sci. 20, 298–307. https://doi.org/10.1021/acscombsci.8b00008

Gouin, S., 2004. Microencapsulation. Trends Food Sci. Technol. 15, 330–347. https://doi.org/10.1016/j.tifs.2003.10.005

Greiner, A., Wendorff, J.H., 2007. Electrospinning: A Fascinating Method for the Preparation of Ultrathin Fibers. Angew. Chem. Int. Ed. 46, 5670–5703. https://doi.org/10.1002/anie.200604646

Grishanov, S., 2011. Structure and properties of textile materials, in: Handbook of Textile and Industrial Dyeing. Elsevier, pp. 28–63. https://doi.org/10.1533/9780857093974.1.28

Groenewoud, W.M., 2001a. THERMOGRAVIMETRY, in: Characterisation of Polymers by Thermal Analysis. Elsevier, pp. 61–76. https://doi.org/10.1016/B978-044450604-7/50003-0

Groenewoud, W.M., 2001b. DIFFERENTIAL SCANNING CALORIMETRY, in: Characterisation of Polymers by Thermal Analysis. Elsevier, pp. 10–60. https://doi.org/10.1016/B978-044450604-7/50002-9

Gulino, G.R., Magnetto, C., Khadjavi, A., Panariti, A., Rivolta, I., Soster, M., Argenziano, M., Cavalli, R., Giribaldi, G., Guiot, C., Prato, M., 2015. Oxygen-Loaded Nanodroplets Effectively Abrogate Hypoxia Dysregulating Effects on Secretion of MMP-9 and TIMP-1 by Human Monocytes. Mediators Inflamm. 2015, 1–11. https://doi.org/10.1155/2015/964838

Gupta, S.C., Patchva, S., Koh, W., Aggarwal, B.B., 2012. Discovery of curcumin, a component of golden spice, and its miraculous biological activities: Multitargeting by curcumin. Clin. Exp. Pharmacol. Physiol. 39, 283–299. https://doi.org/10.1111/j.1440-1681.2011.05648.x

Gurarslan, A., Shen, J., Tonelli, A.E., 2013. Single-component poly(ε-caprolactone) composites. Polymer 54, 5747–5753. https://doi.org/10.1016/j.polymer.2013.08.017

Haase, H., Jordan, L., Keitel, L., Keil, C., Mahltig, B., 2017. Comparison of methods for determining the effectiveness of antibacterial functionalized textiles. PLOS ONE 12, e0188304. https://doi.org/10.1371/journal.pone.0188304

Hadgraft, J., Lane, M.E., 2016. Drug crystallization – implications for topical and transdermal delivery. Expert Opin. Drug Deliv. 1–14. https://doi.org/10.1517/17425247.2016.1140146

Haider, S., Haider, A., A. Alghyamah, A., Khan, R., A. Almasry, W., Khan, N., 2019. Electrohydrodynamic Processes and Their Affecting Parameters, in: Haider, S., Haider, A. (Eds.), Electrospinning and Electrospraying - Techniques and Applications. IntechOpen. https://doi.org/10.5772/intechopen.89929

Haj-Ahmad, R., Khan, H., Arshad, M., Rasekh, M., Hussain, A., Walsh, S., Li, X., Chang, M.-W., Ahmad, Z., 2015. Microneedle Coating Techniques for Transdermal Drug Delivery. Pharmaceutics 7, 486–502. https://doi.org/10.3390/pharmaceutics7040486

Hamburg, M.A., 2012. FDA's Approach to Regulation of Products of Nanotechnology. Science 336, 299–300. https://doi.org/10.1126/science.1205441

Han, J., Zhu, Z., Qian, H., Wohl, A.R., Beaman, C.J., Hoye, T.R., Macosko, C.W., 2012. A simple confined impingement jets mixer for flash nanoprecipitation. J. Pharm. Sci. 101, 4018–4023. https://doi.org/10.1002/jps.23259

Han, Y., Liu, W., Huang, J., Qiu, S., Zhong, H., Liu, D., Liu, J., 2018. Cyclodextrin-Based Metal-Organic Frameworks (CD-MOFs) in Pharmaceutics and Biomedicine. Pharmaceutics 10, 271. https://doi.org/10.3390/pharmaceutics10040271

Hao, J., Ghosh, P., Li, S.K., Newman, B., Kasting, G.B., Raney, S.G., 2016. Heat effects on drug delivery across human skin. Expert Opin. Drug Deliv. 13, 755–768. https://doi.org/10.1517/17425247.2016.1136286

Haque, T., Talukder, M.M.U., 2018. Chemical Enhancer: A Simplistic Way to Modulate Barrier Function of the Stratum Corneum. Adv. Pharm. Bull. 8, 169–179. https://doi.org/10.15171/apb.2018.021

Harpaz, E., Tamir, S., Weinstein, A., Weinstein, Y., 2017. The effect of caffeine on energy balance. J. Basic Clin. Physiol. Pharmacol. 28, 1–10. https://doi.org/10.1515/jbcpp-2016-0090

Hartmann, X., van der Linde, P., Homburg, E., van Breemen, L., de Jong, A., Luttge, R., 2015. Insertion Process of Ceramic Nanoporous Microneedles by Means of a Novel Mechanical Applicator Design. Pharmaceutics 7, 503–522. https://doi.org/10.3390/pharmaceutics7040503

Hassabo, A., Mohamed, A., Nada, A., Zeid, N., 2015. Controlled Release of Drugs from Cellulosic Wound Bandage Using Silica Microsphere as Drug Encapsulator Module. J. Appl. Pharm. Sci. 067–073. https://doi.org/10.7324/JAPS.2015.501211

Hassan, M.M., Sunderland, M., 2015. Antimicrobial and insect-resist wool fabrics by coating with microencapsulated antimicrobial and insect-resist agents. Prog. Org. Coat. 85, 221–229. https://doi.org/10.1016/j.porgcoat.2015.04.016

Hayashi, T., 1994. Biodegradable polymers for biomedical uses. Prog. Polym. Sci. 19, 663–702. https://doi.org/10.1016/0079-6700(94)90030-2

Heckman, M.A., Weil, J., de Mejia, E.G., 2010. Caffeine (1, 3, 7-trimethylxanthine) in Foods: A Comprehensive Review on Consumption, Functionality, Safety, and Regulatory Matters. J. Food Sci. 75, R77–R87. https://doi.org/10.1111/j.1750-3841.2010.01561.x

Heller, W., Klevens, H.B., Oppenheimer, H., 1946. The Determination of Particle Sizes from Tyndall Spectra. J. Chem. Phys. 14, 566–567. https://doi.org/10.1063/1.1724197

Hellwege, K.H., 1969. Landolt-Bornstein, Numerical Data and Functional Relationship in Science and Technology, 6th edition, Vol II/5a, Transport Phenomena (Viscosity and Diffusion). Springer Verlag, Heidelberg.

Herman, A., Herman, A.P., 2013. Caffeine's mechanisms of action and its cosmetic use. Skin Pharmacol. Physiol. 26, 8–14. https://doi.org/10.1159/000343174

Herrmann, J., Bodmeier, R., 1998. Biodegradable, somatostatin acetate containing microspheres prepared by various aqueous and non-aqueous solvent evaporation methods. Eur. J. Pharm. Biopharm. 45, 75–82. https://doi.org/10.1016/S0939-6411(97)00125-2

Hickey, J.W., Santos, J.L., Williford, J.-M., Mao, H.-Q., 2015. Control of polymeric nanoparticle size to improve therapeutic delivery. J. Controlled Release 219, 536–547. https://doi.org/10.1016/j.jconrel.2015.10.006

Holgado, M.A., Martin-banderas, Alvarez-fuentes, Duran-lobato, Prados, J., Melguizo, Fernandez-arevalo, 2012. Cannabinoid derivate-loaded PLGA nanocarriers for oral administration: formulation, characterization, and cytotoxicity studies. Int. J. Nanomedicine 5793. https://doi.org/10.2147/IJN.S34633

Hong, I.K., Ha, J.H., Han, S., Kang, H., Park, S.N., 2018. The Effect of Alkyl Chain Number in Sucrose Surfactant on the Physical Properties of Quercetin-Loaded Deformable Nanoliposome and Its Effect on In Vitro Human Skin Penetration. Nanomaterials 8, 622. https://doi.org/10.3390/nano8080622

Hoseinzadeh, E., Makhdoumi, P., Taha, P., Hossini, H., Stelling, J., Amjad Kamal, M., Md. Ashraf, G., 2017. A Review on Nano-Antimicrobials: Metal Nanoparticles, Methods and Mechanisms. Curr. Drug Metab. 18, 120–128. https://doi.org/10.2174/1389200217666161201111146

Hsiao, K.-H., Huang, C.-M., Lee, Y.-H., 2018. Development of Rifampicin-Indocyanine Green-Loaded Perfluorocarbon Nanodroplets for Photo-Chemo-Probiotic Antimicrobial Therapy. Front. Pharmacol. 9, 1254. https://doi.org/10.3389/fphar.2018.01254

Hu, J., Xiao, Z.-B., Zhou, R.-J., Ma, S.-S., Li, Z., Wang, M.-X., 2011. Comparison of compounded fragrance and chitosan nanoparticles loaded with fragrance applied in cotton fabrics. Text. Res. J. 81, 2056–2064. https://doi.org/10.1177/0040517511416274

Hu, J.-F., Li, S.-F., Raghavan Nair, G., Wu, W.-T., 2012. Predicting chitosan particle size produced by electrohydrodynamic atomization. Chem. Eng. Sci. 82, 159–165. https://doi.org/10.1016/j.ces.2012.07.034

Hubert, S., Briancon, S., Hedoux, A., Guinet, Y., Paccou, L., Fessi, H., Puel, F., 2011. Process induced transformations during Tablet manufacturing: Phase transition analysis of caffeine using DSC and low frequency micro-Raman spectroscopy. Int. J. Pharm. 420, 76–83. https://doi.org/10.1016/j.ijpharm.2011.08.028

Hui, P.C.-L., Wang, W.-Y., Kan, C.-W., Ng, F.S.-F., Wat, E., Zhang, V.X., Chan, C.-L., Lau, C.B.-S., Leung, P.-C., 2013a. Microencapsulation of Traditional Chinese Herbs—PentaHerbs extracts and potential application in healthcare textiles. Colloids Surf. B Biointerfaces 111, 156–161. https://doi.org/10.1016/j.colsurfb.2013.05.036

Hui, P.C.-L., Wang, W.-Y., Kan, C.-W., Ng, F.S.-F., Zhou, C.-E., Wat, E., Zhang, V.X., Chan, C.-L., Lau, C.B.-S., Leung, P.-C., 2013b. Preparation and characterization of chitosan/sodium alginate (CSA) microcapsule containing Cortex Moutan. Colloids Surf. Physicochem. Eng. Asp. 434, 95–101. https://doi.org/10.1016/j.colsurfa.2013.05.043

Hussain, A., Haque, M.W., Singh, S.K., Ahmed, F.J., 2016. Optimized permeation enhancer for topical delivery of 5-fluorouracil-loaded elastic liposome using Design Expert: part II. Drug Deliv. 23, 1242–1253. https://doi.org/10.3109/10717544.2015.1124473

Ikuta, D., Hirata, Y., Wakamori, S., Shimada, H., Tomabechi, Y., Kawasaki, Y., Ikeuchi, K., Hagimori, T., Matsumoto, S., Yamada, H., 2019. Conformationally supple glucose monomers enable synthesis of the smallest cyclodextrins. Science 364, 674–677. https://doi.org/10.1126/science.aaw3053

Islam, M.S., Deng, Y., Tong, L., Faisal, S.N., Roy, A.K., Minett, A.I., Gomes, V.G., 2016. Grafting carbon nanotubes directly onto carbon fibers for superior mechanical stability: Towards next generation aerospace composites and energy storage applications. Carbon 96, 701–710. https://doi.org/10.1016/j.carbon.2015.10.002

Ita, K., 2016. Transdermal iontophoretic drug delivery: advances and challenges. J. Drug Target. 24, 386–391. https://doi.org/10.3109/1061186X.2015.1090442

Izumi, R., Azuma, K., Izawa, H., Morimoto, M., Nagashima, M., Osaki, T., Tsuka, T., Imagawa, T., Ito, N., Okamoto, Y., Saimoto, H., Ifuku, S., 2016. Chitin nanofibrils suppress skin

inflammation in atopic dermatitis-like skin lesions in NC/Nga mice. Carbohydr. Polym. 146, 320–327. https://doi.org/10.1016/j.carbpol.2016.03.068

Jackson, C.J., Tønseth, K.A., Utheim, T.P., 2017. Cultured epidermal stem cells in regenerative medicine. Stem Cell Res. Ther. 8, 155. https://doi.org/10.1186/s13287-017-0587-1

Jain, A.K., Thareja, S., 2019. *In vitro* and *in vivo* characterization of pharmaceutical nanocarriers used for drug delivery. Artif. Cells Nanomedicine Biotechnol. 47, 524–539. https://doi.org/10.1080/21691401.2018.1561457

Jandova, Z., Gill, S.C., Lim, N.M., Mobley, D.L., Oostenbrink, C., 2019. Binding Modes and Metabolism of Caffeine. Chem. Res. Toxicol. 32, 1374–1383. https://doi.org/10.1021/acs.chemrestox.9b00030

Jasim, F., Talib, T., 1992. Some observations on the thermal behaviour of curcumin under air and argon atmospheres. J. Therm. Anal. 38, 2549–2552. https://doi.org/10.1007/BF01974631

Javadi Toghchi, M., Campagne, C., Cayla, A., Bruniaux, P., Loghin, C., Cristian, I., Burgnies, L., Chen, Y., 2019. Electrical conductivity enhancement of hybrid PA6,6 composite containing multiwall carbon nanotube and carbon black for shielding effectiveness application in textiles. Synth. Met. 251, 75–84. https://doi.org/10.1016/j.synthmet.2019.03.026

Jenjob, R., Phakkeeree, T., Seidi, F., Theerasilp, M., Crespy, D., 2019. Emulsion Techniques for the Production of Pharmacological Nanoparticles. Macromol. Biosci. 19, 1900063. https://doi.org/10.1002/mabi.201900063

Jeong, H.J., Nam, S.J., Song, J.Y., Park, S.N., 2019. Synthesis and physicochemical properties of pH-sensitive hydrogel based on carboxymethyl chitosan/2-hydroxyethyl acrylate for transdermal delivery of nobiletin. J. Drug Deliv. Sci. Technol. 51, 194–203. https://doi.org/10.1016/j.jddst.2019.02.029

Jiang, A.-J., Jiang, G., Li, L.-T., Zheng, J.-N., 2015. Curcumin induces apoptosis through mitochondrial pathway and caspases activation in human melanoma cells. Mol. Biol. Rep. 42, 267–275. https://doi.org/10.1007/s11033-014-3769-2

Jin, G., Prabhakaran, M.P., Ramakrishna, S., 2011. Stem cell differentiation to epidermal lineages on electrospun nanofibrous substrates for skin tissue engineering. Acta Biomater. 7, 3113–3122. https://doi.org/10.1016/j.actbio.2011.04.017

Jin, X., Zhu, D.D., Chen, B.Z., Ashfaq, M., Guo, X.D., 2018. Insulin delivery systems combined with microneedle technology. Adv. Drug Deliv. Rev. 127, 119–137. https://doi.org/10.1016/j.addr.2018.03.011

Johnson, B.K., Prud'homme, R.K., 2003. Mechanism for Rapid Self-Assembly of Block Copolymer Nanoparticles. Phys Rev Lett 91, 118302. https://doi.org/10.1103/PhysRevLett.91.118302

Jondhalekar, T.M., Aher, S.S., Saudagar, R.B., 2017. Transethosome: Novel vesicular carrier for enhanced transdermal drug delivery system. Res. J. Pharm. Technol. 10, 1816. https://doi.org/10.5958/0974-360X.2017.00320.1

Jones, A.-A.D., Mi, G., Webster, T.J., 2019. A Status Report on FDA Approval of Medical Devices Containing Nanostructured Materials. Trends Biotechnol. 37, 117–120. https://doi.org/10.1016/j.tibtech.2018.06.003

Joye, I.J., McClements, D.J., 2013. Production of nanoparticles by anti-solvent precipitation for use in food systems. Trends Food Sci. Technol. 34, 109–123. https://doi.org/10.1016/j.tifs.2013.10.002

Jug, M., Mura, P., 2018. Grinding as Solvent-Free Green Chemistry Approach for Cyclodextrin Inclusion Complex Preparation in the Solid State. Pharmaceutics 10, 189. https://doi.org/10.3390/pharmaceutics10040189

Junthip, J., Tabary, N., Chai, F., Leclercq, L., Maton, M., Cazaux, F., Neut, C., Paccou, L., Guinet, Y., Staelens, J.-N., Bria, M., Landy, D., Hédoux, A., Blanchemain, N., Martel, B., 2016. Layer-by-layer coating of textile with two oppositely charged cyclodextrin polyelectrolytes for extended drug delivery: INTRISIC ANTIBACTERIAL ACTIVITY OF MULTILAYER ASSEMBLIES. J. Biomed. Mater. Res. A 104, 1408–1424. https://doi.org/10.1002/jbm.a.35674

Junthip, J., Tabary, N., Leclercq, L., Martel, B., 2015. Cationic β-cyclodextrin polymer applied to a dual cyclodextrin polyelectrolyte multilayer system. Carbohydr. Polym. 126, 156–167. https://doi.org/10.1016/j.carbpol.2015.02.064

Kandimalla, K.K., Kanikkannan, N., Singh, M., 1999. Optimization of a vehicle mixture for the transdermal delivery of melatonin using artificial neural networks and response surface method. J. Controlled Release 61, 71–82. https://doi.org/10.1016/S0168-3659(99)00107-8

Kang, D., Li, B., Luo, L., Jiang, W., Lu, Q., Rong, M., Lai, R., 2016. Curcumin shows excellent therapeutic effect on psoriasis in mouse model. Biochimie 123, 73–80. https://doi.org/10.1016/j.biochi.2016.01.013

Kapoor, M.S., GuhaSarkar, S., Banerjee, R., 2017. Stratum corneum modulation by chemical enhancers and lipid nanostructures: implications for transdermal drug delivery. Ther. Deliv. 8, 701–718. https://doi.org/10.4155/tde-2017-0045

Karpiński, T., 2018. Selected Medicines Used in Iontophoresis. Pharmaceutics 10, 204. https://doi.org/10.3390/pharmaceutics10040204

Kaszuba, M., Corbett, J., Watson, F.M., Jones, A., 2010. High-concentration zeta potential measurements using light-scattering techniques. Philos. Trans. R. Soc. Math. Phys. Eng. Sci. 368, 4439–4451. https://doi.org/10.1098/rsta.2010.0175

Katikaneni, S., Li, G., Badkar, A., Banga, A.K., 2010. Transdermal delivery of a approximately 13 kDa protein--an in vivo comparison of physical enhancement methods. J. Drug Target. 18, 141–147. https://doi.org/10.3109/10611860903287164

Kaur, R., Khullar, P., Mahal, A., Gupta, A., Singh, N., Ahluwalia, G.K., Bakshi, M.S., 2018. Keto–Enol Tautomerism of Temperature and pH Sensitive Hydrated Curcumin Nanoparticles: Their Role as Nanoreactors and Compatibility with Blood Cells. J. Agric. Food Chem. 66, 11974–11980. https://doi.org/10.1021/acs.jafc.8b03893

Ke, X., Tang, H., Mao, H.-Q., 2019. Effective encapsulation of curcumin in nanoparticles enabled by hydrogen bonding using flash nanocomplexation. Int. J. Pharm. 564, 273–280. https://doi.org/10.1016/j.ijpharm.2019.04.053

Keller, H.R., Zhang, X., Li, L., Schaider, H., Wells, J.W., 2017. Overcoming resistance to targeted therapy with immunotherapy and combination therapy for metastatic melanoma. Oncotarget 8. https://doi.org/10.18632/oncotarget.18523

Keroack, D., Zhao, Y., Prud'homme, R.E., 1999. Molecular orientation in crystalline miscible blends. Polymer 40, 243–251. https://doi.org/10.1016/S0032-3861(98)00187-6

Khadjavi, A., Magnetto, C., Panariti, A., Argenziano, M., Gulino, G.R., Rivolta, I., Cavalli, R., Giribaldi, G., Guiot, C., Prato, M., 2015. Chitosan-shelled oxygen-loaded nanodroplets abrogate hypoxia dysregulation of human keratinocyte gelatinases and inhibitors: New insights for chronic wound healing. Toxicol. Appl. Pharmacol. 286, 198–206. https://doi.org/10.1016/j.taap.2015.04.015

Klemm, D., Heublein, B., Fink, H.-P., Bohn, A., 2005. Cellulose: Fascinating Biopolymer and Sustainable Raw Material. Angew. Chem. Int. Ed. 44, 3358–3393. https://doi.org/10.1002/anie.200460587

Kohli, A.K., Alpar, H.O., 2004. Potential use of nanoparticles for transcutaneous vaccine delivery: effect of particle size and charge. Int. J. Pharm. 275, 13–17. https://doi.org/10.1016/j.ijpharm.2003.10.038

Koneru, B., Shi, Y., Munaweera, I., Wight-Carter, M., Kadara, H., Yuan, H., Di Pasqua, A.J., Balkus, K.J., 2016. Radiotherapeutic bandage for the treatment of squamous cell carcinoma of the skin. Nucl. Med. Biol. 43, 333–338. https://doi.org/10.1016/j.nucmedbio.2016.02.010

Koo, S.-W., Hirakawa, S., Fujii, S., Kawasumi, M., Nghiem, P., 2007. Protection from photodamage by topical application of caffeine after ultraviolet irradiation. Br. J. Dermatol. 156, 957–964. https://doi.org/10.1111/j.1365-2133.2007.07812.x

Kou, M.-C., Chiou, S.-Y., Weng, C.-Y., Wang, L., Ho, C.-T., Wu, M.-J., 2013. Curcuminoids distinctly exhibit antioxidant activities and regulate expression of scavenger receptors and heme oxygenase-1. Mol. Nutr. Food Res. 57, 1598–1610. https://doi.org/10.1002/mnfr.201200227

Krausz, A.E., Adler, B.L., Cabral, V., Navati, M., Doerner, J., Charafeddine, R.A., Chandra, D., Liang, H., Gunther, L., Clendaniel, A., Harper, S., Friedman, J.M., Nosanchuk, J.D., Friedman, A.J., 2015. Curcumin-encapsulated nanoparticles as innovative antimicrobial and wound healing agent. Nanomedicine Nanotechnol. Biol. Med. 11, 195–206. https://doi.org/10.1016/j.nano.2014.09.004

Kulac, M., Aktas, C., Tulubas, F., Uygur, R., Kanter, M., Erboga, M., Ceber, M., Topcu, B., Ozen, O.A., 2013. The effects of topical treatment with curcumin on burn wound healing in rats. J. Mol. Histol. 44, 83–90. https://doi.org/10.1007/s10735-012-9452-9

Kumari, A., Yadav, S.K., Yadav, S.C., 2010. Biodegradable polymeric nanoparticles based drug delivery systems. Colloids Surf. B Biointerfaces 75, 1–18. https://doi.org/10.1016/j.colsurfb.2009.09.001

Lademann, J., Knorr, F., Richter, H., Blume-Peytavi, U., Vogt, A., Antoniou, C., Sterry, W., Patzelt, A., 2008. Hair Follicles – An Efficient Storage and Penetration Pathway for Topically Applied Substances. Skin Pharmacol. Physiol. 21, 150–155. https://doi.org/10.1159/000131079

Lalloz, A., Bolzinger, M.-A., Briançon, S., Faivre, J., Rabanel, J.-M., Garcia Ac, A., Hildgen, P., Banquy, X., 2019. Subtle and unexpected role of PEG in tuning the penetration mechanisms of PLA-based nano-formulations into intact and impaired skin. Int. J. Pharm. 563, 79–90. https://doi.org/10.1016/j.ijpharm.2019.02.039

Lalloz, A., Bolzinger, M.-A., Faivre, J., Latreille, P.-L., Garcia Ac, A., Rakotovao, C., Rabanel, J.-M., Hildgen, P., Banquy, X., Briançon, S., 2018. Effect of surface chemistry of polymeric nanoparticles on cutaneous penetration of cholecalciferol. Int. J. Pharm. 553, 120–131. https://doi.org/10.1016/j.ijpharm.2018.09.046

Lam, P.-L., Lee, K.K.-H., Wong, R.S.-M., Cheng, G.Y.M., Cheng, S.Y., Yuen, M.C.-W., Lam, K.-H., Gambari, R., Kok, S.H.-L., Chui, C.-H., 2012. Development of hydrocortisone succinic acid/and 5-fluorouracil/chitosan microcapsules for oral and topical drug deliveries. Bioorg. Med. Chem. Lett. 22, 3213–3218. https://doi.org/10.1016/j.bmcl.2012.03.031

Lam, P.L., Li, L., Yuen, C.W.M., Gambari, R., Wong, R.S.M., Chui, C.H., Lam, K.H., 2013. Effects of multiple washing on cotton fabrics containing berberine microcapsules with anti-*Staphylococcus aureus* activity. J. Microencapsul. 30, 143–150. https://doi.org/10.3109/02652048.2012.704953

Lan, X., She, J., Lin, D., Xu, Y., Li, X., Yang, W., Lui, V.W.Y., Jin, L., Xie, X., Su, Y., 2018. Microneedle-Mediated Delivery of Lipid-Coated Cisplatin Nanoparticles for Efficient and Safe Cancer Therapy. ACS Appl. Mater. Interfaces 10, 33060–33069. https://doi.org/10.1021/acsami.8b12926

Lassalle, V., Ferreira, M.L., 2007. PLA nano- and microparticles for drug delivery: an overview of the methods of preparation. Macromol. Biosci. 7, 767–783. https://doi.org/10.1002/mabi.200700022

Lavagna, L., Massella, D., Pantano, M.F., Bosia, F., Pugno, N.M., Pavese, M., 2018a. Grafting carbon nanotubes onto carbon fibres doubles their effective strength and the toughness of the composite. Compos. Sci. Technol. https://doi.org/10.1016/j.compscitech.2018.03.015

Lavagna, L., Musso, S., Ferro, G., Pavese, M., 2018b. Cement-based composites containing functionalized carbon fibers. Cem. Concr. Compos. 88, 165–171. https://doi.org/10.1016/j.cemconcomp.2018.02.007

Lavino, A.D., Di Pasquale, N., Carbone, P., Marchisio, D.L., 2017. A novel multiscale model for the simulation of polymer flash nano-precipitation. Chem. Eng. Sci. 171, 485–494. https://doi.org/10.1016/j.ces.2017.04.047

Lee, S.-J., Jung, Y.H., Oh, S.Y., Yun, S.P., Han, H.J., 2014. Melatonin enhances the human mesenchymal stem cells motility via melatonin receptor 2 coupling with Gαq in skin wound healing. J. Pineal Res. 57, 393–407. https://doi.org/10.1111/jpi.12179

Lengyel, M., Kállai-Szabó, N., Antal, V., Laki, A.J., Antal, I., 2019. Microparticles, Microspheres, and Microcapsules for Advanced Drug Delivery. Sci. Pharm. 87, 20. https://doi.org/10.3390/scipharm87030020

Leone, F., Cataldo, R., Mohamed, S., Manna, L., Banchero, M., Ronchetti, S., Mandras, N., Tullio, V., Cavalli, R., Onida, B., 2019. Nanostructured ZnO as Multifunctional Carrier for a Green Antibacterial Drug Delivery System—A Feasibility Study. Nanomaterials 9, 407. https://doi.org/10.3390/nano9030407

Leone, F., Gignone, A., Ronchetti, S., Cavalli, R., Manna, L., Banchero, M., Onida, B., 2018. A green organic-solvent-free route to prepare nanostructured zinc oxide carriers of clotrimazole for pharmaceutical applications. J. Clean. Prod. 172, 1433–1439. https://doi.org/10.1016/j.jclepro.2017.10.243

Lephart, E.D., 2016. Skin aging and oxidative stress: Equol's anti-aging effects via biochemical and molecular mechanisms. Ageing Res. Rev. 31, 36–54. https://doi.org/10.1016/j.arr.2016.08.001

Li, H., Gao, A., Jiang, N., Liu, Q., Liang, B., Li, R., Zhang, E., Li, Z., Zhu, H., 2016. Protective Effect of Curcumin Against Acute Ultraviolet B Irradiation-induced Photo-damage. Photochem. Photobiol. 92, 808–815. https://doi.org/10.1111/php.12628

Li, J., Fu, R., Li, L., Yang, G., Ding, S., Zhong, Z., Zhou, S., 2014. Co-delivery of Dexamethasone and Green Tea Polyphenols Using Electrospun Ultrafine Fibers for Effective Treatment of Keloid. Pharm. Res. 31, 1632–1643. https://doi.org/10.1007/s11095-013-1266-2

Li, M., Rouaud, O., Poncelet, D., 2008. Microencapsulation by solvent evaporation: State of the art for process engineering approaches. Int. J. Pharm. 363, 26–39. https://doi.org/10.1016/j.ijpharm.2008.07.018

Li, M.-F., Chen, L., Xu, M.-Z., Zhang, J.-L., Wang, Q., Zeng, Q.-Z., Wei, X.-C., Yuan, Y., 2018. The formation of zein-chitosan complex coacervated particles: Relationship to encapsulation and controlled release properties. Int. J. Biol. Macromol. 116, 1232–1239. https://doi.org/10.1016/j.ijbiomac.2018.05.107

Li, Y., Zhao, X., Zu, Y., Wang, L., Wu, W., Deng, Y., Zu, C., Liu, Y., 2017. Melatonin-loaded silica coated with hydroxypropyl methylcellulose phthalate for enhanced oral bioavailability: Preparation, and in vitro-in vivo evaluation. Eur. J. Pharm. Biopharm. 112, 58–66. https://doi.org/10.1016/j.ejpb.2016.11.003

Limayem Blouza, I., Charcosset, C., Sfar, S., Fessi, H., 2006. Preparation and characterization of spironolactone-loaded nanocapsules for paediatric use. Int. J. Pharm. 325, 124–131. https://doi.org/10.1016/j.ijpharm.2006.06.022

Limongi, T., Canta, M., Racca, L., Ancona, A., Tritta, S., Vighetto, V., Cauda, V., 2019. Improving dispersal of therapeutic nanoparticles in the human body. Nanomed. 14, 797–801. https://doi.org/10.2217/nnm-2019-0070

Lince, F., Marchisio, D.L., Barresi, A.A., 2008. Strategies to control the particle size distribution of poly-ε-caprolactone nanoparticles for pharmaceutical applications. J. Colloid Interface Sci. 322, 505–515. https://doi.org/10.1016/j.jcis.2008.03.033

Lindenberg, C., Schöll, J., Vicum, L., Mazzotti, M., Brozio, J., 2008. Experimental characterization and multi-scale modeling of mixing in static mixers. Chem. Eng. Sci. 63, 4135–4149. https://doi.org/10.1016/j.ces.2008.05.026

Lis Arias, M., Coderch, L., Martí, M., Alonso, C., García Carmona, O., García Carmona, C., Maesta, F., 2018. Vehiculation of Active Principles as a Way to Create Smart and Biofunctional Textiles. Materials 11, 2152. https://doi.org/10.3390/ma11112152

Littringer, E.M., Zellnitz, S., Hammernik, K., Adamer, V., Friedl, H., Urbanetz, N.A., 2013. Spray Drying of Aqueous Salbutamol Sulfate Solutions Using the Nano Spray Dryer B-90—The Impact of Process Parameters on Particle Size. Dry. Technol. 31, 1346–1353. https://doi.org/10.1080/07373937.2013.793701

Liu, C.-H., Huang, H.-Y., 2012. Antimicrobial Activity of Curcumin-Loaded Myristic Acid Microemulsions against Staphylococcus epidermidis. Chem. Pharm. Bull. (Tokyo) 60, 1118–1124. https://doi.org/10.1248/cpb.c12-00220

Liu, Y., Cheng, C., Liu, Y., Prud'homme, R.K., Fox, R.O., 2008. Mixing in a multi-inlet vortex mixer (MIVM) for flash nano-precipitation. Chem. Eng. Sci. 63, 2829–2842. https://doi.org/10.1016/j.ces.2007.10.020

López-Muñoz, F., Marín, F., Álamo, C., 2016. History of Pineal Gland as Neuroendocrine Organ and the Discovery of Melatonin, in: López-Muñoz, F., Srinivasan, V., de Berardis, D., Álamo, C., Kato, T.A. (Eds.), Melatonin, Neuroprotective Agents and Antidepressant Therapy. Springer India, New Delhi, pp. 1–23. https://doi.org/10.1007/978-81-322-2803-5_1

Lowes, M.A., Suárez-Fariñas, M., Krueger, J.G., 2014. Immunology of Psoriasis. Annu. Rev. Immunol. 32, 227–255. https://doi.org/10.1146/annurev-immunol-032713-120225

Lu, Y.-P., Lou, Y.-R., Xie, J.-G., Peng, Q.-Y., Liao, J., Yang, C.S., Huang, M.-T., Conney, A.H., 2002. Topical applications of caffeine or (-)-epigallocatechin gallate (EGCG) inhibit carcinogenesis and selectively increase apoptosis in UVB-induced skin tumors in mice. Proc. Natl. Acad. Sci. 99, 12455–12460. https://doi.org/10.1073/pnas.182429899

Lu, Y.-P., Lou, Y.-R., Xie, J.-G., Peng, Q.-Y., Zhou, S., Lin, Y., Shih, W.J., Conney, A.H., 2007. Caffeine and caffeine sodium benzoate have a sunscreen effect, enhance UVB-induced apoptosis, and inhibit UVB-induced skin carcinogenesis in SKH-1 mice. Carcinogenesis 28, 199–206. https://doi.org/10.1093/carcin/bgl112

Luque-Alcaraz, A.G., Lizardi-Mendoza, J., Goycoolea, F.M., Higuera-Ciapara, I., Argüelles-Monal, W., 2016. Preparation of chitosan nanoparticles by nanoprecipitation and their ability as a drug nanocarrier. RSC Adv. 6, 59250–59256. https://doi.org/10.1039/C6RA06563E

Madan, P.L., 1978. Microencapsulation I. Phase Separation or Coacervation. Drug Dev. Ind. Pharm. 4, 95–116. https://doi.org/10.3109/03639047809055641

Madhaiyan, K., Sridhar, R., Sundarrajan, S., Venugopal, J.R., Ramakrishna, S., 2013. Vitamin B12 loaded polycaprolactone nanofibers: A novel transdermal route for the water soluble energy supplement delivery. Int. J. Pharm. 444, 70–76. https://doi.org/10.1016/j.ijpharm.2013.01.040

Maestá Bezerra, F., García Carmona, Ó., García Carmona, C., Souza Plath, A.M., Lis, M., 2018. Biofunctional wool using β-cyclodextrins as vehiculizer of citronella oil. Process Biochem. https://doi.org/10.1016/j.procbio.2018.11.018

Mahrhauser, D.-S., Reznicek, G., Gehrig, S., Geyer, A., Ogris, M., Kieweler, R., Valenta, C., 2015. Simultaneous determination of active component and vehicle penetration from F-DPPC liposomes into porcine skin layers. Eur. J. Pharm. Biopharm. 97, 90–95. https://doi.org/10.1016/j.ejpb.2015.10.008

Majidinia, M., Reiter, R.J., Shakouri, S.K., Mohebbi, I., Rastegar, M., Kaviani, M., Darband, S.G., Jahanban-Esfahlan, R., Nabavi, S.M., Yousefi, B., 2018. The multiple functions of melatonin in regenerative medicine. Ageing Res. Rev. 45, 33–52. https://doi.org/10.1016/j.arr.2018.04.003

Malucelli, G., 2016. Surface-Engineered Fire Protective Coatings for Fabrics through Sol-Gel and Layer-by-Layer Methods: An Overview. Coatings 6, 33. https://doi.org/10.3390/coatings6030033

Mannhold, R., Dross, K., 1996. Calculation Procedures for Molecular Lipophilicity: a Comparative Study. Quant. Struct.-Act. Relatsh. 15, 403–409. https://doi.org/10.1002/qsar.19960150506

Martí, M., Martínez, V., Rubio, L., Coderch, L., Parra, J.L., 2011. Biofunctional textiles prepared with liposomes: *in vivo* and *in vitro* assessment. J. Microencapsul. 28, 799–806. https://doi.org/10.3109/02652048.2011.621555

Martí, M., Rodríguez, R., Carreras, N., Lis, M., Valldeperas, J., Coderch, L., Parra, J.L., 2012. Monitoring of the microcapsule/liposome application on textile fabrics. J. Text. Inst. 103, 19–27. https://doi.org/10.1080/00405000.2010.542011

Martínez Rivas, C.J., Tarhini, M., Badri, W., Miladi, K., Greige-Gerges, H., Nazari, Q.A., Galindo Rodríguez, S.A., Román, R.Á., Fessi, H., Elaissari, A., 2017. Nanoprecipitation process: From encapsulation to drug delivery. Int. J. Pharm. 532, 66–81. https://doi.org/10.1016/j.ijpharm.2017.08.064

Marto, J., Duarte, A., Simões, S., Gonçalves, L., Gouveia, L., Almeida, A., Ribeiro, H., 2019. Starch-Based Pickering Emulsions as Platforms for Topical Antibiotic Delivery: In Vitro and In Vivo Studies. Polymers 11, 108. https://doi.org/10.3390/polym11010108

Marto, J., Ruivo, E., Lucas, S.D., Gonçalves, L.M., Simões, S., Gouveia, L.F., Felix, R., Moreira, R., Ribeiro, H.M., Almeida, A.J., 2018. Starch nanocapsules containing a novel neutrophil elastase inhibitor with improved pharmaceutical performance. Eur. J. Pharm. Biopharm. 127, 1–11. https://doi.org/10.1016/j.ejpb.2018.01.011

Mather, R., Wilson, J., 2017. Fabrication of Photovoltaic Textiles. Coatings 7, 63. https://doi.org/10.3390/coatings7050063

Mathes, C., Melero, A., Conrad, P., Vogt, T., Rigo, L., Selzer, D., Prado, W.A., De Rossi, C., Garrigues, T.M., Hansen, S., Guterres, S.S., Pohlmann, A.R., Beck, R.C.R., Lehr, C.-M., Schaefer, U.F., 2016. Nanocarriers for optimizing the balance between interfollicular permeation and follicular uptake of topically applied clobetasol to minimize adverse effects. J. Controlled Release 223, 207–214. https://doi.org/10.1016/j.jconrel.2015.12.010

Mathis, R., Mehling, A., 2011. Textiles with cosmetic effects, in: Handbook of Medical Textiles. Elsevier, pp. 153–172. https://doi.org/10.1533/9780857093691.1.153

Mazzarino, L., Travelet, C., Ortega-Murillo, S., Otsuka, I., Pignot-Paintrand, I., Lemos-Senna, E., Borsali, R., 2012. Elaboration of chitosan-coated nanoparticles loaded with curcumin for mucoadhesive applications. J. Colloid Interface Sci. 370, 58–66. https://doi.org/10.1016/j.jcis.2011.12.063

McCarthy, B.J., 2016. An overview of the technical textiles sector, in: Handbook of Technical Textiles. Elsevier, pp. 1–20. https://doi.org/10.1016/B978-1-78242-458-1.00001-7

McConville, A., Hegarty, C., Davis, J., 2018. Mini-Review: Assessing the Potential Impact of Microneedle Technologies on Home Healthcare Applications. Medicines 5, 50. https://doi.org/10.3390/medicines5020050

Meng, F.T., Ma, G.H., Liu, Y.D., Qiu, W., Su, Z.G., 2004. Microencapsulation of bovine hemoglobin with high bio-activity and high entrapment efficiency using a W/O/W double emulsion technique. Colloids Surf. B Biointerfaces 33, 177–183. https://doi.org/10.1016/j.colsurfb.2003.10.003

Mersmann, A., 1999. Crystallization and precipitation. Chem. Eng. Process. Process Intensif. 38, 345–353. https://doi.org/10.1016/S0255-2701(99)00025-2

Miguel, S., Ribeiro, M., Coutinho, P., Correia, I., 2017. Electrospun Polycaprolactone/Aloe Vera_Chitosan Nanofibrous Asymmetric Membranes Aimed for Wound Healing Applications. Polymers 9, 183. https://doi.org/10.3390/polym9050183

Miguel, S.P., Figueira, D.R., Simões, D., Ribeiro, M.P., Coutinho, P., Ferreira, P., Correia, I.J., 2018. Electrospun polymeric nanofibres as wound dressings: A review. Colloids Surf. B Biointerfaces 169, 60–71. https://doi.org/10.1016/j.colsurfb.2018.05.011

Mihailiasa, M., Caldera, F., Li, J., Peila, R., Ferri, A., Trotta, F., 2016. Preparation of functionalized cotton fabrics by means of melatonin loaded β-cyclodextrin nanosponges. Carbohydr. Polym. 142, 24–30. https://doi.org/10.1016/j.carbpol.2016.01.024

Miladi, K., Ibraheem, D., Iqbal, M., Sfar, S., Fessi, H., Elaissari, A., 2014. Particles from preformed polymers as carriers for drug delivery. EXCLI J. 13, 28–57.

Miladi, K., Sfar, S., Fessi, H., Elaissari, A., 2016. Nanoprecipitation Process: From Particle Preparation to In Vivo Applications, in: Vauthier, C., Ponchel, G. (Eds.), Polymer Nanoparticles for Nanomedicines. Springer International Publishing, Cham, pp. 17–53. https://doi.org/10.1007/978-3-319-41421-8_2

Missana, T., Adell, A., 2000. On the Applicability of DLVO Theory to the Prediction of Clay Colloids Stability. J. Colloid Interface Sci. 230, 150–156. https://doi.org/10.1006/jcis.2000.7003

Moballegh Nasery, M., Abadi, B., Poormoghadam, D., Zarrabi, A., Keyhanvar, P., Khanbabaei, H., Ashrafizadeh, M., Mohammadinejad, R., Tavakol, S., Sethi, G., 2020. Curcumin Delivery Mediated by Bio-Based Nanoparticles: A Review. Molecules 25, 689. https://doi.org/10.3390/molecules25030689

Mohanty, B., Gupta, A., Bohidar, H.B., Bandyopadhyay, S., 2007. Effect of gelatin molecular charge heterogeneity on formation of intermolecular complexes and coacervation transition. J. Polym. Sci. Part B Polym. Phys. 45, 1511–1520. https://doi.org/10.1002/polb.21120

Mor, M., Plazzi, P.V., Spadoni, G., Tarzia, G., 1999. Melatonin. Curr. Med. Chem. 6, 501–518.

Mora-Huertas, C.E., Fessi, H., Elaissari, A., 2011. Influence of process and formulation parameters on the formation of submicron particles by solvent displacement and emulsification–diffusion methods. Adv. Colloid Interface Sci. 163, 90–122. https://doi.org/10.1016/j.cis.2011.02.005

Morais, D., Guedes, R., Lopes, M., 2016. Antimicrobial Approaches for Textiles: From Research to Market. Materials 9, 498. https://doi.org/10.3390/ma9060498

Moreno, J.A.S., Mendes, A.C., Stephansen, K., Engwer, C., Goycoolea, F.M., Boisen, A., Nielsen, L.H., Chronakis, I.S., 2018. Development of electrosprayed mucoadhesive chitosan microparticles. Carbohydr. Polym. 190, 240–247. https://doi.org/10.1016/j.carbpol.2018.02.062

Mossotti, R., Ferri, A., Innocenti, R., Zelenková, T., Dotti, F., Marchisio, D.L., Barresi, A.A., 2015. Cotton fabric functionalisation with menthol/PCL micro- and nano-capsules for comfort improvement. J. Microencapsul. 32, 650–660. https://doi.org/10.3109/02652048.2015.1073386

Mostafalu, P., Kiaee, G., Giatsidis, G., Khalilpour, A., Nabavinia, M., Dokmeci, M.R., Sonkusale, S., Orgill, D.P., Tamayol, A., Khademhosseini, A., 2017. A Textile Dressing for Temporal and Dosage Controlled Drug Delivery. Adv. Funct. Mater. 27, 1702399. https://doi.org/10.1002/adfm.201702399

Mottram, D.R., Chester, N. (Eds.), 2018. Drugs in Sport, 7th ed. Routledge, Seventh edition. | Milton Park, Abingdon ; New York, NY : Routledge, 2018. https://doi.org/10.4324/9781315222790

Munaweera, I., Levesque-Bishop, D., Shi, Y., Di Pasqua, A.J., Balkus, K.J., 2014. Radiotherapeutic Bandage Based on Electrospun Polyacrylonitrile Containing Holmium-166 Iron Garnet Nanoparticles for the Treatment of Skin Cancer. ACS Appl. Mater. Interfaces 6, 22250–22256. https://doi.org/10.1021/am506045k

Musazzi, U.M., Marini, V., Casiraghi, A., Minghetti, P., 2017. Is the European regulatory framework sufficient to assure the safety of citizens using health products containing nanomaterials? Drug Discov. Today 22, 870–882. https://doi.org/10.1016/j.drudis.2017.01.016

Musel, A.L., Warshaw, E.M., 2006. Cutaneous Reactions to Transdermal Therapeutic Systems: Dermatitis 17, 109–122. https://doi.org/10.2310/6620.2006.05051

Nada, A., Al-Moghazy, M., Soliman, A.A.F., Rashwan, G.M.T., Eldawy, T.H.A., Hassan, A.A.E., Sayed, G.H., 2018. Pyrazole-based compounds in chitosan liposomal emulsion for antimicrobial cotton fabrics. Int. J. Biol. Macromol. 107, 585–594. https://doi.org/10.1016/j.ijbiomac.2017.09.031

Nagula, R.L., Wairkar, S., 2019. Recent advances in topical delivery of flavonoids: A review. J. Controlled Release 296, 190–201. https://doi.org/10.1016/j.jconrel.2019.01.029

Nairm, J.G., 1995. 3 Coacervation-phase separation technology, in: Advances in Pharmaceutical Sciences. Elsevier, pp. 93–219. https://doi.org/10.1016/S0065-3136(06)80005-1

Nakashima, T., Shimizu, M., Kukizaki, M., 2000. Particle control of emulsion by membrane emulsification and its applications. Adv. Drug Deliv. Rev. 45, 47–56. https://doi.org/10.1016/S0169-409X(00)00099-5

Nastiti, C., Ponto, T., Abd, E., Grice, J., Benson, H., Roberts, M., 2017. Topical Nano and Microemulsions for Skin Delivery. Pharmaceutics 9, 37. https://doi.org/10.3390/pharmaceutics9040037

Natta, F.J. van, Hill, J.W., Carothers, W.H., 1934. Studies of Polymerization and Ring Formation. XXIII. [1] ε-Caprolactone and its Polymers. J. Am. Chem. Soc. 56, 455–457. https://doi.org/10.1021/ja01317a053

Nawrot, P., Jordan, S., Eastwood, J., Rotstein, J., Hugenholtz, A., Feeley, M., 2003. Effects of caffeine on human health. Food Addit. Contam. 20, 1–30. https://doi.org/10.1080/0265203021000007840

Nehlig, A., Daval, J.-L., Debry, G., 1992. Caffeine and the central nervous system: mechanisms of action, biochemical, metabolic and psychostimulant effects. Brain Res. Rev. 17, 139–170. https://doi.org/10.1016/0165-0173(92)90012-B

Nelson, K.M., Dahlin, J.L., Bisson, J., Graham, J., Pauli, G.F., Walters, M.A., 2017. The Essential Medicinal Chemistry of Curcumin: Miniperspective. J. Med. Chem. 60, 1620–1637. https://doi.org/10.1021/acs.jmedchem.6b00975

Nguyen, H., Banga, A., 2018. Electrically and Ultrasonically Enhanced Transdermal Delivery of Methotrexate. Pharmaceutics 10, 117. https://doi.org/10.3390/pharmaceutics10030117

Oguzturk, H., Ciftci, O., Aydin, M., Timurkaan, N., Beytur, A., Yilmaz, F., 2012. Ameliorative effects of curcumin against acute cadmium toxicity on male reproductive system in rats. Andrologia 44, 243–249. https://doi.org/10.1111/j.1439-0272.2012.01273.x

Ohshima, H., 2013. Zeta Potential, in: Tadros, T. (Ed.), Encyclopedia of Colloid and Interface Science. Springer Berlin Heidelberg, Berlin, Heidelberg, pp. 1423–1436. https://doi.org/10.1007/978-3-642-20665-8_162

Ohtaki, A., Akakura, N., Nakasaki, K., 1998. Effects of temperature and inoculum on the degradability of poly-ε-caprolactone during composting. Polym. Degrad. Stab. 62, 279–284. https://doi.org/10.1016/S0141-3910(98)00008-1

Okada, M., 2002. Chemical syntheses of biodegradable polymers. Prog. Polym. Sci. 27, 87–133. https://doi.org/10.1016/S0079-6700(01)00039-9

Omidi, J., Khorram, M., Samimi, A., 2010. Combined method of complex coacervation and electrospray for encapsulate preparation. J. Appl. Polym. Sci. NA-NA. https://doi.org/10.1002/app.30988

Palmer, B., DeLouise, L., 2016. Nanoparticle-Enabled Transdermal Drug Delivery Systems for Enhanced Dose Control and Tissue Targeting. Molecules 21, 1719. https://doi.org/10.3390/molecules21121719

Panahi, Y., Fazlolahzadeh, O., Atkin, S.L., Majeed, M., Butler, A.E., Johnston, T.P., Sahebkar, A., 2019. Evidence of curcumin and curcumin analogue effects in skin diseases: A narrative review: PANAHI ET AL . J. Cell. Physiol. 234, 1165–1178. https://doi.org/10.1002/jcp.27096

Paradkar, M.M., Irudayaraj, J., 2002. Rapid determination of caffeine content in soft drinks using FTIR–ATR spectroscopy. Food Chem. 78, 261–266. https://doi.org/10.1016/S0308-8146(02)00116-4

Parisi, O.I., Scrivano, L., Sinicropi, M.S., Puoci, F., 2017. Polymeric nanoparticle constructs as devices for antibacterial therapy. Curr. Opin. Pharmacol. 36, 72–77. https://doi.org/10.1016/j.coph.2017.08.004

Park, D., Park, H., Seo, J., Lee, S., 2014. Sonophoresis in transdermal drug deliverys. Ultrasonics 54, 56–65. https://doi.org/10.1016/j.ultras.2013.07.007

Pastore, M.N., Kalia, Y.N., Horstmann, M., Roberts, M.S., 2015. Transdermal patches: history, development and pharmacology: History of transdermal patches. Br. J. Pharmacol. 172, 2179–2209. https://doi.org/10.1111/bph.13059

Pawar, A., Thakkar, S., Misra, M., 2018. A bird's eye view of nanoparticles prepared by electrospraying: advancements in drug delivery field. J. Controlled Release 286, 179–200. https://doi.org/10.1016/j.jconrel.2018.07.036

Peila, R., Scordino, P., Shanko, D.B., Caldera, F., Trotta, F., Ferri, A., 2017. Synthesis and characterization of β-cyclodextrin nanosponges for N,N-diethyl-meta-toluamide complexation and their application on polyester fabrics. React. Funct. Polym. 119, 87–94. https://doi.org/10.1016/j.reactfunctpolym.2017.08.008

Peppas, N.A., Narasimhan, B., 2014. Mathematical models in drug delivery: How modeling has shaped the way we design new drug delivery systems. J. Controlled Release 190, 75–81. https://doi.org/10.1016/j.jconrel.2014.06.041

Pereira, R.L., Leites, F.I., Paese, K., Sponchiado, R.M., Michalowski, C.B., Guterres, S.S., Schapoval, E.E.S., 2016. Hydrogel containing adapalene- and dapsone-loaded lipid-core nanocapsules for cutaneous application: development, characterization, *in vitro* irritation and permeation studies. Drug Dev. Ind. Pharm. 42, 2001–2008. https://doi.org/10.1080/03639045.2016.1188110

Perelshtein, I., Ruderman, E., Perkas, N., Tzanov, T., Beddow, J., Joyce, E., Mason, T.J., Blanes, M., Mollá, K., Patlolla, A., Frenkel, A.I., Gedanken, A., 2013. Chitosan and chitosan–ZnO-based complex nanoparticles: formation, characterization, and antibacterial activity. J. Mater. Chem. B 1, 1968. https://doi.org/10.1039/c3tb00555k

Persenaire, O., Alexandre, M., Degée, P., Dubois, P., 2001. Mechanisms and Kinetics of Thermal Degradation of Poly(ε-caprolactone). Biomacromolecules 2, 288–294. https://doi.org/10.1021/bm0056310

Piacentini, E., Drioli, E., Giorno, L., 2014. Membrane emulsification technology: Twenty-five years of inventions and research through patent survey. J. Membr. Sci. 468, 410–422. https://doi.org/10.1016/j.memsci.2014.05.059

Pinkerton, N.M., Behar, L., Hadri, K., Amouroux, B., Mingotaud, C., Talham, D.R., Chassaing, S., Marty, J.-D., 2017. Ionic Flash NanoPrecipitation (iFNP) for the facile, one-step synthesis of inorganic–organic hybrid nanoparticles in water. Nanoscale 9, 1403–1408. https://doi.org/10.1039/C6NR09364G

Pinto, S.S., Diogo, H.P., 2006. Thermochemical study of two anhydrous polymorphs of caffeine. J. Chem. Thermodyn. 38, 1515–1522. https://doi.org/10.1016/j.jct.2006.04.008

Pisoschi, A.M., Pop, A., 2015. The role of antioxidants in the chemistry of oxidative stress: A review. Eur. J. Med. Chem. 97, 55–74. https://doi.org/10.1016/j.ejmech.2015.04.040

Pitt, C.G., Chasalow, F.I., Hibionada, Y.M., Klimas, D.M., Schindler, A., 1981. Aliphatic polyesters. I. The degradation of poly(ϵ-caprolactone) *in vivo*. J. Appl. Polym. Sci. 26, 3779–3787. https://doi.org/10.1002/app.1981.070261124

Poeggeler, B., Reiter, R.J., Tan, D.X., Chen, L.D., Manchester, L.C., 1993. Melatonin, hydroxyl radical-mediated oxidative damage, and aging: a hypothesis. J. Pineal Res. 14, 151–168.

Polat, B.E., Hart, D., Langer, R., Blankschtein, D., 2011. Ultrasound-mediated transdermal drug delivery: Mechanisms, scope, and emerging trends. J. Controlled Release 152, 330–348. https://doi.org/10.1016/j.jconrel.2011.01.006

Poljšak, B., Dahmane, R., 2012. Free Radicals and Extrinsic Skin Aging. Dermatol. Res. Pract. 2012, 1–4. https://doi.org/10.1155/2012/135206

Pourhanifeh, M.H., Mahdavinia, M., Reiter, R.J., Asemi, Z., 2019. Potential use of melatonin in skin cancer treatment: A review of current biological evidence. J. Cell. Physiol. 234, 12142–12148. https://doi.org/10.1002/jcp.28129

Pradhan, R., Lee, D.W., Choi, H.-G., Yong, C.S., Kim, J.O., 2013. Fabrication of a uniformly sized fenofibrate microemulsion by membrane emulsification. J. Microencapsul. 30, 42–48. https://doi.org/10.3109/02652048.2012.692403

Prato, M., Magnetto, C., Jose, J., Khadjavi, A., Cavallo, F., Quaglino, E., Panariti, A., Rivolta, I., Benintende, E., Varetto, G., Argenziano, M., Troia, A., Cavalli, R., Guiot, C., 2015. 2H,3H-Decafluoropentane-Based Nanodroplets: New Perspectives for Oxygen Delivery to Hypoxic Cutaneous Tissues. PLOS ONE 10, e0119769. https://doi.org/10.1371/journal.pone.0119769

Priyadarsini, K., 2014. The Chemistry of Curcumin: From Extraction to Therapeutic Agent. Molecules 19, 20091–20112. https://doi.org/10.3390/molecules191220091

Priyadarsini, K.I., 2009. Photophysics, photochemistry and photobiology of curcumin: Studies from organic solutions, bio-mimetics and living cells. J. Photochem. Photobiol. C Photochem. Rev. 10, 81–95. https://doi.org/10.1016/j.jphotochemrev.2009.05.001

Priyadarsini, K.I., 1997. Free radical reactions of curcumin in membrane models. Free Radic. Biol. Med. 23, 838–843. https://doi.org/10.1016/s0891-5849(97)00026-9

Prow, T.W., Grice, J.E., Lin, L.L., Faye, R., Butler, M., Becker, W., Wurm, E.M.T., Yoong, C., Robertson, T.A., Soyer, H.P., Roberts, M.S., 2011. Nanoparticles and microparticles for skin drug delivery. Adv. Drug Deliv. Rev. 63, 470–491. https://doi.org/10.1016/j.addr.2011.01.012

Puglia, C., Offerta, A., Tirendi, G.G., Tarico, M.S., Curreri, S., Bonina, F., Perrotta, R.E., 2016. Design of solid lipid nanoparticles for caffeine topical administration. Drug Deliv. 23, 36–40. https://doi.org/10.3109/10717544.2014.903011

Qin, Y., Liu, C., Jiang, S., Xiong, L., Sun, Q., 2016. Characterization of starch nanoparticles prepared by nanoprecipitation: Influence of amylose content and starch type. Ind. Crops Prod. 87, 182–190. https://doi.org/10.1016/j.indcrop.2016.04.038

Quintanar-Guerrero, D., Allémann, E., Doelker, E., Fessi, H., 1997. A mechanistic study of the formation of polymer nanoparticles by the emulsification-diffusion technique. Colloid Polym. Sci. 275, 640–647. https://doi.org/10.1007/s003960050130

Quiroz-Reyes, C.N., Ronquillo-de Jesús, E., Duran-Caballero, N.E., Aguilar-Méndez, M.Á., 2014. Development and characterization of gelatin nanoparticles loaded with a cocoa-derived polyphenolic extract. Fruits 69, 481–489. https://doi.org/10.1051/fruits/2014034

Rafiee, Z., Nejatian, M., Daeihamed, M., Jafari, S.M., 2019. Application of different nanocarriers for encapsulation of curcumin. Crit. Rev. Food Sci. Nutr. 59, 3468–3497. https://doi.org/10.1080/10408398.2018.1495174

Rascón-Chu, A., Díaz-Baca, J., Carvajal-Millan, E., Pérez-López, E., Hotchkiss, A., González-Ríos, H., Balandrán-Quintana, R., Campa-Mada, A., 2018. Electrosprayed Core–Shell Composite Microbeads Based on Pectin-Arabinoxylans for Insulin Carrying: Aggregation and Size Dispersion Control. Polymers 10, 108. https://doi.org/10.3390/polym10020108

Rauscher, H., Rasmussen, K., Sokull-Klüttgen, B., 2017. Regulatory Aspects of Nanomaterials in the EU. Chem. Ing. Tech. 89, 224–231. https://doi.org/10.1002/cite.201600076

Rawlings, A.V., 2006. Cellulite and its treatment. Int. J. Cosmet. Sci. 28, 175–190. https://doi.org/10.1111/j.1467-2494.2006.00318.x

Reiter, R.J., Rosales-Corral, S., Tan, D.X., Jou, M.J., Galano, A., Xu, B., 2017. Melatonin as a mitochondria-targeted antioxidant: one of evolution's best ideas. Cell. Mol. Life Sci. 74, 3863–3881. https://doi.org/10.1007/s00018-017-2609-7

Rigon, R., Fachinetti, N., Severino, P., Santana, M., Chorilli, M., 2016. Skin Delivery and in Vitro Biological Evaluation of Trans-Resveratrol-Loaded Solid Lipid Nanoparticles for Skin Disorder Therapies. Molecules 21, 116. https://doi.org/10.3390/molecules21010116

Rincón, M., Calpena, A., Fabrega, M.-J., Garduño-Ramírez, M., Espina, M., Rodríguez-Lagunas, M., García, M., Abrego, G., 2018. Development of Pranoprofen Loaded Nanostructured Lipid Carriers to Improve Its Release and Therapeutic Efficacy in Skin Inflammatory Disorders. Nanomaterials 8, 1022. https://doi.org/10.3390/nano8121022

Roberts, M., Mohammed, Y., Pastore, M., Namjoshi, S., Yousef, S., Alinaghi, A., Haridass, I., Abd, E., Leite-Silva, V., Benson, H., Grice, J., 2017. Topical and cutaneous delivery using nanosystems. J. Controlled Release 247, 86–105. https://doi.org/10.1016/j.jconrel.2016.12.022

Rodrigues, F., Alves, A.C., Nunes, C., Sarmento, B., Amaral, M.H., Reis, S., Oliveira, M.B.P.P., 2016. Permeation of topically applied caffeine from a food by—product in cosmetic formulations: Is nanoscale in vitro approach an option? Int. J. Pharm. 513, 496–503. https://doi.org/10.1016/j.ijpharm.2016.09.059

Rodrigues, M.R., Lanzarini, C.M., Ricci-Junior, E., 2011. Preparation, in vitro characterization and in vivo release of naproxen loaded in poly-caprolactone nanoparticles. Pharm. Dev. Technol. 16, 12–21. https://doi.org/10.3109/10837450903460475

Romita, P., Foti, C., Calogiuri, G., Cantore, S., Ballini, A., Dipalma, G., Inchingolo, F., 2018. Contact dermatitis due to transdermal therapeutic systems: a clinical update. Acta Bio-Medica Atenei Parm. 90, 5–10. https://doi.org/10.23750/abm.v90i1.6563

Roudjane, M., Khalil, M., Miled, A., Messaddeq, Y., 2018. New Generation Wearable Antenna Based on Multimaterial Fiber for Wireless Communication and Real-Time Breath Detection. Photonics 5, 33. https://doi.org/10.3390/photonics5040033

Ru, Q., Wang, Y., Lee, J., Ding, Y., Huang, Q., 2012. Turbidity and rheological properties of bovine serum albumin/pectin coacervates: Effect of salt concentration and initial protein/polysaccharide ratio. Carbohydr. Polym. 88, 838–846. https://doi.org/10.1016/j.carbpol.2012.01.019

Rubio, L., Alonso, C., Coderch, L., Parra, J.L., Martí, M., Cebrián, J., Navarro, J.A., Lis, M., Valldeperas, J., 2010. Skin Delivery of Caffeine Contained in Biofunctional Textiles. Text. Res. J. 80, 1214–1221. https://doi.org/10.1177/0040517509358798

Saad, W., 2007. Drug Nanoparticle Formation via Flash NanoPrecipitation: Conjugation to Encapsulate and Control the Release of Paclitaxel, Chemical Engineering. Princeton University, Princeton.

Saad, W.S., Prud'homme, R.K., 2016. Principles of nanoparticle formation by flash nanoprecipitation. Nano Today 11, 212–227. https://doi.org/10.1016/j.nantod.2016.04.006

Salamanca, C., Barrera-Ocampo, A., Lasso, J., Camacho, N., Yarce, C., 2018. Franz Diffusion Cell Approach for Pre-Formulation Characterisation of Ketoprofen Semi-Solid Dosage Forms. Pharmaceutics 10, 148. https://doi.org/10.3390/pharmaceutics10030148

Salaün, F., 2016. Microencapsulation technology for smart textile coatings, in: Active Coatings for Smart Textiles. Elsevier, pp. 179–220. https://doi.org/10.1016/B978-0-08-100263-6.00009-5

Salehiabar, M., Nosrati, H., Javani, E., Aliakbarzadeh, F., Kheiri Manjili, H., Davaran, S., Danafar, H., 2018. Production of biological nanoparticles from bovine serum albumin as controlled release carrier for curcumin delivery. Int. J. Biol. Macromol. 115, 83–89. https://doi.org/10.1016/j.ijbiomac.2018.04.043

Sami Rtimi, Stefanos Giannakis, Cesar Pulgarin, 2017. Self-Sterilizing Sputtered Films for Applications in Hospital Facilities. Molecules 22, 1074. https://doi.org/10.3390/molecules22071074

Sangermano, M., Bazzano, M., 2018. Chapter 9. Photosynthesis of Polymeric Particles, in: Lalevée, J., Fouassier, J.-P. (Eds.), Polymer Chemistry Series. Royal Society of Chemistry, Cambridge, pp. 274–286. https://doi.org/10.1039/9781788013307-00274

Sayadi, L.R., Banyard, D.A., Ziegler, M.E., Obagi, Z., Prussak, J., Klopfer, M.J., Evans, G.R., Widgerow, A.D., 2018. Topical oxygen therapy & micro/nanobubbles: a new modality for tissue oxygen delivery. Int. Wound J. 15, 363–374. https://doi.org/10.1111/iwj.12873

SCHENIR, 2015. SCENIHR (Scientific Committee on Emerging and Newly Identified Health Risks), Final Opinion on the Guidance on the Determination of Potential Health Effects of Nanomaterials Used in Medical Devices, January 2015.

Schmitt, C., Turgeon, S.L., 2011. Protein/polysaccharide complexes and coacervates in food systems. Adv. Colloid Interface Sci. 167, 63–70. https://doi.org/10.1016/j.cis.2010.10.001

Schneider, M., Stracke, F., Hansen, S., Schaefer, U.F., 2009. Nanoparticles and their interactions with the dermal barrier. Dermatoendocrinol. 1, 197–206. https://doi.org/10.4161/derm.1.4.9501

Schwarzer, H.-C., Schwertfirm, F., Manhart, M., Schmid, H.-J., Peukert, W., 2006. Predictive simulation of nanoparticle precipitation based on the population balance equation. Chem. Eng. Sci. 61, 167–181. https://doi.org/10.1016/j.ces.2004.11.064

Schwöbel, J.A.H., Klamt, A., 2019. Mechanistic skin penetration model by the COSMOperm method: Routes of permeation, vehicle effects and skin variations in the healthy and compromised skin. Comput. Toxicol. 11, 50–64. https://doi.org/10.1016/j.comtox.2019.02.004

Seah, B.C.-Q., Teo, B.M., 2018. Recent advances in ultrasound-based transdermal drug delivery. Int. J. Nanomedicine Volume 13, 7749–7763. https://doi.org/10.2147/IJN.S174759

Şenyiğit, T., Sonvico, F., Rossi, A., Tekmen, I., Santi, P., Colombo, P., Nicoli, S., Özer, Ö., 2016. In Vivo Assessment of Clobetasol Propionate-Loaded Lecithin-Chitosan Nanoparticles for Skin Delivery. Int. J. Mol. Sci. 18, 32. https://doi.org/10.3390/ijms18010032

Seo, K., Kim, M., Kim, D.H., 2015. Re-derivation of Young's Equation, Wenzel Equation, and Cassie-Baxter Equation Based on Energy Minimization, in: Aliofkhazraei, M. (Ed.), Surface Energy. InTech. https://doi.org/10.5772/61066

Sgorbini, B., Cagliero, C., Argenziano, M., Cavalli, R., Bicchi, C., Rubiolo, P., 2017. *In vitro* release and permeation kinetics of *Melaleuca alternifolia* (tea tree) essential oil bioactive compounds from topical formulations. Flavour Fragr. J. 32, 354–361. https://doi.org/10.1002/ffj.3403

Shalmashi, Golmohammad, 2010. SOLUBILITY OF CAFFEINE IN WATER, ETHYL ACETATE, ETHANOL, CARBON TETRACHLORIDE, METHANOL, CHLOROFORM, DICHLOROMETHANE, AND ACETONE BETWEEN 298 AND 323 K. Lat. Am. Appl. Res. 40, 283–285.

Sharkawy, A., Fernandes, I.P., Barreiro, M.F., Rodrigues, A.E., Shoeib, T., 2017. Aroma-Loaded Microcapsules with Antibacterial Activity for Eco-Friendly Textile Application: Synthesis, Characterization, Release, and Green Grafting. Ind. Eng. Chem. Res. 56, 5516–5526. https://doi.org/10.1021/acs.iecr.7b00741

Sharma, R., Pathak, K., 2011. Polymeric nanosponges as an alternative carrier for improved retention of econazole nitrate onto the skin through topical hydrogel formulation. Pharm. Dev. Technol. 16, 367–376. https://doi.org/10.3109/10837451003739289

Shen, H., Hu, X., Szymusiak, M., Wang, Z.J., Liu, Y., 2013. Orally Administered Nanocurcumin to Attenuate Morphine Tolerance: Comparison between Negatively Charged PLGA and Partially and Fully PEGylated Nanoparticles. Mol. Pharm. 10, 4546–4551. https://doi.org/10.1021/mp400358z

Sheng, X., Fan, L., He, C., Zhang, K., Mo, X., Wang, H., 2013. Vitamin E-loaded silk fibroin nanofibrous mats fabricated by green process for skin care application. Int. J. Biol. Macromol. 56, 49–56. https://doi.org/10.1016/j.ijbiomac.2013.01.029

Shi, Y., Wei, Z., Zhao, H., Liu, T., Dong, A., Zhang, J., 2013. Electrospinning of Ibuprofen-Loaded Composite Nanofibers for Improving the Performances of Transdermal Patches. J. Nanosci. Nanotechnol. 13, 3855–3863. https://doi.org/10.1166/jnn.2013.7157

Silva, M.C.D., Leal, R.D.C.A., Silva, H.N.D., Fook, M.V.L., 2020. Biodegradable suture threads as controlled drug delivery systems. Mater. Res. Innov. 24, 161–165. https://doi.org/10.1080/14328917.2019.1619982

Simitzis, P., 2018. Agro-Industrial By-Products and Their Bioactive Compounds—An Ally against Oxidative Stress and Skin Aging. Cosmetics 5, 58. https://doi.org/10.3390/cosmetics5040058

Simovic, L., Skundric, P., Pajic-Lijakovic, I., Ristic, K., Medovic, A., Tasić, G., 2010. Mathematical model of gentamicin sulfate release from a bioactive textile material as a transdermal system under *in vitro* conditions. J. Appl. Polym. Sci. NA-NA. https://doi.org/10.1002/app.31964

Simovic, Lj., Skundric, P., Baralic, A.M., Pajic-Lijakovic, I., Milutinovic-Nikolic, A., 2012. Characterization and behavior of anesthetic bioactive textile complex in vitro condition. J. Biomed. Mater. Res. A 100A, 1–6. https://doi.org/10.1002/jbm.a.33234

Şimşek, S., Eroğlu, H., Kurum, B., Ulubayram, K., 2013. Brain targeting of Atorvastatin loaded amphiphilic PLGA-b-PEG nanoparticles. J. Microencapsul. 30, 10–20. https://doi.org/10.3109/02652048.2012.692400

Singh, D., Pradhan, M., Nag, M., Singh, M.R., 2015. Vesicular system: Versatile carrier for transdermal delivery of bioactives. Artif. Cells Nanomedicine Biotechnol. 43, 282–290. https://doi.org/10.3109/21691401.2014.883401

Siow, L.-F., 2012. Effect of pH on Garlic Oil Encapsulation by Complex Coacervation. J. Food Process. Technol. 04. https://doi.org/10.4172/2157-7110.1000199

Siregar, S., C., Martono, S, M., Rohman,A, 2018. Application of Fourier transform infrared (FTIR) spectroscopy coupled with multivariate calibration for quantitative analysis of curcuminoid in Tablet dosage form. S 151–156. https://doi.org/10.7324/JAPS.2018.8821

Slominski, A., Fischer, T.W., Zmijewski, M.A., Wortsman, J., Semak, I., Zbytek, B., Slominski, R.M., Tobin, D.J., 2005. On the Role of Melatonin in Skin Physiology and Pathology. Endocrine 27, 137–148. https://doi.org/10.1385/ENDO:27:2:137

Solans, C., Morales, D., Homs, M., 2016. Spontaneous emulsification. Curr. Opin. Colloid Interface Sci. 22, 88–93. https://doi.org/10.1016/j.cocis.2016.03.002

Souguir, H., Salaün, F., Douillet, P., Vroman, I., Chatterjee, S., 2013. Nanoencapsulation of curcumin in polyurethane and polyurea shells by an emulsion diffusion method. Chem. Eng. J. 221, 133–145. https://doi.org/10.1016/j.cej.2013.01.069

Souza, J.M., Caldas, A.L., Tohidi, S.D., Molina, J., Souto, A.P., Fangueiro, R., Zille, A., 2014. Properties and controlled release of chitosan microencapsulated limonene oil. Rev. Bras. Farmacogn. 24, 691–698. https://doi.org/10.1016/j.bjp.2014.11.007

Sreekumar, S., Lemke, P., Moerschbacher, B.M., Torres-Giner, S., Lagaron, J.M., 2017. Preparation and optimization of submicron chitosan capsules by water-based electrospraying for food and bioactive packaging applications. Food Addit. Contam. Part A 34, 1795–1806. https://doi.org/10.1080/19440049.2017.1347284

Sun, H., Mei, L., Song, C., Cui, X., Wang, P., 2006. The in vivo degradation, absorption and excretion of PCL-based implant. Biomaterials 27, 1735–1740. https://doi.org/10.1016/j.biomaterials.2005.09.019

Sun, L., Liu, Z., Wang, L., Cun, D., Tong, H.H.Y., Yan, R., Chen, X., Wang, R., Zheng, Y., 2017. Enhanced topical penetration, system exposure and anti-psoriasis activity of two particle-sized, curcumin-loaded PLGA nanoparticles in hydrogel. J. Controlled Release 254, 44–54. https://doi.org/10.1016/j.jconrel.2017.03.385

Sun, Y.-M., Zhang, H.-Y., Chen, D.-Z., Liu, C.-B., 2002. Theoretical elucidation on the antioxidant mechanism of curcumin: a DFT study. Org. Lett. 4, 2909–2911. https://doi.org/10.1021/ol0262789

Suñer-Carbó, J., Calpena-Campmany, A., Halbaut-Bellowa, L., Clares-Naveros, B., Rodriguez-Lagunas, M., Barbolini, E., Zamarbide-Losada, J., Boix-Montañés, A., 2019. Biopharmaceutical Development of a Bifonazole Multiple Emulsion for Enhanced Epidermal Delivery. Pharmaceutics 11, 66. https://doi.org/10.3390/pharmaceutics11020066

Taban, A., Saharkhiz, M.J., Khorram, M., 2020. Formulation and assessment of nano-encapsulated bioherbicides based on biopolymers and essential oil. Ind. Crops Prod. 149, 112348. https://doi.org/10.1016/j.indcrop.2020.112348

Takeuchi, I., Takeshita, T., Suzuki, T., Makino, K., 2017. Iontophoretic transdermal delivery using chitosan-coated PLGA nanoparticles for positively charged drugs. Colloids Surf. B Biointerfaces 160, 520–526. https://doi.org/10.1016/j.colsurfb.2017.10.011

Taktak, F., Bütün, V., Tuncer, C., Demirel, H.H., 2019. Production of LMWH-conjugated core/shell hydrogels encapsulating paclitaxel for transdermal delivery: In vitro and in vivo

assessment. Int. J. Biol. Macromol. 128, 610–620. https://doi.org/10.1016/j.ijbiomac.2019.01.184

Tam, Y.T., To, K.K.W., Chow, A.H.L., 2016. Fabrication of doxorubicin nanoparticles by controlled antisolvent precipitation for enhanced intracellular delivery. Colloids Surf. B Biointerfaces 139, 249–258. https://doi.org/10.1016/j.colsurfb.2015.12.026

Tan, M.X.L., Danquah, M.K., 2012. Drug and Protein Encapsulation by Emulsification: Technology Enhancement Using Foam Formulations. Chem. Eng. Technol. 35, 618–626. https://doi.org/10.1002/ceat.201100358

Tao, J., Chow, S.F., Zheng, Y., 2019. Application of flash nanoprecipitation to fabricate poorly water-soluble drug nanoparticles. Acta Pharm. Sin. B 9, 4–18. https://doi.org/10.1016/j.apsb.2018.11.001

Tapia-Hernández, J.A., Torres-Chávez, P.I., Ramírez-Wong, B., Rascón-Chu, A., Plascencia-Jatomea, M., Barreras-Urbina, C.G., Rangel-Vázquez, N.A., Rodríguez-Félix, F., 2015. Micro- and Nanoparticles by Electrospray: Advances and Applications in Foods. J. Agric. Food Chem. 63, 4699–4707. https://doi.org/10.1021/acs.jafc.5b01403

Tatke, A., Dudhipala, N., Janga, K., Balguri, S., Avula, B., Jablonski, M., Majumdar, S., 2018. In Situ Gel of Triamcinolone Acetonide-Loaded Solid Lipid Nanoparticles for Improved Topical Ocular Delivery: Tear Kinetics and Ocular Disposition Studies. Nanomaterials 9, 33. https://doi.org/10.3390/nano9010033

Thioune, O., Fessi, H., Devissaguet, J.P., Puisieux, F., 1997. Preparation of pseudolatex by nanoprecipitation: Influence of the solvent nature on intrinsic viscosity and interaction constant. Int. J. Pharm. 146, 233–238. https://doi.org/10.1016/S0378-5173(96)04830-2

Thorat, A.A., Dalvi, S.V., 2014. Particle formation pathways and polymorphism of curcumin induced by ultrasound and additives during liquid antisolvent precipitation. CrystEngComm 16, 11102–11114. https://doi.org/10.1039/C4CE02021A

Timilsena, Y.P., Akanbi, T.O., Khalid, N., Adhikari, B., Barrow, C.J., 2019. Complex coacervation: Principles, mechanisms and applications in microencapsulation. Int. J. Biol. Macromol. 121, 1276–1286. https://doi.org/10.1016/j.ijbiomac.2018.10.144

Tobin, D.J., 2017. Introduction to skin aging. J. Tissue Viability 26, 37–46. https://doi.org/10.1016/j.jtv.2016.03.002

Todo, H., 2017. Transdermal Permeation of Drugs in Various Animal Species. Pharmaceutics 9, 33. https://doi.org/10.3390/pharmaceutics9030033

Tolleson, W.H., 2005. Human melanocyte biology, toxicology, and pathology. J. Environ. Sci. Health Part C Environ. Carcinog. Ecotoxicol. Rev. 23, 105–161. https://doi.org/10.1080/10590500500234970

Tordjman, S., Chokron, S., Delorme, R., Charrier, A., Bellissant, E., Jaafari, N., Fougerou, C., 2017. Melatonin: Pharmacology, Functions and Therapeutic Benefits. Curr. Neuropharmacol. 15, 434–443. https://doi.org/10.2174/1570159X14666161228122115

Trojanowska, A., Nogalska, A., Valls, R.G., Giamberini, M., Tylkowski, B., 2017. Technological solutions for encapsulation. Phys. Sci. Rev. 2. https://doi.org/10.1515/psr-2017-0020

Trotta, F., Zanetti, M., Cavalli, R., 2012. Cyclodextrin-based nanosponges as drug carriers. Beilstein J. Org. Chem. 8, 2091–2099. https://doi.org/10.3762/bjoc.8.235

Turino, L.N., Stella, B., Dosio, F., Luna, J.A., Barresi, A.A., 2018. Nanoparticles obtained by confined impinging jet mixer: poly(lactide- *co* -glycolide) vs. Poly-ε-caprolactone. Drug Dev. Ind. Pharm. 44, 934–941. https://doi.org/10.1080/03639045.2017.1421662

Unger, D.R., Muzzio, F.J., 1999. Laser-induced fluorescence technique for the quantification of mixing in impinging jets. AIChE J. 45, 2477–2486. https://doi.org/10.1002/aic.690451203

Utiger, R.D., 1992. Melatonin — The Hormone of Darkness. N. Engl. J. Med. 327, 1377–1379. https://doi.org/10.1056/NEJM199211053271909

Vajragupta, O., Boonchoong, P., Berliner, L.J., 2004. Manganese complexes of curcumin analogues: evaluation of hydroxyl radical scavenging ability, superoxide dismutase activity and stability towards hydrolysis. Free Radic. Res. 38, 303–314.

Valente, I., Celasco, E., Marchisio, D.L., Barresi, A.A., 2012. Nanoprecipitation in confined impinging jets mixers: Production, characterization and scale-up of pegylated nanospheres and nanocapsules for pharmaceutical use. Chem. Eng. Sci. 77, 217–227. https://doi.org/10.1016/j.ces.2012.02.050

van Smeden, J., Janssens, M., Gooris, G.S., Bouwstra, J.A., 2014. The important role of stratum corneum lipids for the cutaneous barrier function. Biochim. Biophys. Acta BBA - Mol. Cell Biol. Lipids 1841, 295–313. https://doi.org/10.1016/j.bbalip.2013.11.006

Ventola, C.L., 2012. The nanomedicine revolution: part 3: regulatory and safety challenges. P T Peer-Rev. J. Formul. Manag. 37, 631–639.

Vineis, C., Varesano, A., 2018. Natural polymer-based electrospun fibers for antibacterial uses, in: Electrofluidodynamic Technologies (EFDTs) for Biomaterials and Medical Devices. Elsevier, pp. 275–294. https://doi.org/10.1016/B978-0-08-101745-6.00014-1

Vitellaro-Zuccarello, L., Cappelletti, S., Rossi, V.D.P., Sari-Gorla, M., 1994. Stereological analysis of collagen and elastic fibers in the normal human dermis: Variability with age, sex, and body region. Anat. Rec. 238, 153–162. https://doi.org/10.1002/ar.1092380202

Vladisavljević, G.T., 2019. Preparation of microemulsions and nanoemulsions by membrane emulsification. Colloids Surf. Physicochem. Eng. Asp. 579, 123709. https://doi.org/10.1016/j.colsurfa.2019.123709

Vladisavljević, G.T., 2015. Structured microparticles with tailored properties produced by membrane emulsification. Adv. Colloid Interface Sci. 225, 53–87. https://doi.org/10.1016/j.cis.2015.07.013

Wan, K.Y., Wong, K.W., Chow, A.H.L., Chow, S.F., 2018. Impact of molecular rearrangement of amphiphilic stabilizers on physical stability of itraconazole nanoparticles prepared by flash nanoprecipitation. Int. J. Pharm. 542, 221–231. https://doi.org/10.1016/j.ijpharm.2018.03.006

Wang, M., Hu, L., Xu, C., 2017. Recent advances in the design of polymeric microneedles for transdermal drug delivery and biosensing. Lab. Chip 17, 1373–1387. https://doi.org/10.1039/C7LC00016B

Wenyi Wang, Patrick Hui, Chi-Wai Kan, 2017. Functionalized Textile Based Therapy for the Treatment of Atopic Dermatitis. Coatings 7, 82. https://doi.org/10.3390/coatings7060082

Wijesirigunawardana, P.B., K. Perera, B.G., 2018. Development of a Cotton Smart Textile with Medicinal Properties Using Lime Oil Microcapsules. Acta Chim. Slov. 65, 150–159. https://doi.org/10.17344/acsi.2017.3727

Williams, H.C., Dellavalle, R.P., Garner, S., 2012. Acne vulgaris. The Lancet 379, 361–372. https://doi.org/10.1016/S0140-6736(11)60321-8

Wong, T.W., John, P., 2015. Advances in Spray Drying Technology for Nanoparticle Formation, in: Aliofkhazraei, M. (Ed.), Handbook of Nanoparticles. Springer International Publishing, Cham, pp. 1–16. https://doi.org/10.1007/978-3-319-13188-7_18-1

Woodruff, M.A., Hutmacher, D.W., 2010. The return of a forgotten polymer—Polycaprolactone in the 21st century. Prog. Polym. Sci. 35, 1217–1256. https://doi.org/10.1016/j.progpolymsci.2010.04.002

Woodward, S.C., Brewer, P.S., Moatamed, F., Schindler, A., Pitt, C.G., 1985. The intracellular degradation of poly(?-caprolactone). J. Biomed. Mater. Res. 19, 437–444. https://doi.org/10.1002/jbm.820190408

World health organization, 1992. IAC MONOGRAHS ON THE EVALUATION OF CARCINOGENIC RISKS TO HUMANS. VOLUME 55 Solar and Ultraviolet Radiation.

Wu, J., Wei, W., Wang, L.-Y., Su, Z.-G., Ma, G.-H., 2008. Preparation of uniform-sized pH-sensitive quaternized chitosan microsphere by combining membrane emulsification technique and thermal-gelation method. Colloids Surf. B Biointerfaces 63, 164–175. https://doi.org/10.1016/j.colsurfb.2007.11.021

Wu, J.H., Cohen, B.A., 2019. The stigma of skin disease: Curr. Opin. Pediatr. 31, 509–514. https://doi.org/10.1097/MOP.0000000000000792

Wysocki, A.B., 1999. Skin anatomy, physiology, and pathophysiology. Nurs. Clin. North Am. 34, 777–797, v.

Xiao, Z., Liu, W., Zhu, G., Zhou, R., Niu, Y., 2014. A review of the preparation and application of flavour and essential oils microcapsules based on complex coacervation technology. J. Sci. Food Agric. 94, 1482–1494. https://doi.org/10.1002/jsfa.6491

Xin, J.H., Fei, B., 2007. N, N-diethyl-m-toluamide–Containing Microcapsules for Bio-Cloth Finishing. Am. J. Trop. Med. Hyg. 77, 52–57. https://doi.org/10.4269/ajtmh.2007.77.52

Xu, B., Cao, Q., Zhang, Y., Yu, W., Zhu, J., Liu, D., Jiang, G., 2018. Microneedles Integrated with ZnO Quantum-Dot-Capped Mesoporous Bioactive Glasses for Glucose-Mediated Insulin Delivery. ACS Biomater. Sci. Eng. 4, 2473–2483. https://doi.org/10.1021/acsbiomaterials.8b00626

Yadav, D.K., Sharma, K., Dutta, A., Kundu, A., Awasthi, A., Goon, A., Banerjee, K., Saha, S., 2017. Purity Evaluation of Curcuminoids in the Turmeric Extract Obtained by Accelerated Solvent Extraction. J. AOAC Int. 100, 586–591. https://doi.org/10.5740/jaoacint.17-0057

Yang, Y., Kalluri, H., Banga, A.K., 2011. Effects of Chemical and Physical Enhancement Techniques on Transdermal Delivery of Cyanocobalamin (Vitamin B12) In Vitro. Pharmaceutics 3, 474–484. https://doi.org/10.3390/pharmaceutics3030474

Yang, Z., Zeng, Z., Xiao, Z., Ji, H., 2014. Preparation and controllable release of chitosan/vanillin microcapsules and their application to cotton fabric: Controllable release of vanillin. Flavour Fragr. J. 29, 114–120. https://doi.org/10.1002/ffj.3186

Yen, F.-L., Wu, T.-H., Tzeng, C.-W., Lin, L.-T., Lin, C.-C., 2010. Curcumin Nanoparticles Improve the Physicochemical Properties of Curcumin and Effectively Enhance Its Antioxidant and Antihepatoma Activities. J. Agric. Food Chem. 58, 7376–7382. https://doi.org/10.1021/jf100135h

Yew, H.-C., Misran, M., 2016. Preparation and characterization of pH dependent κ-carrageenan-chitosan nanoparticle as potential slow release delivery carrier. Iran. Polym. J. 25, 1037–1046. https://doi.org/10.1007/s13726-016-0489-6

Yip, J., Luk, M.Y.A., 2016. Microencapsulation technologies for antimicrobial textiles, in: Antimicrobial Textiles. Elsevier, pp. 19–46. https://doi.org/10.1016/B978-0-08-100576-7.00003-1

Yousef, H., Sharma, S., 2019. Anatomy, Skin (Integument), Epidermis, in: StatPearls. StatPearls Publishing, Treasure Island (FL).

Yu, J.R., Navarro, J., Coburn, J.C., Mahadik, B., Molnar, J., Holmes, J.H., Nam, A.J., Fisher, J.P., 2019. Current and Future Perspectives on Skin Tissue Engineering: Key Features of Biomedical Research, Translational Assessment, and Clinical Application. Adv. Healthc. Mater. 8, 1801471. https://doi.org/10.1002/adhm.201801471

Yuan Gao, Cranston, R., 2008. Recent Advances in Antimicrobial Treatments of Textiles. Text. Res. J. 78, 60–72. https://doi.org/10.1177/0040517507082332

Yun, J., Im, J.S., Lee, Y.-S., Kim, H.-I., 2011. Electro-responsive transdermal drug delivery behavior of PVA/PAA/MWCNT nanofibers. Eur. Polym. J. 47, 1893–1902. https://doi.org/10.1016/j.eurpolymj.2011.07.024

Zelenková, T., Barresi, A.A., Fissore, D., 2015. On the Use of tert-Butanol/Water Cosolvent Systems in Production and Freeze-Drying of Poly-ε-Caprolactone Nanoparticles. J. Pharm. Sci. 104, 178–190. https://doi.org/10.1002/jps.24271

Zelenková, T., Fissore, D., Marchisio, D.L., Barresi, A.A., 2014. Size Control in Production and Freeze-Drying of Poly-ε-Caprolactone Nanoparticles. J. Pharm. Sci. 103, 1839–1850. https://doi.org/10.1002/jps.23960

Zelenková, T., Mora, M.J., Barresi, A.A., Granero, G.E., Fissore, D., 2018. On the Production of Chitosan-Coated Polycaprolactone Nanoparticles in a Confined Impinging Jet Reactor. J. Pharm. Sci. 107, 1157–1166. https://doi.org/10.1016/j.xphs.2017.11.020

Zemljič, L.F., Peršin, Z., Šauperl, O., Rudolf, A., Kostić, M., 2018. Medical textiles based on viscose rayon fabrics coated with chitosan-encapsulated iodine: antibacterial and antioxidant properties. Text. Res. J. 88, 2519–2531. https://doi.org/10.1177/0040517517725117

Zhang, C., Pansare, V.J., Prud'homme, R.K., Priestley, R.D., 2012. Flash nanoprecipitation of polystyrenenanoparticles. Soft Matter 8, 86–93. https://doi.org/10.1039/C1SM06182H

Zhang, S., Campagne, C., Salaün, F., 2019. Influence of Solvent Selection in the Electrospraying Process of Polycaprolactone. Appl. Sci. 9, 402. https://doi.org/10.3390/app9030402

Zhang, S., Kawakami, K., 2010. One-step preparation of chitosan solid nanoparticles by electrospray deposition. Int. J. Pharm. 397, 211–217. https://doi.org/10.1016/j.ijpharm.2010.07.007

Zhang, Y., Feng, J., McManus, S.A., Lu, H.D., Ristroph, K.D., Cho, E.J., Dobrijevic, E.L., Chan, H.-K., Prud'homme, R.K., 2017. Design and Solidification of Fast-Releasing Clofazimine Nanoparticles for Treatment of Cryptosporidiosis. Mol. Pharm. 14, 3480–3488. https://doi.org/10.1021/acs.molpharmaceut.7b00521

Zhang, Z., Michniak-Kohn, B.B., 2012. Tissue Engineered Human Skin Equivalents. Pharmaceutics 4, 26–41. https://doi.org/10.3390/pharmaceutics4010026

Zhu, Z., 2014. Flash Nanoprecipitation: Prediction and Enhancement of Particle Stability via Drug Structure. Mol. Pharm. 11, 776–786. https://doi.org/10.1021/mp500025e

Zhuang, Y., Xu, Y., Wang, H., Wang, L., Liu, C., Xu, W., Yang, H., 2019. Preparation of pure egg albumen fiber through coaxial wet-spinning. Mater. Lett. 253, 63–66. https://doi.org/10.1016/j.matlet.2019.06.035

Zlotos, Darius.P., Jockers, R., Cecon, E., Rivara, S., Witt-Enderby, P.A., 2014. MT_1 and MT_2 Melatonin Receptors: Ligands, Models, Oligomers, and Therapeutic Potential. J. Med. Chem. 57, 3161–3185. https://doi.org/10.1021/jm401343c

Zorec, B., Zupančič, Š., Kristl, J., Pavšelj, N., 2018. Combinations of nanovesicles and physical methods for enhanced transdermal delivery of a model hydrophilic drug. Eur. J. Pharm. Biopharm. 127, 387–397. https://doi.org/10.1016/j.ejpb.2018.03.008